UNIVERSIDADE DO ALGARVE

Faculdade de Ciências e Tecnologia

Performance Analysis of OFDM Technology on Radio-over-Fiber Systems

Tashi Arthur Ravach

Master in Electronic Engineering and Telecommunications

2011

UNIVERSIDADE DO ALGARVE

Faculdade de Ciências e Tecnologia

Performance Analysis of OFDM Technology on Radio-over-Fiber Systems

Tashi Arthur Ravach

Dissertation supervised by:

Professora Doutora Maria do Carmo Raposo de Medeiros

Master in Electronic Engineering and Telecommunications

2011

Declaration

I hereby declare that this dissertation is the result of my original work and research, and that it is expressed in my own words. Any consulted sources of information are duly acknowledged at their point of use, and are referenced in the included list.

Student:

(Tashi Arthur Ravach)

Supervisor:

(Doutora Maria do Carmo Raposo de Medeiros)

Supervisory Committee:

(Doutor António Eduardo de Barros Ruano)

(Doutora Maria do Carmo Raposo de Medeiros)

(Doutora Paula Raquel Viegas dos Santos Nunes Laurêncio)

Abstract

Nowadays, the demand for high speed, high quality and diversity in distributed services presents a challenge for telecommunication technology. Wireless systems provide the accessibility to end-user, but are not the solution for long distance links. Currently, the ideal technology for long-range transmissions at high data rates is optical fiber. Hence, a new concept for high capacity networks emerges, with centralized services into Base Stations (BS) engineered to provide flexibility and control over the system, and to perform operations such as electrical to optical domain conversion and modulation. Such Radio-over-Fiber (RoF) networks also appear as an attractive technology because they are efficient and cost effective.

Orthogonal Frequency Division Multiplexing (OFDM) technology is widely used in a number of standards. For instance, it is actually the Multi-Carrier Modulation (MCM) technique applied in 802.11a/g/n wireless standards and in Digital Video Broadcasting-Terrestrial (DVB-T), among other prevailing systems, which makes this subject one particularly pertinent to study. OFDM systems are an appealing choice for waveform modulation, as they are very bandwidth efficient comparing to others MCM, and provide flexibility in data transmission rates. Additionally, an important advantage dwells in its natural robustness against severely interfering environments.

In this thesis, fundamentals on OFDM technology are extensively described, and its application to wireless and optical fiber networks is introduced. The combined channel effects of these technologies on OFDM signals are investigated. In terms of performance analysis, this exposition focuses on understanding the importance of OFDM modulation parameters, and explores some OFDM signal properties. To achieve this, a simulator was implemented with *Matlab* to create arbitrary OFDM waveforms and emulate channel effects. This study also investigates the efficiency of OFDM technology over a real Radio Frequency (RF) system with an ideal communication channel. Finally, an experimental RoF configuration is implemented and its performance is assessed.

Keywords: OFDM, FFT, 802.11, RoF, EVM, and Matlab.

Resumo

Na área das telecomunicações, as tecnologias dominantes são aquelas que oferecem serviços diversificados e de qualidade superior a custos acessíveis para os utilizadores, proporcionando simultaneamente flexibilidade e controlo aos fornecedores de serviços. Actualmente, a fibra óptica é o meio de transmissão predominante para estabelecer sistemas de comunicação para longas distâncias, isto porque suporta taxas de transmissão muito elevadas introduzindo menor atenuação e menos interferências do que os meios clássicos. No que respeita à distribuição e acessibilidade de serviços de comunicação, verificou-se nos últimos anos, e ainda presentemente com o sucesso notável dos sistema de redes sem fios, que estes são os mais adequados para fornecer o acesso final aos utilizadores. Tal se deve principalmente à facilidade de acesso e à mobilidade associados a estes sistemas, bem como a crescente capacidade em termos de taxas de transmissão e de segurança. Deste modo, um conceito surge para um tipo de rede que tira partido das vantagens associadas a estas duas tecnologias conhecido como Rádio sobre Fibra (Radio-over-Fiber - RoF), sendo que o sinal rádio eléctrico pode ser com fios ou sem fios. Este tipo de redes composta é introduzido em [1], e é descrito pelos autores como um sistema constituído por um Sítio Central (Central Site - CS) ligado por fibra óptica a um Sítio Remoto (Remote Site - RS). A ideia consiste na implementação de um RS simples e de baixo custo, com capacidade para executar de forma centralizada operações como a conversão directa do domínio eléctrico para óptico e a modulação de sinais ópticos. Um cenário possível poderia ser um conjunto de utilizadores a transmitir informação para o RS através de uma rede sem fios. No RS, os sinais rádio eléctricos são combinados e directamente convertidos para o domínio óptico, e a informação é encaminhada para o CS.

Um dos sistemas de redes locais sem fios mais usados é definido pelo standard IEEE 802.11g. Este standard pertence à categoria de especificações designadas como IEEE 802.11 que são minuciosamente descritas em [2], dentro da qual aperfeiçoamentos e novas especificações compatíveis com versões anteriores têm sidos desenvolvidas ao longo dos anos. O standard IEEE 802.11g foi concebido de forma a ser compatível com os standards anteriores IEEE 802.11a e IEEE 802.11b, e a definição da sua camada física baseia-se nestes. Assim, este standard mantém-se actual e usado em larga escala, pelo que se torna um tópico de estudo particularmente interessante. O standard IEEE 802.11a é um dos primeiros sistemas do género a fazer uso de um método de modulação de dados conhecido como Multiplexagem por Divisão de Frequências Ortogonais (Orthogonal Frequency Division Multiplexing - OFDM).

Esta técnica de modulação, descrita ao pormenor para um modelo de rede sem fios em [3], surgiu na década de 1960. É uma tecnologia que tem sido cada vez mais adoptada em sistemas

eléctricos com fios e sem fios devido às diversas vantagens que a caracterizam. Em primeiro lugar, comparada com outras técnicas de modulação com múltiplas portadoras, a modulação OFDM proporciona uma utilização muito mais eficiente da largura de banda. Esta eficiência deve-se à disposição particular das suas sub-portadoras (Subcarriers - SC), isto é, à ortogonalidade existente entre as suas frequências. Esta propriedade possibilita a sobreposição espectral de componentes das SCs, cada uma delas centrada numa frequência múltipla da frequência de base, sem que sejam introduzidas interferências entre elas. Outra vantagem associada a esta tecnologia é a sua grande robustez em ambientes que introduzem altos níveis de distorção e atrasos no sinal, tais como ambientes de multi-percurso. Sendo o sinal composto por SCs com frequências distintas, os efeitos de atenuação dependentes da frequência apenas influenciam algumas delas, ou seja, apenas parte da informação transmitida é corrompida. Esta característica, aliada de mecanismos de codificação da fonte, permite recuperar grande parte da informação distorcida. No que respeita a atrasos, o principal mecanismo de protecção baseia-se em gerar uma periodicidade no sinal através do Prefixo Cíclico (Cyclic Prefix - CP), que estende a duração do símbolo OFDM. Este prefixo é simplesmente constituído por uma cópia de parte das amostras que definem o sinal, que são colocadas a frente de cada símbolo durante o Intervalo de Guarda (Guard Interval - GI). Recorrendo ao uso de SCs piloto, erros de fase são facilmente estimados e corrigidos sem necessitar de recorrer a equalizadores complexos e dispendiosos. Algumas desvantagens também estão associadas a esta tecnologia. Em primeiro lugar, é extremamente sensível a erros de sincronismo, quer a nível de frequência, quer a nível de tempo. Em segundo lugar, na modulação OFDM existe uma tendência em se gerar altos níveis de Relação Pico-Valor Médio de Potência (Peak-to-Average Power Ratio - PAPR). Tal acontece porque no processo de multiplexagem as SCs são somadas entre elas. Quando várias destas portadoras são somadas num período, se em dado instante todas têm elevadas amplitudes, tal é reflectido no sinal OFDM resultante através de um pico naquele instante, elevando-se muito acima da média. Estes altos picos exigem muito por parte dos amplificadores que podem saturar, bem como dos filtros e conversores analógico/digital existentes num sistema real.

Nesta dissertação, como primeiro objectivo pretende-se estudar de forma compreensiva os comportamentos conhecidos da modulação OFDM em diversas situações, baseando as características dos sinais gerados nas especificações de modulação e de tempo descritas no standard IEEE 802.11a. Mecanismos de sincronismo e de estimação do canal são igualmente baseados nestas especificações. Numa primeira fase, um simulador desenvolvido em *Matlab* é usado para gerar formas de ondas OFDM complexas em banda base. Estas são sujeitas a modelos de distorção por falta de sincronismo, por canais multi-percurso e ruído Gaussiano, pondo à prova os mecanismos de recuperação e demonstrando os seus efeitos. O principal mecanismo de análise do desempenho consiste no cálculo da Magnitude do Vector de Erro (Error Vector Magnitude - EVM), implementado

conforme descrito no standard IEEE 802.11a. Além disso, as influências sobre os sinais são observadas através de representações clássicas, como a Relação Sinal-Ruído (Signal-to-Noise Ratio – SNR) e a contagem percentual da Taxa de Bits Errados (Bit Error Rate – BER). De modo a observar os efeitos dos filtros e de pequenos desvios que podem ocorrer numa transmissão real, o simulador também é implementado para sinais em banda.

O segundo objectivo deste trabalho consiste em estudar o comportamento da técnica de modulação OFDM num sistema RoF, implementando fisicamente uma rede e recorrendo a instrumentos para gerar os sinais e para adquiri-los de volta. De modo a formar um sistema completo, flexível e controlado a partir do simulador, foram desenvolvidas ferramentas para comunicação com os instrumentos através de um interface GPIB, bem como para geração e extracção de ficheiros específicos à cada instrumento. A configuração implementada representa um RS em comunicação com um CS. Assim, o RS recebe quatro sinais rádio centrados em frequências distintas, em que um deles é o sinal OFDM em estudo. Estes sinais são combinados, passando a circular todos juntos pelo mesmo meio eléctrico. O sinal eléctrico é então modulado directamente numa portadora óptica pelo RS, e esta é transmitida. No receptor, que corresponde ao sinal que chega no CS vindo do RS, o sinal é convertido de volta para o domínio eléctrico usando um foto-detector, e o sinal OFDM é separado dos restantes e processado digitalmente. Por fim, a análise das constelações é efectuada, sendo caracterizada através do cálculo do EVM.

Palavras Chaves: OFDM, FFT, 802.11, RoF, EVM, e Matlab.

Acknowledgments

I would like to express my appreciation to my dissertation supervisor, whose expertise and guidance were important for the conception of this master thesis.

In addition, I want to acknowledge my colleagues from the CEOT who always listened to my questions and helped me find my way.

Finally, and most importantly, I wish to thank my family for the support they provided me continuously and in many ways through my entire life.

Table of Contents

DECLARATION I
ABSTRACT III
RESUMO V
ACKNOWLEDGMENTS IX
TABLE OF CONTENTS XI
LIST OF FIGURES XV
LIST OF TABLES XIX
ABBREVIATIONS XXI
CHAPTER 1. INTRODUCTION 1
1.1. Wireless Radio-over-Fiber Networks 1
1.2. OFDM Technology in RoF Networks 1
1.3. Dissertation Outline 2
CHAPTER 2. FUNDAMENTALS ON OFDM SYSTEMS 5
2.1. Introduction 5
2.2. An Overview on OFDM Technology 5
2.3. OFDM Model for a Transmission System 7
2.3.1. The Concept of Orthogonality between Subcarriers 9
2.3.2. Scrambling, Convolutional Coding and Interleaving 11
2.3.3. OFDM Modulation/Demodulation using IFFT/FFT Algorithm 12
2.3.4. The Importance of the Guard Interval and the Cyclic Prefix 12
2.3.5. Pulse Shaping and Windowing applied to OFDM Systems 14
2.4. Mathematical Characterization 15
2.4.1. OFDM Modulation 15
2.4.2. OFDM Signal over a Time-Dispersive Channel 17
2.4.3. OFDM Demodulation 18
2.4.4. Relating the OFDM Subcarriers to the Noise 19
2.4.5. Time Synchronization Errors 20
2.4.6. Frequency Synchronization Errors 21
2.4.7. Time and Frequency Synchronization Errors 23
2.5. Main Advantages of OFDM Technology 23
2.6. Important Drawbacks of OFDM Technology 24

2.7. Summary 25
CHAPTER 3. OFDM IN WIRELESS AND OPTICAL NETWORKS 27
3.1. Introduction 27
3.2. OFDM as Part of the IEEE 802.11 Standard for Wireless Networks 28
3.2.1. IEEE 802.11a Specifications for OFDM Modulation 29
3.2.2. Preview on the IEEE 802.11a PHY Frame Structure 31
3.2.3. Frame Detection using the Short Training Sequence 34
3.2.4. Frequency Offset Estimation using the Short Training Sequence 35
3.3. OFDM Application to Optical Networks 36
3.4. Propagation Characteristics of the Channel 38
3.4.1. Additive White Gaussian Noise 39
3.4.2. Shadowing 39
3.4.3. Multipath Channel Model 39
3.4.4. Doppler Shift 41
3.4.5. Optical Fiber Impairments 42
3.5. Tools for Performance Analysis 43
3.5.1. Error Vector Magnitude 43
3.5.2. Signal-to-Noise Ratio 45
3.5.3. Relating EVM to SNR 46
3.5.4. Peak-to-Average Power Ratio 46
3.6. Summary 49
CHAPTER 4. OFDM SYSTEM SIMULATION USING MATLAB 51
4.1. Introduction 51
4.2. Matlab Simulation Model 51
4.2.1. Base Structure of the Simulator 52
4.2.2. Baseband to Passband Conversion 53
4.2.3. Construction of IEEE 802.11a PHY Frames 54
4.3. The Effect of Time Synchronization Errors 58
4.4. The Effect of Frequency Synchronization Errors 59
4.5. The Effect of AWGN Channel 61
4.6. The Effect of Rayleigh Multipath Channel 63
4.7. Windowing and Spectral Regrowth 64
4.8. Improving the PAPR 65
4.8.1. Source Scrambling 66
4.8.2. Peak Clipping 68

4.9. Summary 69
CHAPTER 5. EXPERIMENTAL OFDM IMPLEMENTATION AND PERFORMANCE ANALYSIS 71
5.1. Introduction 71
5.2. Interfacing with the Instruments 71
5.3. Configuration of the Transmitter and Receiver 72
5.3.1. Synchronizing the Instruments 73
5.3.2. Sampling Frequency and Oversampling 74
5.4. Transmission of IEEE 802.11a PHY Frames 75
5.4.1. Defining the Source Length 76
5.4.2. Performing the Transmission 77
5.5. Summary 82
CHAPTER 6. OFDM PERFORMANCE ON A ROF NETWORK 83
6.1. Introduction 83
6.2. RoF Network Architecture 83
6.2.1. The RSOA as an Optical Modulator and Amplifier 84
6.2.2. Overall System Configuration 86
6.3. Performance Evaluation 87
6.3.1. The Influence of the RSOA Gain 88
6.3.2. The Intermodulation Interference 90
6.3.3. The Experimental Configurations 92
6.4. Summary 98
CHAPTER 7. CONCLUSIONS AND FUTURE WORK 99
7.1. Conclusions 99
7.2. Future Work 104
APPENDIX A. THE FOURIER TRANSFORM AND ITS USE WITH MATLAB 105
A.1. The Discrete Fourier Transform (DFT) 105
A.2. Mathematical Background 106
A.3. Understanding the FFT with *Matlab* 107
A.3.1. The FFT as a tool for Frequency Spectrum Analysis 107
A.3.2. The FFT and the effect of Zero Padding 109
A.3.3. The FFT as a Modulator and Multiplexer for OFDM Systems 111
APPENDIX B. MODULATING ARBITRARY OFDM SIGNALS 115
B.1. Complex or Real OFDM Modulation 115
B.2. Generating Arbitrary Baseband OFDM Signals 116

APPENDIX C. INSTRUMENTS SPECIFICATIONS 123
C.1. Keithley Model 2910 RF Signal Generator 123
C.2. Tektronix RSA 2203A Real-Time Spectrum Analyzer DC-3GHz 124
C.3. Relating the Baseband Transmission to the Acquisition 126
APPENDIX D. EXPERIMENTAL RESULTS FOR RCE, BER AND PER METRICS 129
D.1. Channel Spacing of 5 MHz, 2-fold Oversampling 129
D.2. Channel Spacing of 5 MHz, 5-fold Oversampling 132
REFERENCES 135

List of Figures

Figure 2.1 – Block diagram of a simple OFDM point-to-point transmission model [3]. 7
Figure 2.2 – SCs in parallel by column, OFDM symbols by row. 8
Figure 2.3 – Influence of the transmitter/receiver hardware transfer funtion on the design of an OFDM system [3]. 8
Figure 2.4 – MCM techniques in FDM. a) conventional; b) orthogonal [3]. 10
Figure 2.5 – a) Orthogonal SCs in TD [10]; b) their sum over the period. 10
Figure 2.6 – Generating a Cyclic Prefix [21]. 13
Figure 2.7 – Applying a window to an OFDM symbol [3]. 15
Figure 3.1 – SC frequency allocation based on IEEE 802.11a definitions. 30
Figure 3.2 – PPDU frame format [2]. 32
Figure 3.3 – OFDM training structure. Timing is for 20 MHz of channel spacing [2]. 32
Figure 3.4 – PLCP Preamble composed by the STS and by the LTS, for a 20 MHz channel spacing. 33
Figure 3.5 – Flow structure of the Delay and Correlate algorithm [27]. 35
Figure 3.6 – A multipath fading environment. 39
Figure 3.7 – Random complex Rayleigh multipath channels: 10 impulses on the left; 20 impulses on the right. 40
Figure 3.8 – Multipath delay spread. 41
Figure 3.9 – Representation of multimode distortion [29]. 42
Figure 3.10 – Representation of Constellation Error [2]. 43
Figure 3.11 – Clipping of 2 dB for a complex OFDM symbol of 20 MHz channel spacing, with 4-fold oversampling. 48
Figure 4.1 – Flow diagram for the base structure of the *Matlab* simulator. 52
Figure 4.2 – Up/Down-Conversion with IQ Modulation/Demodulation [39]. 54
Figure 4.3 – Diagram of the implemented *Matlab* simulator, based on IEEE 802.11a PHY. 55
Figure 4.4 – Influence of a timing offset δt = 0.5 μs, corresponding to a 1 sample offset within the GI on the received BPSK constellation. "+" represent the ideal constellations state and "o" the rotated received samples. 58
Figure 4.5 – ICI originated by Carrier Synchronization Error. 59
Figure 4.6 – Constellations distorted by ICI caused by frequency offsets δf = ΔF/16 on the left, and δf = ΔF/16×10 on the right, where ΔF = 312.5 kHz is the SC spacing for a 20 MHz channel spacing. 60
Figure 4.7 – Averaged EVM for different frequency offsets. The SC spacing is ΔF = 312.5 kHz for a 20 MHz channel spacing, and the frequency offset varies within the interval δf = [-ΔF: ΔF]. 60

Figure 4.8 – BER versus E_b/N_0 in AWGN channel for the modulation schemes used in IEEE 802.11a standard. The dashed lines are the theoretical curves for conventional systems, obtained using *Matlab* built-in *berawgn()* function. 62
Figure 4.9 – BER versus E_b/N_0 in AWGN channel for the modulation schemes used in IEEE 802.11a standard with convolutional coding. The dashed lines are the theoretical curves for conventional systems. 62
Figure 4.10 – BER versus E_b/N_0 in AWGN and Rayleigh channels with 10 taps and 20 taps, without convolutional coding nor interleaving. The dashed lines are the theoretical curves for conventional systems, obtained using *Matlab* built-in *berfading()* function. 64
Figure 4.11 – OFDM power spectrum for several windowed transition lengths. 65
Figure 4.12 – PAPR Distribution for different numbers of SCs, with 4-fold oversampling. The dashed lines are the theoretical approximation (due to oversampling, with $\alpha = 3.3$). 66
Figure 4.13 – PSD and PAPR distribution or unscrambled and scrambled transmissions of a picture. 67
Figure 4.14 – The effects of clipping on OFDM signals, with $N_{FFT} = 64$, $N_{GI} = 16$, $N_{WIN} = 2$ and Oversampling = 4. 68
Figure 5.1 – Computer-to-Instruments communication schematic. 72
Figure 5.2 – Instruments synchronization diagram [41] [42]. 73
Figure 5.3 – OFDM Spectrums for different Pulse Shaping Filters, with 4-fold oversampling. In the first illustration, $N_{FFT} = 64$ and 4-fold oversampling is applied. In the second figure, $N_{FFT} = 128$ (64 zeros padded) and 2-fold oversampling is applied. 74
Figure 5.4 – IEEE 802.11a PHY frame with 5-fold oversampling; its corresponding windowed power spectrum. 78
Figure 5.5 – Coarse/Fine Detection of the Frame Starting Sample. 79
Figure 5.6 – Constellations recovery of an OFDM signal in Back-to-Back Transmission: a) Received; b) De-rotated. 81
Figure 6.1 – Suggested RoF Network Architecture 84
Figure 6.2 – Spontaneous Emission of the RSOA for a range of bias current sources. 85
Figure 6.3 – Amplification factor of the RSOA for a range of Input Optical Power. 85
Figure 6.4 – TF of the RSOA for a range of bias current sources; an amplified view for the frequency range of the carriers used in the RoF architecture. 86
Figure 6.5 – The influence of the Optical Amplification of the RSOA on the EVM and the PER. 89
Figure 6.6 – The four carriers with frequency location from left to right: f_{c1}, f_{c2}, f_{c3} and f_{c4}. 90
Figure 6.7 – The effect of a frequency offset at carrier f_{c3} on the intermodulation product frequency location, for 10.5 dBm of electrical power. 90

Figure 6.8 - Example of acquired OFDM Constellations in the presence of interfering intermodulation product outside DC, with 10.5 dBm of electrical power: a) Received 2C2S-IMD-RSOA; b) De-rotated 2C2S-IMD-RSOA; 91
Figure 6.9 – Examples of acquired OFDM Constellations, with 0.5 dBm of electrical power: a) Received 2C2S; b) De-rotated 2C2S; c) Received 2C2S-RSOA; d) De-rotated 2C2S-RSOA; e) Received 2C2S-RSOA-11k; f) De-rotated 2C2S-RSOA -11k. 92
Figure 6.10 – Examples of acquired OFDM Constellations, with 0.5 dBm of electrical power: a) Received 2C2S-IMD; b) De-rotated 2C2S-IMD; c) Received 2C2S-IMD-RSOA; d) De-rotated 2C2S-IMD-RSOA; e) Received 2C2S-IMD-RSOA-11k; f) De-rotated 2C2S-IMD-RSOA -11k..... 93
Figure 6.11 – The effect of the different experimental configurations on the EVM and the PER. 95
Figure A.1 – (a) Sine wave with f_0 = 2 Hz; (b) Sine wave with f_0 = 4 Hz; (c) Sine wave with f_0 = 6 Hz; (d) The summed sines (a)+(b)+(c) 108
Figure A.2 – Frequency spectrums obtained using the FFT for: (a) a sine wave with f_0 = 2 Hz; (b) a sine wave with f_0 = 4 Hz; (c) a sine wave with f_0 = 6 Hz; (d) the summed sines (a)+(b)+(c). 108
Figure A.3 – Two-sided and centered frequency spectrums with amplitude normalization for: (a) a sine wave with f_0 = 2 Hz; (b) a sine wave with f_0 = 4 Hz; (c) a sine wave with f_0 = 6 Hz; (d) the summed sines (a)+(b)+(c). 109
Figure A.4 – Sine wave with f_0 = 4 Hz and 8 samples per period; curve padded with zeros to reach 64 samples; curve padded again with zeros to reach 128 samples. 110
Figure A.5 – Frequency spectrum of: the signal computed with no zero padding; the signal computed with 64 samples; the signal computed with 128 samples. 110
Figure A.6 – The sum of three sine waves at 1.5 Hz, 2 Hz and 2.5 Hz; Frequency spectrum with no zero padding; Frequency spectrum with an 8-fold resolution increase. 111
Figure A.7 – A generic OFDM signal generated in three different ways: (a) Periodic waveforms created separately and summed together; (b) Periodic waveforms created separately with IFFT and summed together; (c) A single IFFT operation that provides the same output..... 113
Figure A.8 – Frequency spectrum of: (a) Periodic waveforms created separately and summed together; (b) Periodic waveforms created separately with IFFT and summed together; (c) A single IFFT operation that provides the same output..... 113
Figure B.1 – Transmission with (left) and without (right) additional IQ modulation [10]. 115
Figure B.2 – a) Original bits stream; b) Convolutionally coded bits stream at rate 3/4..... 116
Figure B.3 – Modulated complex data samples using 4-QAM modulation scheme. 117
Figure B.4 – SCs frequency allocation before IFFT operation for: a complex output on top; a real output at bottom. 118

Figure B.5 – The first FD OFDM chunk prepared for the IFFT operation, with 2-fold oversampling by zero padding: complex output on top; real output at bottom..... 119
Figure B.6 – Raised-cosine window shape applied to each OFDM Symbol, with 2-fold oversampling: applied to the complex samples on top; applied to the real samples at bottom. 120
Figure B.7 – The first TD OFDM symbols, with 2-fold oversampling by zero padding: real part of complex output on top; real output at bottom. 121
Figure B.8 – Two-sided frequency spectrum of the OFDM signal. 121
Figure B.9 – Superimposed constellations of the transmitted and recovered SCs. 122

List of Tables

Table 3.1 – OSI model reference [23]. 28
Table 3.2 – Overview of IEEE 802.11 PHYs [23]. 29
Table 3.3 – Standard IEEE 802.11a modulation-dependent parameters [2]. 30
Table 3.4 – Standard IEEE 802.11a timing-related parameters [2]. 30
Table 3.5 – Differences between typical OFDM Systems and typical Optical Systems [5]. 37
Table 3.6 – Comparison between Wireless and Optical channels [7]. 38
Table 3.7 – Allowed RCE versus Data Rate as specified in IEEE 802.11 standard [2]. 45
Table 5.1 – PSDU length variation of the DATA field with 128 OFDM symbols and a 5 MHz channel spacing. 76
Table 5.2 – IEEE 802.11a OFDM Modulation-dependent Parameters for a 13.5 Mb/s Transmission.. 77
Table 5.3 – IEEE 802.11a PHY FRAME Timing-dependent Parameters for a 13.5 Mb/s Transmission. 77
Table 6.1 – Experimental Configurations. 88
Table B.1 – Complex and Real OFDM modulation parameters. 116
Table B.2 – First 12 samples of 4-QAM modulated data in series. 117
Table B.3 – First 3 chunks of 4-QAM modulated samples in parallel. 118
Table B.4 – Modulated data prepared for IFFT with a complex output of N samples. 119
Table B.5 – Modulated data prepared for IFFT with a real output of 2N samples (Hermitian symmetry). 119
Table C.1 – Keithley Model 2910 supported sampling rates for ARB waveforms playback [42]. 123
Table C.2 – Tektronix RSA 2203A acquisition parameters for IQT data [41]. 124
Table C.3 – Tektronix RSA 2203A span-dependent parameters for IQT acquisition [41]. 125
Table D.1 – Results for the electrical configurations, with 2-fold oversampling. 129
Table D.2 – Results for the RSOA polarizations, with 2-fold oversampling. 130
Table D.3 – Results for the RoF configurations, with 2-fold oversampling. 131
Table D.4 – Results for the electrical configurations, with 5-fold oversampling. 132
Table D.5 – Results for the RSOA polarizations, with 5-fold oversampling. 133
Table D.6 – Results for the RoF configurations, with 5-fold oversampling. 134

Abbreviations

ACO-OFDM	Asymmetrically Clipped Optical OFDM
ADC	Analog-to-Digital Conversion
ADSL	Asymmetric Digital Subscriber Lines
AGC	Automatic Gain Control
AP	Access Point
ARB	Arbitrary Waveform
AWGN	Additive White Gaussian Noise
BER	Bit Error Rate
CD	Coherent-Detection
CDF	Cumulative Distribution Function
CIR	Channel Impulse Response
COFDM	Coded OFDM
CO-OFDM	Coherent Optical OFDM
CP	Cyclic Prefix
CS	Central Site
CSMA/CA	Carrier Sense Multiple Access with Collision Avoidance
CSMA/CD	Carrier Sense Multiple Access with Collision Detection
DAB	Digital Audio Broadcasting
DAC	Digital-to-Analog Conversion
DC	Direct Current
DCO-OFDM	DC-Biased Optical OFDM
DD	Direct-Detection
DDC	Digital Down Converter
DDO-OFDM	Direct-Detection Optical OFDM
DFB	Distributed Feedback
DFT	Discrete Fourier Transform
DSP	Digital Signal Processing
DSSS	Direct Sequence Spread-Spectrum
DSSS/CCK	Direct Sequence Spread-Spectrum Complementary Code Keying
EMI	Electromagnetic Interference
EVM	Error Vector Magnitude
FD	Frequency Domain
FDM	Frequency Division Multiplexing
FEC	Forward Error Correction
FFT	Fast Fourier Transform
FHSS	Frequency Hopped Spread-Spectrum
FM	Frequency Modulation
FTP	File Transfer Protocol
GI	Guard Interval
GIF	Graphics Interchange Format
GPIB	General Purpose Interface Bus
HDSL	High-bit-rate Digital Subscriber Lines

HDTV	High Definition TeleVision
ICI	Interchannel (Intercarrier) Interference
IDFT	Inverse Discrete Fourier Transform
IEEE	Institute of Electrical and Electronics Engineers
IF	Intermediate Frequency
IFFT	Inverse Fast Fourier Transform
IM	Intensity Modulation
IMD	Intermodulation Distortion
IP	Internet Protocol
IPv6	Internet Protocol Version 6
IQ	In-Phase/Quadrature
IR	Infrared
ISI	Intersymbol Interference
JPEG	Joint Photographic Experts Group
LAN	Local Area Network
LASER	Light Amplification by Stimulated Emission of Radiation
LFM	Linear Field Modulation
LLC	Logical Link Control
LoS	Line-of-Sight
LPF	Low-Pass Filter
LTS	Long Training Sequence
MAC	Medium Access Control
MAN	Metropolitan Area Network
MCM	Multi-Carrier Modulation
MMF	Multimode optical Fiber
MPDU	MAC Protocol Data Unit
MPEG	Moving Picture Experts Group
MSB	Most Significant Bit
OFDM	Orthogonal Frequency Division Multiplexing
OSI	Open Systems Interconnection
PAP	Peak-to-Average Power
PAPR	Peak-to-Average Power Ratio
PHY	Physical Layers
PLCP	Physical Layer Convergence Procedure
PMD	Physical Medium Dependent
POF	Plastic (Polymer) Optical Fiber
PPDU	PLCP Protocol Data Unit
PSD	Power Spectral Density
PSDU	PHY Service Data Unit
PSK	Phase Shift Keying
QAM	Quadrature Amplitude Modulation
RCE	Relative Constellation Error
RF	Radio Frequency
RFI	Radio Frequency Interference
RMS	Root Mean Square
RoF	Radio-over-Fiber

RS	Remote Site
RSOA	Reflective Semiconductor Optical Amplifier
SC	Subcarrier (Subchannel)
SCP	Session Control Protocol
SCPI	Standard Commands for Programmable Instruments
SDM	Spacial Division Multiplexing
SMF	Single Mode optical Fiber
SMTP	Simple Mail Transfer Protocol
SNR	Signal-to-Noise Ratio
STS	Short Training Sequence
TCP	Transmission Control Protocol
TD	Time Domain
TF	Transfer Function
TIFF	Tagged Image File Format
UDP	User Datagram Protocol
VCO	Voltage Controlled Oscillator
VDSL	Very-high-speed Digital Subscriber Lines
WDM	Wavelength Division Multiplexing
WFA	Wi-Fi Alliance
WLAN	Wireless Local Area Network
ZIP	Zone Information Protocol

Chapter 1. Introduction

1.1. Wireless Radio-over-Fiber Networks

In present days, the demand for high speed, high quality and diversity in distributed services through networks presents as a challenge for telecommunication technology. Wireless systems provide the accessibility to end-user, but are not a solution for long distance links. Currently, the ideal technology for long-range transmissions at high data rates, with reduced distortions and lower power consumption is optical fiber. By combining electrical and optical technologies, a new concept of networks emerges, which is known as RoF.

A RoF consists of a Central Site (CS) connected to a Remote Site (RS) through an optical fiber link. This is a technology where electrical signals, which can be baseband data, modulated Intermediate Frequency (IF) or an RF carrier, are used to modulate the optical source. Using this approach the optical network can deliver directly the RF signal to the RS, thus avoiding the need to generate and process high frequency carriers at the antenna site. Hence, by concentrating most of the expensive high frequency equipment for electronic signal processing at a centralized location, the RS become simpler and more cost effective [1]. The main reasons that lead RoF networks to appear as especially attractive technology can be summarized into the following:

- Transparency for bandwidth or modulation techniques is provided [4].
- Remote stations become small, simple and low cost [1].
- Centralized operation is possible [1].

The underlying idea in implementing a Wireless RoF system is to combine the mobility and accessibility of the wireless technologies with the massive bandwidth offered by optical fiber.

1.2. OFDM Technology in RoF Networks

Orthogonal Frequency Division Multiplexing (OFDM) is a technology used in many broadband wired and wireless systems, mainly due to its robustness against Intersymbol Interferences (ISI) caused by a dispersive channel [5]. In addition, OFDM technology is an appealing choice for waveform modulation, as it is very bandwidth efficient comparing to other Multi-Carrier Modulation (MCM) techniques, and it provides flexibility in data transmission rates [3]. Currently, many studies are showing that OFDM is also a promising technology for optical communications [5].

However, there are known drawbacks associated to this technology, namely a very high sensitivity to time and frequency synchronization, and the large dynamic range of the signal.

Frequency shifts, usually resulting from unequal local oscillator frequency at the transmitter and receiver, cause the orthogonality between Subcarriers (SC) to be lost, thereby introducing Intercarrier Interferences (ICI). Time deviations, such as delay spreads, cause adjacent data symbols to overlap and interfere with each other, thus introducing ISI. Large peaks cause saturation in power amplifiers, which results in Intermodulation Distortion (IMD) and in out-of-band radiation, thereby leading to ICI [3].

In addition to these impairments, by combining an optical distribution system with a traditional wireless network an additional propagation delay is introduced by the fiber link [6]. Merging a wireless system with an optical fiber system also implies considering the limitations inherent to each technology. For example, wireless communications experience severely interfering multipath propagation characteristics, while optical systems endure effects such as chromatic dispersion, or multimode distortion [7].

The foremost goal of this dissertation is to study the performance of OFDM technology on a RoF network, while taking into account the deterioration sources mentioned above. In order to do so, a simulator was implemented with *Matlab*, which allows for the generation of arbitrary OFDM complex and real waveforms. The simulator includes channel propagation effects with essential signal detection and recovery mechanisms, and time/frequency offset simulation. The parameters chosen to perform the OFDM modulation in this particular study are described in the IEEE 802.11a [2] standard amendment for WLANs. To complete this research, a small practical RoF system was implemented and evaluated. In this dissertation, the main approach for performance evaluation will rely on the estimation of Error Vector Magnitude (EVM) in interfering scenarios, and in understanding the consequences associated to synchronization issues. In addition, the Peak-to-Average Power Ratio (PAPR) will be studied to quantify the large dynamic range of the signal, which is a significant negative aspect of this technology.

1.3. Dissertation Outline

This first chapter consists in a general introduction to the technologies discussed in this dissertation. In particular, an overview is made on RoF networks and on OFDM technology application in electrical-based and optical-based technology.

The second chapter develops a number of topics in which a generic model for a wireless OFDM system is described in detail. The fundamental characteristics of this modulation technique are explained, and mathematical models that define the modulation, demodulation, synchronization and channel effects are introduced.

The third chapter discusses the use of OFDM technology in IEEE 802.11a wireless standard, as well as its application to optical networks. The expected channel effects are presented, focusing on the aspects of wireless channels and optical fiber, as Wireless RoF communication systems are affected by both. The main tools chosen for performance evaluation are also defined.

The fourth chapter is dedicated to the *Matlab* simulation of an OFDM system based on the parameters described in the IEEE 802.11a wireless standard. The previously introduced models are simulated to understand the effects of synchronization errors and dispersive multipath channels.

The fifth chapter exposes the procedures adopted to perform real transmissions using instruments. The experimental parameters and the instruments configuration are defined.

The sixth chapter consists in studying the influence of a wired RoF system on an OFDM signal. The system architecture is briefly described, and the OFDM signal acquired for different situations is analyzed.

The seventh chapter presents the general conclusion concerning the subjects approached and the results obtained in this thesis, as well as potential future work and development on this dissertation subject.

Chapter 2. Fundamentals on OFDM Systems

2.1. Introduction

This chapter introduces the theoretical background for wireless OFDM-based transmission systems, and different properties of OFDM technology.

First, a model for wireless transmission systems is presented. The use of schemes to prevent data loss and to correct erroneous bits resulting from transmission impairments is introduced. The importance of the Guard Interval (GI), the Cyclic Prefix (CP) and Windowing is also discussed. In addition, fundamental theory that defines OFDM technology, namely orthogonality and the use of Discrete Fourier Transform (DFT) to perform modulation is explained.

In order to understand OFDM technology, it is necessary to study the mathematical background that characterizes it. A detailed mathematical model is used to design OFDM symbols, and to define several steps of major importance in the transmission sequence. Namely, the modulation of OFDM symbols, the mathematical definition of a transmission affected by a multipath channel with additive white noise, the demodulation and the degradation brought on by time/frequency/phase offsets.

2.2. An Overview on OFDM Technology

The idea of using parallel-data transmission and multiplexing can be traced back to the 1950s, and was further explored in the 1960s [3]. The principles of OFDM technology emerged as an evolution of the conventional Frequency Division Multiplexing (FDM) systems [8]. In 1966, a first suggestion to make use of orthogonal frequencies for transmission was made in a patent by Chang of Bell Labs [5]. In 1980, the Cyclic Prefix was introduced, which has turned to be essential in most OFDM systems [5]. It was later in 1970 that OFDM technology was patented in the US. In 1971, Weinstein and Ebert introduced the DFT as part of the modulation and demodulation process for parallel-data systems [9]. It was only in the 1980s that OFDM was considered for high-speed modems and digital mobile communications [3]. In 1987, Lassalle and Alard pointed out the importance of Forward Error Correction (FEC) [5]. Finally, in the 1990s, OFDM technology was applied to wideband data communications over mobile radio FM channels, High-bit-rate Digital Subscriber Lines (HDSL), Asymmetric Digital Subscriber Lines (ADSL), Very-high-speed Digital Subscriber Lines (VDSL), Digital Audio Broadcasting (DAB), and High Definition Television (HDTV) terrestrial broadcasting [3]. Nowadays, OFDM systems are widely employed in diverse data delivery systems such as digital radio

and television, phone lines and different wireless networking systems [8]. It is only recently that OFDM technology was introduced to optical communication systems. Many theoretical and practical studies on its performance are currently in progress for a number of optical systems and fiber types, such as Single Mode Optical Fiber (SMF), Multimode Optical Fiber (MMF) and Plastic Optical Fiber (POF) [5].

In conventional single carrier transmission schemes, data symbols are modulated and placed over a carrier wave that occupies the entire available frequency spectrum [10]. Distinctively, OFDM scheme belongs to a broad class of Multi-Carrier Modulation (MCM) in which a high-rate data stream is split up into a set of low-rate substreams that share the available frequency spectrum space [3] [7]. Each SC contains previously modulated data using well-known modulation techniques such as Phase Shift Keying (PSK) or Quadrature Amplitude Modulation (QAM) [3] [11]. However, a fundamental characteristic distinguishes OFDM systems from other MCM systems: the particular spectral overlap resulting from the arrangement of the SCs. This overlap is made possible without any ICI due to the mathematical orthogonality existing between them. It allows the saving of a large amount of bandwidth compared to other parallel-data systems such as FDM, making this technology very bandwidth efficient [3].

Another important attribute of OFDM technology is that its SCs can be modulated and multiplexed using DFT algorithm [3]. This is possible because the DFT has orthogonality properties inherent to its very definition [8]. The use of DFT allows the OFDM modulation and demodulation to be entirely digitally implemented, consequently reducing drastically the complexity and cost of practical systems [3].

OFDM technology in the present days is widely used in telecommunication systems due to its natural immunity to interfering environments [12]. Conventional digital systems are not capable of operating well in multipath environment, where a receiver has to cope with a signal that is weak and contains many echoes and interferences [11]. On the contrary, OFDM is a technology capable of operating in adverse conditions that characterize multipath channels, where the signal is subject to high frequency attenuation, narrowband interferences and frequency-selective fading [12]. In fact, robustness against channel dispersion and simplicity for phase offsets and channel estimation are two fundamental advantages of this technology [7].

OFDM technology experiences two main drawbacks. The first one, usually referred to as Peak-to-Average Power Ratio (PAPR), consists in the large dynamic range of the signal. The second is its sensitivity to time and frequency synchronization errors [13].

2.3. OFDM Model for a Transmission System

The model depicted in Figure 2.1 illustrates the entire communication process of a typical wireless OFDM transmission system. At the transmitter, the data is coded using Forward Error Correction (FEC) code. FEC coding is an important aspect for the robustness of the system because the frequency-selective radio channel can severely attenuate the data symbols transmitted over the SCs, resulting in bit errors [3]. Typically, convolutional coding is used, and sometimes concatenation with Reed-Solomon coding. Frequency and/or time interleaving is also usually applied [12].

As the bit coding process is completed, the coded bits are mapped into symbols using Gray coding, which are then modulated into complex data constellations using conventional modulation schemes like Phase Shift Keying (PSK) and Quadrature Amplitude Modulation (QAM) [3]. Using Gray coding ensures that the bit pattern transmitted by adjacent constellation samples changes only by one bit. This way, when a constellation sample deviates into the location of an adjacent sample, Gray coding combined with FEC coding improves the error correction, making the system more resilient [12]. The resulting FD constellation samples are then allocated on the data SCs, on an OFDM symbol-by-symbol basis. In Figure 2.2, the modulated samples are first distributed from left to right on the first OFDM symbol, then again on the second, then on the next one, until all the samples are allocated.

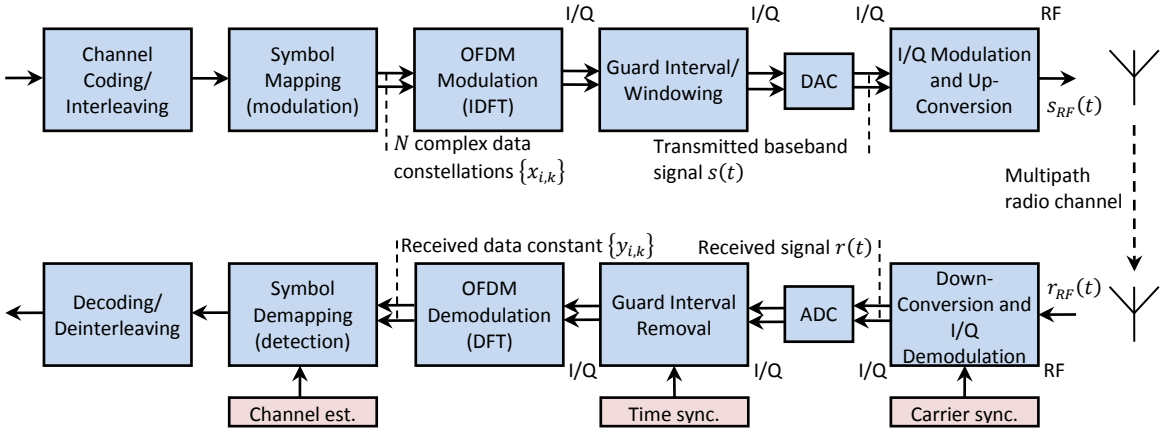

Figure 2.1 – Block diagram of a simple OFDM point-to-point transmission model [3].

Generally, in an OFDM system several types of SCs are used. The majority of them will contain modulated data samples, but some will also be pilot SCs used to perform channel estimation at the receiver. Usually a number of SCs remain empty as well, which in terms of FFT will result in "increased" sampling resolution, and also, by allowing the number of SCs to be a power of two, in higher computational efficiency [14]. However, there is a more practical motivation for this, which is the use of Low-Pass Filters (LPF) at the Analog-to-Digital Conversion (ADC) and Digital-to-Analog

Conversion (DAC) of the transmitted and received baseband signals. Figure 2.3 illustrates how the hardware Transfer Function (TF) of a communication system can affect its design. The SCs close to the Nyquist frequency $f_s/2$ will be attenuated by these filters, and therefore cannot be used for data transmission. The Direct Current (DC) SC might also suffer from serious distortions caused by DC offsets of the ADCs and DACs, and therefore should be avoided for data transmission [2] [3].

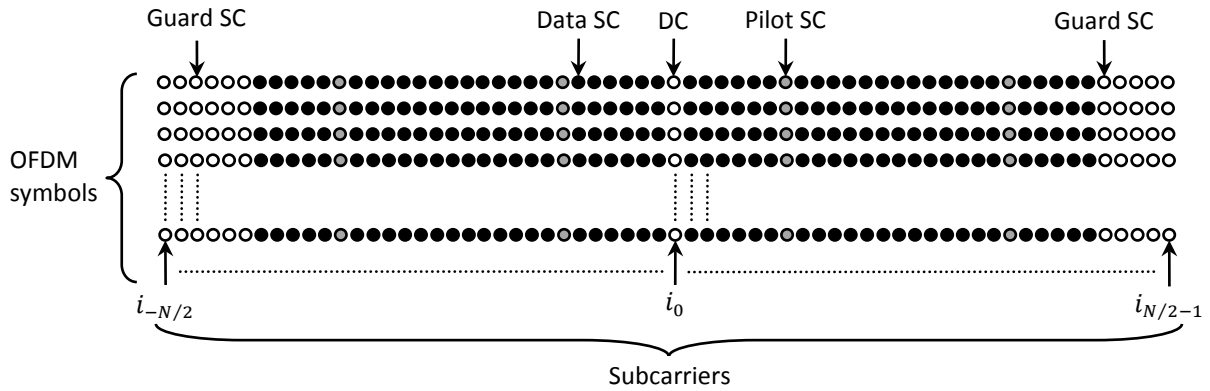

Figure 2.2 – SCs in parallel by column, OFDM symbols by row.

To generate Time Domain (TD) OFDM symbols, the Inverse Discrete Fourier Transform (IDFT) with predetermined length is applied to each set of data, which are composed by the modulated SCs. In other words, the PSK or QAM modulated source samples are the information in the Frequency Domain (FD) that is placed on SCs, and then converted and multiplexed into TD samples [8]. The IDFT block takes N data constellation points at a time, where N is the number of SCs in the system. In Figure 2.1, i is a SC index and k is an OFDM symbol index. Each chunk of N input symbols has a period of T seconds, depending on the channel spacing [3] [8]. The N output samples generated by the IDFT block compose the TD baseband signal that carries the data symbols. By applying the IDFT to generate the OFDM symbols, a set of orthogonal frequencies is applied to the SCs, and as the SCs spectrum overlap, high spectral efficiency is achieved. Due to the orthogonality property, the SCs do not influence each other [3].

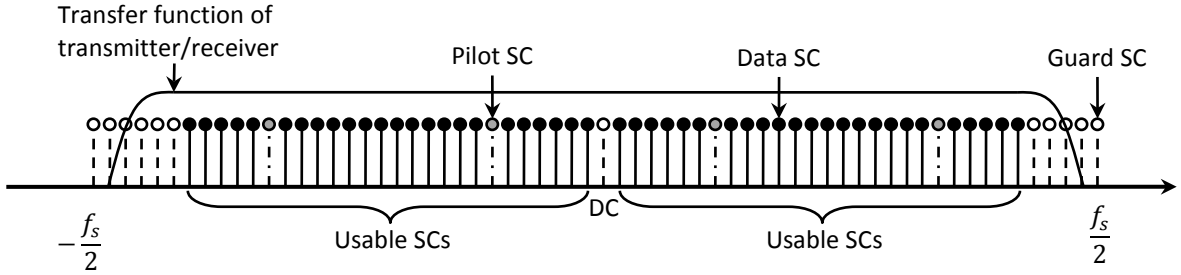

Figure 2.3 – Influence of the transmitter/receiver hardware transfer funtion on the design of an OFDM system [3].

In OFDM systems, the transmission data rate per SC is lowered, which means that the symbol duration is increased. This implies that the sensitivity of the system to frequency selective fading due

to multipath channel is greatly reduced [10]. The bandwidth occupied in OFDM systems is greater than the correlation bandwidth of the fading channel. This is an important advantage because this way multipath fading will degrade some of the carriers only, and the majority of the carriers will be properly received, even before using more data recovering schemes [11]. Additionally, a simple way of maintaining orthogonality over a dispersive channel is to introduce a Cyclic Prefix (CP) during the Guard Interval (GI) between adjacent OFDM symbols [3]. This fundamental mechanism creates the robustness to multipath reflective environments of OFDM technology.

In order to perform the real RF transmission, the generated OFDM complex baseband signals must be processed by an In-Phase/Quadrature (IQ) modulator and up-converted to be transmitted through an RF carrier. When designing an OFDM receiver, time and frequency synchronization must be the main concern to identify the start of an OFDM symbol and to align the local frequencies of the modulator/demodulator. Any failure to maintain synchronization results in partial loss of the SCs orthogonality. In other words, ISI and ICI are introduced [3].

2.3.1. The Concept of Orthogonality between Subcarriers

As introduced formerly, OFDM modulation technique can be seen as a special case of Frequency Division Multiplexing (FDM) modulation. In typical parallel-data systems similar to FDM, *N* non-overlapping frequency subchannels share the available frequency band, and each subchannel is modulated with a distinct symbol. A guard band is defined between each subchannel in order to avoid spectral overlap and eliminate ICI. Finally, the total subchannels are frequency multiplexed. Because this technology resulted into inefficient use of the available spectrum, the suggestion of using overlapping subchannels was explored in the 1960s [3]. This is one of the great improvements achieved in OFDM technology, reflected in the saving of nearly 50% of the bandwidth. However, to achieve this a fundamental mathematical property called “orthogonality” must exist between the frequencies of the SCs in order to avoid cross talk between them [3]. Figure 2.4 illustrates the difference between conventional non-overlapping multi-carrier techniques and orthogonal overlapping multi-carrier techniques.

Two function $\emptyset_i(t)$, $\emptyset_j(t)$ are orthogonal over a time period T if:

$$\int_0^T \emptyset_i(t)\emptyset_j(t)\,dt = \begin{cases} k, & (i = j) \\ 0, & (i \neq j) \end{cases}, \quad (k \neq 0) \tag{2.1}$$

In OFDM systems, the carriers are chosen to be in phase and to have frequencies that are multiple between each other. Therefore, integrating any two such carriers over one period $T = 1/f_0$ equals to zero [15].

$$\int_0^T cos(2\pi n f_o t) cos(2\pi m f_o t)\, dt = 0, \quad (n \neq m) \tag{2.2}$$

Where: n and m are two unequal integers; f_o is the fundamental frequency; T is the period over which the integral is taken.

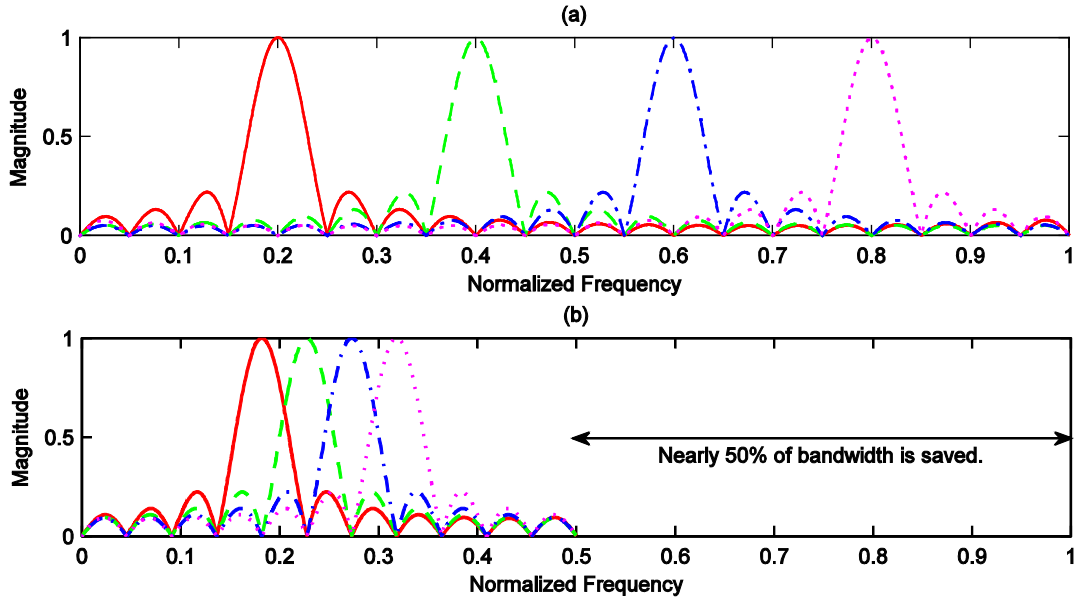

Figure 2.4 – MCM techniques in FDM. a) conventional; b) orthogonal [3].

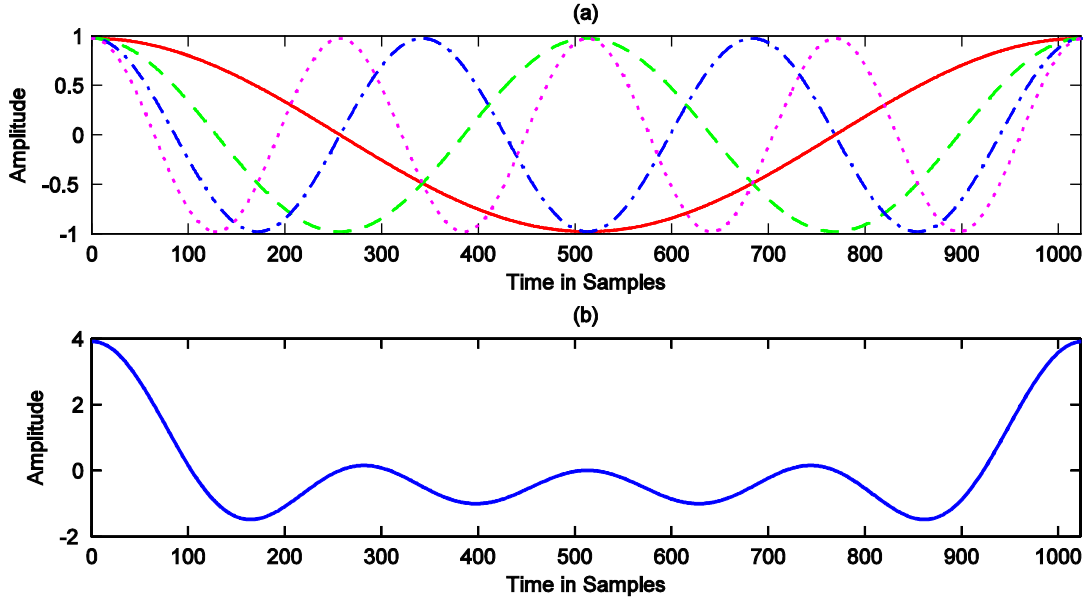

Figure 2.5 – a) Orthogonal SCs in TD [10]; b) their sum over the period.

In general, integer frequencies multiples are all orthogonal to each other, and are known as harmonics. In OFDM systems, the SCs are separated by multiples of $1/T$, thus guaranteeing that an integer number of cycles per period separates the SCs in one period [10] [15]. An example can be seen in Figure 2.5. Knowing that, it is easy to understand why the SCs being mathematically orthogonal imply that, when the receiver takes each carrier down to DC and integrates the signal

over a symbol period, if the other carriers have a whole number of cycles in the symbol period T, then the integration process results in zero contribution from all these other carriers.

Signals and systems theory is another way of understanding how orthogonality allows SCs to overlap without generating any interference. The sinusoids of a DFT are all orthogonal to each other, thus a signal in the vector space of a DFT can be acknowledged as a linear combination of the orthogonal sinusoids. For a certain frequency, if the input signal has energy, a peak will be in the correlation of the signal and the source sinusoid at that corresponding frequency. This means that by correlating the information as the DFT is performed for a particular SC, and because the root functions of the DFT are uncorrelated, only the energy for that particular SC can be seen [8].

2.3.2. Scrambling, Convolutional Coding and Interleaving

A scrambler consists in a device that randomizes data before transmission. In a telecommunication system, when transmitting information, long sequences of zeros or ones are likely to occur because the data does not follow a random distribution. The use of scrambling removes such sequences, which eases mechanisms such as synchronization and Automatic Gain Control (AGC) at the receiver [2] [16]. In addition, by dispersing the data, the resulting signal power spectrum is more likely to comply with maximum PSD requirements, as concentration of power in a narrow frequency band is avoided. It also improves the PAPR by reducing the probability of high peaks above the average to occur.

Convolutional coding is a FEC coding technique commonly used in wireless communication systems. This technique has become popular due to its good performance and flexibility in achieving different coding rates [17]. Convolutional coding involves introducing information redundancy at the transmitter, therefore increasing the bit stream at an extent depending on the coding rate. At the receiver, the redundant information is then used to detect and correct bit errors [3] [17].

Interleaving consists in reordering adjacent symbols before transmission, which prevents burst errors by making them appear as random errors [17]. Transmission errors generally have a strong time/frequency correlation. By providing diversity, interleaving plays a crucial task in channel coding as it breaks that correlation, thus enabling the decoder to eliminate or reduce fading all over the band and over the whole interleaving depth [11].

Frequency interleaving takes advantage of the frequency diversity in wide-band transmissions by averaging local deep fading over the whole bandwidth of the system [17]. In OFDM systems, frequency interleaving should be implemented for all the data symbols in a single OFDM

symbol, which means that the depth of the frequency interleaver should equal the number of bits per OFDM symbol [2] [17].

Time interleaving uses the time diversity of the channel to average local time deep fading in some OFDM symbols over all OFDM symbols. Its depth should exceed the maximum TD burst error. Time interleaving is not used in WLAN transmissions due to the slow fading characteristics of the channel [17].

Data distribution in OFDM systems is made over multiple SCs, and it is unlikely that all the SCs will suffer distortions over a transmission, which means that the selective fading will cause some information bits to be received with errors, and others correctly. This assumption can be made because in OFDM technology a conversion occurs from the wideband frequency-selective channel into a series of narrowband and frequency-non-selective fading subchannels. Convolutional coding and time/frequency interleaving are crucial mechanisms that take advantage of this property to prevent loss of information [11]. In WLAN systems, both convolutional coding and frequency interleaving are used. In this way, if some information degrades over one SC, it is recoverable by using related information extracted from another SC, thereby exploiting the wideband channel's frequency diversity. OFDM systems implemented with error correction coding schemes are usually referred to as Coded OFDM (COFDM) [3] [11].

2.3.3. OFDM Modulation/Demodulation using IFFT/FFT Algorithm

In terms of practical implementation, for a large number of channels, the arrays of sinusoidal generators and coherent demodulators required grow to be unduly expensive and complex. It was shown, however, that a multitone data signal corresponds to the Inverse Fourier Transform of the original serial data stream, and that the coherent demodulator is effectively a Fourier Transform generator [9].

Using special purpose hardware to perform the FFT, entirely digital implementation can now be accomplished, replacing the bank of SC oscillators and coherent demodulators [3]. A demonstration is available in Appendix A that shows how OFDM modulation and multiplexing are performed using the Fourier Transform.

2.3.4. The Importance of the Guard Interval and the Cyclic Prefix

Most wireless systems undergo multipath environments and RF signal reflection on several kinds of objects, resulting in frequency fading phenomenon, which translates in ISI and ICI. These reflecting effects lead the receiver to detect multiple versions of the signal, with different delays and attenuation factors [8] [18].

A solution to this problem resides in creating a GI between the transmitted OFDM symbols. If the GI has greater length than the time span of the channel, it is enough for the ISI distortion to occur only over the first few samples, thus affecting no more than the GI itself preceding the OFDM symbol [8] [19]. Therefore, to be effective the GI must have a length that surpass the maximum delay τ_{max} of the multipath propagation channel. At the receiver, the GI can simply be discarded as it contains no useful information [3] [15].

However, in a practical system a GI composed just by empty samples does not prevent OFDM symbols from interfering with themselves [8]. To solve this issue the cyclic prefix/postfix was introduced and has become a fundamental principle of OFDM systems. Creating the CP consists in taking a copy of a number of samples from the tail of an OFDM symbol, and to insert them at its head during the GI between consecutive OFDM symbols. By doing so, the transmitted signal becomes periodic, thus turning the time-dispersive effect of the multipath channel equivalent to a cyclic convolution. Cyclic convolution properties dictate that the effect of multipath channel is limited to a point-wise multiplication of the transmitted data constellations by the TF of the Channel Impulse Response (CIR). This means that the SCs remain orthogonal as long as the time deviation introduced by the channel is lower that the GI duration [3] [20]. Figure 2.6 illustrates that as long as the starting sample is chosen according to the criteria $\tau_{max} < T_x < T_{GI}$, the contributions from all the multipath components influence all the samples. Hence, all the acquired samples undergo the same channel and ICI is prevented [20].

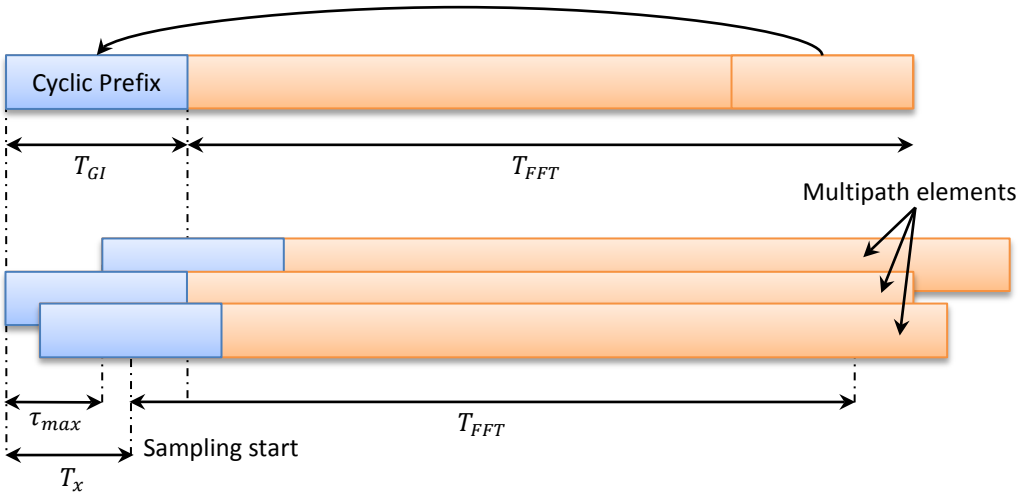

Figure 2.6 – Generating a Cyclic Prefix [21].

To detect the data constellation, the inverse of the estimated channel TF is multiplied element-wise to the DFT output. For phase modulation schemes, multiplying by the complex conjugate of the channel estimation can perform the equalization. Additionally, differential detection can be used, where the symbol constellation of adjacent SCs are compared to recover the data [3].

The disadvantage that comes with this solution dwells in the slight loss of effective transmitted power due to GI transmission, and in an increased use of bandwidth. Typically the GI length is about a quarter of the OFDM symbol period to a tenth, leading to a Signal-to-Noise Ratio (SNR) loss of 0.5 dB to 1 dB [3] [15].

2.3.5. Pulse Shaping and Windowing applied to OFDM Systems

In any data transmission systems, the main objective is to use a transmitter to send data, and a receiver to detect the incoming data. Pulse shaping consists in transmitting this data in a way that, at the receiver, the signal can be sampled at an optimal point in the pulses interval, thus allowing maximum probability of an accurate decision. In order to achieve this, the fundamental shape of the pulses must be designed to guarantee that they do not interfere with one another at the optimal sampling point. Two basic conditions define a proper pulse shape that ensures non-interference. The first is that the shaped pulses must show a zero crossing at the sampling point, and the second is that the amplitude of each pulse must drop rapidly outside the pulse interval. These conditions are important because any real system will contain timing jitter, which may cause the optimal sampling point to move and miss the zero crossing point [22]. Another important purpose of pulse shaping is the limitation of the occupied bandwidth by smoothing the transitions between symbols [23].

The rectangular pulse meets the criteria introduced above, but occupies a very large bandwidth due to its Fourier Transform being the familiar $sinc(x) = sin(\pi x)/\pi x$, which has side lobes repeating to infinity. This is why for band-limited data transmission the rectangular pulse shape is not the ideal choice [3] [22]. A solution to this problem dwells in the use of windowing. Windowing is a well-known technique to reduce the level of these side lobes, thereby reducing the signal power transmitted out of band [3].

A wide variety of modern data transmission schemes use raised-cosine function as a filter to put into practice this windowing. Consider a raised-cosine shape with pulse width τ seconds. The shape of the raised-cosine filter is precisely defined by the parameter α. This parameter varies in $0 < \alpha < 1$, and rules the occupied bandwidth and the rate at which the pulse decays. When $\alpha = 0$, the narrowest bandwidth is obtained. When $\alpha = 1$, the bandwidth used is $1/\tau$, but the TD shape descends rapidly, offering a double-sided bandwidth of $2/\tau$ that matches the main lobe of a rectangular pulse shape. In other words, a larger value of α will result in using more bandwidth, but reduces the susceptibility to jitter. Therefore, the parameter α offers the system designer some flexibility by allowing a trade-off between increased data rate and TD tail suppression [22].

In OFDM systems, pulse shaping is achieved on the entire OFDM symbols, by windowing the transitions between symbols. When consecutives OFDM symbols are assembled, the end of one

symbol has rarely the same amplitude and phase as the following one, which causes spectral regrowth. Spectral regrowth consists of a range of frequencies that expend on each side of a carrier and extends into adjacent frequency bands, consequently creating interferences. One way to reduce or remove this effect is to introduce windowing and cyclic suffix (also referred to as postfix) into the OFDM model. By combining windowing with the cyclic suffix, a smooth transition can be achieved between consecutive symbols, thus avoiding spectral regrowth. However, due to the decreased redundancy caused by the effective GI length reduction, part of the multipath immunity is lost in this process [23] [24].

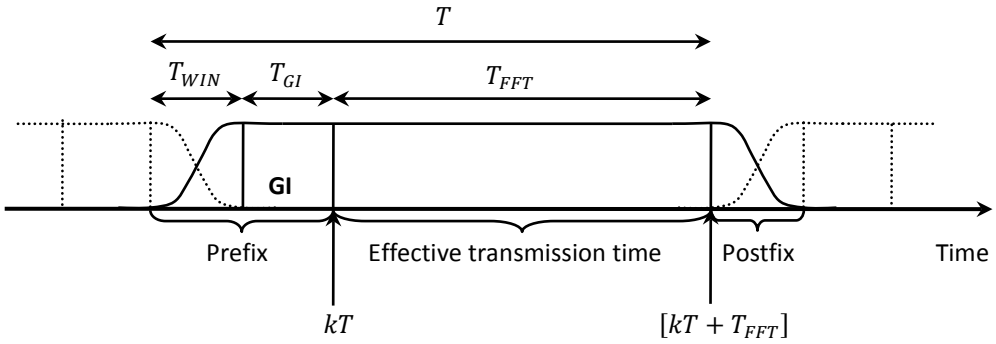

Figure 2.7 – Applying a window to an OFDM symbol [3].

Raised-cosine function applied to an OFDM systems can be seen as a convolution of the extended rectangular pulse of duration T with a sine half-wave. It is important to make sure that the applied window will not influence the signal during its effective period. Hence, the window is applied to part of the existing CP and to a generated cyclic postfix with the length of the cosine shape at the rightmost edge of the symbol. The extended parts used for prefix and postfix are shaped as depicted in Figure 2.7. On the other hand, to maintain the efficiency in bandwidth occupancy, it is important to have minimal non-data samples in each OFDM symbol. That is why the number of samples of the OFDM symbols is preserved by summing the windowed samples from the end of each symbol to the windowed samples at the beginning of the following symbol [3] [24]. The DFT at the receiver implements a rectangular filter that, after estimating correctly the DFT start time kT, restores the orthogonality of the SCs [3].

2.4. Mathematical Characterization

2.4.1. OFDM Modulation

Mathematically, an OFDM signal can be expressed as a sum of the SCs pulses shifted in time and frequency, and multiplied by the data symbols. Ramjee Prasad [3] presents a continuous-time mathematical notation of the kth OFDM symbol written as the following approach:

$$S_{RF,k}(t-kT) = \begin{cases} Re\left\{ w(t-kT) \sum_{i=-N/2}^{N/2-1} x_{i,k} e^{j2\pi\left(f_c+\frac{i}{T_{FFT}}\right)(t-kT)} \right\}, & kT - T_{WIN} - T_{GI} \le t \le kT + T_{FFT} + T_{WIN} \\ 0, & otherwise \end{cases} \quad (2.3)$$

Where each symbol is defined as:

T	Symbol time - the total OFDM symbol time
T_{FFT}	FFT time - the effective OFDM symbol time
T_{GI}	GI time - the CP duration
T_{WIN}	Window time - the windowed prefix/postfix duration for spectral shaping
f_c	Center frequency of the occupied frequency spectrum
N	FFT length - the number of FFT points
k	Index of the transmitted OFDM symbol
i	Index of the SC, where $i \in \{-N/2, \dots, -1, 0, 1, \dots, N/2-1\}$
$x_{i,k}$	Signal constellation point (data, pilot or null) of the ith SC of the kth OFDM symbol

From the information above, the frequency spacing between each adjacent SC can be calculated as $\Delta F = 1/T_{FFT}$. The sampling period can also be computed as $T_s = 1/(N \times \Delta F)$. In addition, a transmitter pulse shape can be defined as:

$$w(t) = \begin{cases} \frac{1}{2}[1 - cos\pi(t + T_{WIN} + T_{GI})/T_{WIN}], & -T_{WIN} - T_{GI} \le t \le -T_{GI} \\ 1, & -T_{GI} \le t \le T_{FFT} \\ 1 - \frac{1}{2}[1 - cos\pi(t - T_{FFT})/T_{WIN}], & T_{FFT} \le t \le T_{FFT} + T_{WIN} \end{cases} \quad (2.4)$$

Based on this notation, a continuous sequence of modulated OFDM symbols is expressed as the following:

$$s_{RF}(t) = \sum_{k=-\infty}^{\infty} S_{RF,k}(t-kT) \quad (2.5)$$

Now, based on the equations above the complex envelope of the OFDM signal is given directly by writing the low-pass equivalent transmitted signal [3]:

$$s(t) = \sum_{k=-\infty}^{\infty} S_k(t-kT) \quad (2.6)$$

$$s_k(t-kT) = \begin{cases} w(t-kT)\sum_{i=-\frac{N}{2}}^{\frac{N}{2}-1} x_{i,k} e^{j2\pi\left(\frac{i}{T_{FFT}}\right)(t-kT)}, & kT - T_{WIN} - T_{GI} \le t \le kT + T_{FFT} + T_{WIN} \\ 0, & otherwise \end{cases} \quad (2.7)$$

By comparing the equation above to the equation below of a Fourier Series, similarities can be observed [3]:

$$v(t) = \sum_{n=-\infty}^{\infty} c(nf_o) e^{j2\pi f_o t} \quad (2.8)$$

Where the following relations stand out: the complex Fourier Coefficients $c(nf_o)$ correspond to the complex signal constellation points $x_{i,k}$ in the FD; the frequencies nf_o correspond to the SC frequencies i/T_{FFT}; $v(t)$ is the modulated OFDM waveform in TD. In a digital implementation of the OFDM modulation, the data constellation samples $c(nf_o) = x_{i,k}$ are the input of the IFFT block, and the OFDM modulated TD symbols come at the output.

2.4.2. OFDM Signal over a Time-Dispersive Channel

At the receiver, the OFDM signal is expected to have suffered the influence of a time-dispersive channel and Additive White Gaussian Noise (AWGN). The Channel Impulse Response (CIR) is designated as $h(\tau, t)$ [3]:

$$r(t) = h(\tau, t) * s(t) + n(t) = \int_0^{\tau_{max}} h(\tau, t) s(t-\tau)\, d\tau + n(t) \quad (2.9)$$

Where: $r(t)$ is the received degraded signal; $h(\tau, t)$ is the CIR; $s(t)$ is the original transmitted signal; $n(t)$ is the added random noise; τ is the excess delay.

Outside the boundary $[0, \tau_{max}]$ the CIR is zero, hence the range of the convolutional integration is confined within this limit. The time at which the first waveform arrives at the receiver defines the excess delay $\tau = 0$ of the channel, and τ_{max} is the maximum delay of the channel. To simplify the derivation of the received signal, two assumption are made: the channel is considered to be nearly static during the transmission of the OFDM symbol k; the maximum excess delay $\tau_{max} < T_{GI}$. Thereby, $h(\tau, t)$ simplifies to $h_k(\tau)$, and there is no interference of one OFDM symbol onto the effective period of the consecutive one. With the last assumption, ISI is avoided in case of sufficiently accurate time synchronization [3].

2.4.3. OFDM Demodulation

Conceptually, the demodulation of the OFDM signal is performed by a set of filters matched to the effective part $[kT, kT + T_{FFT}]$ of the OFDM symbol, as shown in Figure 2.7. In other words, the OFDM demodulation is performed by extracting back the Fourier Coefficients from the TD OFDM signal [3]:

$$c(nf_o) = \frac{1}{T_o} \int_{T_o} v(t) e^{-j2\pi f_o t}\, dt \tag{2.10}$$

Where: T_o is the integration period equivalent to T_{FFT}; $v(t)$ is the received baseband signal; $c(nf_o)$ are the recovered Fourier coefficients. In a digital implementation of the OFDM demodulation, the TD symbols are the input of the inverse operation, which is the FFT algorithm, and the recovered FD data samples $y_{i,k} = c(nf_o)$ come at the output.

After determining the exact instant kT at which the OFDM symbols starts, the transmitted constellation is extracted from the received signal $r(t)$ as the received constellation $y_{i,k}$ by integrating [3]:

$$\begin{aligned} y_{i,k} &= \frac{1}{T_{FFT}} \int_{t=kT}^{kT+T_{FFT}} r(t) e^{-j2\pi \frac{i}{T_{FFT}}(t-kT)}\, dt \\ &= \frac{1}{T_{FFT}} \int_{t=kT}^{kT+T_{FFT}} \left[\int_{\tau=0}^{\tau_{max}} h_k(\tau) s(t-\tau)\, d\tau + n(t) \right] e^{-j2\pi \frac{i}{T_{FFT}}(t-kT)}\, dt \end{aligned} \tag{2.11}$$

Due to the assumption made previously, it is known that there is no influence from contiguous OFDM symbols. Hence, $s(t)$ can be replaced by $s_k(t)$:

$$\begin{aligned} y_{i,k} = \frac{1}{T_{FFT}} &\int_{t=kT}^{kT+T_{FFT}} \left[\int_{\tau=0}^{\tau_{max}} h_k(\tau) \sum_{i'=-N/2}^{N/2-1} x_{i',k} e^{j2\pi \frac{i'}{T_{FFT}}(t-kT-\tau)}\, d\tau \right] e^{-j2\pi \frac{i}{T_{FFT}}(t-kT)}\, dt \\ &+ \frac{1}{T_{FFT}} \int_{t=kT}^{kT+T_{FFT}} n(t) e^{-j2\pi \frac{i}{T_{FFT}}(t-kT)} \end{aligned} \tag{2.12}$$

In the equation above, the integration is performed in the range where the window is $w(t - kT) = 1$. Hence, the window segment of the equation is ignored. At this point, the expression can be simplified for further solving by introducing $u = t - kT$ [3]:

$$y_{i,k} = \sum_{i'=-N/2}^{N/2-1} x_{i',k} \frac{1}{T_{FFT}} \int_{u=0}^{T_{FFT}} \left[\int_{\tau=0}^{\tau_{max}} h_k(\tau) e^{-j2\pi \frac{i'}{T_{FFT}}(u-\tau)} d\tau \right] e^{-j2\pi \frac{i}{T_{FFT}}u} du + n_{i,k}$$
$$= \sum_{i'=-N/2}^{N/2-1} x_{i',k} \frac{1}{T_{FFT}} \int_{u=0}^{T_{FFT}} \left[\int_{\tau=0}^{\tau_{max}} h_k(\tau) e^{-j2\pi \frac{i'}{T_{FFT}}\tau} d\tau \right] e^{-j2\pi \frac{i-i'}{T_{FFT}}u} du + n_{i,k} \quad (2.13)$$

The inmost integral of the last expression in the equation above describes the Fourier Transform of $h_k(\tau)$ at the frequency instant $i'/T_{FFT} = i'\Delta F$, which corresponds to the sampled channel TF at instant kT. Hence, the channel coefficients are as follows [3]:

$$h_{i',k} = FT\{h_k(\tau)\} = \int_{\tau=0}^{\tau_{max}} h_k(\tau) e^{-j2\pi \frac{i'}{T_{FFT}}\tau} d\tau = H(i'\Delta F, kT) \quad (2.14)$$

Based on this notation, the output of the receiver filter, which is the FFT in a digital implementation, is shortened into the following expression:

$$y_{i,k} = \sum_{i'=-N/2}^{N/2-1} x_{i',k} h_{i',k} \frac{1}{T_{FFT}} \int_{u=0}^{T_{FFT}} e^{-j2\pi \frac{i-i'}{T_{FFT}}u} du + n_{i,k} \quad (2.15)$$

By solving the integral in the equation above, if $i = i'$ the result is one. Otherwise, the integral becomes zero. Hence, the final expression is [3]:

$$y_{i,k} = x_{i,k} h_{i,k} + n_{i,k} \quad (2.16)$$

With this expression, considering the assumptions introduced formerly, the received constellation $y_{i,k}$ describes the received constellation with the effect of a multipath channel and random noise $n_{i,k}$. The multipath channel introduces attenuation/amplification and phase rotation according to the complex-valued channel coefficients $h_{i,k}$.

2.4.4. Relating the OFDM Subcarriers to the Noise

To retrieve correctly the data from the constellation, it is necessary to estimate the channel and compensate the phase and amplitude deviations. There are several ways to estimate the channel. One technique is based on transmitting a preamble made of a specific sequence known by the receiver, which is used to estimate the channel TF coefficients. Another technique is the differential detection, where the phases and amplitudes of symbols transmitted over neighboring SCs or succeeding OFDM symbols are compared [3].

Ideally, the SCs of an OFDM systems can be thought of as parallel Gaussian channels. This statement remains true under perfect time and carrier synchronization, and assuming that multipath

channel effects are subdued by the GI. Hence, each SC has an individual Signal-to-Noise Ratio (SNR) due to the attenuation/amplification of the OFDM signal. The SNR per SC is defined as [3]:

$$\left(\frac{E_c}{N_o}\right)_{i,k} = \frac{E\left\{\left|x_{i,k}\right|^2\right\}\left|h_{i,k}\right|^2}{\sigma_N^2} \tag{2.17}$$

Where: $\sigma_N^2 = E\left\{\left|n_{i,k}\right|^2\right\}$ is the noise variance; k is the index of the transmitted OFDM symbol; i is the index of the SC, where $i \in \{-N/2, \dots, -1, 0, 1, \dots, N/2-1\}$.

The normalized received power is expressed as $P_o = E\left\{\left|h_{i,k}\right|^2\right\}$. Hence, the averaged SNR becomes:

$$\overline{\left(\frac{E_c}{N_o}\right)} = \frac{E\left\{\left|x_{i,k}\right|^2\right\}P_o}{\sigma_N^2} \tag{2.18}$$

Usually, the signal energy is normalized to unity, therefore becoming $E\left\{\left|x_{i,k}\right|^2\right\} = 1$.

2.4.5. Time Synchronization Errors

Timing offset can be linked to the starting sample of the FFT at the receiver, but also to sampling frequency offsets. A small sampling frequency offset leads to a gradually increasing timing offset and, consequently, to a growing phase rotation at an increasing slope. Larger inaccuracies provoke ICI because the SC spacing at the receiver no longer equals the SC spacing at the transmitter. The effect of an FFT timing offset δt at the receiver can be observed by shifting the integration interval of Equation (2.11), which becomes $t \in [kT + \delta t, kT + T_{FFT} + \delta t]$ [3]:

$$y_{i,k} = \frac{1}{T_{FFT}} \int_{t=kT+\delta t}^{kT+T_{FFT}+\delta t} r(t) e^{-j2\pi \frac{i}{T_{FFT}}(t-kT-\delta t)}\, dt \tag{2.19}$$

δt is assumed to be small enough not to create ISI due to the timing error. That is, the offset is small enough for the CIR to remain within the GI. Hence, the receiver window does not overlap with the preceding or with the following OFDM symbol. Thereby, no energy from the adjacent symbols is introduced, and the demodulated signal can still be expressed from the transmitted symbol $s_k(t)$. By making again the change $u = t - kT - \delta t$, the following expression is obtained just as in the previous section [3]:

$$y_{i,k} = \sum_{i'=-N/2}^{N/2-1} x_{i',k} \frac{1}{T_{FFT}} \int_{u=0}^{T_{FFT}} \left[\int_{\tau=0}^{\tau_{max}} h_k(\tau) e^{-j2\pi \frac{i'}{T_{FFT}}\tau}\, d\tau \right] e^{-j2\pi \frac{(i-i')u + i'\delta t}{T_{FFT}}}\, du + n_{i,k} \tag{2.20}$$

By moving the term $e^{-j2\pi \frac{i'\delta t}{T_{FFT}}}$ out of the integration, the expression that define the received constellation including a timing error is obtained [3]:

$$y_{i,k} = x_{i,k} h_{i,k} e^{-j2\pi \frac{i' \delta t}{T_{FFT}}} + n_{i,k} = x_{i,k} h_{i,k} e^{-j2\pi \frac{i \delta t'}{N}} + n_{i,k} \quad (2.21)$$

Where: $\delta t'$ is the timing offset in samples. It can now be concluded that the timing offset produces a phase rotation of the signal constellation, with the phase rotation being null at the center frequency and increasing linearly towards the edges of the frequency band. In addition, it can be deduced from the equation above that a timing offset in one sample results in a phase shift of $\pm\pi$ in the farthest SCs, with the FFT length making no difference [3].

When coherent detection is used, the phase rotation is detected with channel estimation. The equalization is performed at the receiver by a SC-wise multiplication of the received symbols by the inverse of the estimated channel coefficients. This way, small timing errors can be corrected, thus avoiding performance degradation. Nevertheless, if the timing offset δt exceeds the GI duration, ISI and ICI are introduced. That is, energy is added from an adjacent OFDM symbol, leading to a partial loss of orthogonality [3].

When differential detection is used, the progressive phase rotation detection is performed by comparing the phases and amplitudes of symbols transmitted over neighboring SCs or succeeding OFDM symbols. However, if the detection follows the frequency direction, the distance between the compared constellation points is reduced, which can cause performance degradation [3].

2.4.6. Frequency Synchronization Errors

Frequency offsets usually consist in a small deviation of the local oscillators at the transmitter and at the receiver. Another source of frequency change to consider is the Doppler shift. Doppler shifts are insignificant for fixed position stations and can be ignored in indoor environments, but will affect the link quality otherwise [3] [25].

The frequency error can be considered as errors at the frequency instants at which the signal is demodulated with the FFT. The frequency offset can be described mathematically as a frequency shift δf and a phase offset θ in the baseband signal [3]:

$$r'(t) = r(t) e^{j(2\pi \delta f t + \theta)} \quad (2.22)$$

By applying this notation as previously in Equation (2.11), this expression for the received constellations is obtained:

$$y_{i,k} = \frac{1}{T_{FFT}} \int_{t=kT}^{kT+T_{FFT}} r(t) e^{j(2\pi\delta f t+\theta)} e^{-j2\pi\frac{i}{T_{FFT}}(t-kT)}\, dt$$
$$= e^{j2\pi\theta} \frac{1}{T_{FFT}} \int_{t=kT}^{kT+T_{FFT}} \left[\int_{\tau=0}^{\tau_{max}} h_k(\tau) s(t-\tau)\, d\tau + n(t) \right] e^{j2\pi\delta f t} e^{-j2\pi\frac{i}{T_{FFT}}(t-kT)}\, dt \quad (2.23)$$

Following the same steps that led from Equation (2.11) to Equation (2.15), the equation develops into:

$$y_{i,k} = e^{j(2\pi\delta f kT+\theta)} \sum_{i'=-N/2}^{N/2-1} x_{i',k} h_{i',k} \frac{1}{T_{FFT}} \int_{u=0}^{T_{FFT}} e^{-j2\pi\left(\frac{i-i'}{T_{FFT}}-\delta f\right)u}\, du + n_{i,k} \quad (2.24)$$

The integral does not equal zero for $i = i'$ and neither for $i \neq i'$ in the presence of frequency error. Hence, orthogonality between SCs is lost to a certain extent. Two conditions come from this expression: for $i = i'$, an equal phase rotation and attenuation of the SCs is expected. For $i \neq i'$, ICI is introduced [3].

$$y_{i,k} = e^{j(2\pi\delta f kT+\theta)} x_{i,k} h_{i,k} \frac{1}{T_{FFT}} \int_{u=0}^{T_{FFT}} e^{-j2\pi\delta f u}$$
$$+ e^{j(2\pi\delta f kT+\theta)} \sum_{i'=-N/2}^{N/2-1} x_{i',k} h_{i',k} \frac{1}{T_{FFT}} \int_{u=0}^{T_{FFT}} e^{-j2\pi\left(\frac{i-i'}{T_{FFT}}-\delta f\right)u}\, du + n_{i,k} \quad (2.25)$$

As long as the condition $\delta f < 0.5\, SC\ spacing$ is complied with, the previous mathematical expressions are valid. Otherwise, for larger frequency offsets the transmitted data symbols $x_{i,k}$ are shifted by one or more positions in the frequency direction, which means that the ith SC appears as the $(i + \delta f_i)$th to the receiver, where $\delta f_i = round(\delta f / \Delta F)$ is the integer part of the frequency error in SCs [3].

The ICI component can be considered as a noise for small values in relation to the SC spacing, which means that it only translates into SNR degradation. Studies have shown that frequency offset δf of up to 2% of the SC spacing ΔF are insignificant, and acceptable for up to 10% in some cases. The following expression describes the evaluation of the phase rotation and attenuation due to a frequency error [3]:

$$y_{i,k} = x_{i,k} h_{i,k} sinc(\delta f T_{FFT}) e^{j(2\pi\delta f(kT+T_{FFT}/2)+\theta)} + n'_{i,k} \quad (2.26)$$

With:

$$\frac{1}{T_{FFT}}\int_{t=0}^{T_{FFT}} e^{j2\pi\delta f t}\,dt = \frac{1}{j2\pi\delta f T_{FFT}}\left[e^{j2\pi\delta T_{FFT}} - 1\right] = e^{j2\pi\delta T_{FFT}}\frac{sin(\pi\delta f T_{FFT})}{\pi\delta f T_{FFT}} = e^{j2\pi\delta f_{FFT}} sinc(\delta f_{FFT}) \quad (2.27)$$

Where: $n'_{i,k}$ is the noise term that includes the additional noise from ICI.

2.4.7. Time and Frequency Synchronization Errors

Taking into account the time offsets δt, the frequency offsets δf and the phase offsets θ, the model for general cases appears as follows [3]:

$$y_{i+\delta f_{i,k}} = x_{i,k} h_{i,k} sinc[(\delta f - \delta f_i \Delta F)T_{FFT}] e^{j\Psi_{i,k}} + n'_{i,k} \quad (2.28)$$

Where: $n'_{i,k}$ is the noise including the additional ICI; $\Psi_{i,k}$ is the phase distortion due to synchronization errors given by:

$$\Psi_{i,k} = \theta + 2\pi\delta f\left(kT + \frac{T_{FFT}}{2} + \delta t\right) + 2\pi\delta t\frac{i}{T_{FFT}} \quad (2.29)$$

It is common practice to designate the timing offset in samples, where $\delta t' = t/T_s$, and to normalize the frequency offset to the SC frequency spacing with $\delta f' = \delta f/\Delta F$. Thus, in terms of samples, Equation (2.29) can be rewritten as:

$$\Psi_{i,k} = \theta + 2\pi\delta f'\left(\frac{1}{2} + k\frac{N + N_{GI} + N_{WIN}}{N} + \frac{\delta t'}{N}\right) + 2\pi\delta t'\frac{i}{N} \quad (2.30)$$

2.5. Main Advantages of OFDM Technology

Spectral Efficiency - In OFDM technology, the spectrums of the SCs with orthogonal frequencies overlap without influencing each other. For a high number of SCs, the frequency spectrum becomes nearly rectangular, thus resulting in a high spectral efficiency [3] [26].

Digital Implementation - Simple digital implementation is possible by using the efficient and powerful FFT algorithm to perform modulation and demodulation of OFDM symbols, thus reducing the complexity and cost of OFDM systems [3] [26].

Adaptive Data Modulation - Different conventional data modulation schemes can be employed for each individual SC, such as MPSK or MQAM. This provides flexibility in the choice of data transmission volume per SC by squeezing more or less bits in the same bandwidth, and therefore control on the overall data transmission rate per OFDM symbols. In addition, when the channel has

slow variation in time, its capacity can be improved by adapting the data rate per SC according to the SNR of the SC [3] [22].

Resistance to Narrowband Interferences - In a single carrier system, a single interference can lead the whole connection to fail. In contrast, in a multi-carrier system only a small percentage of the SCs will be affected. For this reason, OFDM systems have strong natural resistance to narrowband interferences [3].

Resilience to Multipath Surroundings - In OFDM systems, very high data rates are converted into very low parallel-data rates, thus ensuring flat fading for all the subchannels because a wideband signal becomes a set of narrowband signals. Therefore, it is an efficient way to deal with multipath since no equalizer is needed at the receiver, thus reducing the complexity of the communication system. This resilience to frequency-selective fading channels by using multi-carrier techniques makes it ideal for high-speed data transmission [3].

2.6. Important Drawbacks of OFDM Technology

Spectral Efficiency Loss due to the GI - The GI consists in transmitting redundant samples copied from the end of an OFDM symbol to its beginning, in order to emulate periodicity. Although this provides the essential additional robustness against delays from multipath fading environments, it also results in spectral efficiency loss because the redundant samples use bandwidth and power during the transmission, and then they are discarded at the receiver. Therefore, when defining the OFDM model parameters, there is a trade-off to be found between Doppler and phase noise effects and the loss due to GI [3] [26].

Sensitivity to Doppler Spreads - Doppler spreads consist in very fast channel variations, resulting in changes in the phases of the arriving waves that lead to time-variant multipath propagation. Hence, Doppler spreads causes loss of orthogonality between SCs, therefore introducing ICI [3] [26].

Vulnerability to Time/Frequency Errors - Accurate frequency and time synchronization are critical in OFDM systems, as they are extremely sensitive to frequency offset and to phase noise. Without time synchronization, ISI is introduced, and with no frequency synchronization, ICI is introduced [3].

The PAPR Problem - The PAPR, or crest factor, is a measurement calculated from the peak amplitude of a waveform that is divided by the Root Mean Square (RMS) value of that waveform. When N signals are summed coherently with the same phase, peak power is produced with N times the average power [3]. MCM systems using OFDM technology are more sensitive to High Power Amplifier

(HPA) non-linearities than single-carrier modulated systems [26]. OFDM systems in particular tend to have large values of PAPR, which involve disadvantages such as increased complexity of the ADC and DAC converters, and strong reduction of the power efficiency of the RF power amplifier [3].

2.7. Summary

In this chapter, a description of a generic model for a wireless OFDM system was presented. Some of the fundamental aspects of this technology were further developed, and a mathematical model was introduced. The main advantages and drawbacks of this technology were uncovered.

OFDM modulation is an excellent choice as a communication technology. OFDM systems are rather simple and inexpensive to implement, as they can be digitally modulated and demodulated using FFT algorithm, which makes them very practical. In addition, the FFT also performs multiplexing over a number of SCs with overlapping spectrums while producing orthogonality between them. Hence, OFDM is a MCM system with much lower bandwidth occupancy when compared to others for the same data rate. By using simple mechanisms, high robustness against multipath, frequency-selective fading environment is achieved. Because the SCs can be modulated with different data modulation schemes, adaptive data transmission rate is made possible. Finally, the receiver for an OFDM system is easier to implement, as no complex equalization is necessary to recover the signal.

The main drawbacks of this technology are its high sensitivity to time and frequency synchronization errors, and Doppler spreads, because they result in loss of orthogonality between SCs, therefore introducing ISI and ICI. The large dynamic range of the signal, which translates into high PAPR, is another important disadvantage of OFDM systems, especially because high PAPR originates saturation in power amplifiers.

Chapter 3. OFDM in Wireless and Optical Networks

3.1. Introduction

OFDM technology has been present in wireless systems for several years now, and has proven to be an excellent modulation technique, as explained in the previous section. This chapter consists in an introduction to the application of OFDM technology to wireless over optical networks. In this dissertation, we focus on wireless systems based on IEEE 802.11a standard since nowadays Wireless Local Area Network (WLAN) is a well-established technology, widely employed by end-users. The IEEE 802.11 standard for WLAN, extensively described in [2] [23], presents itself as a good choice for analysis, as it is a standard used in a large scale and exposed to a large number of interference sources. Besides, this technology is still evolving towards greater speed, improved security, and with perspective for new applications and investments.

The parameters mandatory to IEEE 802.11a standard for OFDM modulation and timing specifications are introduced, and a preview is made on frame generation with a preamble used for synchronization and simplified equalization.

The combination of OFDM systems with optical technology is also reviewed in this chapter. These are technologies with important differences in their basic conception, such as the polarity of the signal, the detection techniques or the type of signal in use.

In an ideal transmission channel, a signal passes through a field defined as a single direct path, and is perfectly recovered at the receiver without having suffered any modification. However, in a real channel many destructive effects modify the transmitted signal and must be taken into consideration.

For the RoF network studied here in particular, the RF signal travels through a medium composed by two main segments: electrical wire and optical fiber. Therefore, the specific effect of the mediums involved must be taken into account. Obviously, the whole channel model that will affect the signal is defined by the combination of all possible interference sources, from all the segments of the network (wireless path, optical fiber, connectors, electrical to optical conversion, etc…). However, the wireless transmission media is expected to have a much stronger impact on the signal quality than the fiber link.

Some tools chosen for performance evaluation will also be introduced, which are appropriate to observe the channel effects and the PAPR phenomenon inherent to OFDM technology.

3.2. OFDM as Part of the IEEE 802.11 Standard for Wireless Networks

In the last decade, WLANs has been through remarkable growth with the large-scale production of IEEE 802.11 compliant devices. This was due mainly to the evolution in semiconductor technology, as well as to WLAN standardization with IEEE 802.11, which led to a dramatic cost reduction and therefore to an increased adoption of this technology. In 1999, the Wi-Fi Alliance (WFA) was formed to certify the interoperability between IEEE 802.11 devices from different manufacturers. WLAN technology is still growing in a sustainable way because it has become very affordable, but also due to the many advantages that it provides. With WLANs, the costs, time and efforts necessary to implement a wired network, involving deploying cables and tearing up walls can be avoided. In addition, with the wide propagation of laptops and mobile technology, WLAN offers connectivity virtually anytime and anywhere simply by installing Access Points (AP). In present days, most existing WLAN systems are based on the IEEE 802.11a/b/g standard amendments, which provide throughput enhancements over the original IEEE 802.11 PHY [23]. In 2009, the IEEE 802.11n specification for WLAN was published.

OSI Reference Model layers	Description	Examples	Layer categories
Application	Interacts with software applications that implement a communicating component	Telnet, FTP, SMTP	Application
Presentation	Coding and conversion functions that are applied to application layer data	QuickTime, MPEG, GIF, JPEG, TIFF	
Session	Establishes, manages, and terminates communication sessions	ZIP, AppleTalk, SCP, DECnet Phase IV	
Transport	Accepts data from the session layer and segments the data for transport across the network	TCP, UDP	Data transport
Network	Defines the network address	IP, IPv6	
Data link	Transit of data across a physical network link	802.2 LLC	
Physical	Electrical, mechanical, procedural, and functional specifications	802.11 PHY	

Table 3.1 – OSI model reference [23].

The first development of the IEEE 802.11 group was centered on a common Medium Access Control (MAC) layer for multiple PHY layers to standardize WLAN. IEEE 802.11 is a member of the IEEE 802 family for Local Area Networks (LAN) and Metropolitan Area Network (MAN) standard, and therefore shares some of their characteristics. It incorporates 802.1 architecture, management, and interworking, and 802.2 Logical Link Control (LLC) [2]. The 802.2 LLC and IEEE 802.11 MAC and PHY compose the data link and physical layers of the Open Systems Interconnection (OSI) reference model, as described in Table 3.1.

For collision detection, IEEE 802.11 uses a variation of the mechanism applied to shared Ethernet LANs, called Carrier Sense Multiple Access with Collision Avoidance (CDMA/CA). Wired LANs use Carrier Sense Multiple Access with Collision Detection (CDMA/CD), where the detection is made electrically and almost instantly when the transmitter receives back its own transmission. When a collision is detected, the stations wait for a random period before transmitting again. For WLANs, there is no way to detect a collision in such direct manner. However, the station can detect that the medium is busy or inactive if no response or acknowledge is received from the remote station once a frame has been transmitted [3] [23].

	802.11	802.11a	802.11b	802.11g	802.11n
PHY technology	DSSS	OFDM	DSSS/CCK	OFDM, DSSS/CCK	SDM/OFDM
Data rates	1, 2 Mb/s	6-54 Mb/s	5.5, 11 Mb/s	1-54 Mb/s	6-600 Mb/s
Frequency band	2.4 GHz	5 GHz	2.4 GHz	2.4 GHz	2.4 GHz and 5 GHz
Channel spacing	25 MHz	20 MHz	25 MHz	25 MHz	20 MHz and 40 MHz

Table 3.2 – Overview of IEEE 802.11 PHYs [23].

Originally, the IEEE 802.11 standard published in 1997 included three PHYs: Infrared, 2.4 GHz Frequency Hopped Spread Spectrum (FHSS), and 2.4 GHz Direct Sequence Spread Spectrum (DSSS). Later, several standard amendments were produced, namely the IEEE 802.11a to create a new PHY in 5 GHz, and IEEE 802.11b to increase the data rate in 2.4 GHz DSSS PHY [2] [23]. OFDM technology was introduced to the IEEE 802.11 standard with the development of the IEEE 802.11a amendment. It was the first packet-based system to make use of OFDM technology for its PHY standard. Until then, OFDM technology was used only in systems such as DAB and DVB [3]. In 2001, the use of OFDM in 2.4 GHz band was authorized. Afterward, as the IEEE 802.11g amendment was developed based on IEEE 802.11a PHY, OFDM also became part of this standard in 2003. With the introduction of the new IEEE 802.11g standard, backward compatibility and interoperability was maintained with the older IEEE 802.11b devices. This ensured for new IEEE 802.11g client cards to work in existing IEEE 802.11b hotspots, or older IEEE 802.11b client devices to connect with any new IEEE 802.11g AP. The IEEE 802.11g standard amendment experienced very large market success due to this ensured compatibility and due to new data rates of up to 54 Mb/s [23].

3.2.1. IEEE 802.11a Specifications for OFDM Modulation

The IEEE 802.11a amendments endow with MAC and PHY specifications for transmission data rates. A list of modulation-dependent and timing-related parameters supported by this standard is

available in Table 3.3 and Table 3.4. In addition, Figure 3.1 shows the SCs allocation in frequency as it is described in the standard.

Modulation	Coding rate (R)	Coded bits per SC (N_{BPSC})	Coded bits per OFDM symbol (N_{CBPS})	Data bits per OFDM symbol (N_{DBPS})	Data rate (Mb/s) (20 MHz channel spacing)	Data rate (Mb/s) (10 MHz channel spacing)	Data rate (Mb/s) (5 MHz channel spacing)
BPSK	1/2	1	48	24	6	3	1.5
BPSK	3/4	1	48	36	9	4.5	2.25
QPSK	1/2	2	96	48	12	6	3
QPSK	3/4	2	96	72	18	9	4.5
16-QAM	1/2	4	192	96	24	12	6
16-QAM	3/4	4	192	144	36	18	9
64-QAM	2/3	6	288	192	48	24	12
64-QAM	3/4	6	288	216	54	27	13.5

Table 3.3 – Standard IEEE 802.11a modulation-dependent parameters [2].

Parameters	Value (20 MHz channel spacing)	Value (10 MHz channel spacing)	Value (5 MHz channel spacing)
Number of data SCs (N_{SD})	48	48	48
Number of pilot SCs (N_{SP})	4	4	4
Total number of SCs ($N_{ST} = N_{SD} + N_{SP}$)	52	52	52
SC frequency spacing ($\Delta_F = B/N_{FFT}$)	$\frac{20\ MHz}{64} = 0.3125\ MHz$	$\frac{10\ MHz}{64} = 0.15625\ MHz$	$\frac{5\ MHz}{64} = 0.078125\ MHz$
IFFT / FFT duration ($T_{FFT} = 1/\Delta_F$)	$\frac{1}{0.3125\ MHz} = 3.2\ \mu s$	$\frac{1}{0.15625\ MHz} = 6.4\ \mu s$	$\frac{1}{0.078125\ MHz} = 12.8\ \mu s$
GI duration ($T_{GI} = T_{FFT}/4$)	$\frac{3.2\ \mu s}{4} = 0.8\ \mu s$	$\frac{6.4 \mu s}{4} = 1.6 \mu s$	$\frac{12.8 \mu s}{4} = 3.2\ \mu s$
Symbol duration ($T_{SYM} = T_{GI} + T_{FFT}$)	$0.8\ \mu s + 3.2\ \mu s = 4\ \mu s$	$1.6\ \mu s + 6.4\ \mu s = 8\ \mu s$	$3.2\ \mu s + 12.8\ \mu s = 16\ \mu s$

Table 3.4 – Standard IEEE 802.11a timing-related parameters [2].

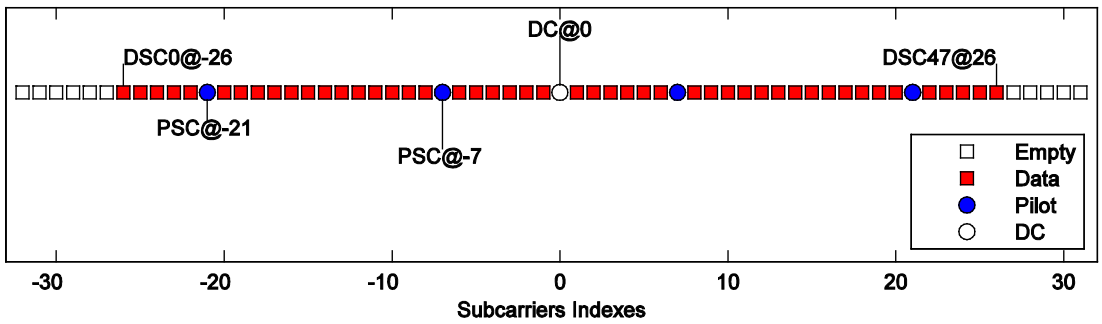

Figure 3.1 – SC frequency allocation based on IEEE 802.11a definitions.

This wireless standard uses 64 SCs, where 48 SCs carry data and 4 SCs are used as pilots for simple estimation of phase offsets caused by FFT timing errors. From the remaining SCs, 11 are

empty and behave as guard band. The SC at DC also remains empty to avoid distortions from ADC and DAC offsets [2].

Variable bit rate is achieved by changing the convolutional coding rate, as well as the data modulation order; that is, the information data bits per OFDM symbols is regulated. The channel spacing also controls the bit rate by specifying the duration of OFDM symbols transmission.

The standard also specifies the length of the GI with duration $N_{GI} = N_{FFT}/4$ of the FFT period, which means that an OFDM symbol is formed by 80 samples. As introduced in Section 2.3.4 and Section 2.3.5, the GI consists in a cyclic extension and in a windowed section to reduce the spectral sidelobes of the transmitted waveform. Typically, the transition time T_{WIN} duration is about 100 ns, but the standard allows flexibility in both the transition duration and shape [2]. For a 20 MHz channel spacing, this transition time translates into $N_{WIN} = (100\ ns * 80)/4\ \mu s = 2$ samples. A greater transition time improves the spectral efficiency, but reduces the effective length of the GI. Hence, a compromise should be reached between both when the system is being designed.

3.2.2. Preview on the IEEE 802.11a PHY Frame Structure

The main purpose of the OFDM PHY is to transmit the MAC Protocol Data Unit (MPDU). Two elements define the OFDM PHY: Physical Layer Convergence Procedure (PLCP) and the Physical Medium Dependent (PMD) sub-layers [15].

The MAC layer communicates with the PLCP through a PHY service AP. The PLCP prepares the MPDUs for transmission under MAC instruction, and also conveys frames incoming from the wireless medium to the MAC layer. By mapping MPDUs into a frame format that is appropriate for transmission by the PMD, the PLCP sub-layer minimizes the dependence of the MAC layer on the PMD sub-layer [2] [16].

The PMD provides transmission and reception of PHY units between two stations through the wireless medium under the oversight of the PLCP. To supply this service, the PMD interfaces directly with the air medium and provides modulation and demodulation of the frame transmissions. The PLCP and PMD communicate using service primitives to manage the transmission and reception functions [2] [16].

The PLCP Protocol Data Unit (PPDU) frame structure for IEEE 802.11a specification is depicted in Figure 3.2 and Figure 3.3. The first part of the frame is the PLCP preamble, which is composed by 10 short symbols from t_1 to t_{10}, and 2 long symbols T_1 and T_2 with a GI having doubled length. The next part of the frame is the SIGNAL field, which is followed by a number of additional OFDM symbols with the DATA [2].

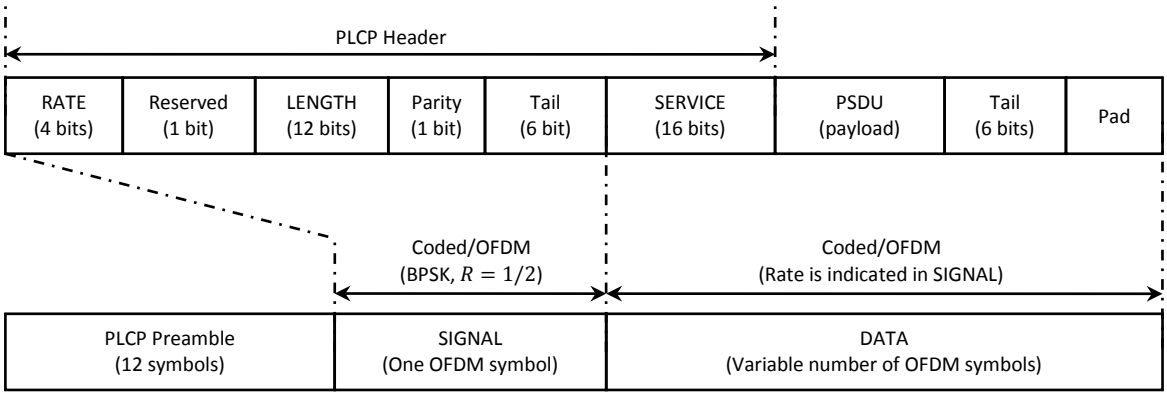

Figure 3.2 – PPDU frame format [2].

The PLCP Preamble field is used to detect the frames at the receiver through cross-correlation, and to synchronize the demodulator, which is the FFT for a digital system. The short symbols are used to adjust the AGC at the receiver, and for coarse estimation of the carrier frequency and time offsets. The long symbols are used to perform fine-tuning of the frequency offsets and the channel estimation [2].

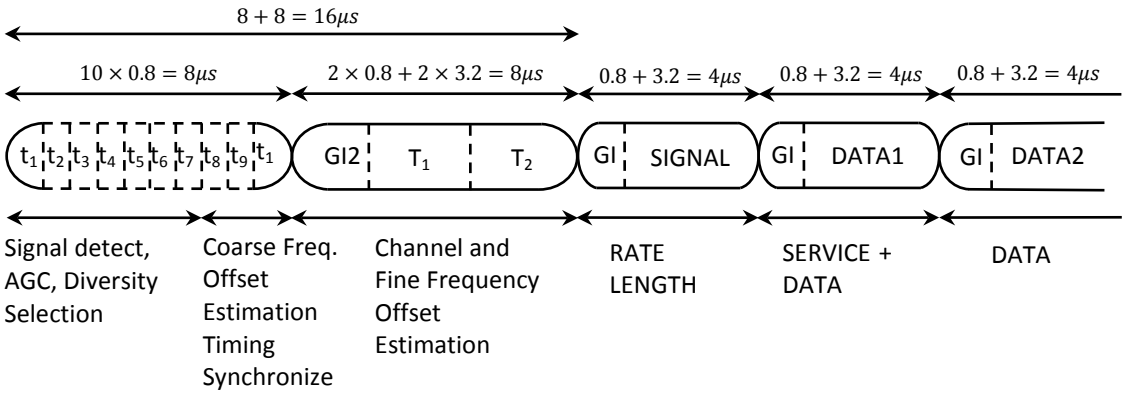

Figure 3.3 – OFDM training structure. Timing is for 20 MHz of channel spacing [2].

The Short Training Sequence (STS) consists of 12 SCs, which are modulated by the elements of the sequence S, given by [2]:

$$S_{-26,26} = \sqrt{13/6}\{0,0,1+j,0,0,0,-1-j,0,0,0,1+j,0,0,0,-1-j,0,0,0,-1-j,0,0,0,1 + j,0,0,0,0,0,0,0,-1-j,0,0,0,-1-j,0,0,0,1+j,0,0,0,1+j,0,0,0,1 + j,0,0,0,1+j,0,0\}$$

The multiplication by a factor of $\sqrt{13/6}$ normalizes the average power of the resulting OFDM symbol, which utilizes 12 out of 52 SCs. Only spectral lines of $S_{-26,26}$ with indices that are a multiple of 4 have non-zero amplitude, which results in a periodicity of $T_{FFT}/4 = 0.8\ \mu s$ when the bandwidth is 20 MHz [2].

A Long Training Sequence (LTS) consists of 53 SCs, which include a zero value at DC and are modulated by the elements of the sequence L, given by [2]:

$$L_{-26,26} = \{1, 1, -1, -1, 1, 1, -1, 1, -1, 1, 1, 1, 1, 1, 1, -1, -1, 1, 1, -1, 1, -1, 1, 1,$$
$$1, 1, 0, 1, -1, -1, 1, 1, -1, 1, -1, 1, -1, -1, -1, -1, -1, 1, 1, 1, -1,$$
$$-1, 1, -1, 1, -1, 1, 1, 1, 1\}$$

Two periods of the long sequence are transmitted for improved channel estimation accuracy, with a GI length of half the size of one sequence. Hence, $T_{LONG} = 1.6 + 2 \times 3.2 = 8\ \mu s$ for a 20 MHz channel spacing [2].

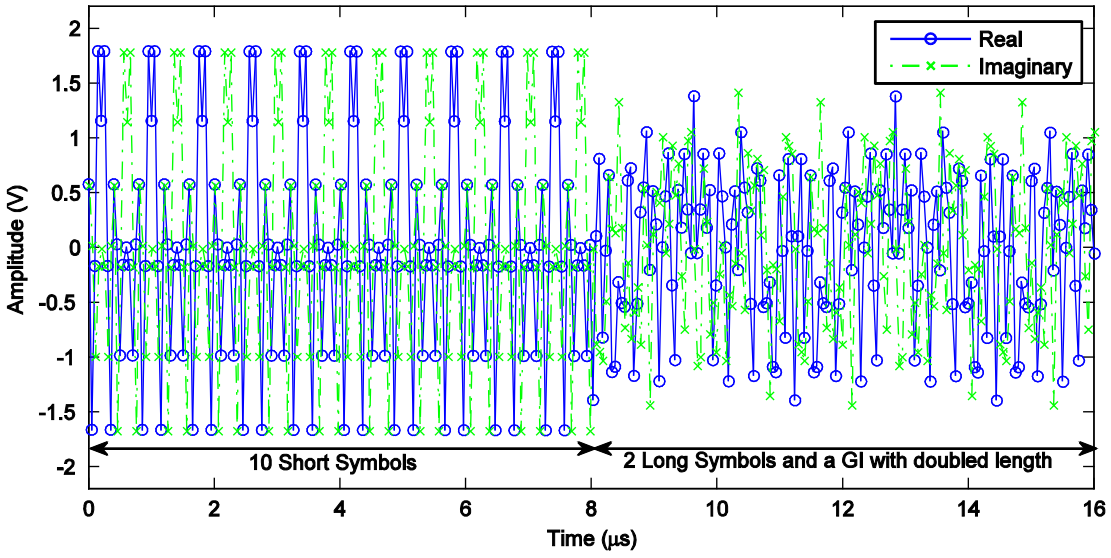

Figure 3.4 – PLCP Preamble composed by the STS and by the LTS, for a 20 MHz channel spacing.

The SIGNAL field contains the LENGTH and RATE of the PHY Service Data Units (PSDU), and consists in 24 bits. It is transmitted with the lowest rate to guarantee unfailing reception, which is BPSK modulation with convolutional coding at rate $R = 1/2$, and without being scrambled [2].

The RATE is formed by a sequence of 4 bits defined in the specifications depending on the modulation parameters [2].

The LENGTH is computed by converting the 12-bit unsigned integer indicating the number of octets in the PSDU that the MAC is requesting the PHY to transmit into binary digits, with the Most Significant Bit (MSB) to the right. The maximum number of octets allowed per frame is 4095, which corresponds to the highest 12-bit binary representation of the converted length ($4095_{10} = 111111111111_2$) [2].

The PARITY bit is used as a basic form of error detection based on the LENGTH bits. Even parity is mandatory, meaning that the number of ones included within LENGTH and PARITY together must be even [2].

Finally, the DATA fields are transmitted at the DATA RATE indicated in the SIGNAL field. The first 16 bits define the SERVICE field, which is followed by the PSDU, some TAIL bits and padding [2].

The SERVICE field is composed by 16 bits, where the first part are zeros that allow the descrambler at the receiver to synchronize, and the remaining 9 bits are reserved and also zeros [2].

The remaining TAIL bits are required to return properly the convolutional encoder to the zero state. This improves the error probability at the receiver because de decoder relies on future bits when decoding. Since there is no guarantee that there will be padding at the end of the payload, TAIL insertion is necessary. Hence, the PLCP TAIL bit field is produced by replacing six scrambled zero bits following the message by six non-scrambled zero bits [2].

The number of PAD bits depends on the length of the PSDU, that is, the number of bits in the DATA field must be a multiple of N_{CBPS}, which is the number of coded bits in an OFDM symbol. To do so, the original message must be extended in order to become a multiple of N_{DBPS}, which is the number of data bits per OFDM symbol. Therefore, the number of PAD bits are computed from the PSDU LENGTH as described in [2]:

$$N_{SYM} = ceil((16 + 8 \times LENGTH + 6)/N_{DBPS}) \tag{3.1}$$

$$N_{DATA} = N_{SYM} \times N_{DBPS} \tag{3.2}$$

$$N_{PAD} = N_{DATA} - (16 + 8 \times LENGTH + 6) \tag{3.3}$$

Where: N_{SYM} is the number of OFDM symbols; N_{DATA} is the number of bits in the DATA field and $\mathrm{N_{PAD}}$ is the number of padded bits. The appended bits are set to zeros and are scrambled with the rest of the bits in the DATA field [2].

3.2.3. Frame Detection using the Short Training Sequence

In systems using IEEE 802.11a PHY, the receiver knows the structure of the preamble. This is valuable information that is used by the receiver to perform frame detection. In fact, in this standard the preambles are designed to help the detection of the starting edge of a packet. The standard leaves the choice of the algorithm for packet detection to the developer [27]. In this dissertation, the approach presented by Schimdl and Cox is used for coarse frame detection. It is known as the Delay and Correlate algorithm, and takes advantage of the periodicity of the sort training symbols at the start of the preamble.

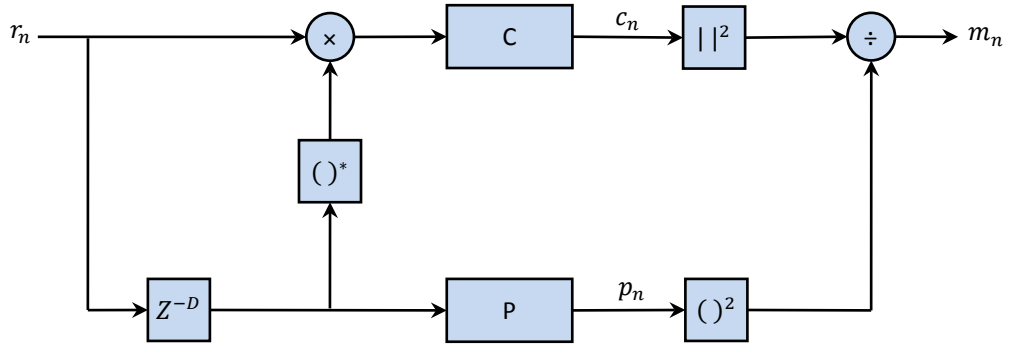

Figure 3.5 – Flow structure of the Delay and Correlate algorithm [27].

$$c_n = \sum_{k=0}^{L-1} r_{n+k} r_{n+k+D}^* \tag{3.4}$$

$$p_n = \sum_{k=0}^{L-1} r_{n+k+D} r_{n+k+D}^* = \sum_{k=0}^{L-1} |r_{n+k+D}|^2 \tag{3.5}$$

$$m_n = \frac{|c_n|^2}{(p_n)^2} \tag{3.6}$$

Two sliding windows C and P can be seen in Figure 3.5. The C window is a cross-correlation between the received signal and a delayed version of the received signal. The delay Z^{-D} is equal to the period of the start of the preamble, which is the period of the short training symbols with length $D = 16$ in the IEEE 802.11a standard. The P window calculates the received signal energy during the cross-correlation window. The value of the P window is used to normalize the decision statistic m_n, in order for it to be independent on absolute received power level [27].

3.2.4. Frequency Offset Estimation using the Short Training Sequence

The periodicity of the short training sequence is engineered to provide optimal conditions for both timing and frequency synchronization, due to its energy distribution and periodicity. The estimation of frequency offset is achieved by taking advantage of this periodicity to determine the difference between the transmitted frequency and the received one. It is given by the relation $\Delta f = f_{TX} - f_{RX}$. Based on the definitions in Chapter 2, the received baseband signal is defined, without modeling the noise, as:

$$r(t) = s(t) e^{j2\pi\Delta f t} \tag{3.7}$$

Where: $s(t)$ is the transmitted signal; $r(t)$ is the received signal; Δf is the frequency offset.

Since the STS is periodic, by introducing a one period delay δt to the equation above it becomes [28]:

$$r(t-\delta t) = s(t)e^{j2\pi\Delta f(t-\delta t)} \tag{3.8}$$

Both $r(t)$ and $r(t-\delta t)$ are known by the receiver, as well as the original sequence $s(t)$. Thus, the following relation can be calculated:

$$\begin{aligned} r(t-\delta t)r^*(t) &= s(t)e^{j2\pi\Delta f(t-\delta t)}s^*(t)e^{-j2\pi\Delta ft} \\ &= |s(t)|^2 e^{-j2\pi\Delta f\delta t} \end{aligned} \tag{3.9}$$

Finally, by finding the angle of each side of the equation above, the expression to discover the frequency offset is deduced [28]:

$$\begin{aligned} &\measuredangle[r(t-\delta t)r^*(t)] = \measuredangle\left[|s(t)|^2 e^{-j2\pi\Delta f\delta t}\right] \\ (=)\ &\measuredangle[r(t-\delta t)r^*(t)] = -2\pi\Delta f\delta t \\ (=)\ &\Delta f = \frac{\measuredangle[r(t-\delta t)r^*(t)]}{-2\pi\delta t} \end{aligned} \tag{3.10}$$

3.3. OFDM Application to Optical Networks

At the end of the 20th century, around the 1980s, electrical-based technology was getting to a point of saturation in terms of capacity and reach. A typical coaxial link needed regenerators every 1 km for a data rate of 200 Mb/s, involving very high costs [7]. Consequently, the need for new solutions was growing, and a promising technology that was already under development, known as optical fiber, became one of the main alternatives chosen for investigation. As coherent source for optical transmitters became achievable by using Light Amplification by Stimulated Emission of Radiation (LASER), the problem of finding an appropriate transmission medium emerged. In 1966, Kao and Hockman proposed optical fiber for lightwave transmission, and stated that the attenuation from optical fiber was caused by fiber impurities that could be removed [7]. However, at that time optical fiber was unacceptably expensive to become a practical solution. Later, optical fiber networks became an attractive technology due to their low loss, but the optical systems were still limited to distances generally lower than 100 km due to the need for optical signal regeneration. In the late 1980s, coherent detection communication systems were introduced to improve the transmission distance of electrical-based systems. Nevertheless, as the optical amplifier was invented in the 1990s a new generation of communication systems was arising, in which it became possible to transmit substantial quantity of signals over a single optical fiber using Wavelength-Division Multiplexing (WDM) technology [7].

OFDM systems have many strong advantages turning them into an appealing technology, which is why they are widely used in a number of communication standards, and are especially popular in wireless telecommunications [7]. Nonetheless, it is only recently that OFDM technology was applied to optical communications, mostly due to the increasing demand for higher data rates across dispersive optical links, and also because Digital Signal Processing (DSP) at optical data rates has become possible [5]. An important barrier in applying OFDM technology to optical networks resides in the elementary differences existing in the conception of these systems [5]. These differences are uncovered in Table 3.5. In conventional OFDM systems, the information is carried on the electrical field where the signal can have both positive and negative values. At the receiver, a local oscillator is used and Coherent-Detection (CD) is performed. On the contrary, in typical optical systems the information is transported on the intensity of the optical signal and thus can only be positive. At the receiver, Direct-Detection (DD) is used [5].

Typical OFDM System	Bipolar	Information carried on electrical field	Local Oscillator at receiver	Coherent Reception
Typical Optical System	Unipolar	Information carried on optical intensity	No Local Oscillator (laser) at receiver	Direct Detection

Table 3.5 – Differences between typical OFDM Systems and typical Optical Systems [5].

The application of OFDM technology to optical networks can be separated in two main modulation types: Intensity Modulation (IM) and Linear Field Modulation (LFM) [5].

IM is usually applied to optical wireless systems and other systems where many modes are received, and where the OFDM signal must be represented as intensity. This implies that the modulating signal must be both real and positive, despite the baseband OFDM signals generally being complex and bipolar [5]. One way to achieve this is by constraining the baseband signal to have Hermitian symmetry, as described in [7]. The modulated complex data samples and their complex conjugate in the FD are placed in such a way that guarantees this symmetric property before proceeding to OFDM modulation. At this point, a real baseband signal is obtainable, but it is still necessary to turn it into a unipolar signal. In order to achieve this unipolar OFDM signal, two solutions exist: DC-Biased Optical OFDM (DCO-OFDM) and Asymmetrically Clipped Optical OFDM (ACO-OFDM). In the first solution, a DC bias is added to the signal, but due to the large PAPR of OFDM, even with a large bias some negative peaks will be clipped, thus resulting in interferences [5]. In the latter solution, the OFDM signal is clipped at the zero level, removing all the negative part of the signal. If only the odd frequency OFDM SCs are non-zero at the Inverse Fast Fourier Transform (IFFT) input, the interferences resulting from the clipping affects only the even SCs, thus preventing impairments on the odd data carrying SCs [5].

LFM is used to achieve linearity between the transmitter IFFT input and the receiver FFT output in SMF. It consists in mapping each discrete OFDM SC frequency in the baseband electrical domain to a single discrete frequency in the optical domain. This way a linear relationship is created between the optical field of the transmitted signal and the OFDM baseband signal. At the receiver, the signal is mixed with a component at the optical carrier frequency. The component at the optical frequency can be transmitted with the OFDM signal as in Direct-Detection Optical OFDM (DDO-OFDM), or coherent detection can be used where the receiver signal is mixed with a carrier produced locally as in Coherent Optical OFDM (CO-OFDM) [5].

DDO-OFDM offers the advantages of a simpler receiver, but to avoid interferences from unwanted mixing product some of the optical frequencies must remain unused. This is achieved by inserting a guard band between the optical carrier and the OFDM SCs, thus resulting in spectral efficiency loss and consumption of additional power. CO-OFDM requires a laser at the receiver and is sensitive to phase noise [5].

3.4. Propagation Characteristics of the Channel

Wireless environment is usually characterized as severely interfering scenario, in particular because it behaves as a reflective, frequency-selective fading, and multipath channel. Therefore, the signal detected by the receiver is usually distorted by random noise and multipath propagation. At a given instant, the receiver can only distinguish a combination of several replicas of the original signal that are attenuated, reflected, refracted and diffracted. The channel model for wireless communications is frequently referred to as time and frequency-selective fading channel [25].

	Mathematical Model	Nonlinearity	Speed
Wireless OFDM	Time domain multiple discrete Rayleigh fading	None	Can be fast for mobile
Optical OFDM	Continuous frequency domain dispersion	Significant	Medium

Table 3.6 – Comparison between Wireless and Optical channels [7].

Optical fiber environments are much less likely to degrade the signal due to random noise, namely because they are immune to Radio Frequency Interferences (RFI) and Electromagnetic Interferences (EMI). Nonetheless, they are sensitive to physical vibrations that translate into random noise. Moreover, the signal can be impaired by multimode dispersion (when MMF is used) or chromatic distortion (when SMF is used) [7].

3.4.1. Additive White Gaussian Noise

Usually, any real transmission system is affected by some degree of white noise, which, depending on the medium type, is caused by different sources. White noise can be defined as noise having a frequency spectrum that is continuous and uniform over a specified frequency band, thus having equal power per Hertz over the specified frequency band [29].

3.4.2. Shadowing

Shadowing consists in Line-of-Sight (LoS) loss, and signal diffraction over an obstacle. This generally happens around apartment buildings or hills that obstruct the path from the transmitter to the receiver, and causes the signal to be strongly attenuated or even undetectable at the receiver [3]. Communication systems using higher frequencies are more susceptible to shadowing. To overcome this issue, the transmitters are typically placed at high locations [25]. Smaller cells can be deployed as well to resolve this problem, but this implies costs for additional base stations and backbones [3].

3.4.3. Multipath Channel Model

3.4.3.1. Rician Fading and Rayleigh Fading

A transmitted RF signal can be reflected from objects such as vehicles, constructions or other natural obstacles. As a result, besides the direct LoS radio wave, multiple paths are detected at the receiver [3]. The phase relation between the several detected signals can generate constructive or destructive interferences, usually over short distances [25].

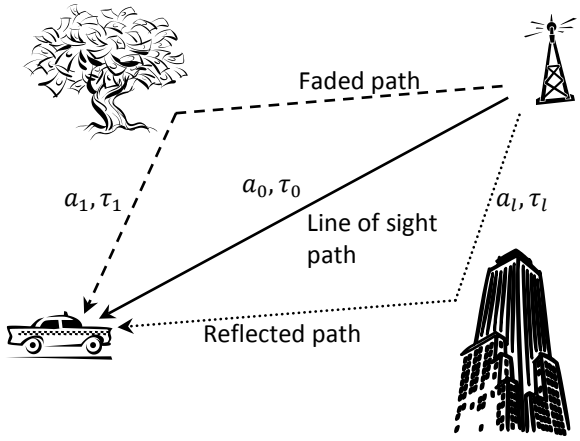

Figure 3.6 – A multipath fading environment.

Two stochastic models describe multipath fading channels. A multipath interfering environment is classified as Rician fading when one of the paths, typically the LoS path, is much stronger than the additional delayed and attenuated interfering paths. In Rician fading, the

amplitude gain is characterized by a Rician distribution. Rayleigh fading can be seen as a special case of Rician fading, where there is no direct LoS path. In Rayleigh fading, the amplitude gain is characterized by a Rayleigh distribution. A typical wireless channel can be modeled as a summarization of the multiple paths, each undergoing a Rayleigh process, given by [7]:

$$h(t,\tau) = \sum_{l-1}^{L} a_l g_l(t)\delta(\tau - \tau_l) \tag{3.11}$$

Where: a_l is a complex constant of path gain; $g_l(t)$ is the Rayleigh fading process; τ_l is the delay for the lth path. The difference in path time can be expressed as $\Delta\tau = \tau_l - \tau_0$.

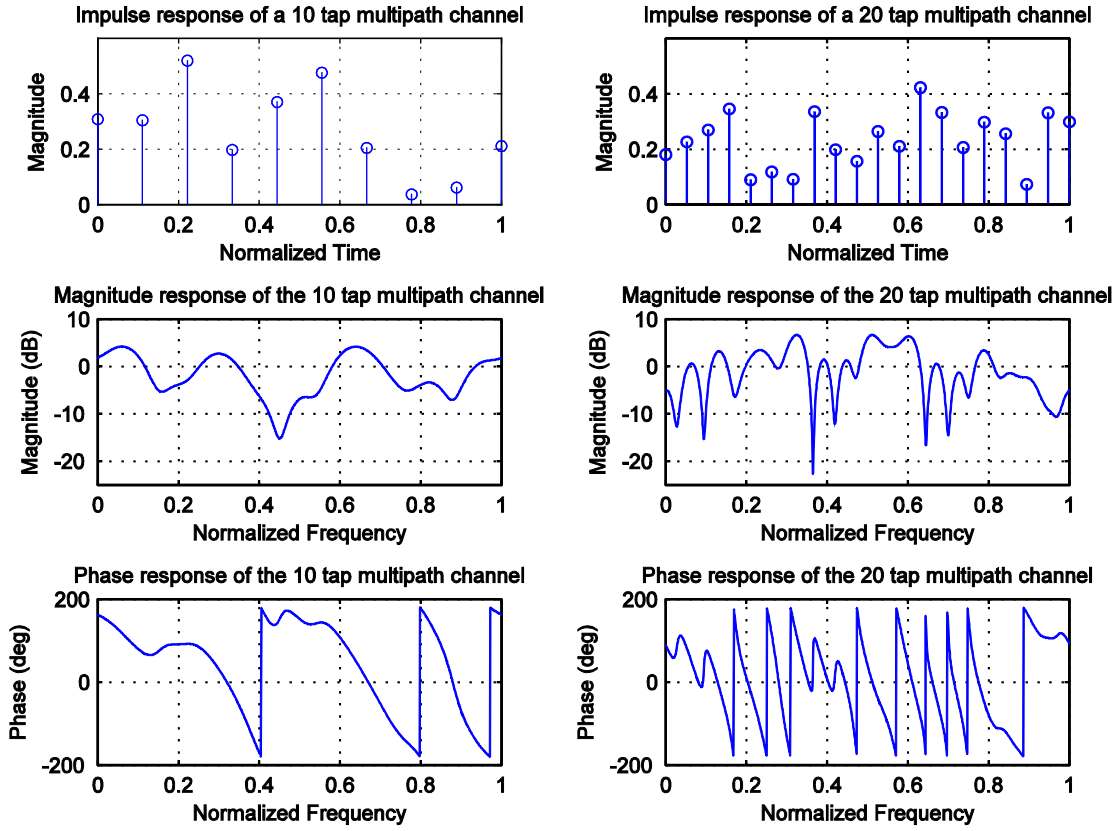

Figure 3.7 – Random complex Rayleigh multipath channels: 10 impulses on the left; 20 impulses on the right.

3.4.3.2. Frequency-Selective Fading

By definition, selective fading is a kind of fading that varies for different frequencies over a frequency band, hence causing distortions that vary in nature at different instants. In a wireless transmission, some frequencies are canceled due to reflections. For narrow bandwidth transmission, when this destructive effect occurs at transmission frequency, the entire signal can be lost. In OFDM systems, because the original signal is spread over a wide bandwidth, the frequency cancelation is unlikely to occur on all the SCs [3] [25]. Additionally, by using FEC coding and interleaving the

robustness is furtherly increased, as described in Section 2.3.2. In opposition to frequency-selective fading, flat fading occurs when the coherence bandwidth if the channel is larger than the bandwidth of the signal. It that situation, all the frequency components of the signal are exposed to the same magnitude of fading.

3.4.3.3. Delay Spread

Usually, in multipath environment the receiver detects the direct LoS signal added to multiple extra paths. These additional paths are likely to travel along different distances before reaching the receiver. Therefore, besides being attenuated, these supplementary paths arrive later at the receiver [3] [12]. Due to these delays, the detected signals energy is spread in time. The delay spread is the time extension between the arrival of the first and last multipath signal at the receiver [25]. Filters at the transmitter and receiver can also cause additional delay spread [23]. The delay spread causes adjacent data symbols to overlap and interfere with each other, thus introducing ISI [26]. The main mechanism to combat delay spread is the GI with a CP, as introduced in Section 2.3.4.

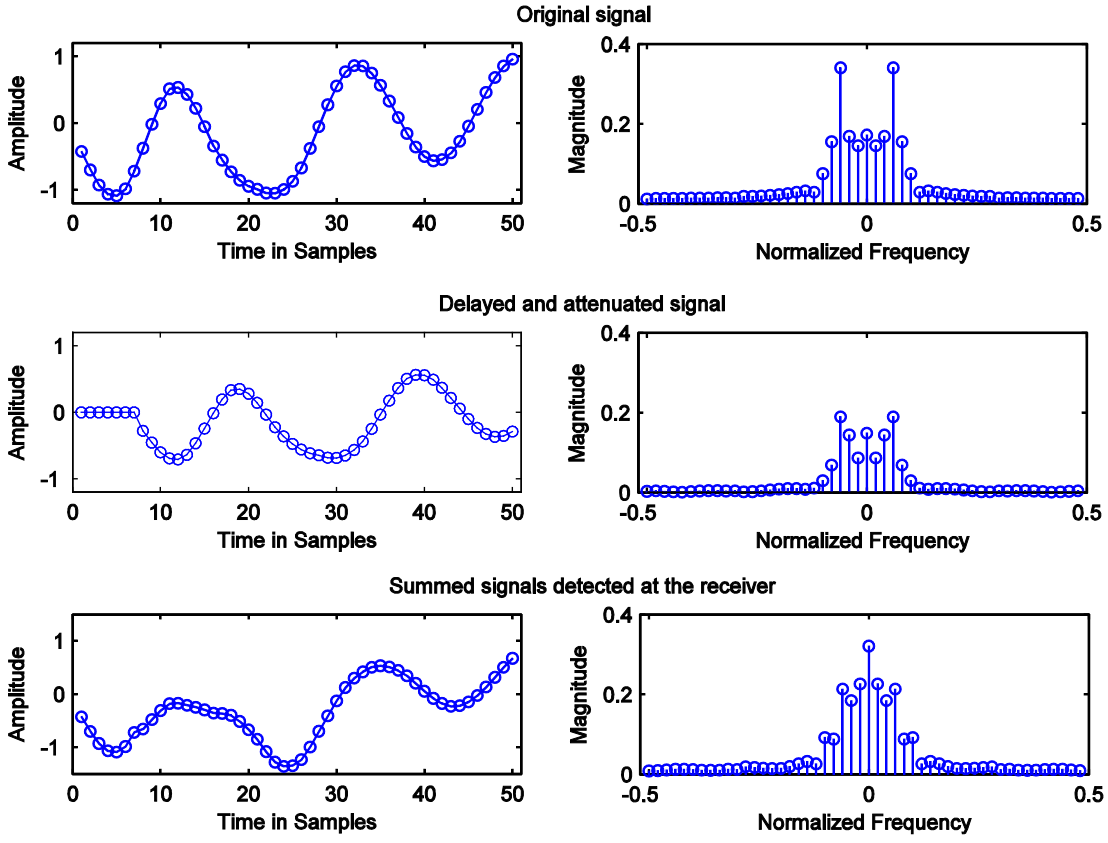

Figure 3.8 – Multipath delay spread.

3.4.4. Doppler Shift

Doppler shift is defined simply as a change in frequency. The shifting in frequency is caused by movements of the transmitter and of the receiver in relation to one another [12]. Doppler shifts

are insignificant for fixed position stations. However, for a mobile station the Doppler shift will affect the link quality [26]. The relative motion between the transmitter and the receiver defines the quantity of frequency variation. The Doppler shift in frequency can be written as [25]:

$$\Delta f = \pm f_o(v/c) \tag{3.12}$$

Where: Δf is the frequency change in the signal seen by the receiver; f_o is the transmitted frequency; v is the difference between the transmitted and the received frequency; c is the speed of light.

3.4.5. Optical Fiber Impairments

3.4.5.1. Chromatic Dispersion

Chromatic dispersion is a well-known optical fiber impairment, and usually manifests in SMF. It is caused by different velocities among distinct spectral components within the same mode, and is defined by two constituents: material dispersion and waveguide dispersion. Material dispersion results from the sensitivity of the speed of light in a medium in relation to its wavelength. Waveguide dispersion results from the physical design of the optical fiber, and is caused by the fact that a given wavelength travels at different speeds in the core and cladding of an SMF. It occurs when the refractive indices of a core-cladding are just nearly equal and the light is not confined in the fiber core [7].

3.4.5.2. Multimode Distortion

Multimode distortion consists in signal spread in time. This occurs in MMF because the propagation speed is not the same for all the modes, and therefore the difference in mode path lengths produces a difference in arrival times ate the receiver [7] [29]. An analogy can be established between this effect and the existing multipath propagation in wireless communications [29].

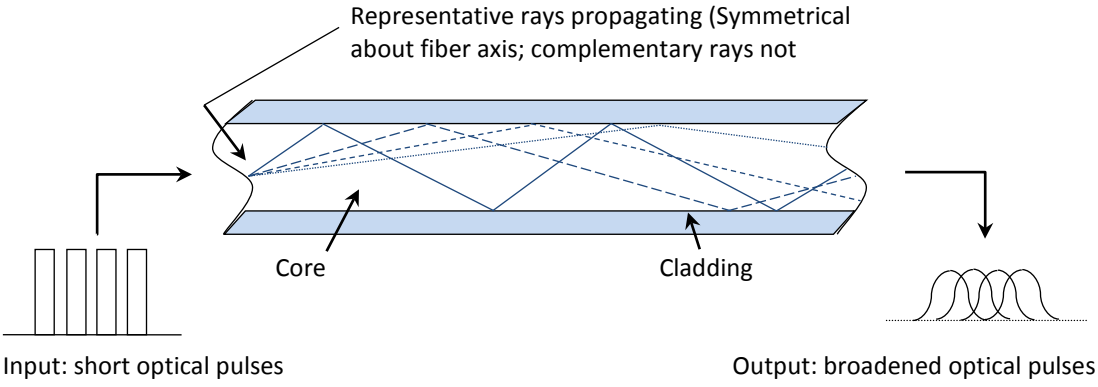

Figure 3.9 – Representation of multimode distortion [29].

In MMF the direct signal can be distorted by the arrival of the reflected signal with a small delay. This delay takes place because in a step-index optical fiber, rays taking more direct paths through the fiber core will undergo fewer reflections at the core-cladding boundary. Similarly to wireless multipath propagation, this results in signal distortion and limitations in signal bandwidth. One way to reduce significantly this effect is by using a core with graded refractive index [29]. In addition, by limiting the number of propagating modes to a fundamental one the multimode dispersion can be effectively eliminated. MMF and graded-index fiber suffer highly from modal dispersion over short distances, and as a result material dispersion and chromatic dispersion never become degradation factors [7].

3.5. Tools for Performance Analysis

3.5.1. Error Vector Magnitude

In a real communication system, different kinds of impairments are expected to distort the received signal in amplitude and phase. Typically, in the presence of ISI and noise, the measured signal will appear to be randomly varying around the ideal signal, translating into an error cloud around the ideal constellation point [30].

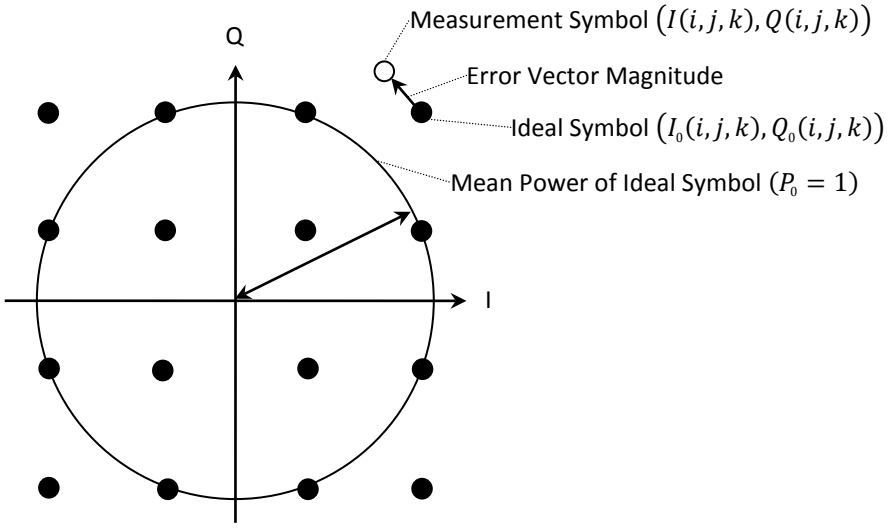

Figure 3.10 – Representation of Constellation Error [2].

Error Vector Magnitude (EVM) can be defined as an estimation of the quality of a communication system. This evaluation is made by measuring the error between the original symbols and the received data constellation points after decimating the recovered waveform, hence also providing a direct measure of modulation accuracy in the presence of impairments [31] [32]. In an OFDM system, EVM has the advantage of providing an assessment of the quality of the transmission

system even before data demodulation is performed, and of granting a prediction for the expected Bit Error Rate (BER), since BER is proven to be a consequence of EVM [31].

Based on the definitions given in [33], the RMS EVM computed with a reference signal for a sequence of constellation samples can be described as the following:

$$EVM_{RMS} = \sqrt{\frac{\frac{1}{N}\sum_{k=1}^{N}\left(\left(I(k) - I_0(k)\right)^2 + \left(Q(k) - Q_0(k)\right)^2\right)}{\frac{1}{N}\sum_{k=1}^{N}(I_0(k)^2 + Q_0(k)^2)}} \times 100 \tag{3.13}$$

Where: $I_0(k)$ is the ideal reference value in phase for the kth symbol in the burst; $Q_0(k)$ is the ideal reference value in quadrature for the kth symbol in the burst; $I(k)$ is the received reference value in phase for the kth symbol in the burst; $Q(k)$is the received reference value in quadrature for the kth symbol in the burst; N is the number of constellation samples processed.

If the calculations are performed for a normalized constellation power as depicted in Figure 3.10, then the denominator of the equation above corresponds to the mean power of the ideal symbols:

$$P_0 = \sqrt{\frac{1}{N}\sum_{k=1}^{N}(I_0(k)^2 + Q_0(k)^2)} = 1 \tag{3.14}$$

For performance evaluation the Relative Constellation Error (RCE) metric was considered in this dissertation. RCE is defined as the RMS averaged magnitude error of all the constellation points in a number of frames. In other words, it is an average of the EVM computed for a number of frames. The following expression, given in [2], describes the RMS error estimation process for a block of OFDM-based frames:

$$Error_{RMS} = \frac{\sum_{i=1}^{N_f}\sqrt{\frac{\sum_{j=1}^{L_p}\left[\sum_{k=1}^{N_{SC}}\left\{\left(\left(I(i,j,k) - I_0(i,j,k)\right)^2 + \left(Q(i,j,k) - Q_0(i,j,k)\right)^2\right)\right\}\right]}{N_{SC} \times L_p \times P_0}}}{N_f} \tag{3.15}$$

Where: L_p is the length of the packet (the number of OFDM symbols in the frame); N_f is the number of frames for the measurement; $\left(I_0(i,j,k), Q_0(i,j,k)\right)$ denotes the ideal symbol point of the ith frame, jth OFDM symbol of the frame, kth SC of the OFDM symbol in the complex plane; $\left(I(i,j,k), Q(i,j,k)\right)$ denotes the observed symbol point of the ith frame, jth OFDM symbol of the frame, kth SC of the OFDM symbol in the complex plane; P_o is the average power of the ideal constellation ($P_0 = 1$).

While the EVM is commonly presented in percentage, the RCE is usually given in decibels. It can be related to the RMS error through the following expression:

$$RCE_{dB} = 20 \times log_{10}(Error_{RMS}) \tag{3.16}$$

The IEEE 802.11 specifications states that the test should be performed over at least 20 frames (N_f), and that the RMS average should be taken. The packets under test must be at least 16 OFDM symbols long. In addition, random data must be used to generate the OFDM symbols [2]. Moreover, the specifications indicate the RCE averaged over SCs, OFDM symbols and entire frames should not exceed the data rate dependent values according to Table 3.7 below.

Relative Constellation Error (dB)	Modulation	Coding Rate (R)
-5	BPSK	1/2
-8	BPSK	3/4
-10	QPSK	1/2
-13	QPSK	3/4
-16	16-QAM	1/2
-19	16-QAM	3/4
-22	64-QAM	2/3
-25	64-QAM	3/4

Table 3.7 – Allowed RCE versus Data Rate as specified in IEEE 802.11 standard [2].

3.5.2. Signal-to-Noise Ratio

To compute correctly the SNR in OFDM technology, where the SNR is given by the E_b/N_0 (the energy per bit to noise power spectral density ratio), the data modulation order and the OFDM modulation parameters must be taken into account. The SNR for each modulation scheme must consider the number of bits per symbol, thus the signal power corresponds to the energy per bit times the number of bits per symbol. A higher E_b/N_0 required for transferring data means that more energy is required for each bit transfer [34].

Considering all these parameters, the OFDM E_s/N_0 (the energy per symbol to noise power spectral density ratio) given in decibels can be obtained by performing the following calculation [34]:

$$\left[\frac{E_s}{N_0}\right]_{dB} = \left[\frac{E_b}{N_0}\right]_{dB} + 10log_{10}\left(\frac{N_{SC}}{N_{FFT}}\right) + 10log_{10}\left(\frac{T_{FFT}}{T_{FFT}+T_{GI}}\right) + 10log_{10}\left(log_2(M)\right) \tag{3.17}$$

Where: $[E_b/N_0]_{dB}$ is the energy per bit to noise power spectral density ratio in decibels; N_{SC} is the number of occupied SCs; N_{FFT} is the FFT length in samples; T_{FFT} is the FFT duration; T_{GI} is the GI duration; M is the data modulation order.

So far, Equation (3.17) does not account for the additional energy required per bit if FEC coding is applied. Here, convolutional code with rate R determines this added amount of power. Considering this, the equation above can be rewritten as:

$$\left[\frac{E_s}{N_0}\right]_{dB} = \left[\frac{E_b}{N_0}\right]_{dB} + 10log_{10}\left(\frac{N_{SC}}{N_{FFT}}\right) + 10log_{10}\left(\frac{T_{FFT}}{T_{FFT}+T_{GI}}\right) + 10log_{10}\left(log_2(M)\right) + 10log_{10}(R) \quad (3.18)$$

3.5.3. Relating EVM to SNR

EVM and SNR are common measuring tools used for performance assessment in communication systems, and both can be related to BER. Finding the relation between EVM and other performance metrics can provide additional insight on the system performance, while avoiding the need to develop expensive modules. When data-aided EVM estimation is calculated, it is assumed that the EVM is measured using known data sequences or that the SNR is high enough so that symbol errors are insignificant [35].

It has been demonstrated in [32] [35] and [36] that for a Gaussian noise model the ratio of normalized noise power to the normalized power of the ideal constellation can be replaced by their non-normalized quantities, and that the relation between data-aided EVM and SNR is given by:

$$EVM_{RMS} \approx \sqrt{\frac{N_0}{E_S}} = \sqrt{\frac{1}{SNR}} \quad (3.19)$$

Where: N_0 is the normalized noise power and E_S is the normalized power of the ideal constellation.

3.5.4. Peak-to-Average Power Ratio

3.5.4.1. PAPR Evaluation

PAPR evaluation is an important aspect of the system performance because it provides a measurement for a major disadvantage of OFDM technology, which is the large dynamic range of its signals. PAPR provides a quantification of amplitude variation in an OFDM signal, therefore giving an estimation of the degradation. High PAPR indicates that there are high peaks in relation to the average value of the OFDM symbols. For instance, if N signals summed together compose the OFDM symbols, then it is possible that, at a given instant, the amplitude of one symbol is the maximum amplitude of each N signals summed [3] [37]. Unfortunately, large peaks cause saturation in power amplifiers, which results in intermodulation product among the SCs, and leads to ICI. Such situations are expected to occur, and result in peaks with amplitude much higher than the average. In [7] [37] PAPR is presented as:

$$PAPR = \frac{\underset{t\in[0,T]}{max}|x(t)|^2}{\varepsilon \in \{|x(t)|^2\}} = \frac{max[x(t)x(t)^*]}{\varepsilon \in [x(t)x(t)^*]} \tag{3.20}$$

Where: $x(t)$ is the signal; $\varepsilon \in \{.\}$ designates the expectation; $()^*$ corresponds to the conjugate operator. In decibels, the PAPR is:

$$PAPR_{dB} = 10 \times log_{10}(PAPR) \tag{3.21}$$

3.5.4.2. PAPR Distribution

The complex baseband signal of an OFDM symbol with N SCs is described in [3] through the following expression:

$$x(t) = \frac{1}{\sqrt{N}} \sum_{n=1}^{N} a_n e^{j\omega_n t} \tag{3.22}$$

Where: a_n are the modulating symbols. The amplitude of the OFDM signal has Rayleigh distribution with zero mean and variance of N times the variance of one complex sinusoid, because the real and the imaginary values of $x(t)$ become Gaussian distributed for large numbers of SCs, each with a mean of zero and a variance of $1/2$ [3] [37]. Therefore, the amplitude of the OFDM signal has a Rayleigh distribution. The power distribution becomes a central chi-square distribution with two degrees of freedom and zero mean with a cumulative distribution given by [3]:

$$F(z) = 1 - e^{-z} \tag{3.23}$$

Assuming the samples to be mutually uncorrelated, which is true when there is no oversampling, the Cumulative Distribution Function (CDF) for the PAPR per OFDM symbol is defined in [3] [37] as the probability that the PAPR of the OFDM signal exceeds a certain threshold:

$$P\{PAPR \leq z\} = (1 - e^{-z})^N \rightarrow P\{PAPR > z\} = 1 - (1 - e^{-z})^N \tag{3.24}$$

Where: N is the number of SCs and z is the threshold.

The peak power distribution is difficult to present as an exact solution. When oversampling is applied, the samples can no longer be assumed to be mutually uncorrelated, and the expression above is no longer valid. An approximation is proposed in [3], which is made by assuming that the distribution for αN SCs and oversampling can be approximated by the distribution for αN SCs without oversampling, with $\alpha > 1$. Hence, the effect of oversampling is approximated by adding a certain number of extra independent samples. Considering this, the PAPR distribution accounting for oversampling becomes:

$$P\{PAPR \leq z\} = (1 - e^{-z})^{\propto N} \tag{3.25}$$

3.5.4.3. PAPR Reduction

There are several ways to reduce the Peak-to-Average Power (PAP). The simplest approach to reduce PAP is to clip the signal. Clipping is performed on OFDM symbols by defining a threshold over the amplitude in time domain, and setting any value greater than the limit equal to the boundary. However, this solution can be associated to some inconvenient. In the first place, by directly cutting the peaks in amplitude a distortion is introduced in the OFDM signal, which will degrade the BER. In second place, the non-linear distortion introduced by clipping results is an increased out-of-band radiation [3] [37].

The clipping operation can be seen as the multiplication of the OFDM signal to a rectangular window function, where the window amplitude is one where no clipping is needed, and lower than one where clipping is needed. Using the same concept, the out-of-band interferences can be minimized if a non-rectangular shaped window, ideally as narrow as possible, is multiplied to the large signal peaks. On the other hand, the window should not be too long, because it implies that more samples will be affected, therefore also increasing BER degradation [3].

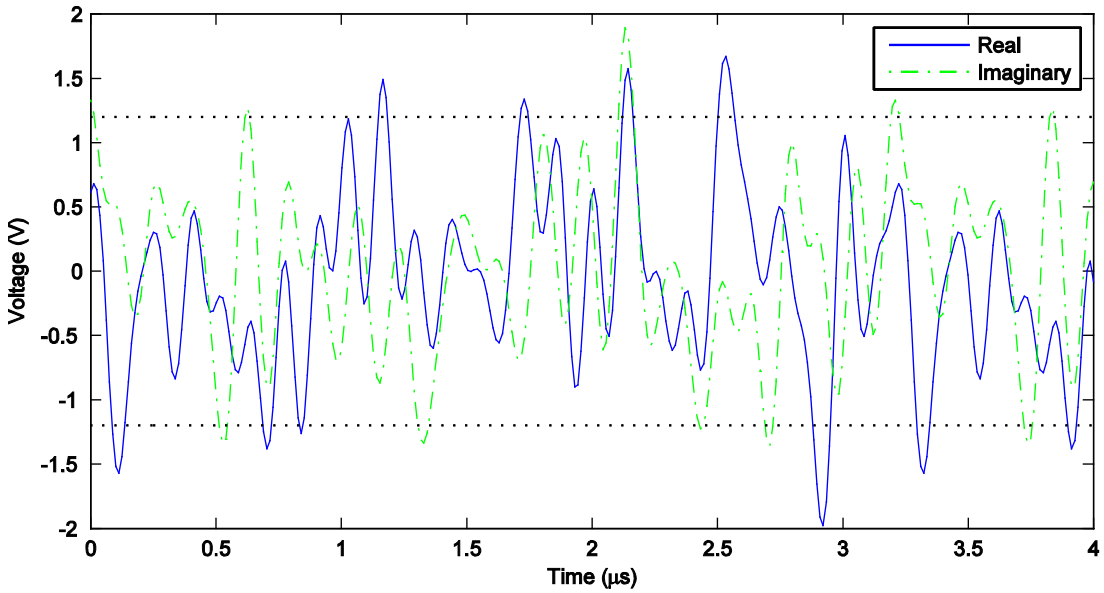

Figure 3.11 – Clipping of 2 dB for a complex OFDM symbol of 20 MHz channel spacing, with 4-fold oversampling.

The clipping operation can be described mathematically as an approximated signal where a certain threshold limits the amplitude while the phase is left unmodified [15]:

$$\bar{x}(t) = \begin{cases} x(t), & |x(t)| \leq A \\ Ae^{jarg(x(t))}, & |x(t)| > A \end{cases} \tag{3.26}$$

Where: $x(t)$ is the original signal; $\bar{x}(t)$ is the clipped signal; A is the maximum amplitude allowed and $arg\big(x(t)\big)$ is the phase of $x(t)$.

The clipping operation must be performed on the analog signal, or on an upsampled version of the digital signal, because as the signal is converted from digital to analog, the high peaks can occur between discrete samples. A relation between the clipping power and the original signal's power is given in [15] as the clipping power ratio, which the following equation defines in decibels as:

$$CR_{dB} = 20 \times log_{10}(A/\sigma) \tag{3.27}$$

Where: σ^2 is the power of $x(t)$.

In packet-based systems, the error probability increases as the PAPR gets worse. When a transmission fails, the packet is retransmitted. If its PAPR is too high, the situation might happen where the packet never passes through. One other way of reducing PAPR in a packet-based transmission system is the use of a standard scrambler. By generating a new random seed for each transmission, the scrambler can ensure that the transmitted data is uncorrelated with preceding and following transmissions. Hence, by scrambling with different seeds at each transmission, independent PAPR can be assured between retransmissions, which results in independent error probability [3].

3.6. Summary

In this chapter, an introduction was made to OFDM application in wireless IEEE 802.11a packet-based system, because it is the OFDM modulation reference chosen for further development in this dissertation. In addition, an overview was made on the use of OFDM technology with optical systems. The main channel effects typical to each domain were introduced, and some mathematical models were also presented. It was seen that if a RoF network is considered, the dispersion and interference sources from both electrical domain and optical domain must be considered in order to perform an accurate analysis of the system performance.

Analysis methods that allow assessment of the system were described as well. EVM provides an effective way of measuring the distance between the expected complex constellation location and the received one. EVM analysis is a good evaluation choice, because with simple calculations an estimate of the constellation degradation can be obtained even before needing any further processing, such as demodulation and decoding. PAPR is a significant drawback on OFDM systems, and therefore it is important to monitor its level and effect for different parameters in the model used.

Chapter 4. OFDM System Simulation using Matlab

4.1. Introduction

The importance of the numerous parameters that define the OFDM model was introduced in the previous sections. It was explained that several of them, such as FEC coding and cyclic extension, are fundamental to ensure the OFDM transmission's robustness against different error sources. However, they also imply losses in transmission efficiency in terms of bandwidth, power and bit rate. Therefore, it is desirable to understand the relation between the benefits they provide and the efficiency loss.

Other parameters, such as the complexity of the data modulation scheme and windowing, can also contribute to the sensitivity of the overall system. This will be studied by exposing the model to several common adverse situations, such as random noise and reflective environments that cause multiple paths with different delays and attenuations.

Carrier and timing synchronism are of vital importance in OFDM systems. Failures in synchronism have strong negative impact on the system, because they origin ICI and ISI. In this chapter, these effects will be demonstrated.

An important weakness inherent to OFDM technology is its tendency to engender high PAPR. There are several ways of reducing PAPR. One technique known as peak power clipping will be investigated. In addition, by providing entropy to the transmitted data, scrambling can also improve the PAPR. Scrambling should also enhance the power distribution over the band. It will be verified as well that by windowing the transition between adjacent OFDM symbols, less energy is lost due to spectral regrowth.

In this chapter, the performance of the OFDM system will be studied using classic references, such as SNR and BER. Furthermore, EVM will be used to measure the system's performance.

4.2. Matlab Simulation Model

Matlab is a software tool developed by *The MathWorks* for numerical computing and programming language. It is designed for engineering analysis and mathematical computing and visualization. *Matlab* is built to perform fast computing and manipulation of large arbitrary matrices. Currently, *Matlab* includes many toolboxes that support a large number of application areas. Amongst many others, the toolboxes of most interest for this project are Communications Systems, Digital Signal Processing and Data Acquisition [38].

4.2.1. Base Structure of the Simulator

The main simulator was implemented by developing a number of functions in a modular way, following closely the model introduced in Figure 2.1. It allows the creation of arbitrary OFDM waveforms in both baseband and passband, for arbitrary modulation and timing parameters. The base simulator structure is presented in Figure 4.1. In the process of building arbitrary OFDM signals from an information source, the data states can be categorized into four distinct types, which are: binary digits; modulated constellation samples; OFDM modulated samples; RF signal samples.

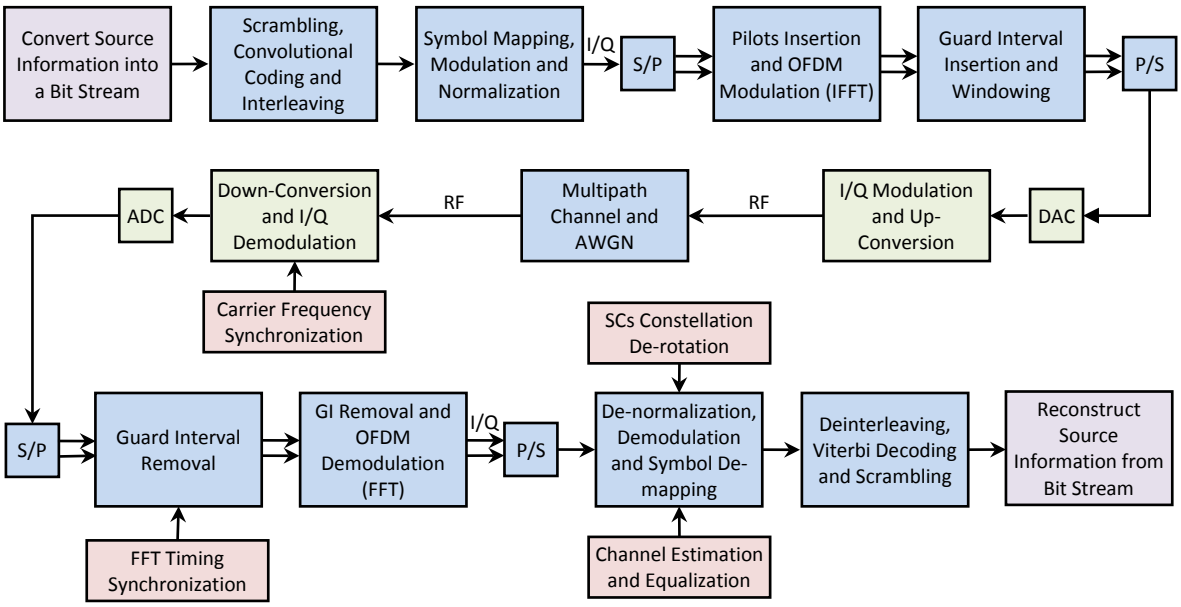

Figure 4.1 – Flow diagram for the base structure of the *Matlab* simulator.

Based on user input, a set of functions defines the configurations for each of these states, and returns the simulation configurations as *Matlab* structures. They are used for both transmission and reception definitions, and they provide control by enabling or disabling simulation parameters, such as source coding, modulation schemes, signal shaping, channel effects and channel compensation.

The user can provide objects for transmission, such as JPEG, BMP and PNG pictures, or TXT files. The simulator extracts the information into binary format representation, performs the simulation, and attempts to reconstruct the files. Scrambling becomes particularly useful in that situation, because this kind of data does not have a random distribution. In addition, large binary random sequences can be generated.

For the binary state, the configuration structure includes flags to control the activation of scrambling, convolutional coding and interleaving. The chosen coding rate is also part of this

structure. The estimation of BER is achieved by comparing the original binary stream to the received bit streams.

When the bit stream has been manipulated as required by the user, the constellation modulation takes place. The configuration structure contains the modulation parameters for the data SCs, such as the modulation order and type, the number of bits per modulated symbol, and the normalization power. As the signal is received, the EVM is estimated using the reference constellation samples and the received ones, with and/or without previous channel compensation.

The next stage consists in the OFDM modulation, which depends on a fair number of parameters. The user controls the base properties of the OFDM signal, such as the FFT length, the number of data SCs and pilot SCs, the GI length, the windowed transition length and oversampling. From that information, the simulator determines the SCs indexes and the symbol timing-dependent parameters in samples. The resulting structure holds all the information necessary to perform the OFDM modulation while taking into account the expected baseband signal type. The series-to-parallel conversion, and vice-versa, also depends on the number of data SCs. As the baseband OFDM signal is created, the CDF of the PAPR can be determined, and PAP reduction techniques like clipping can be investigated. At the receiver, if the phase offset correction is enabled, the pilot SCs are used to correct any rotation of the constellation samples.

To observe the effect of carrier frequency offsets, as well as IQ amplitude and phase imbalance, IQ modulation can be simulated. When a passband RF signal is generated this way, the multipath channel is simulated by creating the signal as seen by the receiver, that is, as the sum of several delayed and attenuated versions of the original RF signal. For baseband implementation, the carrier and time synchronization errors models and the time-dispersive channel model in use are those introduced in Chapter 2. AWGN and Rayleigh multipath channel models can be applied to the signal if required by the user. For AWGN channel, the specified SNR is given as E_b/N_0 and is converted to E_s/N_0 considering the OFDM modulation characteristics. For multipath environment, N taps are specified by the user, and N random complex impulses are generated. Then, the CIR is convoluted with the baseband TD signal to create the received signal.

4.2.2. Baseband to Passband Conversion

In a typical communication system, the signal is up-converted at the transmitter and down-converted at the receiver. Up-conversion consits in taking the baseband signal and converting it to passband. This is also known as mixing, and is achieved by multiplying the signal with a complex sinusoidal carrier with a specific center frequency. At the receiver, the signal is down-converted by multiplying the real RF carrier with a complex sinusoidal signal having the same center frequency.

The signal resulting from down-conversion is complex and has unchanged energy content. The down-conversion process also includes low-pass filtering to remove the negative frequencies and noise outside the desired bandwidth [39].

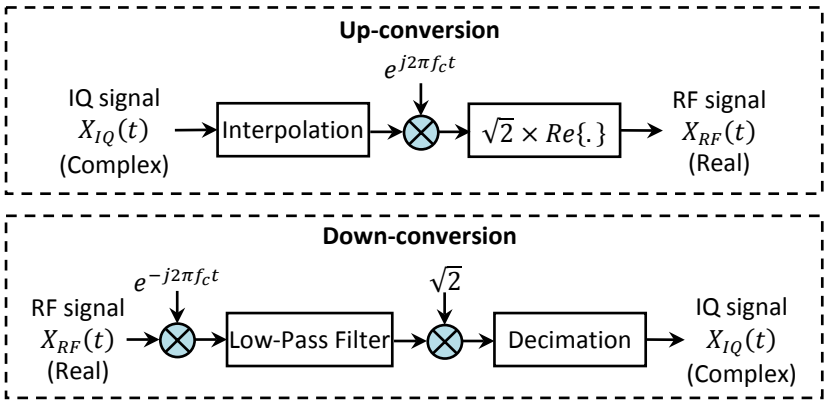

Figure 4.2 – Up/Down-Conversion with IQ Modulation/Demodulation [39].

In a practical transmission, it is usually necessary to oversample the signal because the TF of the transmitter and receiver hardware reduces the useable bandwidth, if compared to the theoretical one given by the sampling theorem [3]. The Nyquist sampling theorem states that the frequency content of a signal can be completely reconstructed if the sampling rate exceeds a minimum of twice the frequency of the highest frequency component of the signal. For this reason, IQ modulators are usually preceded by a data interpolation filter to up-sample before up-converting, which is reversed at the demodulator by a decimation filter to down-sample the data back to its original sampling rate. The factor $\sqrt{2}$ is multiplied at both the transmitter and the receiver to account for the loss of energy in the signal that occurs by taking only the real part of the complex signal [39].

This baseband to passband conversion was implemented for completeness, in order to observe the effect of the filters and of carrier frequency offsets on the signal with more than just the baseband models described in Chapter 2. Pulse shaping with oversampling can be applied, such as a Square Root Raised Cosine transmission filter with a matching filter at the receiver. Alternatively, direct oversampling can be experimented at the signal generation by inserting more empty guard SCs, that is, by increasing the IFFT length while maintaining the same number of SCs. The signal is recovered with simple low-pass filtering when the receiver down-converts the signal.

4.2.3. Construction of IEEE 802.11a PHY Frames

A less flexible version of the main simulator was also adapted to put into practice the IEEE 802.11a standard chosen for this dissertation. When applied, the scrambling, convolutional coding, interleaving, and pilot SCs are generated based on the specifications available in [2]. This implementation of the simulator allows for the generation of frames as described in Section 3.2, that

is, the PLCP Preamble and the SIGNAL sequence are created and are inserted before each DATA packet. These additional components of the frame are used by the receiver to carry out the synchronization, to perform the channel estimation and to apply phase offset corrections.

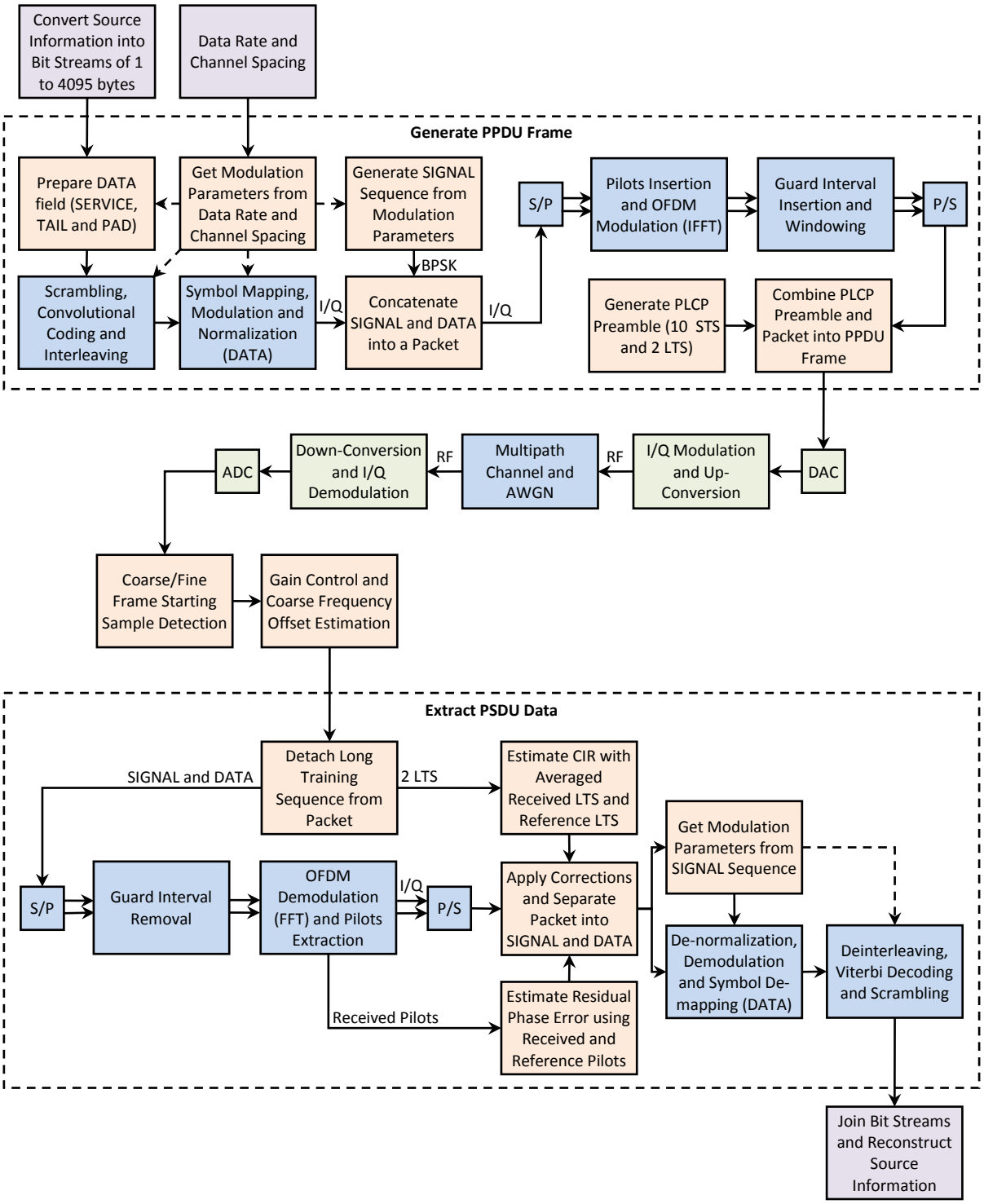

Figure 4.3 – Diagram of the implemented *Matlab* simulator, based on IEEE 802.11a PHY.

The complex OFDM signal is created based on the DATA RATE, the CHANNEL SPACING and the source provided by the user. The PSDU length can also be specified, but it must remain within 1

byte to 4095 bytes to comply with the specifications. Based on this information, the simulator determines the corresponding modulation-dependent parameters, and if necessary breaks the bit stream generated at the source into a number of packets. The OFDM modulation-dependent parameters, such as the number of SCs, the FFT length and the GI length, are those specified by the standard and must remain unmodified in this version of the simulator. For each packet of binary digits, the PPDU frame is generated as described below.

Based on the modulation-dependent parameters, which include the convolutional coding rate and the modulation order, and on the PSDU length, the SIGNAL bits are defined. Then, the SIGNAL is modulated at the lowest supported data rate, which is BPSK with convolutional coding at rate $R = 1/2$. This way the loss probability of this symbol is minimized, which is important because it contains the information that the receiver needs to perform the OFDM demodulation. The modulated SIGNAL consists in precisely 48 samples, corresponding to the 48 data SCs.

The DATA field is also relying on the modulation-dependent parameters. This field is properly prepared by appending SERVICE, TAIL and PAD bits to the source bits. The PAD bits depend on the coding rate and the number of bits per constellation sample, that is, the number of coded bits per SC. As this is completed, the prepared bits are scrambled, convolutionally coded and interleaved. The scrambler randomizes the bit stream to avoid any concentration of power in narrow frequency bands. Convolutional coding introduces redundancy, hence increasing the system's capacity to recover from errors. Finally, interleaving ensures frequency diversity, thus enhancing the robustness of the system. Source coding is entirely implemented based on the specifications available in [2].

At this point, the DATA packet is modulated using conventional schemes, and serial-to-parallel conversion takes place to pre-allocate each FD sample to its corresponding SC within its OFDM symbol. The modulated samples are normalized to an average power $P_o = 1\ W$, as indicated in [2]. Then, the 48 SIGNAL samples and the N_{SYM} segments of DATA, each with 48 samples, can be concatenated into a single block before proceeding to the OFDM modulation.

In this simulator, the generation and insertion of pilot SCs is part of the OFDM modulation process, as they depend on the number of symbols that will be generated. First, the samples from each chunk of data are distributed among the available frequencies. This is done by starting the allocation on the negative frequencies to the left, and going towards the positive frequencies to the right. The SC at the center is DC, and remains empty because it is likely to endure higher distortions. The BPSK modulated pilot SCs are generated and they are allocated among the data SC. This process is illustrated in Figure 3.1 from Chapter 3, and an example is also given for arbitrary modulation in Appendix B. Once the SC placement has ended, each chunk of samples is shifted to the correct position by taking all samples from the central to the rightmost position, and moving them to the left

of the remaining samples. The modulation is then achieved by applying the IFFT to each chunk of samples, resulting in TD complex OFDM baseband symbols with $N_{FFT} = 64$ samples (without oversampling by IFFT zero padding).

By default, a GI is created with a CP by copying samples from the end of each symbol to the beginning, with length set to $N_{GI} = N_{FFT}/4 = 16$ samples, and with a windowed transition that shapes $N_{WIN} = N_{GI}/8 = 2$ samples. Hence, the resulting effective cyclic extension is composed by $N_{GI} - N_{WIN} = 14$ samples, while each OFDM symbol is composed by 80 samples. The CP creates periodicity for each OFDM symbol, which greatly improves the resilience to time-dispersive multipath channel effects. The windowed section reduces spectral regrowth by smoothing the transition between symbols. Once this is concluded, the OFDM symbols are placed in series to generate the OFDM baseband signal.

To complete the frame construction process, the PLCP preamble is created and placed at the beginning of the OFDM signal. The result of this final combination is an IEEE 802.11a PHY baseband frame ready for up-conversion, which is composed by 10 Short Training Symbols, 2 Long Training Symbols, 1 SIGNAL symbol and N_{DSYM} DATA symbols.

As it was established previously, the application of channel effects and hardware impairments, such as local oscillator frequency offsets or IQ imbalance, depends on whether the simulation is performed for a baseband or for a passband signal. To experiment the synchronization mechanisms, each transmitted frame can be placed in a random position between sections of random noise, having variable amplitude and length.

The PLCP preamble is the main synchronization mechanism of this standard. The receiver knows the characteristics of the original PLCP preamble. Hence, the knowledge of properties like the periodicity and the power distribution of the preamble can be used to enhance synchronization, estimate the necessary amplification gain and compensate for carrier frequency offsets. As the signal is down-converted, the receiver takes advantage of the good cross-correlation properties of the STS to estimate coarsely the frame start. In this study, to improve the detection conditions, null powered intervals are introduced between adjacent frames. Then, based on the coarsely detected starting sample of the frame, windowed refined estimation can provide a more accurate location of the starting sample. Assuming the synchronization to be successful, the STS is then used to determine the amplification gain needed to get the correct signal power, and also to correct roughly carrier frequency offsets on the frame.

At this point, the receiver can proceed to PPDU frame dismantlement and PSDU data extraction. The process begins by first separating the PLCP Preamble from the remaining part of the

frame. The two long symbols that compose the LTS are extracted from the PLCP preamble, OFDM demodulated and averaged. Using this average together with the known long sequence, the TF of the CIR is estimated. The rest of the frame is converted from series-to-parallel and OFDM demodulated. Channel distortion compensation is achieved by doing a point-wise multiplication of the FD received data chunks with the estimated CIR. As long as the time-dispersion introduced by the CIR remains within the GI range, the effect of timing errors are restrained and introduce only a phase rotation. By interpolating between the pilot SCs along the FFT length, an estimate of the linear phase rotation is determined for each individual OFDM symbol. This final rectification is achieved through point-wise multiplication of each OFDM symbol in the FD by its phase rotation estimate.

After the received SIGNAL samples are detached from the DATA samples, they are demodulated and decoded, and the resulting binary digits are used to define the DATA demodulation parameters. Based on these definitions, the demodulation, deinterleaving, decoding and scrambling of the DATA packet takes place. Finally, the PSDU payload is recovered by discarding the SERVICE, TAIL and PAD bits, and can be recombined into the received information.

4.3. The Effect of Time Synchronization Errors

Time synchronization errors can occur in several different ways, namely due to delays introduced by filters, delay spread from a multipath channel, sampling frequency offsets or an error in frame starting sample detection.

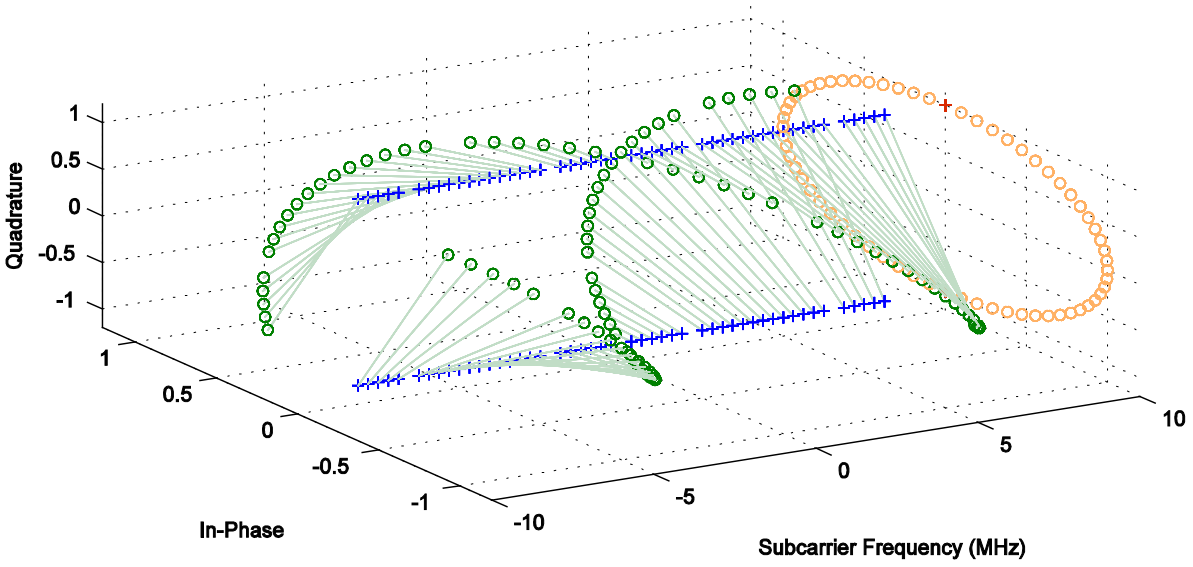

Figure 4.4 – Influence of a timing offset δt = 0.5 μs, corresponding to a 1 sample offset within the GI on the received BPSK constellation. "+" represent the ideal constellations state and "o" the rotated received samples.

As discussed previously, the CP inserted in the GI is the main mechanism employed to combat timing errors in OFDM transmission. However, if the time in samples exceeds the length of

the GI, then it can be said that the CIR is generating time synchronization errors, and therefore ISI arises. It was seen in Section 2.4.5 that a timing offset translates into a shift in the integration interval of the receiver filter, which is the FFT. Hence, to simplify the concept it can be said that a timing offset is related to the starting sample of the FFT window. A timing offset existing in one sample introduces a FD phase shift of $\pm\pi$ in the SCs at the edges of the FFT window. Therefore, a progressive linear phase rotation is inflicted to the samples composing the signal constellations.

Figure 4.4 demonstrates this effect. As the SC frequencies grow, the respective phase rotation increases progressively. The superposition of all the constellations samples appears as a circular effect where samples spread radially to the left and right of the ideal location. This is true as long as the time shifted FFT window remains within the OFDM symbol boundary (within the GI duration). If not, part of the demodulated samples belongs to the adjacent OFDM symbol, which results in severe distortion of the received constellation.

4.4. The Effect of Frequency Synchronization Errors

Carrier synchronization errors usually occur when there is a small frequency mismatch between the local oscillators of the transmitter and the receiver, which causes frequency offsets. In other words, instead of being centered on DC at $0\ Hz$, the received baseband signal is centered at a frequency δf.

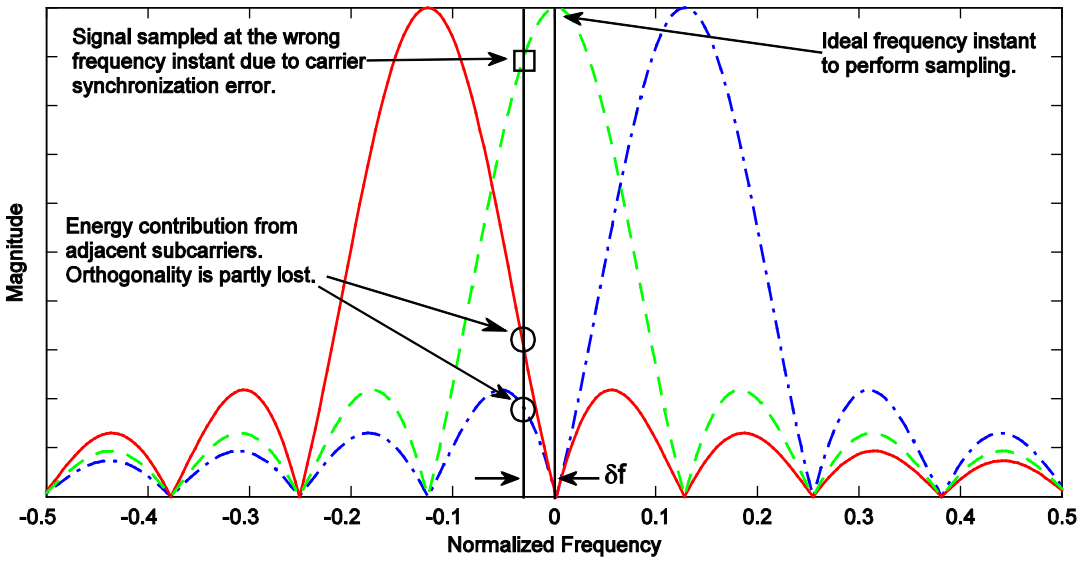

Figure 4.5 – ICI originated by Carrier Synchronization Error.

It was discussed in Section 2.4.6 that a frequency offset appears in the received signal as a frequency shift alongside a phase offset. The frequency shift causes the sampling points at the receiver to take place outside the ideal peak power location in the spectrum, where the energy

contribution from the overlapping SCs is not null. Thus, the frequency shift causes orthogonality between adjacent SCs to be partially lost and introduces ICI. Such situation is illustrated in Figure 4.5, where the magnitude of three overlapping SCs is presented, which are superimposed in the OFDM signal spectrum. Due to the existing frequency offset, the received signal is sampled at the wrong frequency instants by the FFT demodulation, and ICI arises.

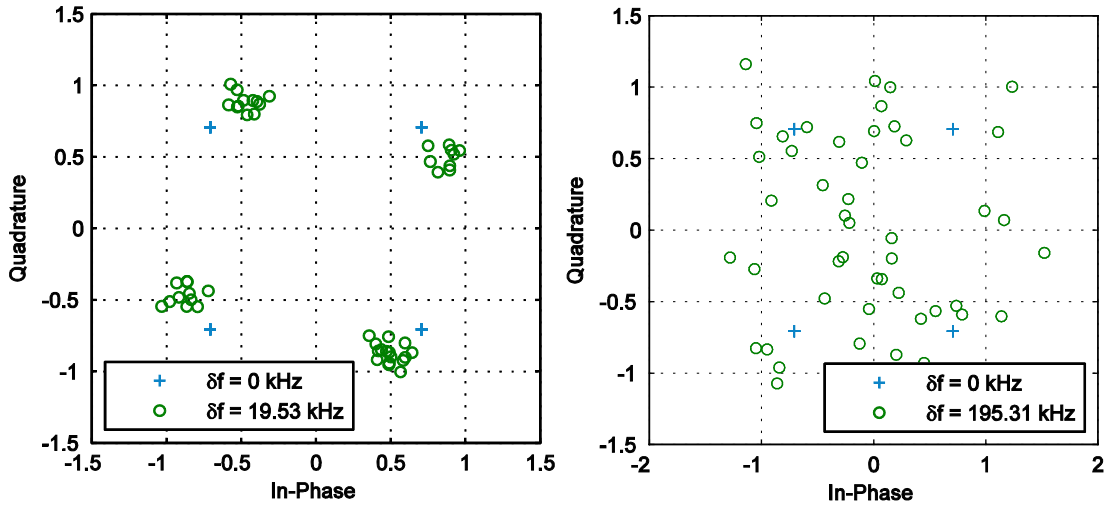

Figure 4.6 – Constellations distorted by ICI caused by frequency offsets δf = ΔF/16 on the left, and δf = ΔF/16×10 on the right, where ΔF = 312.5 kHz is the SC spacing for a 20 MHz channel spacing.

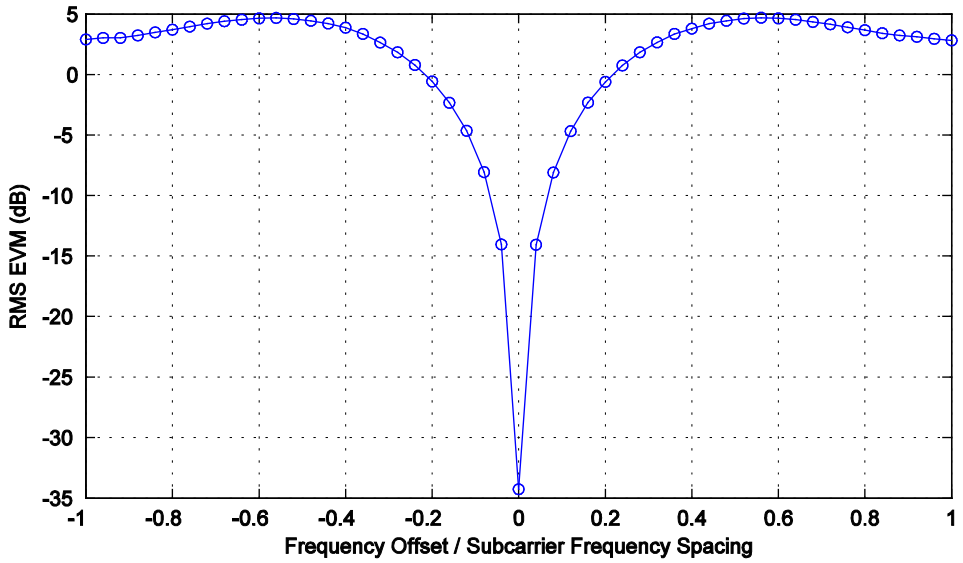

Figure 4.7 – Averaged EVM for different frequency offsets. The SC spacing is ΔF = 312.5 kHz for a 20 MHz channel spacing, and the frequency offset varies within the interval δf = [-ΔF: ΔF].

As mentioned previously in Section 2.4.6, for small frequency offsets the effect of the generated ICI can be modeled as additive random noise that affects the SNR. In addition, the phase offset causes a global rotation of the data constellation. Such behavior can be observed in Figure 4.6, where the "+" show the correct constellation state, and the "o" denote the received samples distorted by ICI. For a frequency offset of $\delta f = 19.53\,kHz$, a global phase rotation of the

constellation is clearly noticeable, together with a slight dispersion of the samples. For worst cases, the constellation appears as a "cloud" of samples, as it is observed when $\delta f = 195.3\ kHz$.

Figure 4.7 presents an average of the RMS EVM computed for a sweep of frequency offsets in AWGN channel. Notice that, as expected, while the condition $\delta f < \Delta F$ is observed, the EVM degrades towards smaller negative values as δf approaches ΔF. That is, the error percentage in constellation deviations is increasing. For larger frequency offsets, the transmitted data symbols are shifted by one or more positions in the frequency direction, which means that the current SC appears as the adjacent one to the receiver. When this occurs, the receiver can no longer distinguish the correct SC from those introducing undesired energy contributions, which means that orthogonality has been lost.

Note that the IEEE 802.11a standard specifies a frequency accuracy of $\pm 25\ ppm$ around the center frequency. For a $5\ GHz$ carrier frequency, this corresponds to a frequency variation considered acceptable, that is, a maximum frequency deviation within the range:

$$\delta f = (5\ GHz \times \pm 25\ ppm)/1000000 = \pm 125\ kHz.$$

For instance, considering a channel spacing of $20MHz$ and a FFT length of 64 samples, the SC spacing is given by $\Delta F = 312.5\ kHz$. This means that the carrier frequency deviation must be confined within values under $\delta f = \pm 156.25\ kHz$ in order to be correctable.

4.5. The Effect of AWGN Channel

In AWGN channels, the unaltered OFDM modulation is expected to achieve neither performance improvement nor loss. As in single carrier systems, it is the data modulation order that dictates the sensitivity to random noise, that is, the energy required to attain a determined level of BER. In terms of simulation, it is important to scale properly the signal as discussed in Section 3.5.2 to compare fairly the different schemes. Figure 4.8 a) illustrates this statement, where the theoretical curves generated using *Matlab* built-in functions are the dashed lines. To achieve this ideal relation, the OFDM signal is modulated without creating a GI because, as it was discussed in Section 2.3.4, the cyclic extension involves a loss in SNR due to the additional power used for transmission. It can be seen that the empirical OFDM BER curves fit perfectly the theoretical curve for conventional non-multi-carrier systems. Hence, it can be concluded that the uniform noise contributes to the SNR of each SC in the OFDM system, and that the overall result is equivalent to the effect on single channel systems.

The SNR loss caused by the GI is represented in Figure 4.8 b), and is estimated to be nearing 1 dB for a GI composed by a CP with 1/4 of the 64 samples of the FFT. The SNR loss observed is a small

inconvenient compared to the greatly improved robustness of OFDM technology against time synchronization errors, which are common in multipath interfering scenarios.

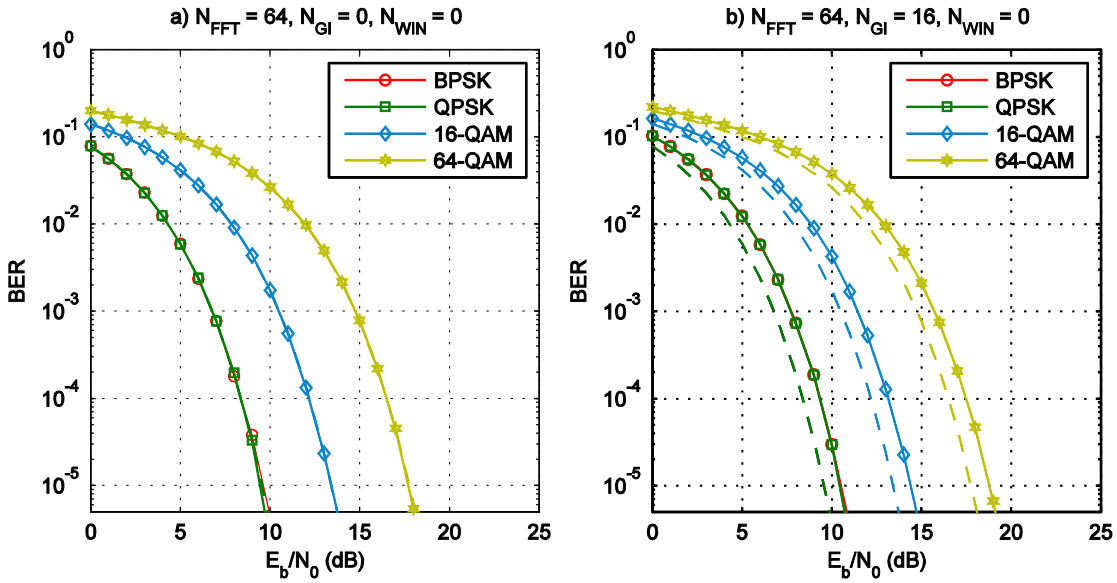

Figure 4.8 – BER versus E_b/N_0 in AWGN channel for the modulation schemes used in IEEE 802.11a standard. The dashed lines are the theoretical curves for conventional systems, obtained using *Matlab* built-in *berawgn()* function.

Notice that the curves for BPSK and QPSK modulation schemes are almost equivalent. This happens because QPSK can be seen as two orthogonal BPSK systems, one in the real component and the other in the imaginary component of the system. Therefore, in terms of energy per bit, BPSK uses twice the energy of QPSK because the imaginary part of the signal is unexploited. In other words, if the rate and power are the same for BPSK and QPSK, then BPSK systems use twice as much bandwidth as QPSK to achieve the same BER.

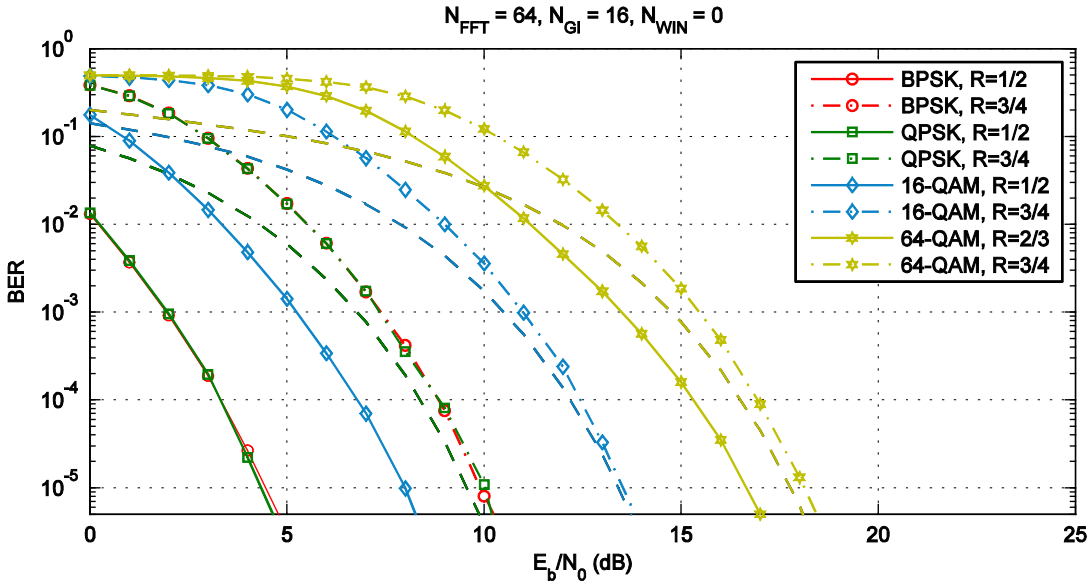

Figure 4.9 – BER versus E_b/N_0 in AWGN channel for the modulation schemes used in IEEE 802.11a standard with convolutional coding. The dashed lines are the theoretical curves for conventional systems.

Channel coding techniques, such as convolutional coding, involve information redundancy. Thus, in terms of energy used to execute a transmission, it means that additional power is required, because more bits are transmitted to achieve the same communication. In general, for coded but non-punctured transmissions the results in Figure 4.9 show significant improvements. However, when observing the BER as a function of the E_b/N_0 necessary to achieve a correct reception with punctured transmissions, an improvement is noticeable only at a certain point, which varies from a situation to another. For instance, the BER of the 64-QAM modulation scheme with a coding rate of 2/3 degrades when $E_b/N_0 < 10\ dB$, but then improves for higher values. These results suggest that a random distribution of the errors along the received signal, which is more likely to occur as the E_b/N_0 increases, is more prone to be corrected by the decoder. Hence, for severe E_b/N_0 conditions, if too many errors occur with higher modulation orders and with punctured coding, the incapacity of the convolutional decoder to recover translates into a loss of performance.

4.6. The Effect of Rayleigh Multipath Channel

One of the important characteristics of OFDM systems is the strong resilience to multipath time and frequency-selective fading environments. This is due mainly to the cyclic extension of the symbols, and is improved even more by using channel FEC coding techniques and creating diversity with interleaving.

The Rayleigh multipath channel model in use is frequency-selective. However, it was seen in previous sections that the channel is expected to appear as a flat fading channel for each SC, that is, each SC is expected to experience independent Rayleigh fading. Therefore, the OFDM signal passing through multipath Rayleigh fading channel should have a BER versus E_b/N_0 relation very similar to one from a single sub-channel experiencing Rayleigh flat fading.

For simulation purpose, the concept of multipath surrounding can be seen as a single impulse at the transmitter that is received as a train of impulses, where each impulse has different delay and attenuation. The complex component of each tap can be defined as a Gaussian random variable with zero mean and variance 1/2.

It was demonstrated in Section 2.4 that, as long as the number of taps in the channel is lower than the GI duration, ISI and ICI are prevented. The GI created with a CP generates a periodicity in each OFDM symbol, and it is known that the sum of a sinusoidal with a delayed version of itself modifies the phase and amplitude, but not the frequency components of the sinusoidal. Hence, orthogonality is maintained even in a multipath environment as long as no delay forces the FFT window at the receiver to take samples from an adjacent OFDM symbol. Figure 4.10 a) presents such situation, where the OFDM signal with a GI of 16 samples passes through a 10 taps multipath

channel. In these examples, the channel is assumed to be perfectly estimated at the receiver, thus providing optimal results. As expected under these conditions, the experimental data follows the theoretical curve when the maximum delay is restricted within the GI duration.

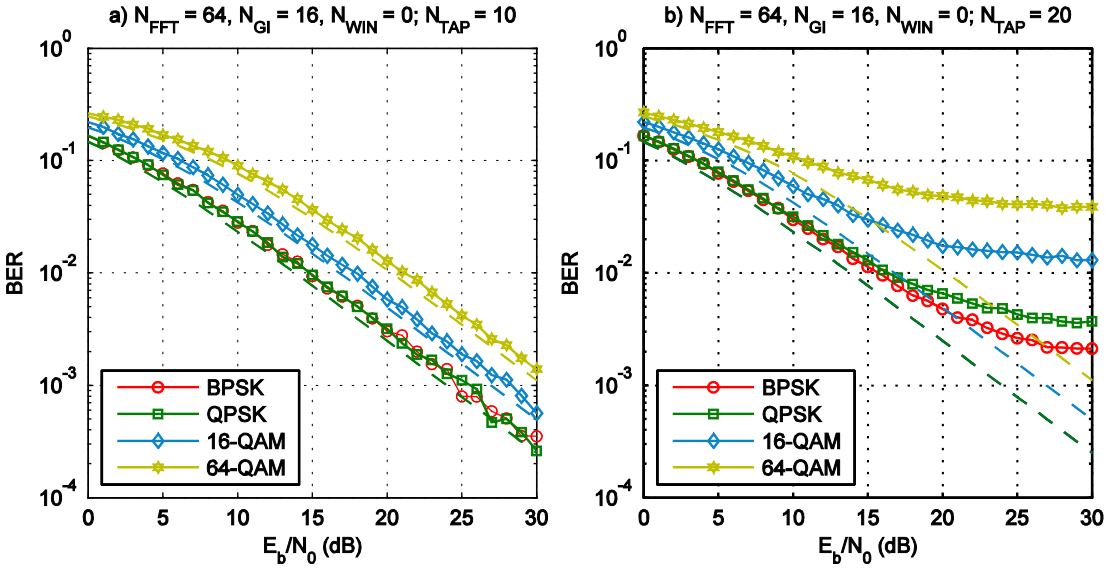

Figure 4.10 – BER versus E_b/N_0 in AWGN and Rayleigh channels with 10 taps and 20 taps, without convolutional coding nor interleaving. The dashed lines are the theoretical curves for conventional systems, obtained using *Matlab* built-in *berfading()* function.

In contrast, when the maximum delay caused by the channel overcomes the GI duration, severe distortion is introduced by ISI, even when the channel TF is known. As demonstrated in Figure 4.10 b), the BER no longer follows the theoretical Rayleigh curve and reveals more degradation, despite the increasing SNR.

When OFDM symbol windowing is applied, a portion of the symbols edges are modified by the window function that smoothly brings the samples down to zero amplitude. Then, these smoothed transition samples are summed between symbols so that the proper symbol length is not exceeded. Hence, these transition samples cannot be considered as part of the added periodicity, which means that they reduce slightly the effectiveness of the GI.

4.7. Windowing and Spectral Regrowth

In OFDM systems, each symbol is modulated individually. Then, the OFDM symbols in parallel are converted to series. However, it was explained in Section 2.3.5 that when assembling the OFDM symbols in series, two adjacent symbols rarely have the same phase and amplitude, which results in spectral regrowth. In this case, spectral regrowth is seen as power on a range of frequencies extending on each side of the OFDM power spectrum. This effect reduces the power efficiency of the spectrum, and creates interferences. Windowing is one way to reduce spectral regrowth. In OFDM systems, this is usually achieved by windowing each OFDM symbol, and summing the windowed

transitions from one symbol to another. In this dissertation, OFDM symbol windowing is implemented in time domain. The result is a smooth transition between adjacent OFDM symbols, and an effective decline in the amount of power distributed out of the band.

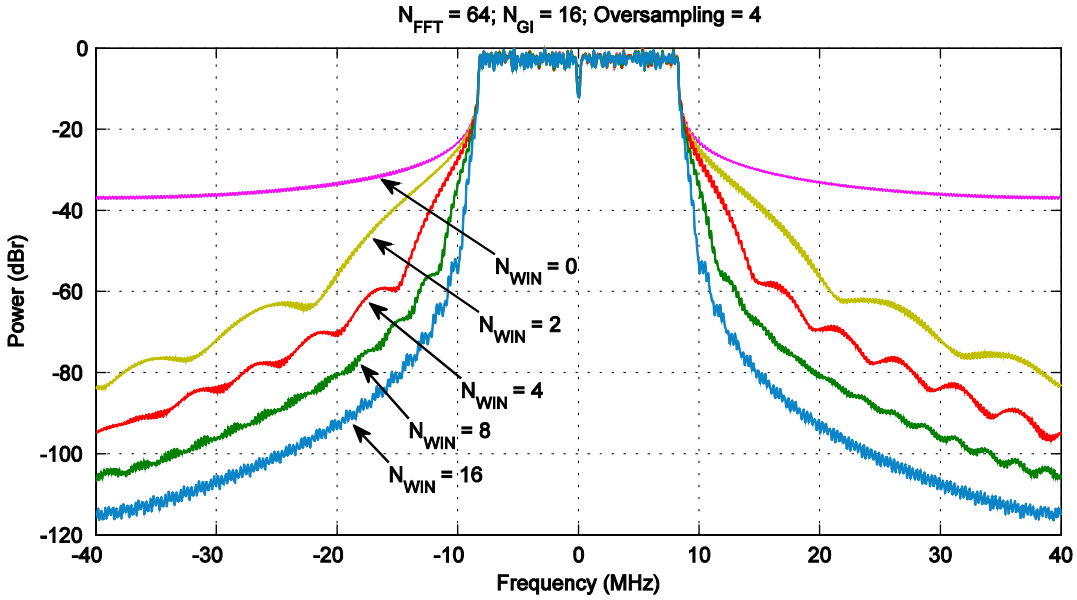

Figure 4.11 – OFDM power spectrum for several windowed transition lengths.

It can be observed in Figure 4.11 that windowing improves the power spectrum very effectively. As the number of windowed samples increases, the amount of power located outside the band diminishes greatly. However, it is important to recall that the windowed section of the symbols modifies the CP that is placed in the GI. Hence, although the GI duration remains the same, the effective CP that creates the periodicity for each OFDM symbol becomes smaller as the windowed transition length increases. Therefore, windowing reduces the OFDM system's robustness to multipath fading environments. This means that the system designer must reach a compromise between improving the spectral efficiency and increasing the resilience to the time-dispersive effects of the channel .

4.8. Improving the PAPR

The theoretical introduction to this subject given in Section 3.5.3 suggests that PAPR increases with the number of SCs. This makes sense, since it is known that the OFDM signal consist in a sum of SCs with orthogonal frequencies (verified in Appendix A). PAPR rises when many of the SCs that are summed have high amplitude, that is, when constructive superposition of the SCs occurs. Hence, if there are less SCs, then the probability to generate high peaks in the resulting OFDM signal is reduced. Figure 4.12 shows the distribution of PAP increasing as the number of SCs increases.

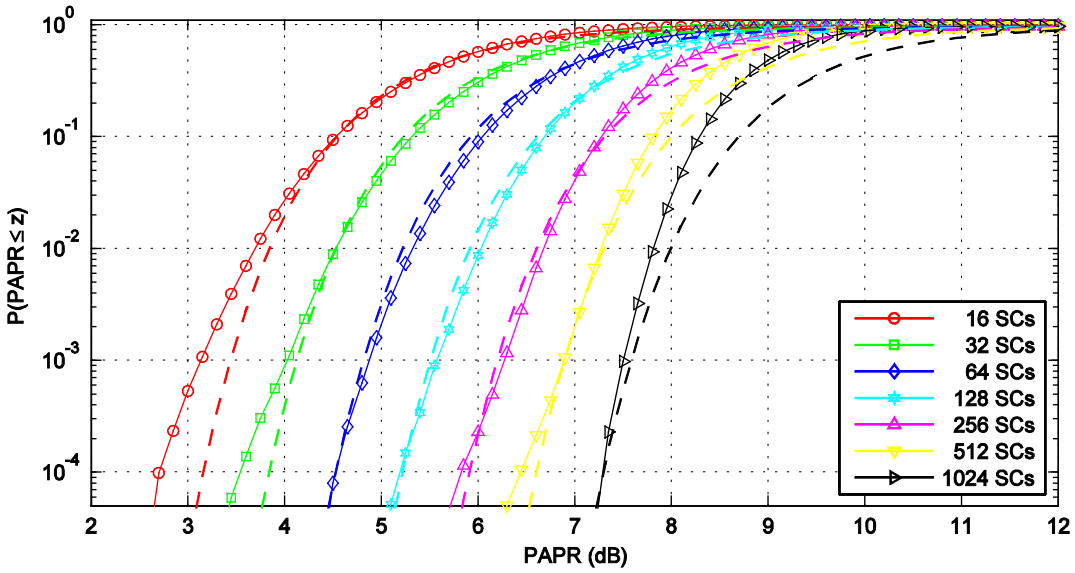

Figure 4.12 – PAPR Distribution for different numbers of SCs, with 4-fold oversampling. The dashed lines are the theoretical approximation (due to oversampling, with α = 3.3).

Based on the definitions, it becomes easy to understand that the worst possible case of PAPR expected to occur in IEEE 802.11a standard should never reach values beyond approximately $10 \times log_{10}(48 + 4) = 17.17\ dB$. That is, the highest potential peak in relation to the average has its amplitude limited by the number of used SCs. However, when a scrambler is used, such situation is very unlikely to occur.

PAPR is the main drawback intrinsic to OFDM modulation. In real transmission systems, high peak power can be demanding on power amplifiers backoff and efficiency, and also on ADC/DAC complexity to support large dynamic ranges. Non-ideal power amplifiers can saturate and distort non-linearly the signal, and non-linear distortions generate intermodulation product that translates into ICI. Besides this, high peaks imply lesser efficiency due to greater power consumption.

4.8.1. Source Scrambling

When real data is transmitted, long sequences of zeros or ones are likely to be present in its binary representation. Such sequences may result in long chains with the same modulated samples. As they are OFDM modulated, these samples represent frequencies that are summed as the SCs are multiplexed. In such situation, the resulting OFDM signal's high PAP occurrence probability increases, and the energy distribution along the frequency spectrum becomes less efficient. One way to compensate for this is to break these long sequences and redistribute them. The mechanism used here to achieve this improved distribution is scrambling. Scrambling consists in randomizing the source bits at the transmitter, and in reversing the operation at the receiver. Figure 4.13 demonstrates the differences between the unscrambled and the scrambled transmission of a picture.

The power spectrum of the scrambled transmission denotes a great improvement in power allocation, with fewer in-band fluctuations and with a reduced out-of-band radiation range.

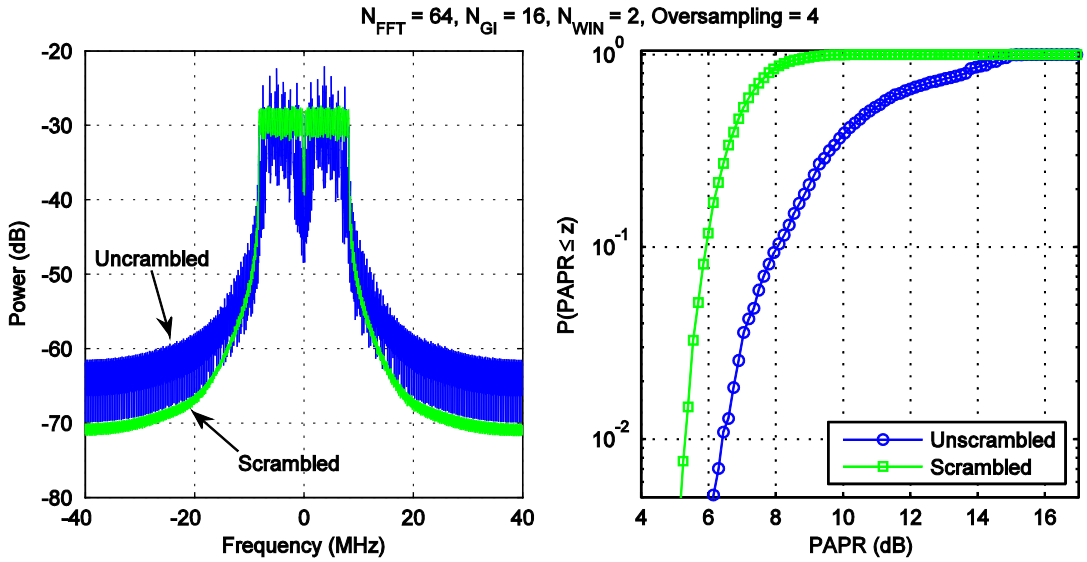

Figure 4.13 – PSD and PAPR distribution or unscrambled and scrambled transmissions of a picture.

For the unscrambled transmission, the PAPR is distributed mostly between 6 dB to 16 dB. This corresponds to peaks with at least 4 to an unlikely maximum of 39.8 times more power than the average. In contrast, the scrambled transmission PAPR is distributed between 5 dB to 9 dB. This indicates that scrambling reduced significantly the amount of power located in high peaks above the average. That is, most of the peaks remain somewhere within 3.2 to 7.9 times the average power. The results indicate that the maximum factor, which is unlikely to occur, has decreased significantly. The distribution curve of the scrambled transmission falls abruptly and its range has shortened. This means that the probability of the signal, at a given instant, to be lower than or equal to the current maximum peak has increased. In other words, the power is better distributed, and it has become less likely to find very high peaks in relation to the average.

4.8.2. Peak Clipping

One of the simplest crest factor reduction technique used to diminish the PAPR is peak clipping. In this dissertation, clipping is performed by setting a clipping level somewhere above the average power of the signal. Hence, the level indicates the percentage of amplitude where the threshold is defined. Anything above the threshold is clipped. This technique is effective, but it introduces non-linear distortions that reflect as in-band and out-of-band radiation in the power spectrum of the clipped signal, leading to ICI and spectrum efficiency loss. Filtering can be used after clipping to control the out-of-band radiation. Figure 4.14 demonstrates how clipping impacts on the spectrum and on the constellation.

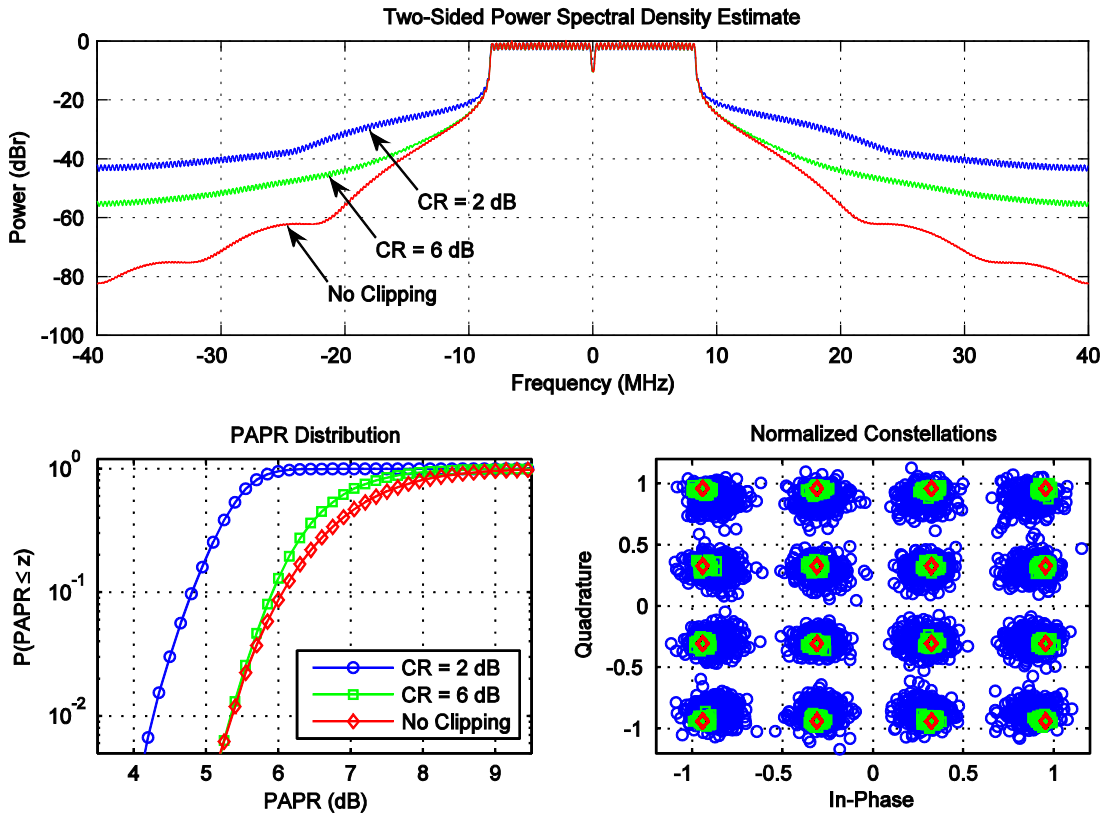

Figure 4.14 – The effects of clipping on OFDM signals, with N_{FFT} = 64, N_{GI} = 16, N_{WIN} = 2 and Oversampling = 4.

In this example, a severe clipping level was applied and the out-of-band radiation is not filtered for demonstration purpose. With a 2 dB clipping ratio to the signal, the CDF illustration shows a considerable PAPR improvement, which indicates the reduction of high peaks in relation to the average. The averaged spectrum for that clipping level shows a significant out-of-band radiation. Its corresponding constellation is marked by "o", and it can be seen that in this case there is a strong intermodulation interference causing ICI. It was seen previously that ICI can be modeled as random noise that degrades the SNR by adding in-band noise. Therefore, the scattering observed in the constellation is consistent with the expected BER degradation. Hence, for lower clipping levels (lower

threshold, meaning more amplitude cut-off), the PAPR can be improved significantly at the expense of SNR.

In the case of a 6 dB clipping above the mean power, the observed out-of-band radiation is significantly lowered compared to the 2 dB case, and the scattering in the constellation is greatly reduced, but the PAPR improvement is also much lower. The original signal has a PAPR distributed between about 5 dB to 9 dB. The CDF indicates the probability of the power to be lower or equal to a specified PAPR value. This means that there is a high probability that the PAPR will not go beyond 9 dB (about 8 times the average power). For a clipping ratio of 6 dB, the PAPR is distributed between 5 dB and 8 dB, which means that there is a small improvement of about 1 dB. For a 2 dB clipping, the distribution range and the maximum value of the PAPR are largely reduced, going from about 4 dB to 6 dB (somewhere between 2.5 and 4 times the average power).

Judging by the results obtained, clipping does appear as an effective way to reduce the PAPR in OFDM signals. However, it is verified that clipping comes with a cost in terms of efficient use of the available spectrum due to the generation of out-of-band radiation. In addition, clipping increases the EVM due to in-band interferences, consequently degrading the BER to some extent. By introducing a filter after performing the clipping operation, the out-of-band radiation can be compensated to diminish the spectrum efficiency loss. However, even with out-of-band filtering, this PAPR reduction technique always introduces some degree of distortion. Hence, if the clipping ration is not too severe, peak clipping can effectively lessen the PAPR and improve the transmission performance.

4.9. Summary

The most important issues inherent to OFDM technology were investigated based on the developed simulator for IEEE 802.11a specifications. This chapter was introductory to several impairments likely to occur in further practical implementation.

It was verified that frequency offsets causes adjacent SC energy to be taken by the demodulation filter. As this ICI increases, the constellation EVM degrades due to constellation scattering and global rotation. A maximum error is reached when the frequency offset attains half the SCs spacing. Over that limit, it becomes impossible to model the error perfectly, as it is no longer possible to determine which SC is being taken by the FFT.

In terms of timing offsets, it was confirmed that they influence the constellation samples by introducing a phase error, which increases linearly towards $\pm\pi$ as the SCs distance to DC increases. Hence, this linear phase skewing of the samples creates a bidirectional rotational effect, leading the samples to rotate away from their intended location. However, this observation is valid only if the

time offsets remain within the GI extent. Otherwise, the received signal becomes strongly distorted by ISI.

It is also interesting to see how SNR impact on BER in OFDM systems remains a modulation-dependent relation. Putting aside the additional energy required for the cyclic extension, the simulated BER versus E_b/N_0 fits perfectly the theoretical curve for single carrier modulation. Hence, OFDM technology brings neither enhancement nor impairment in the presence of white noise with Gaussian distribution.

The results from the simulation of an OFDM signal passing through a Rayleigh frequency-selective channel are in accordance with the theoretical basis. As expected, the curve for the OFDM signal fits well the curve for single carrier modulation. However, if the CIR exceeds the extension of the GI, severe degradation occurs.

The effect of peak clipping as a PAPR improvement method was investigated. It was verified that clipping is a very simple means of effectively reducing PAPR. However, this technique creates non-linear distortions and out-of-band radiation. Although the filtering can compensate for the out-of-band energy, this technique remains limited due to the inevitable distortions introduced. On the other hand, using a scrambler can efficiently reduce the PAPR and improve the power distribution over the band.

Chapter 5. Experimental OFDM Implementation and Performance Analysis

5.1. Introduction

The OFDM modulation technique was studied in detail in the previous chapters, where the different aspects of key importance were discussed and their effects demonstrated, such as the sensitivity of this technology to synchronization errors and its behavior in time-dispersive channels. The IEEE 802.11a standard was also introduced, namely the generation of frames, where the preambles are used for synchronization and channel estimation.

In this chapter, the objective is to understand how to use communication instruments that enable the practical application of the previously generated OFDM signals to a communication system. To achieve this, a *Keithley Model 2910 RF Signal Generator* is used as the transmitter that performs up-conversion with IQ modulation, and a *Tektronix RSA 2203A Real-Time Spectrum Analyzer DC-3GHz* acts as a receiver that performs down-conversion.

The OFDM transmission process is described in a back-to-back connection of the instruments.

5.2. Interfacing with the Instruments

Finding proper means of interfacing the simulator with the instruments was of great importance to this project. Both instruments available support Standard Commands for Programmable Instruments (SCPI), General Purpose Interface Bus (GPIB) communication, Ethernet networking communication and removable pen drives. However, the idealized system to perform experiments on OFDM signal is one that is fast, robust and flexible altogether. Therefore, making use of the SCPI with GPIB communication became the obvious choice, as *Matlab* offers excellent programming support for communication with instruments. This way the complete transmission process is controllable from the workstation: OFDM modulation, transmission, reception, and finally OFDM demodulation.

Communication with the transmitter from *Matlab* brought no particular difficulty. The user manual of the instrument provided all the details necessary to create Arbitrary Waveform (ARB) non-binary files with the correct structure. In addition, more information on how to send and create ARB files inside *Keithley Model 2910 RF Signal Generator*, and playback the file for RF transmission can be found in [40].

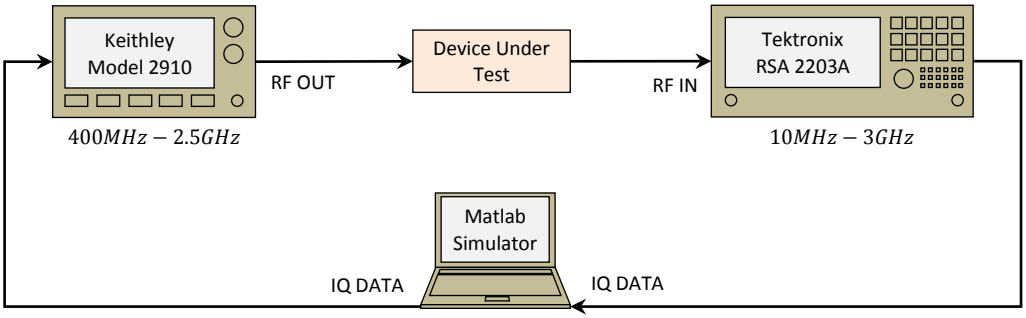

Figure 5.1 – Computer-to-Instruments communication schematic.

Recovering the IQ samples from the receiver revealed a challenging task. First, the captured IQ versus Time (IQT) data is stored into a binary file format intended to be instrument-only for saving and recalling data. In second place, the IF filter response introduces phase and amplitude deviations. The information necessary to perform corrections is also stored in the IQT files. Whether the IQ data is received through GPIB or read from an IQT file, the samples should undergo this correction to achieve improved accuracy. Nonetheless, many advanced details on the file structure are available in the user manual for this instrument given in [41]. Tektronix support team also provided valuable indications on how to achieve this.

The receiver used is in fact a Spectrum Analyzer, and therefore provides a wide selection of tools to analyze signals. In the FD, data can also be extracted in the form of Trace (TRC) files. Detailed information concerning the structure of these non-binary files is available in the user manual referenced in [41].

The ability to convert complex OFDM signals directly from *Matlab* environment into ARB waveforms inside the transmitter, combined with the capacity to receive and extract the complex baseband signal, proved to be fundamental to complete the remaining sections of this dissertation. A small *Matlab* toolbox was designed to support these key operations with the instruments, as well as other useful SCPI command sequences to control instrument parameters such as the center frequency, the transmission power or triggering.

5.3. Configuration of the Transmitter and Receiver

Before attempting any advanced experiment, one should know how to make optimal use of the tools available. This means that all the transmission parameters must be chosen according to the capacity of the instruments. Ideally, perfect timing and frequency synchronization between the two instruments should be achieved, because the main objective in this section and the next one is to characterize how the device under test is affected by the transmission medium. Hence, all

experiments must be performed under the same conditions in terms of instruments configurations, which must be known and have minimal influence over the signal. Here, these conditions were separated in two groups: the synchronization between instruments, and the relation between their respective sampling frequencies.

5.3.1. Synchronizing the Instruments

The first aspect to consider in this communication system is the synchronization between the measuring device in use and the source. Both instruments possess input and output ports to provide synchronization through reference oscillator frequency and triggering. The diagram depicted in Figure 5.2 shows how the synchronization was achieved between the instruments in terms of physical connections. The transmitter plays back the ARB waveform, and wraps back to the start of the waveform as it reaches the end. This process repeats continuously, and at each wrap point, a synchronization pulse is generated by the source. The signal analyzer, which is sharing the same 10 MHz reference, picks up that signaling pulse and synchronizes the acquisition.

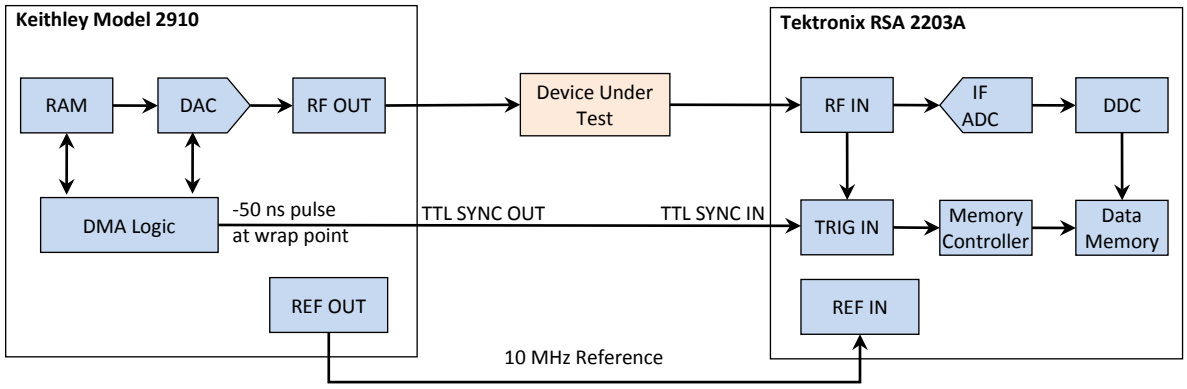

Figure 5.2 – Instruments synchronization diagram [41] [42].

By synchronizing the instruments this way, carrier frequency offsets and sampling frequency errors are minimized. However, even with the instruments synchronized, timing errors can still be generated by taking the first sample of a transmission in the wrong place, that is, by introducing a timing offset in the transmission. Two mechanisms were implemented to maximize the precision for the detection of the starting point of a transmitted frame. The first is the use of guard intervals with zero power between frames. A function was developed to detect these null powered intervals. The second mechanism is the use of the coarse/fine timing synchronization implemented based on the IEEE 802.11a frame preambles, as described in Section 3.2.3.

5.3.2. Sampling Frequency and Oversampling

The second important aspect common to any transmission systems is the choice for the sampling frequency. The sampling theorem states that, in order to recover completely a signal, the sampling frequency must be at least twice the maximum frequency of the signal being sampled. In other words, if the Nyquist frequency exceeds the highest frequency of the signal being sampled, then all the information necessary to reconstruct the signal is present. This means that in theory, if the receiver can sample the signal twice as fast as its highest sampled frequency component, aliasing should be avoided and the signal entirely recovered. In this context, aliasing occurs if the Nyquist condition fails to be satisfied, and consists in adjacent overlapping spectral "copies" of the signal, where any frequency above $f_s/2$ is impossible to differentiate from a lower-frequency component. Aliasing can be avoided in two ways: by increasing the sampling rate to above twice the highest frequency, or by introducing an anti-aliasing filter in the system.

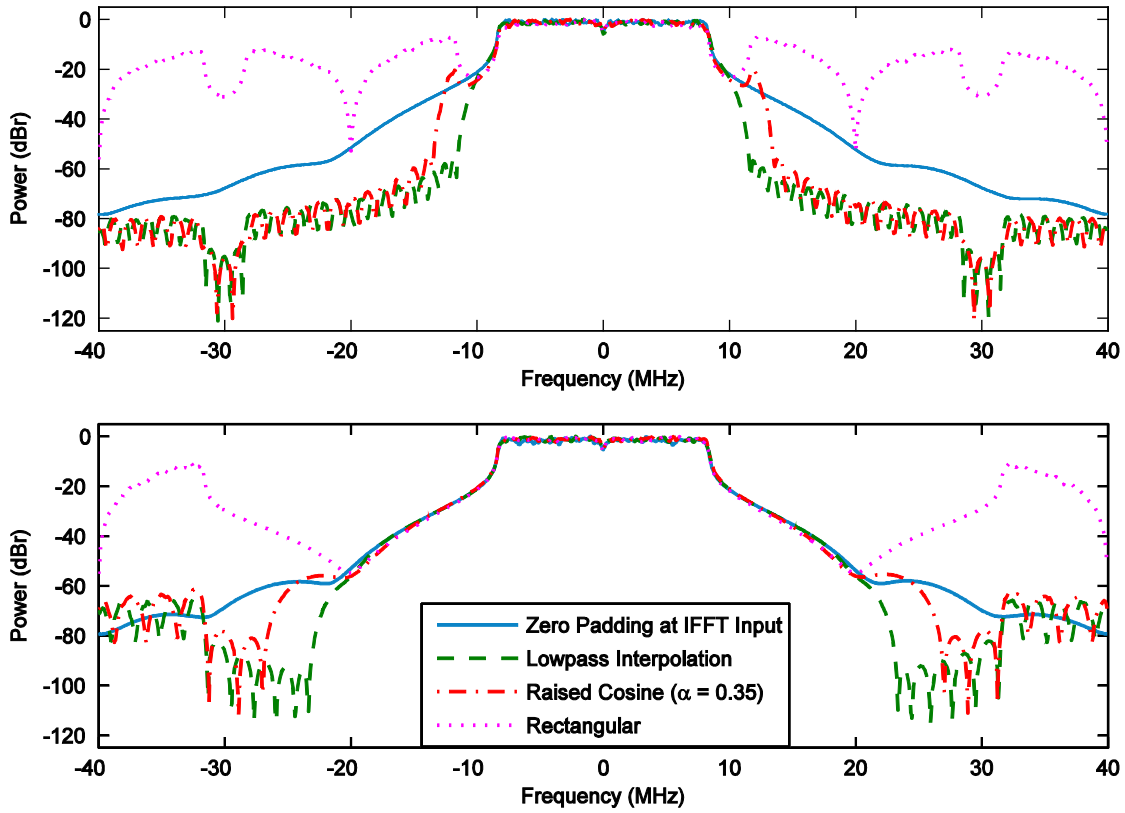

Figure 5.3 – OFDM Spectrums for different Pulse Shaping Filters, with 4-fold oversampling. In the first illustration, N_{FFT} = 64 and 4-fold oversampling is applied. In the second figure, N_{FFT} = 128 (64 zeros padded) and 2-fold oversampling is applied.

In a practical implementation, the sampling rate should be greater than only twice the rate, especially due to real instruments limitations. This increased rate is known as the oversampling rate. Oversampling increases the bandwidth of the signal, because more samples are transmitted during the same symbol period, with lower time interval between samples. Besides improving the effect of

anti-aliasing, oversampling also improves the frequency resolution and reduces the presence of noise. Anti-aliasing filters complexity can be reduced and become less expensive if oversampling is used, because it does not need to be exceedingly sharp nor fast. It also allows the DACs and ADCs to be cheaper while supporting high resolution, as long as the noise remains uniformly distributed. Finally, the SNR can be improved because, if random noise is uncorrelated from one sample to another, then when N samples are taken and averaged, the noise variance is reduced by a factor of $1/N$ [43].

In this OFDM system implementation, two distinct methods can be used to oversample the signal. The first is the conventional oversampling, which is achieved through pulse shaping filters and interpolation of the TD signal. The latter is direct "internal" IFFT oversampling through zero padding, which is typically used in OFDM systems.

This second methodology is an interesting choice, because with zero padding the frequencies above $f_s/2$ are forced to be zero. Hence, zero padding is equivalent to increasing the guard band around the frequencies used to transport information. It is known that de DAC causes periodic spectral replication, which must be suppressed by a reconstruction filter. Thus, oversampling through FFT zero padding can improve greatly the received signal, because by increasing the distance between spectral replicas, it allows reasonably sharp and less expensive reconstruction filters to restore properly the signal [5] [7]. Different approaches are represented in Figure 5.3. The required oversampling factor depends on the system design, but is most likely within a range of 10-30% [5].

The parameters supported by each instrument are available in Appendix C. Details are also provided, on a general basis, on how a packet of samples in baseband can be transmitted in the correct conditions, received, and acquired back, while taking into account the timing and memory related parameters of the instruments in use.

5.4. Transmission of IEEE 802.11a PHY Frames

In this sub-section, an illustration is made of the steps performed to achieve a complete back-to-back transmission, while relating correctly the instruments. Additional information on this subject is available in Appendix C. This transmission demonstrates how the communication can be performed with all means available to improve the robustness of the system, such as synchronization, source coding and basic channel estimation.

In this case, the back-to-back configuration consists in using a direct cable connection with impedance of 50 Ω as the device under test. This is the best possible situation, since the transmitter output connector and receiver input connector share this same impedance. Hence, ideally this

configuration involves no unforeseen loss. However, even under these conditions a small loss was observed when only an empty carrier is transmitted, nearing 0.5 dBm. Hence, for a transmission powered with 0.5 dBm, the receiver get a signal with about 0 dBm.

5.4.1. Defining the Source Length

One important notion to have in mind is that a specific binary source length results in different transmission length due to the varying number of bits per modulated samples. Therefore, the analysis should not be done for the same source length, but rather for the same number of OFDM symbols, that is, the packet length. This is important, because a fair comparison of EVM implies that the same number of modulated samples should be analyzed, under similar conditions. To perform the forthcoming analysis, the number of data OFDM symbols per transmission will be $N_{DSYM} = 128$, and the number of data SCs $N_{SD} = 48$. This implies the number of generated random bits per transmission, that is, the PSDU length in bits, to vary based on the following assumption:

$$N_{\mathrm{PSDU}} = (N_{\mathrm{DSYM}} - 1) \times N_{\mathrm{SD}} \times R \times log_2(M) \tag{5.1}$$

$$N_{\mathrm{PSDU}} = N_{\mathrm{PSDU}} + rem(N_{\mathrm{PSDU}}, 8) \tag{5.2}$$

Where: N_{SD} is the number of data SCs; R is the coding rate; $log_2(M)$ is the number of bits per modulated symbol. The DATA length N_{DSYM} is reduced by one OFDM symbol to accounts for the SERVICE, TAIL and some PAD bits. The second operation guarantees that the PSDU length in bits can be converted to octets without decimal part. The table below presents the estimated PSDU length associated to each data rate for a channel spacing of 5 MHz.

Data rate (Mb/s)	Modulation	Coding Rate	Coded bits per SC	PSDU Length (octets)
1.5	BPSK	1/2	1	381
2.25	BPSK	3/4	1	572
3	QPSK	1/2	2	762
4.5	QPSK	3/4	2	1143
6	16-QAM	1/2	4	1524
9	16-QAM	3/4	4	2286
12	64-QAM	2/3	6	3048
13.5	64-QAM	3/4	6	3429

Table 5.1 – PSDU length variation of the DATA field with 128 OFDM symbols and a 5 MHz channel spacing.

By doing this, each EVM computation is based on a constant reference given by $(N_{DSYM} + 1) \times (N_{SD} + N_{SP}) = (128 + 1) \times (48 + 4) = 6708$ constellation samples. This is valid for all modulations and coding rates, and includes both the PSDU symbols and the SIGNAL symbol, for all data SCs and all pilot SCs. This way, although the number of padded bits during the frame construction process might vary slightly, the number of samples used for analysis is constant.

5.4.2. Performing the Transmission

The transmission system implemented starts with the generation of the baseband OFDM signal. In this case, the generated signal is based on the highest bit rate specified in the IEEE 802.11a standard for a 5 MHz channel spacing, which is 13.5 Mb/s. The base parameters used to create the frame in this example are described in detail in Table 5.2 and Table 5.3 below, and are established in accordance with the definitions introduced in Section 3.2.

Modulation-dependent	Timing-dependent
Modulation Scheme: 64-QAM	Channel Spacing: $B = 5\ MHz$
Data Subcarriers: $N_{SD} = 48$	$N_{FFT} = 64\ samples$
Pilot Subcarriers: $N_{SP} = 4$	$N_{GI} = N_{FFT}/4 = 16\ samples$
Coding Rate: $R = 3/4$	$N_{WIN} = N_{GI}/8 = 2\ samples$
$N_{BPSC} = log_2(64) = 6\ bits$	$\Delta_F = B/N_{FFT} = 78.125\ kHz$
$N_{CBPS} = N_{SD} \times N_{BPSC} = 288\ bits$	$N_{SYM} = N_{FFT} + N_{GI} = 80\ samples$
$N_{DBPS} = N_{CBPS} \times R = 216\ bits$	$T_{SYM} = N_{SYM}/BW = 16\ \mu s$
DATA RATE	$R_b = N_{DBPS}/T_{SYM} = 13.5\ Mb/s$

Table 5.2 – IEEE 802.11a OFDM Modulation-dependent Parameters for a 13.5 Mb/s Transmission.

PLCP PREAMBLE	$N_{STS} = 10 \times 16 = 160\ samples$
	$N_{LTS} = 2 \times 64 + 32 = 160\ samples$
	$N_{PLCP} = N_{STS} + N_{LTS} = 320\ samples$
	$T_{PLCP} = 2 \times (2 \times T_{SYM}) = 64\ \mu s$
SIGNAL	$N_{SIG} = 64 + 16 = 80\ samples$
	$T_{SIG} = 1 \times T_{SYM} = 16\ \mu s$
DATA	$PSDU = 8 \times 3429\ bytes = 27432\ bits$
	$SERVICE = 16\ bits$
	$TAIL = 6\ bits$
	$N_{DSYM} = ceil((16 + 27432 + 6)/N_{DBPS}) = 128\ symbols$ $N_{DATA} = N_{DSYM} \times N_{DBPS} = 27648\ bits$ $PAD = N_{DATA} - (16 + 27432 + 6) = 194\ bits$ $N_{PKT} = N_{DSYM} \times N_{SYM} = 10240\ samples$ $T_{PKT} = (N_{DSYM}/N_{SYM}) \times T_{SYM} = 2.048\ ms$
PHY FRAME	$N_{FRM} = N_{PLCP} + N_{SIG} + N_{PKT} = 10640\ samples$
	$T_{FRM} = T_{PLCP} + T_{SIG} + T_{PKT} = 2.128\ ms$

Table 5.3 – IEEE 802.11a PHY FRAME Timing-dependent Parameters for a 13.5 Mb/s Transmission.

In this dissertation, a packet refers to the PSDU payload wrapped into the DATA field within a frame, with the frame being the entire transmitted structure (PREAMBLE, SIGNAL and DATA). For this particular transmission, the transmitted frame contains a payload of 128 OFDM symbols for a PSDU length of 27432 bits, corresponding to 3429 bytes.

Since the receiver can sample at a rate of 51.2 MHz, then the theoretical limit for transmission is of 25.6 MHz. However, oversampling is required to enable optimal results. To

maintain the designated data rate of 13.5 Mb/s while oversampling the signal, and considering the sampling rates supported by both the transmitter and the receiver, a choice should be made between two oversampling rates: 2-fold oversampling with a sampling rate of 10 MHz, or 5-fold oversampling with a sampling rate of 25 MHz. Although both alternatives provide similar results, an oversampling factor of 5 was chosen to proceed with this project.

In Table 5.3, the entire frame length in samples and in time was calculated. With no oversampling and a channel spacing of 5 MHz, the time required to transmit a single frame without any frame guard is 2.128 ms. Hence, by oversampling the signal with a factor of 5, the number of samples becomes $N_{FRM_{OS}} = 5 \times 10640 = 53200$. However, since the selected sampling rate for transmission is also increased to $SR = 5 \times 5\,MHz = 25\,MHz$, effectively the time required to transmit a frame and the bit rate remains the same. The oversampled baseband complex OFDM signal and its spectrum are depicted in Figure 5.4.

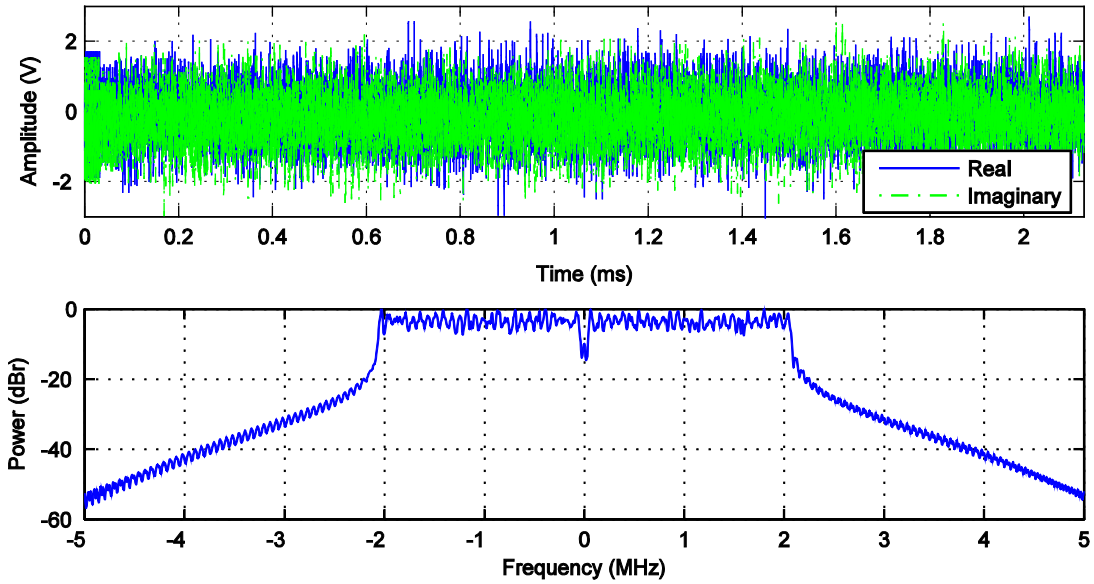

Figure 5.4 – IEEE 802.11a PHY frame with 5-fold oversampling; its corresponding windowed power spectrum.

If a frame guard is inserted before each frame to ease the synchronization, then the extra samples must be accounted for if the acquisition is to include them. Here, a frame guard with arbitrary length of $N_{FG} = 5 \times 256 = 1280$ zeros is introduced. Hence, the total number of transmitted samples is $N_{TOTAL} = 62800 + 1280 = 54480$. These are the samples sent from *Matlab* to *Keithley Model 2910* by means of a GPIB. The time required to transmit the additional frame guard is given by $T_{FG} = 256/N_{SYM} \times T_{SYM} = 51.2\,\mu s$. Consequently, the complete transmission has duration $T_{TOTAL} = T_{FG} + N_{FRM} = 2.1792\,ms$.

At this point, the frames are being continuously transmitted by *Keithley Model 2910*, and constantly acquired by *Tektronix RSA 2203A*. Appendix C provides more details on the way to relate the instruments. The selected frequency span is 10 MHz. Thus, the acquisition sampling rate is 12.8

MHz, and its frame time is 80 µs per chunks of 1024 complex samples. With a trigger starting position set to 25%, the number of acquired samples must be adapted in order for the instrument to analyze enough samples to recover correctly the full transmission. Consequently, in order to achieve a complete analysis, a block with a minimum of $ceil(ceil(2.1792\ ms/80\ \mu s)/(1-25/100)) = 38$ frames must be acquired, which corresponds to a total of $38 \times 1024 = 38912$ samples. In conclusion, the actual acquisition recovered back in *Matlab* environment consists in $37912 \times (1-25/100) = 29184$ complex samples, at a sampling rate of 12.8 MHz.

At this point, downsampling the signal can be performed for two different OFDM demodulation choices. One way is to reduce the sampling rate down to its original 5 MHz, with 80 samples per OFDM symbol, and then demodulate the signal. The other consists in performing a sampling rate conversion back to 25 MHz, with 400 samples per OFDM symbol, and then proceeding to an oversampled OFDM demodulation. Since the original signal was oversampled by IFFT zero padding, the received block is resampled by a ratio of $12.8\ MHz/25\ MHz = 0.512$. As a result, the 25 MHz sampling rate is recovered, and the received re-sampled block has a length of $29184/0.512 = 57000$ samples.

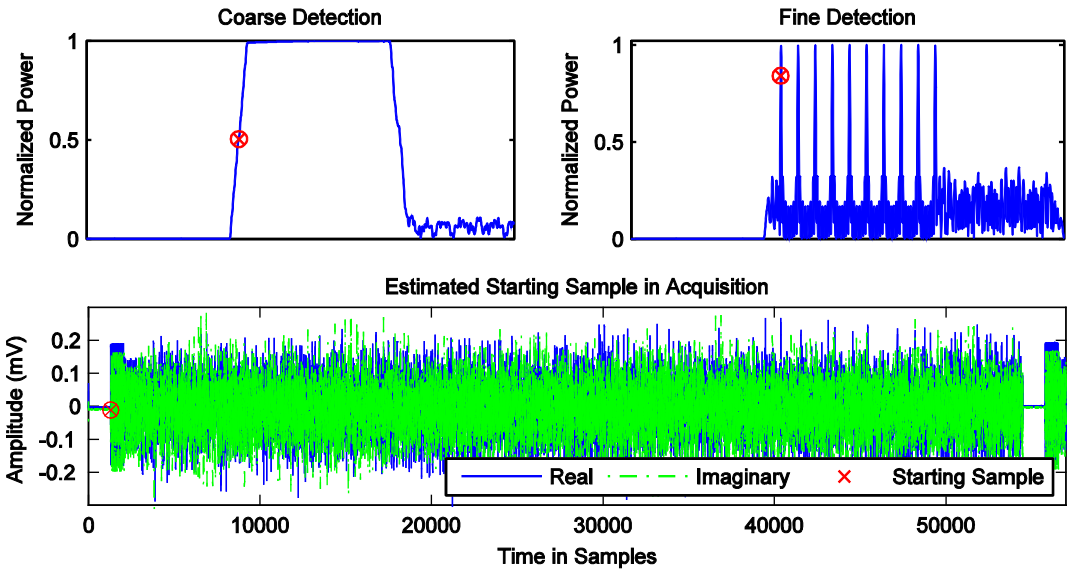

Figure 5.5 – Coarse/Fine Detection of the Frame Starting Sample.

Back into the simulator and with the received block sampled at 25 MHz, the frame detection and synchronization can now take place. The first step consists in distinguishing the low powered frame guard from the rising signal power. This frame guard is helpful in two ways: it determines roughly the instant at which windowed coarse synchronization can take place; its low amplitude also makes the plateau resulting from coarse estimation stand out more clearly. In this case, since the instruments are synchronized, the starting sample of the acquired signal corresponds approximately

to the beginning of the frame guard. Without triggering and external oscillating frequency reference, the acquired frames circulate constantly within the acquisition window. In such situation, the frame guard reveals much more helpful in the process of detecting the starting sample of the frame, hence improving the robustness of the implemented system. In this case, by making use of the instruments triggering it becomes even easier to detect the frame start, at it is always located somewhere around the beginning of the acquisition.

The second step consists in applying the Delay and Correlate algorithm described in Section 3.2.3, with the known STS and over a specified time window, to perform coarse time synchronization. Figure 5.5 illustrates this process. A time window is selected to estimate the moving average on subsets of samples with the length of one short symbol, that is, a period of 16 samples. The result is the formation of a plateau with higher energy around the location of the STS. The starting edge of the plateau denotes crudely the location of the starting sample of the acquired signal. In this implementation, the user, by setting a threshold over which the signal is estimated to be starting, controls the decision. This parameter was deliberately set to a lowered value, at 50% of maximum normalized power, in order to provide a greater margin to the refined estimator that follows.

The starting sample can be very precisely determined by cross-correlating the start of the coarsely estimated frame samples with one period of the STS. This refined estimation was achieved using built-in *Matlab* cross-correlation function, also over a time window correlated with one short period, and results in very distinct peaks marking the beginning of each of the 10 short periods. The maximum normalized power of the first peak should indicate precisely the location of the starting sample. This mechanism is also executed based on a user-controlled threshold, at which the starting sample is estimated to be located. In theory, the power of each peak should reach the maximum normalized power, which means that the detection for a 100% threshold should indicate exactly the starting sample. However, some peaks might be strongly attenuated by channel distortions, leading to a synchronization error. To prevent this, the threshold was set to 80%, thus ensuring that the first peak is detected. In the absence of oversampling, this threshold level is practically equivalent to 100% in terms of detected sample, because the closest sample is usually the peak itself. However, when the signal is oversampled, since more samples define the peak, the closest sample might not be the correct one, leading to a slightly inaccurate synchronization. Still, although a small delay might be introduced, due to the GI only a linearly increasing phase error is introduced, which is easy to correct.

When time synchronization is completed, the STS can be used to estimate the gain factor necessary to amplify the signal, by calculating the average power ration of the received sequence with the expected known sequence. Still based on the STS, the coarse frequency offset estimation can finally take place. In this case, since the instruments share the same reference oscillator

frequency, there is virtually no carrier frequency offsets. However, even with the trigger, the starting sample detection has great influence on the recovered constellations, which is why additional time synchronization is so important.

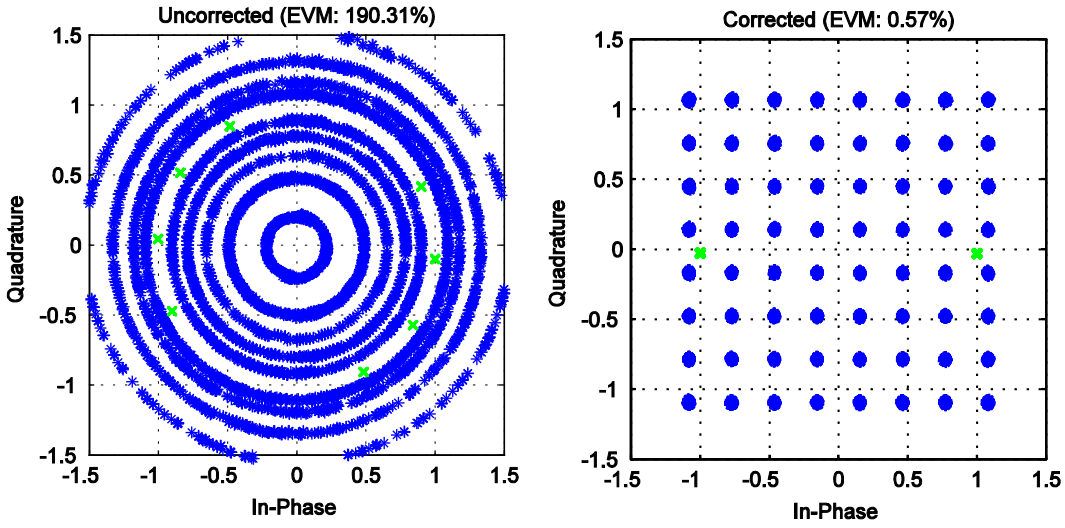

Figure 5.6 – Constellations recovery of an OFDM signal in Back-to-Back Transmission: a) Received; b) De-rotated.

The final step for synchronization and recovery is based on the LTS and the pilot SCs. As it was discussed in Chapter 2, one advantage of OFDM technology dwells in its robustness combined with straightforward equalization techniques. In IEEE 802.11a standard, the LTS allows for even less demanding channel estimation. This known LTS is used to estimate the TF of the channel by averaging the two long symbols that compose it. Channel compensation can then be achieved very simply by performing a point-wise multiplication of each OFDM symbol in the FD by the TF of the estimated CIR. Furthermore, by interpolating between the received pilot SCs and doing the same with the original ones, for each of the OFDM symbols additional phase offset compensation is also performed with the respective estimated TF.

Figure 5.6 demonstrates how the superimposed 48 SC constellations improve as the corrections are applied. Notice that in this case, as the link introduces no significant distortion, the uncorrected samples are already clustered with reduced dispersion. However, although no considerable scattering is observed, the constellation is globally rotated, and a progressive linear phase rotation is evident. Since the instruments are synchronized and the cable provides almost ideal conditions, considering that this particular synchronization is performed on an oversampled signal, this suggests that a minor delay was introduced in the FFT timing synchronization process. A small offset might also have been introduced by the instrument DDC filters and by the sampling rate conversions. It was described in the previous section that a small sampling frequency offset also causes linear phase skewing. In the process of acquiring back the original samples, they are

downconverted and resampled by the Spectrum Analyzer, and then resampled again in the simulator to recover the original sampling rate. By performing these steps, and because the sampling rate conversion ratios are usually not integer values, small sampling frequency errors can occur that have an effect on each SC to a different degree. Since this also influences the LTS, when estimating the TF of the CIR most of these effects are accounted for and compensated. Any remaining phase offsets caused by timing synchronization deviations are then balanced using the pilot SCs, and the SCs constellations are fully recovered.

Besides using the EVM metric, a greater insight on the performance of the transmission system can be attained by estimating the BER of each frame, and by computing the Packet Error Rate (PER) for a block of frames. In this case, a single frame was transmitted in an ideal configuration, resulting in a BER of 0%, which means that no bit errors occured. In the same way, the PER quantifies the amount of packets that contain errors in relation to the total number of packets. In this thesis, any packet with a BER greater than 0% is accounted as erroneous.

5.5. Summary

A brief description of the methodology used to transmit and receive data using instruments in an ideal back-to-back link was made. The transmitter and the receiver configurations have been defined, and the physical synchronization mechanisms put into practice were presented. This is an important step to analyze and compare properly the effect of different devices under test in the remaining part of this study.

It was also explained how the IEEE 802.11a PHY frame is generated with a constant length, in order to compute the averaged EVM for the same number of samples in every situation, thus ensuring a fair EVM comparison as the situation changes.

As a transmission is performed, different parameters require some degree of adjustments. Namely, to comply with the IEEE 802.11a data rates for a 5 MHz channel spacing while taking into consideration both instruments capabilities, the choice of transmission sampling rate and oversampling must be adapted. In addition, given the frequency span and the triggering position of the receiver, it is important to configure correctly the receiver so that the transmission can be entirely acquired.

Chapter 6. OFDM Performance on a RoF Network

6.1. Introduction

In this chapter, a RoF network model for an uplink transmission from the RS to the CS is presented. The system is designed as a RS where DSP operations, carriers coupling, electrical to optical domain conversion of the RF signal and amplified optical source modulation are achieved. This is an implementation of the concept of centralized operation. The long distance transmission is covered by the optical fiber link. At the CS, the signal is converted back from optical to electrical domain, split into the original distinct carriers, and the data is acquired and analyzed.

The main purpose of this section consists in studying the performance of OFDM technology in such RoF system, with intermodulation. To do so, one of the coupled carriers is an OFDM-modulated signal, following the IEEE 802.11a specifications. The performance of this technology is then evaluated under the influence of the network. While the configuration of the transmitter and the receiver remains unchanged, the device under test can vary from a simple cable to some couplers, or to a complete RoF architecture.

6.2. RoF Network Architecture

The architecture designed in this project consists in a model for a RS and its link to the CS. It is intended to couple several carriers with different frequencies in the electrical domain, to modulate the resulting RF signal optically, and to transmit it through a fiber link. The suggestion is to cover the long distance transmission between the CS and the RS by means of optical fiber, to perform DSP operation and domain conversion directly in the sites, and to distribute the service through conventional electrical systems, such as wireless APs. In this dissertation, the main objective is to study the effect of the RoF system together with intermodulation on one of the carriers that is an OFDM signal. Figure 6.1 illustrates the structural design under investigation.

Four carriers are generated independently with different center frequencies, and are coupled in the electrical domain. The resulting RF signal is then taken from the output of the couplers, and it is supplied to a Reflective Semiconductor Optical Amplifier (RSOA). The RSOA is seeded by a Distributed Feedback (DFB) laser. The optical fiber in use is type SMF. The RSOA uses the electrical RF signal and the incoming optical source to perform electrical to optical domain conversion and to modulate the optical source, to amplify the resulting optical signal and to reflect it back through the optical port. Afterward, the optical signal emitted by the RSOA enters the circulator, which redirects

the optical signal towards the photo-detector. The photo-detector converts the optical signal back to the electrical domain. The resulting RF signal subsequently passes through a cable to reach splitters, which separate back the input into four signals. Finally, the Spectrum Analyzer centered on a specific carrier frequency receives and acquires back the signal for a specified frequency span.

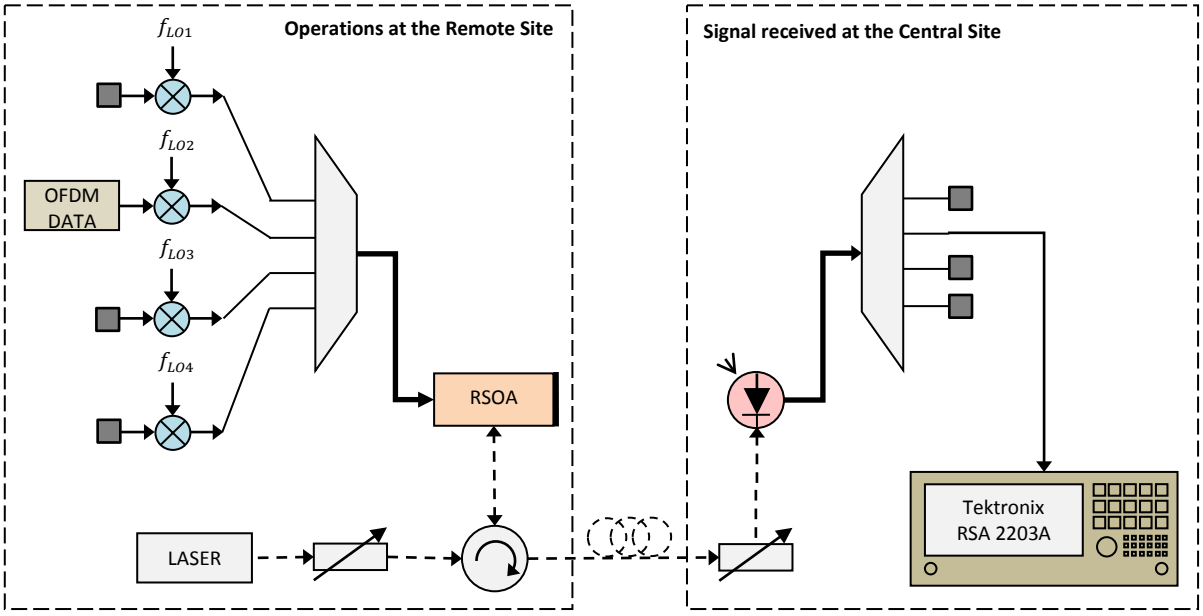

Figure 6.1 – Suggested RoF Network Architecture.

6.2.1. The RSOA as an Optical Modulator and Amplifier

One of the fundamental components available for the realization of this project is the *SOA-RL-OEC-1550*, developed by *CIP Technologies*. It is designed to operate on a wavelength of 1.55 µm, and provides high gain for small signal while ensuring low polarization dependent gain, with 1.2 GHz of electrical bandwidth.

Before proceeding to the experimental RoF system, the parameters used at the RSOA were chosen by considering three main factors: the spontaneous emission of the RSOA, the optical gain and the transfer function.

The spontaneous emission of the RSOA was characterized for a sequence of bias current sources in the absence of any optical input, by measuring the optical output power for a range of wavelengths. In Figure 6.2 it can be observed that, as the source current increases the optical output power increases as well, with the highest values neighboring a wavelength of 1550 nm. From the shape of the curves, it can also be seen that for higher input currents, the peak tends to shift to lower wavelengths, and that it is transferred to greater wavelengths as lower bias currents are applied. In addition, higher current results in more significant ripple at the peak of the curve, which means that the robustness of the system can be affected. Therefore, a compromise must be reach between the

optical gain and the wavelength of the optical signal. In this case, an appropriate choice of operation with the RSOA can be selected at wavelengths around 1.55 µm, with a bias current of 60 mA.

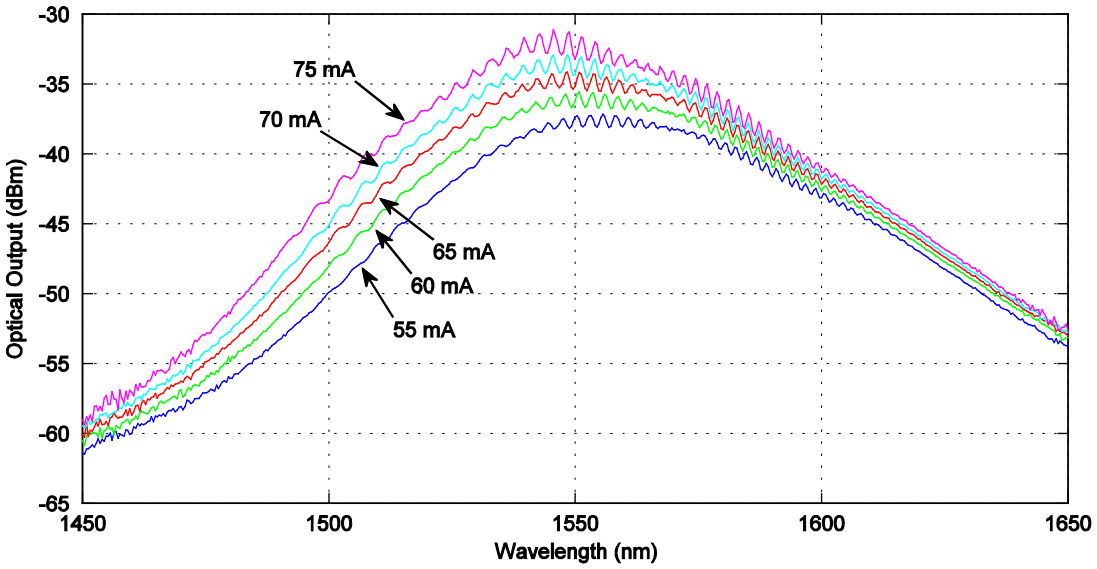

Figure 6.2 – Spontaneous Emission of the RSOA for a range of bias current sources.

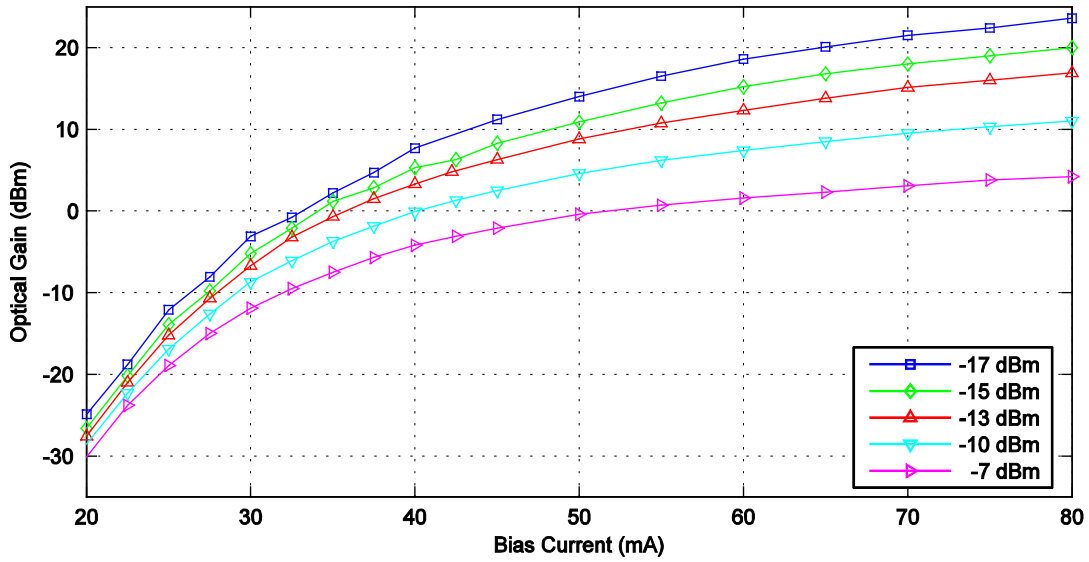

Figure 6.3 – Amplification factor of the RSOA for a range of Input Optical Power.

Another important aspect of the RSOA is its response to different optical source power, for a sequence of polarization currents. Power efficiency is one of the requirements of good telecommunication systems, for both commercial and environmental reasons. In addition, practical materials usually have limited capacity. In the case of this RSOA, the optical power should not exceed 2 dBm in order to avoid saturation. Hence, in general it is desirable to work with small signals when it is possible. Figure 6.3 illustrates the reaction of the RSOA to different optical power levels. It is very clear that the RSOA is able to amplify with greater optical gain as the optical source power decreases.

The transfer function of the RSOA for a constant -17 dBm optical source and several input currents is depicted in Figure 6.4. It is evident that the optical output power decreases as the frequency increases, for all bias currents. The TF is very similar for all currents, with only small power oscillations occurring, depending on the frequency location. This is important because it implies that by varying the bias current of the RSOA, that is, by changing the amplification gain, the optical output signal is consistent from one situation to another.

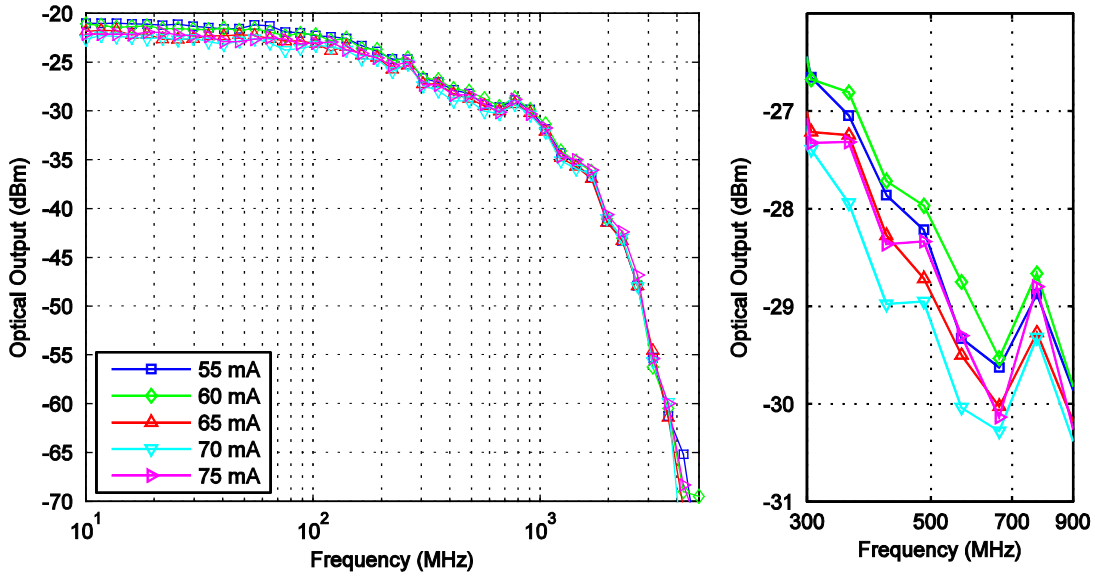

Figure 6.4 – TF of the RSOA for a range of bias current sources; an amplified view for the frequency range of the carriers used in the RoF architecture.

6.2.2. Overall System Configuration

The four generated carriers are each centered on distinct frequencies, which are $f_{c1} = 300\ MHz$, $f_{c2} = 500\ MHz$, $f_{c3} = 700\ MHz$ and $f_{c4} = 900\ MHz$, respectively. The carrier centered on f_{c2} is the one investigated in this report. It consists in the OFDM waveform transmitted by *Keithley Model 2910*, designed using the IEEE 802.11a specifications, as explained in the previous chapter. Subsequently, the carriers are all coupled into a single RF signal in the following manner: f_{c1} and f_{c2} are coupled into f_{c12}; f_{c3} and f_{c4} are coupled into f_{c34}; and finally f_{c12} and f_{c34} are coupled into f_{c1234}. Afterward, the resulting RF signal continues to enter the RSOA. The couplers/splitters consist in the same devices, which act differently depending on the selected input and output. Each coupler introduces an intensity loss on the signals of around 6 dBm. A minor deviation of the attenuation can occur as the carrier frequency varies. Hence, the RF signal entering the RSOA suffers a gradual attenuation has it passes through the couplers (two per carrier), which sums up to roughly 12 dBm. Therefore, for a set of carriers transmitted with a power of 0.5 dBm, the electrical RF signal entering the RSOA has about -11.5 dBm.

The laser in use provides an optical signal power of 4 dBm, with a wavelength of 1551.8 nm. This wavelength was obtained by calibrating the laser so that its beam corresponds to the location where the spontaneous emission of the RSOA is at its peak, that is, when the RSOA provides maximum optical amplification through reflection. To feed the RSOA, a Bias-T injects a source current together with the RF signal into the device. The RSOA source current is set to 60 mA, with its thermistor having an impedance of about 12.15 kΩ. The injected current controls the amplification factor of the RSOA, and the thermistor its operating temperature. In this case, this corresponds to a temperature of 25 °C.

Two optical attenuators are placed in the network to regulate both the optical source power and the modulated optical carrier power. The attenuator placed between the laser and the circulator is used to regulate the optical source power as intended, which is reduced from 4 dBm to about -15.5 dBm before entering the circulator. Since the circulator induces an attenuation nearing 1.2 dBm, the optical signal power entering the RSOA is of approximately -16.7 dBm. With this configuration, the RSOA provides an amplification bordering 20 dBm. Another attenuator can be seen foregoing the photo-detector. It is used to control the power of the optical carrier emitted by the RSOA, hence avoiding saturation of the photo-detector. For the -16.7 dBm input, the RSOA configuration provides an optical output power rounding 3.27 dBm. Thus, after passing through the circulator the optical signal has around 2.07 dBm. This signal is deliberately attenuated to approximately -13.3 dBm before it enters the photo-detector, to avoid saturation. Finally, the electrical signal returned by the photo-detector enters the splitters, from which the *Tektronix RSA 2203A* filters and analyzes the signal.

As a final point, the data acquired by the spectrum analyzer is transferred back into the computer, and *Matlab* is used for further digital processing. The channel is then estimated, and EVM and PER are computed for a number of packets.

6.3. Performance Evaluation

The RoF network introduced in Section 6.2 represents the entire system implemented. To study individually the influence of the several important segments of the circuit, different experimental configurations were implemented by modifying the network connections, and by changing the transmission conditions. The EVM is estimated with normalized constellations, for blocks of 20 packets, each with length of 128 OFDM symbols. All the results presented in this section can be found in Appendix D.

Domain	Label	Description
Electrical	B2B	Back-to-Back - The cable is the “ideal” device under test.
	2C2S	2 Couplers, 2 Splitters.
	2C2S-IMD	2 Couplers, 2 Splitters, with Intermodulation.
Electrical and Optical	2C2S-IMD-RSOA	2 Couplers, 2 Splitters, with Intermodulation, with Optical Fiber.
	2C2S-IMD-RSOA-11k	2 Couplers, 2 Splitters, with Intermodulation, with 11 km of Optical Fiber.
	2C2S-RSOA	2 Couplers, 2 Splitters, with Optical Fiber.
	2C2S-RSOA-11k	2 Couplers, 2 Splitters, with 11 km of Optical Fiber.

Table 6.1 – Experimental Configurations.

6.3.1. The Influence of the RSOA Gain

To observe the impact of this component on the transmission, controlled variations were applied on the input current of the RSOA to vary the optical amplification conditions, and measurements were taken. To generate Figure 6.5, the effect of the RSOA parameters on a single carrier centered on 500 MHz was measured. The transmitted signal is OFDM modulated as described in the IEEE 802.11a specifications for a 5 MHz channel spacing, and no intermodulation is introduced by additional RF carriers. Nonetheless, the RF signal passes through two couplers, which introduce an attenuation of about 12 dBm. Three source power configurations are experimented on the generated carrier in the electrical domain: -10.5 dBm, 0.5 dBm, 10.5 dBm. Several important observations can be made from this analysis.

In the first place, the results obtained indicate clearly that the RCE is not modulation-dependent, since it is approximately constant as the data rate increases. Only tiny variations are noticeable in the computed RCE within the same optical amplification and the same electrical signal power. This observation is verified for each system configuration. However, the Packet Error Rate (PER) fluctuates as the RCE remains the same. This occurs because as the data rate increases, the SCs constellation order increases, and the convolutional coding rate varies. Therefore, the data rate influences the robustness of the system, and this effect on the PER is expected. As the data rates increase, the system becomes more susceptible to distortions of the signal, which results in higher PER.

Nonetheless, it can be seen that both the electrical source power and the optical amplification are extremely important to the system performance. Although the RSOA provides high gain for small signals, it is observed for instance that for a -10.5 dBm signals with 12 dBm of attenuation, which results in an average power of only -22.5 dBm, the RCE remains very high for all optical amplifications. As the electrical power is increased to 0.5 dBm and above, the recorded RCE

suggests that the RSOA is operating more comfortably. In terms of the optical amplification, it can be seen that as the amplification increases the RCE also rises for any electrical source. However, for higher optical amplification factors, when the electrical source power is at 10.5 dBm, although the amount of constellation errors decreases in relation to smaller electrical signals, the distance between results from different optical amplification becomes more evident. Hence, for small electrical signals, even lesser optical amplification introduces distortions. As the electrical signal power increases, the distortion level decreases and higher levels of optical amplification are supported.

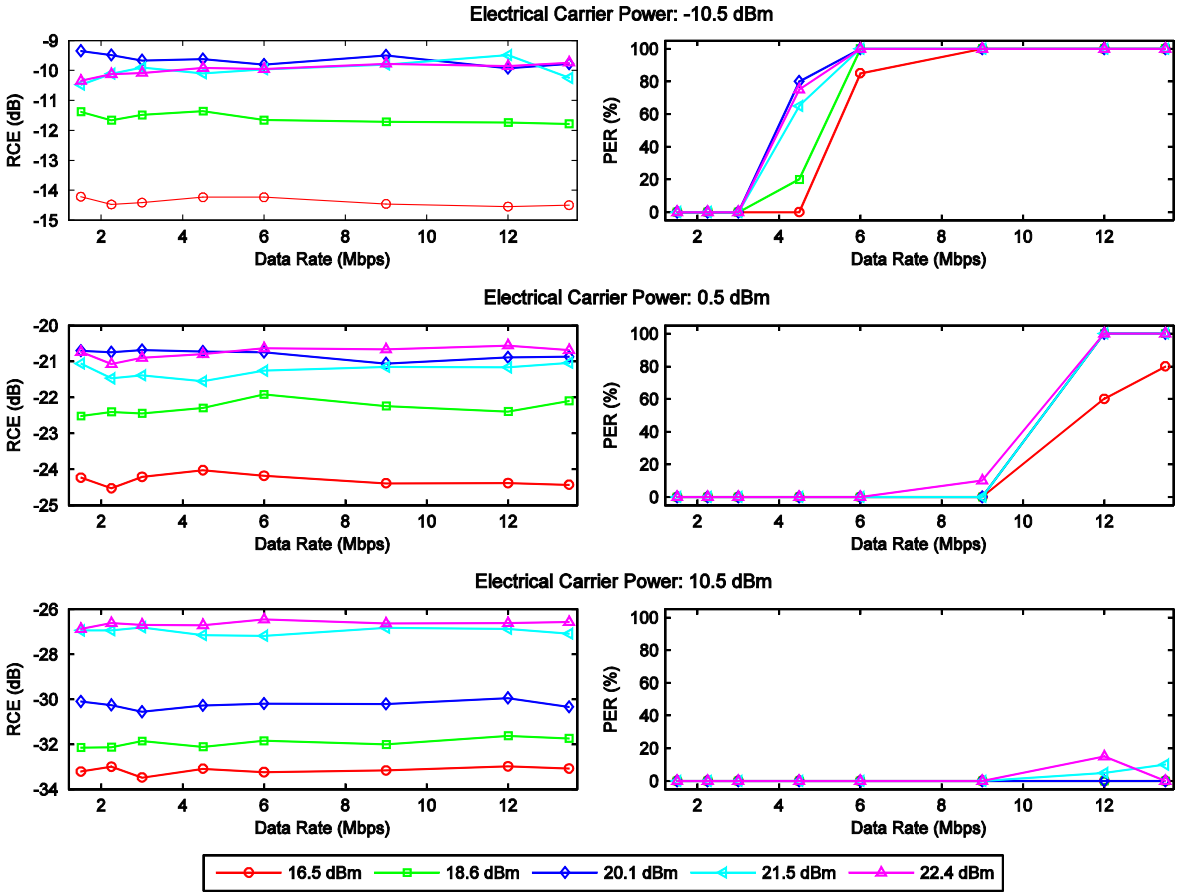

Figure 6.5 – The influence of the Optical Amplification of the RSOA on the EVM and the PER.

When the RoF system is configured, the laser is tuned so that its wavelength corresponds to the highest point in the reflective capacity curve of the RSOA. Although more amplification is provided this way, it is not its most stable state, and oscillations can be introduced which are more important as the amplification factor is increased. Therefore, a compromise should be reached between the amount of power required and the vulnerability of the system to distortions while setting the RSOA optical amplification.

6.3.2. The Intermodulation Interference

Intermodulation is an important aspect of this study, because the idea intrinsic to a RoF network of this nature is the distribution of multiple services through several channels using the same communication medium.

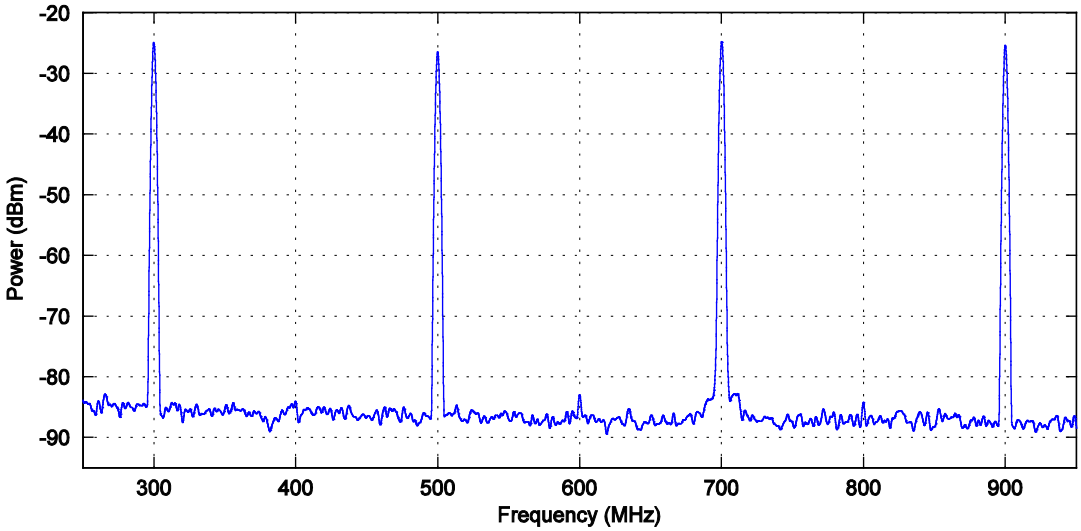

Figure 6.6 – The four carriers with frequency location from left to right: f_{c1}, f_{c2}, f_{c3} and f_{c4}.

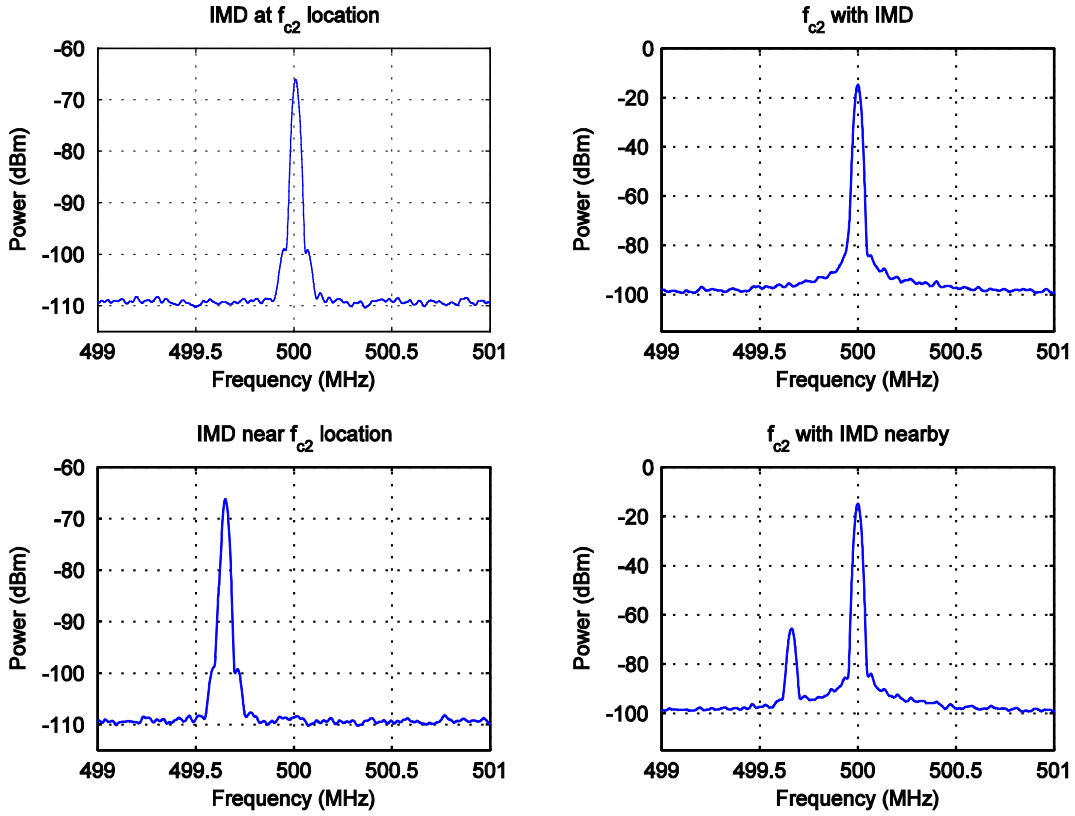

Figure 6.7 – The effect of a frequency offset at carrier f_{c3} on the intermodulation product frequency location, for 10.5 dBm of electrical power.

Intermodulation interferences normally appear from intermodulation product in a band of consecutive channels. The intermodulation product is usually associated to an order, depending on the non-linearity that instigates the products [44]. In this study, four carriers $f_{c1} = 300\,MHz$, $f_{c2} = 500\,MHz$, $f_{c3} = 700\,MHz$ and $f_{c4} = 900\,MHz$ are created, and f_{c2} is the carrier being studied. Therefore, it is the frequencies causing intermodulation product falling on frequency f_{c2} that are particularly relevant. A mathematical notation for 3rd order interferences is given in [44], where the second harmonic of a frequency A that intermodulates with a frequency B produces an interference at a frequency C. It is given by $2A - B = C$. Knowing this, and the range of frequencies in use, it is evident that $2 \times 700\,MHz - 900\,MHz = 500\,MHz$, which means the carriers f_{c3} and f_{c4} interfere with carrier f_{c2}.

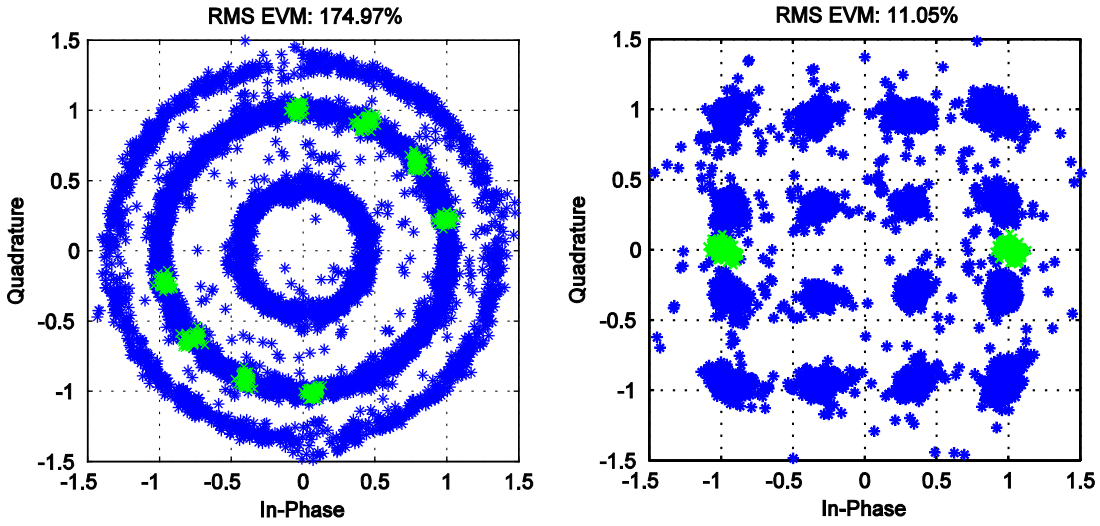

Figure 6.8 - Example of acquired OFDM Constellations in the presence of interfering intermodulation product outside DC, with 10.5 dBm of electrical power: a) Received 2C2S-IMD-RSOA; b) De-rotated 2C2S-IMD-RSOA;

The material available allowed for the introduction of intermodulation in the RoF architecture to be possible. However, the only carrier frequency really transporting information is the OFDM modulated carrier f_{c2}. The remaining RF carriers are always emitted with the same electrical power as the main carrier. In the OFDM carrier, the energy is spread along the wide frequency band. On the other hand, the remaining RF carriers are not modulated with data, and therefore have stronger energy limited to a narrow band. Hence, the interfering energy is quite strong when higher levels of electrical power are in use, which can severely degrade the received constellations. In theory, as long as this energy falls precisely on the DC SC, although there is intermodulation product, no degradation of the constellations is introduced, because there is no information on DC.

Another aspect to consider is the fact that a Voltage Controlled Oscillator (VCO) that is slightly sensitive to temperature generates carrier f_{c3}. It was observed that, as the experiments took place, small positive or negative variations were introduced in the center frequency, with up to 2 MHz of deviation. These oscillations were normally much smaller, but still enough to interfere

sometimes with the SCs next to DC. In addition, the produced carrier presents a small amount of out-of-band radiation. For high power levels, this situation occasionally introduces very high distortions, because by shifting the center frequency of f_{c3} to a nearby frequency, the intermodulation product also diverges a little bit. When this occurs, the interfering energy of the intermodulation product no longer falls on the DC SC, and instead distortions are introduced to data carrying SCs around DC. This effect is depicted in Figure 6.7. Hence, the CIR cannot be assumed as approximately constant from a block of acquisitions to another when intermodulation is present, especially when higher electrical power is used.

6.3.3. The Experimental Configurations

The methodologies chosen to characterize the system performance are RCE and PER. This analysis is settled on the study of the received constellations under varying network configurations, for all the transmission rates comprised in IEEE 802.11a specifications for a 5 MHz channel spacing. Figure 6.9 and Figure 6.10 consist in the superposition of the constellations of all the SCs existing in the transmission of a single packet, for transmissions at a data rate of 6 Mb/s. The illustrations present the constellations as they are received and the result of the corrections by point-wise multiplication of the channel TF estimate.

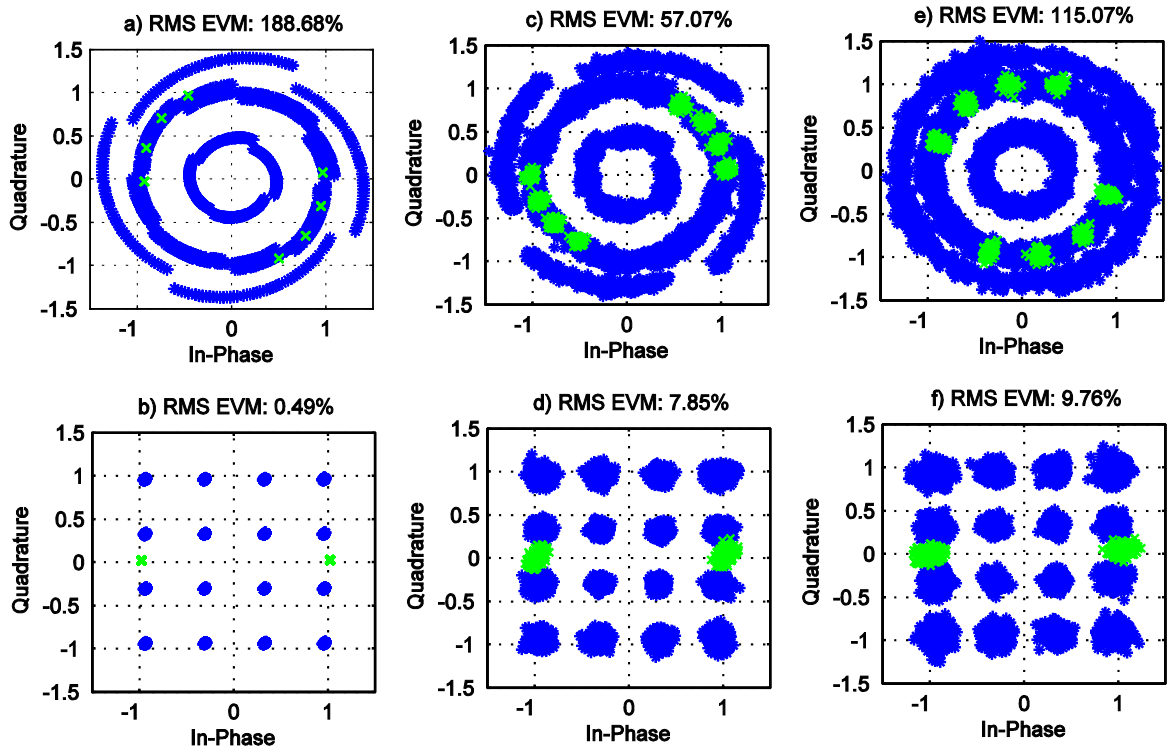

Figure 6.9 – Examples of acquired OFDM Constellations, with 0.5 dBm of electrical power: a) Received 2C2S; b) De-rotated 2C2S; c) Received 2C2S-RSOA; d) De-rotated 2C2S-RSOA; e) Received 2C2S-RSOA-11k; f) De-rotated 2C2S-RSOA -11k.

The instruments share a common oscillating frequency reference, which virtually excludes any carrier frequency offsets. However, although a trigger synchronizes the instruments, two effects studied in Chapter 4 are observed in all acquisitions: a global phase rotation of the constellations; a progressive phase rotation of the constellations.

The global phase rotation is possibly caused by a small global timing offset, which can be the result of a small delay introduced by the DDC filters of the spectrum analyzer. If all the frequency components of the signal are affected in a similar way by the filters, then the consequence is a constant phase error that affects the whole transmission, which is why the rotation occurs at the same distance and in the same circular direction for all constellation samples. Despite the existence of a common reference oscillating frequency, it also viable that a small phase error is introduced between instruments.

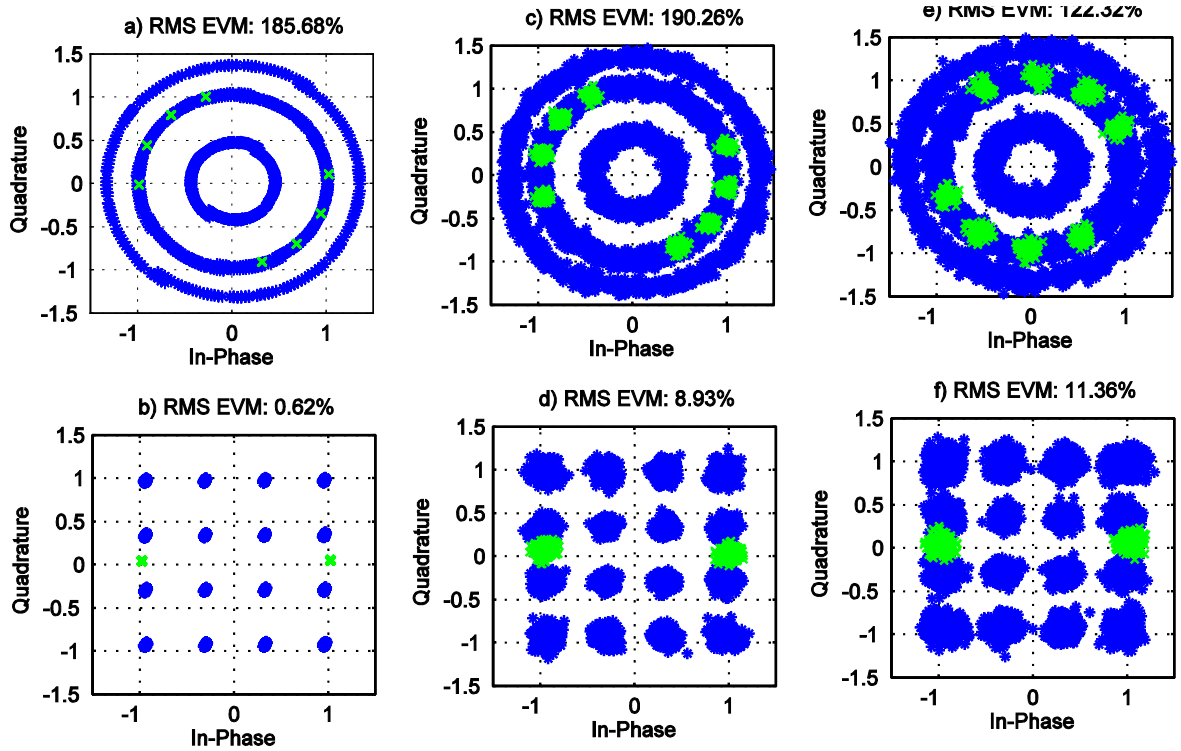

Figure 6.10 – Examples of acquired OFDM Constellations, with 0.5 dBm of electrical power: a) Received 2C2S-IMD; b) De-rotated 2C2S-IMD; c) Received 2C2S-IMD-RSOA; d) De-rotated 2C2S-IMD-RSOA; e) Received 2C2S-IMD-RSOA-11k; f) De-rotated 2C2S-IMD-RSOA -11k.

As it was discussed previously, the progressive phase rotation can be caused by several situations, but in this case, there are mainly two possible conditions: a small sampling rate error; a timing offset in the FFT filter at the receiver, smaller than the duration of the GI. In this case, both causes are probably originating this phase skewing. The first one might be introduced during the sampling rate conversions, when the acquired samples are taken from 12.8 MHz back to 25 MHz (or down to 5 MHz, depending on the FFT length chosen at the receiver). Because the rate conversion ratio is not an integer value, for long transmissions a small progressive sampling frequency error can

be introduced. The second cause is linked to the detection of the starting sample of the acquisition. In the final detection step, the mechanism implemented depends on a user-defined threshold to select a sample, within the normalized power peaks of the cross-correlated STS. This threshold was deliberately set to relatively low value (80%), because as the transmission conditions worsen (ex: low electrical power with intermodulation and 11 km of optical fiber), sometimes the first peaks are more attenuated and suffer more distortions, and they fail to reach a normalized power of 1. The threshold used remains the same for all experimental conditions. In addition, by detecting an oversampled signal, more samples define the peaks, which increase the chance of locating the starting sample with an offset of one or two samples in time within the GI. Since the effective CP has a duration of 14 samples (without oversampling), and due to the introduced periodicity property, the information in frequency is guaranteed not to be lost. However, in practical terms, this situation is equivalent to introducing a timing offset in the FFT window of the receiver, which causes a linearly increasing phase rotation towards $\pm\pi$ on the SCs as their distance from DC increases.

Fortunately, this effect is easily corrected with the TF estimate of the CIR. In this experiment, the electrical part of the network is composed by different components that are connected by coaxial cables. This means that, unlike in wireless transmissions, the system does not endure severe multipath interferences. Moreover, the optical fiber in use is of type SMF. Hence, although a degree of chromatic dispersion is expected to occur, no multimode dispersion (common in MMF, with interferences comparable to a wireless multipath environment) should take place. For these reasons, within an experimental setting there is not a strong variation of the channel as the signal travels, which means that all the OFDM symbols endure approximately the same conditions. This is why the final OFDM symbol-by-symbol phase offset estimation using the pilot SCs does not bring a significant additional improvement to the previously corrected constellations.

In terms of blocks of acquisitions, it was explained in the section above that in the presence of intermodulation product with higher electrical power, the CIR cannot be assumed as unchanging. In addition, several other points of the RoF network are adjusted manually, such as the optical power feeding the RSOA and the photo-detector. However, in terms of the OFDM symbols of a packet, that is, within the duration of a single transmission, since any delay that might be introduced in the process is always lower than the effective GI, it is acceptable to assume that the channel is approximately constant.

The final aspect of this study is a comparison of the RCE estimated for every implemented configuration, for all data rates and for each level of electrical carrier power. As before, it can be seen in the curves from Figure 6.11 that the constellation error remains approximately constant as the

data rate increases. It is the PER that varies within an experimental setting, as the modulation order and the convolutional coding rate change when the data rate changes.

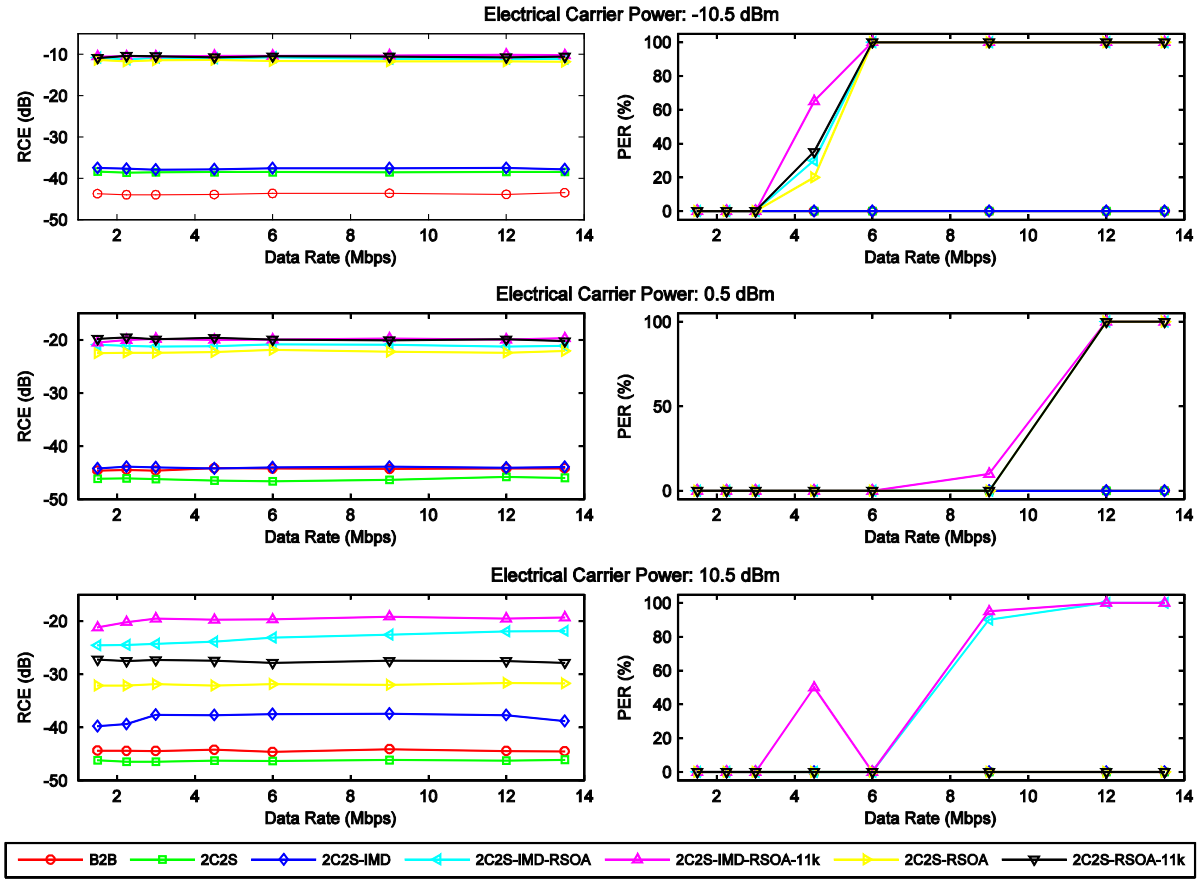

Figure 6.11 – The effect of the different experimental configurations on the EVM and the PER.

For a low electrical power of -10.5 dBm, the computed RCE are definitely separated into two groups: the electrical domain results; the RoF network results. As expected, the results from the electrical domain have very low constellation error. In back-to-back, the RCE remains constant at about -44 dB. In the presence of the coupler/splitters, the RCE rises slightly to around -38 dB and – 37 dB, with and without IMD, respectively. Conversely, for any transition to the optical domain, constellation error is quite poor, remaining within -11 dB.

While in the electrical domain there is no PER at all, in all RoF configurations the constellation scattering is so important that only the lowest data rates, up to 3 Mb/s, have good PER. Although the modulation order for 3 Mb/s is the same as for 4.5 Mb/s, in the latter the convolutional coding rate is punctured from rate 1/2 to rate 3/4. In this case, the constellation dispersion has become too severe for the decoder to consistently detect and correct the erroneous bits, and PER rises. For the remaining data rates, the PER rapidly grows to 100%.

In general, with so little electrical power, the intermodulation product has practically no effect on the transmissions. In terms of the results in the optical domain, they are consistent with the observations from Section 6.3.1. It was seen that the wavelength of the laser used to generate the

optical source is placed at the location where the RSOA provides maximum amplification. However, the RSOA is not perfectly stable at that location, as some ripple is observed. For this reason, although the RSOA can effectively amplify very small signals, they are also more sensitive to this effect.

As the electrical power grows to 0.5 dBm, the same grouping of RCE values as previously appears. Interestingly, the signal attenuated by the couplers/splitters without IMD has a better RCE, which is of -46 dB. This suggests that more accuracy is achieved for acquisitions above a certain electrical power level. About the results with IMD, a small improvement is also noticeable, since the RCE values equal approximately the -44 dB shared by the back-to-back acquisitions. In the optical domain, the RCE curves are again grouped, but in this case around -21 dB, which corresponds to about -10 dB of improvement in relation to the previous case. Although the difference in RCE between RoF configurations is quite insignificant, the error measurements tend to be better when no IMD exists, without the long distance fiber.

As it is predictable, the PER of the electrical domain results is constantly null. However, in the RoF configurations the growth in electrical power also introduced PER improvements when no IMD exists. Above 6 Mb/s, the PER begins to increase when 11 km of fiber are used, and above 9 Mb/s all optical fiber configurations loose packets at maximum rate.

With this level of electrical power, the intermodulation product generates small distortions, perceptible mostly when the optical fiber is used. It is interesting to observe that when there is no IMD, the RCE with optical fiber remains somewhat high. This indicates that 0.5 dBm is not enough electrical power to completely overcome the effect of the ripple from the RSOA, which appears to have much more influence than the IMD. In the constellations from Figure 6.9 and Figure 6.10, it can be seen very clearly that, independently of the IMD and without the long fiber link, the samples recovered after crossing the optical sections of the networks are heavily spread around the ideal constellation location. As the 11 km of fiber are introduced, the constellations suffer additional degradation.

Finally, the experimental configurations were tested with 10.5 dBm of electrical power per carrier. The distinction in performance from one structure to another has now become evident in terms of RCE. For the back-to-back and the couplers/splitters links, there is no important difference in relation to the previous case. Yet, the IMD now visibly affects the constellation error in the electrical domain. Although the RCE remains quite good, it has worsened to around -38 dB. For the RoF networks, in the absence of IMD the RCE has greatly improved. Without the long fiber link, the RCE is fixed near -31 dB. With the 11 km of optical fiber link, the RCE is approximately at -27 dB. These results, as any below -25 dB, are in agreement with the IEEE 802.11a specifications for the

maximum RCE per data rate, for the highest data rate of 13.5 Mb/s. In the presence of IMD, the distance between RCE results for the short and the long fiber link is also noticeable. While the RCE of the short optical fiber link configuration is near -24 dB, the 11 km long link remains close to -20 dB.

In this situation, it is now possible to detect more clearly that when the signal travels through the 11 km of optical fiber, a higher degree of distortions is measured on the constellations. This is a relatively small distance in terms of optical fiber link. In addition, whatever the RoF setting in use, the RSOA optical source, and the optical power at the photo-detector input are both approximately constants. When the long fiber link is employed, this is achieved by manually allowing more power to enter the link, in a way that its output is always approximately -13.3 dBm. Hence, attenuation in the long link does not appear as a good cause of deterioration. Since the optical fiber used is a SMF, one explanation to this additional scattering could be a small amount of chromatic dispersion.

Except for the configurations with IMD, the RCE values from optical configurations are always located below -25 dB. Consistently, the PER computed for these transmissions remains always at 0%. In the case of the IMD settings in the RoF network, it appears as the distortions caused by intermodulation product are amplified to a certain extent, as they seem to have much stronger negative influence on the recovered samples. One possible cause to this effect is that different frequency components of a signal might be amplified to slightly different factors by the RSOA. This could result in greater amplification of the carriers causing the intermodulation product, which in turn would have stronger impact on the main carrier. Concerning the PER in these circumstances, with the short optical link configuration, almost every packet transmitted at data rates above 6 Mb/s are considered lost, and all packets transmitted above 9 Mb/s are lost.

When the signal crosses the 11 km optical link, there is an unexpected course in the PER results. Strangely, at 4.5 Mb/s small BER values result in 50% of the packets to be lost. Then, at 6 Mb/s the PER decreases to 0%, and it finally rises back to 100%. The recorded BER for all packets lost during these experiments is always low. Thus, one theory that explains this is once again the punctured coding rate 3/4, which is taken from rate 1/2. Since IMD is present, if one or more of the SCs are affected at the same frequencies along every OFDM symbol within a frame, a greater dispersion should occur consistently, leading to complete loss of these SCs. Such situation combined with the fact that the coding rate has been weakened by puncturing could lead to the inability of the convolutional decoder to recover the erroneous bits. At 6 Mb/s, even though the modulation order increases in complexity, the coding rate is not punctured, and is therefore much more robust.

6.4. Summary

A RoF network was implemented for a variety of experimental conditions, namely the use of short and long fiber links, with and without IMD. The mechanisms used to study the different aspects of the system with OFDM signals were presented, and the different configurations were experimented for a number of parameters. This prototype of a structure for a communication system consists in performing the signal generation, the electrical-to-optical conversion/modulation, the optical-to-electrical conversion and the acquisition with real components and instruments. Furthermore, between each transmission/acquisition cycle, the OFDM signal is created by simulation, and additional DSP is performed on the acquired data.

Based on the analysis of a previous characterization of the RSOA, values were defined to polarize the RSOA, and to determine an appropriate optical source power and wavelength. As this was completed, the previously developed *Matlab* simulator and toolbox to communicate with the instruments were used to transmit and acquire cyclically significant amounts of IEEE 802.11a standard-based frames, with EVM calculation, and BER and PER estimation.

In this chapter, the result of the experimental work was presented. It was demonstrated that by introducing optical fiber into a conventional electrical system this way, the transmitted OFDM signal is modified in several ways by the components of the circuit, each potentially introducing distortions of varying nature. The response of these components to the electrical power, to the combination of carriers and to the optical paths was studies by comparing the estimated RCE for each situation.

To conclude this practical implementation, all theoretical concepts of this dissertation such as the OFDM modulation, the channel effects and the importance of synchronization were fundamental. In addition, the previous simulation of wireless OFDM transmissions was essential to recognize the different impairments endured by the OFDM signal, and to understand how these channel effects can be compensated for.

Chapter 7. Conclusions and Future Work

7.1. Conclusions

This aim of this project is to contribute to the introduction of OFDM technology to a Radio-over-Fiber network, where several services are distributed through the coupling of multiple optical and electrical carriers. The general idea behind this architecture is to simplify and centralize DSP operations between a RS and a CS, while reducing the costs for the service provider. Such configuration also improves the end-users experience by enabling the simultaneous distribution of many services, with higher data transmission rates. Three technologies are fundamental to this architecture: the conventional electrical-based systems for user access; the optical fiber to cover for long distances between RS and CS; and finally the modulation techniques.

An important part of this dissertation focused on the characteristics of OFDM modulation, and to its applicability to optical fiber with WLAN-based modulation parameters. The theoretical foundation to this technology was investigated in Chapter 2, where it was shown that OFDM systems present many advantages, but also a few downsides.

The key aspects of IEEE 802.11a frame creation were introduced in Chapter 3, together with some of the notions to consider for OFDM introduction to optical technology. A brief description of the channel effects of each technology was also made, and the performance metrics were defined.

A simulator was developed to understand and confirm all the important aspects of OFDM technology, such as modulation-dependent parameters, the timing-dependent parameters and the synchronization issues. The effect of the channel models were also accounted for. This empirical study was fundamental as a preparation to the remaining part of the project.

The methodologies used to configure the instruments, the implementation of the practical RoF architecture and the performance evaluation can be found in Chapter 5 and Chapter 6.

Due to the concept of orthogonality, OFDM is one of the most bandwidth efficient MCM techniques. Orthogonality allows multiple SCs to overlap in frequency without interfering with each other, because the energy of each subchannel is undetectable to the others. In addition, the modulation can be performed digitally by using the IFFT/FFT algorithm. This is possible because the DFT theory is constructed upon LTI system theory, and perceives any periodic signal as a sum of harmonically related sinusoids, which by nature are orthogonal to each other. Therefore, with the

IFFT/FFT it is possible to modulate and multiplex the SCs, and to perform the opposite operations efficiently and at very low cost.

This technique is very flexible in terms of data rates and robustness, because variable FEC coding rates can be applied on the source bits, and different modulation orders can be used. The FEC coding affects the data rate by introducing a known extent of redundancy into the bit stream, which is used at the receiver to recover from errors. The more redundancy is introduced, the lower the data rate, but the recovery probability increases. The modulation order also influences the transmission rate by grouping variable numbers of bits into symbols. The greater the modulation order, the higher the data rate, but the error probability increases. This was verified through simulations in Chapter 4. From the results, it can be concluded as well that the SNR in OFDM signals is equivalent to the SNR distributed into the SCs. Hence, the influence of the E_b/N_0 on BER for OFDM systems in AWGN channel corresponds to that from conventional systems. In other words, the probability of bit error in OFDM signals also depends on the modulation order and on the coding rate, which are sensitive to noise power.

This technology is very resistant to narrowband interferences. In narrowband transmission systems, if the channel strongly interferes within the frequency band in use, the signal is highly distorted or entirely lost. OFDM systems are wideband, which means that a large number of frequency bands are used simultaneously during transmission. Thus, the channel affects only a percentage of the SCs. Therefore, by combining this wideband diversity with source coding techniques, such as convolutional coding and frequency interleaving, the decoder at the receiver is able to recover more of the erroneous bits.

OFDM modulation has become a valuable technique to wireless transmission systems due to its strong resilience to multipath time and frequency-selective fading environments. To cope with these effects, a very simple solution was introduced to OFDM-based systems: the GI with a CP. Creating the CP for each OFDM symbol has the effect of introducing periodicity. This means that as long as the largest time delay introduced by the channel propagation has duration smaller than the GI period, no information is lost, and only a linearly increasing phase shift is introduced on the received constellations. Hence, the GI duration is a parameter to control the sensitivity of the system to delay spreads. However, if was shown that this symbols extension results in a small loss of SNR, because it represents additional transmitted energy that is discarded at the receiver. Besides, windowing the transition between adjacent OFDM symbols reduces spectral regrowth, but also reduces slightly the effectiveness of the GI. Using the simulator, the effect of a Rayleigh multipath channel model was evaluated for OFDM signals. It was verified that the OFDM signal passing through the Rayleigh multipath channel has a BER versus E_b/N_0 relation identical to the theoretical curve for narrowband systems. Hence, the SCs are experiencing independent Rayleigh flat fading.

Carrier frequency and time synchronization are probably the most vulnerable aspect of this technology. It was seen that a small carrier offset causes the receiver FFT filter to take energy somewhere around the ideal frequency instant. Hence, part of the orthogonality is lost and ICI is introduced, which means that some of the detected energy belongs to adjacent SCs. It was verified by simulation that small frequency errors result in constellation scattering modeled as noise, and global phase rotation. As the error increases, the constellation becomes a highly distorted cloud of samples. Above half the SCs frequency spacing, it is impossible for the receiver to known which carrier is being demodulated. In terms of timing offset, it was also verified by simulation that as long as it is smaller than the GI duration, a linearly increasing phase error is introduced in the direction of $\pm\pi$ as the SCs frequencies go apart from DC. Timing offsets can also be originated by small sampling frequency errors.

Another issue of OFDM systems comes with the level of PAP that rapidly rises. These peaks are very demanding for the amplifiers, and can result in saturation. It was demonstrated that both scrambling and clipping could reduce PAPR effectively. Clipping is simpler, but it involves distortions in the signal that can lead the SNR to degenerate rapidly, because the peaks above a certain threshold are simply cut-off. The task of the scrambler is primarily to avoid large sequences of repeated bits to occur by randomizing the source bits. This process results in a better distribution of the energy of the power spectrum. Consequently, it was verified that the PAPR improves because the probability of the modulated SCs to be multiplexed when all have high energy levels is reduced. For the practical part of the dissertation, since IEEE 802.11a frames are transmitted, scrambling is the technique used.

This dissertation concludes with the application of OFDM technology to a practical RoF architecture. For this part of the work, the objective is to compare the performance of IEEE 802.11a packet-based transmissions for a number of experimental configurations.

From the previous study of OFDM systems, it was acknowledged that it is imperative for the instruments to be well synchronized, so that the relation between them remains approximately constant. The channel spacing of 5 MHz for the transmissions was chosen from the IEEE 802.11a timing-related parameters. It was discussed in Chapter 2 and in Chapter 5 that usually oversampling is necessary to compensate for the limitations of the hardware TF. Based on both instruments specifications, an oversampling factor of 5 was chosen for discussion. This way, transmissions were accomplished within data rates defined in IEEE 802.11a standard, which provides RCE references.

Before proceeding to experiences with the RoF structure, the response of the RSOA to several situations was studied. Based on the spontaneous emission of the RSOA for a range of polarization currents, a good location for optical source tuning was defined. It was observed that the

polarization current of the RSOA influences significantly the optical amplification factor, and that increased values result in a decline in operational wavelength. This allowed the identification of wavelengths near 1550 nm where high reflection occurs with tolerable ripple. Then, for several optical sources the optical amplification factors were measured, and it was verified that reduced power resulted in greater amplification. Finally, the TF of the RSOA for a -17 dBm optical source was observed to make sure that different bias current would not introduce undesired effects.

This part of the experiment was executed for several levels of electrical power, without IMD and with a short fiber link. The performance metric consists in RMS EVM computation, BER and PER for blocks of 20 frames. For all electrical power levels and all RSOA polarization currents, the EVM computed for a set of packets, frequently referred to as RCE, remains approximately constant as the data rate increases. This is in agreement with the suggestion that EVM measurements can provide an approximation of the SNR metric, which can be related to the BER. On the contrary, the PER worsens as the data rate increases. This is the consequence of two modulation-dependent parameters: the convolutional coding rate and the modulation order. Clearly, as the coding rate decreases or the modulation order increases, the PER degrades. From this study, it can be concluded that a higher polarization current, that is, more optical amplification, results in degradation of the RCE. As the RCE degrades, the PER also degrades more for higher data rates. In addition, the RCE improves as the electrical carrier power increases.

Another aspect of the experiment to consider is the IMD. Although four frequencies are used when IMD is active, only some of them have an influence on the frequency being analyzed. The study of the IMD resulted in three main conclusions. The first is that for low electrical carrier power the intermodulation product is very small and its influence becomes negligible. The second is that for higher levels of electrical carrier power, from a block of acquisition to another, the channel conditions are not necessarily the same. However, from the viewpoint of all the OFDM symbols in a packet, the channel is approximately constant. This was verified by observing that one of the interfering carriers, which is generated by a VCO, is not perfectly pure nor stable. The third is that the intermodulation product effect is more evident when the optical fiber is part of the experiment. It is important to remember that the OFDM carrier has its energy spread over a wide band of frequencies. On the contrary, the three remaining carriers are empty, and therefore have all their energy concentrated on a narrow frequency. This means that if the intermodulation product deviates from DC, for 10.5 dBm of electrical carrier power the interference is strong enough to interfere severely with data carrying SCs.

The final section of this dissertation is focused on comparing OFDM performance as the different experimental configurations are tested. Although this aspect is present in all previous acquisitions, it is in this section that the effect of channel estimation for timing errors is discussed.

The constellations used to represent an example of each investigational situation have an evident common impairment: global rotation and linearly increasing phase error. As introduced theoretically in Chapter 2, and further verified by simulation in Chapter 4, it is unmistakable that the constellation samples, independently of the degree of scattering, are affected by this phenomena. Since a common reference oscillating frequency connects the instruments, it is unlikely that any carrier offset was introduced. This effect is most likely the result of a sampling frequency error caused by the rate conversions, combined with an error margin introduced by the low threshold used for packet starting sample detection. Sampling frequency conversion is unavoidable, as it is depending on the rates supported by each instrument. As for the low detection threshold, which is most likely the main cause, it was intentionally lowered to ensure that in the event of high attenuation or distortion of the IEEE 802.11a STS, the frame would still be detected at the first peak. Since this timing error is very small, ISI is never introduced due to the GI, and therefore the point-wise multiplication by the CIR estimate is enough to correct it.

In terms of RCE and PER, for low electrical carrier power the results remain essentially poor for any application in the optical domain, but excellent for all acquisitions performed only in the electrical domain. As the carriers power increases to 0.5 dBm, a significant improvement is observed in the optical domain, and the IMD interference remains barely perceptible. The grouping of the RCE of all optical domain acquisition, despite the differences in fiber length and IMD, indicates that the distortions are still depending mainly on the RSOA. However, with more electrical power, it is evident that each experiment separates from the others. In the optical domain, the measured RCE without IMD is in agreement with IEEE 802.11a specifications for all data rates. Still, as the IMD is introduced, it is obvious that the RCE degrades in both the electrical and the RoF configurations. However, the effect is substantially stronger in the presence of optical fiber. In the electrical domain, the acquisitions remain excellent. A reason to this might be that different frequency components of a signal are amplified to different factors by the RSOA. This could result in greater amplification of the two carriers that are generating the intermodulation product, which then influences the main carrier. The use of an 11 km long optical fiber also introduces noticeable changes to the RCE, which points to the presence of a small amount of chromatic dispersion. Attenuation caused by the long fiber link is not considered as a possible cause, because the optical power is adjusted to ensure that the photo-detector always receives an optical signal with approximately -13.3 dBm.

These results were obtained with the idea of observing the effect of IEEE 802.11a compliant frames in a RoF network, which explains the choices made for oversampling and sampling rate. However, with these instruments they can be improved. For instance, one way to do so is by increasing the oversampling factor under the same remaining conditions (which would effectively

reduce the channel spacing, and therefore the data rates). It was explained in Chapter 5 that oversampling could improve the SNR. Since SNR and EVM can be related, this suggests that the RCE and the PER should improve. Nonetheless, although both RCE and PER would greatly improve for higher oversampling factors (at reduced data rates), the differences in terms of RCE from one experiment to another should remain quite similar, as the same degree of improvement is applied to all of them.

7.2. Future Work

The proposed RoF network architecture experimented in this project demonstrates high potential as a hybrid system. It is fit to answer the needs of both the service providers and the consumers. It enables cost reduction for the infrastructures, provides control and centralized DSP operation, while allowing for service diversity and improvements.

In this project, the IMD is implemented by generating empty RF carriers at specific frequencies. Since they carry no information, the energy is all concentrated into a narrowband frequency. Under these conditions, the intermodulation product consists in a relatively high peak that can strongly interfere, but with only some frequencies of the OFDM signal, because its energy is spread along a wideband. By introducing the system to IMD with modulated carriers, the results might change dramatically. The intermodulation product could interfere with less energy, but on a wider frequency band.

Another aspect to consider is the implementation of the same system with wireless carriers in the electrical domain. The channel effects of the RoF network as it was implemented include mainly distortions introduced by the components, and time delays. Accounting for the severe effects of the wireless multipath channel would provide a more realistic approach of this network.

Appendix A. The Fourier Transform and its use with Matlab

A.1. The Discrete Fourier Transform (DFT)

The DFT is a mathematical tool developed by Jean Baptiste Joseph, Baron de Fourier (1768-1830). Fourier realized that by summing up simple sine and cosine waves, complicated waveforms could be created. In the same way, by performing the opposite operation, intricate signals can be decomposed into a number of summed simple signals [45]. This is known as the Fourier Series, and it enables the representation of any periodic signal as a sum of harmonically related sinusoids. In addition, almost any signal can be represented as an infinite sum of non-harmonically related sinusoids [46].

Based on this theory, Fourier later developed the DFT. The DFT is capable of taking a discrete signal in TD and transforming that signal into its FD representation. It is possible to examine an unknown signal with the DFT by identifying the various frequencies that compose it, and measure their relative "quantity" in the signal [45].

Fourier theory is stated upon Linear Time Invariant (LTI) system theory. Therefore, the DFT seen as a system with input and output signal (sinusoids) is fully consistent with LTI systems requirements, which are scalability, additivity and time invariance. Scalability means that alterations in the input signal amplitude result in matching changes in the output signal amplitude. Additivity implies that signals added at the input result in signals added at the output. Time invariance means that the characteristics of the system are not time dependent, and therefore a shift in the input signal will produce an equivalent shift in the output signal. This is why the Fourier analysis is possible: a complex signal is decomposed into a number of simple signals, each simple signal is analyzed independently, and the complex signal is recomposed into the original signal [47].

In present days, the DFT is a fundamental tool in the area of frequency spectrum analysis, which is employed in many technological fields, such as thermal analysis, image processing, quantum mechanics, physics and of course digital signal processing. In telecommunications, usually hardware generates and receives a signal carrying information, which is transmitted through a medium. Both the hardware and the medium usually corrupt the signal. Since the expected signal has a well-defined spectrum, if the receiver can perform a spectral analysis, it can determine which parts of the signal are information or distortions, and extract the information [45].

In particular, OFDM systems take full advantage of the DFT abilities because with IFFT/FFT operations, the OFDM signal can be modulated, demodulated, multiplexed and analyzed. A data sample given in the FD is modulated by performing an IFFT at the transmitter. OFDM demodulation is

achieved simply by performing an FFT to the TD signal at the receiver. Multiplexing is carried out by feeding the IFFT with a sequence of adjacent samples in the FD. At the IFFT input, each sample is seen as a harmonic frequency. Hence, the output results in a TD waveform that is equivalent to the sum of each individual curve. Demultiplexing is done in a similar way with the FFT performing the reverse operation. In other words, IFFT performs modulation and multiplexing with orthogonality, and FFT performs demultiplexing and demodulation.

Periodicity: Fourier analysis states that any periodic waveform can be represented by a sum of simpler waveforms. The DFT is periodic, and extends from $f = 0$ to $f = f_s$, where f_s if the sampling frequency [14].

Symmetry: When the region of a spectrum is examined, symmetry can be observed between 0 and f_s, around the center point $0.5f_s$. This center point is the Nyquist frequency. Therefore, the region going from $0.5f_s$ to f_s is a mirror image of the data going from 0 to $0.5f_s$. This symmetry adds redundant information [14].

Orthogonality: By definition, sine and cosine are orthogonal to each other. Fourier theory describes a periodic signal as a sum of harmonically related sinusoids. This implies that the harmonics have integer number of cycles in a period. Therefore, all the harmonics are orthogonal to each other. In terms of spectral analysis, this means that even if they overlap, the frequencies will not interfere with one another [45].

Fast Fourier Transform (FFT): The FFT is an algorithm that computes fast and efficiently the DFT. It is due to the speed and discrete nature of the FFT that discrete-time to discrete-frequency transform can be performed with *Matlab*, or in real-time using microprocessors and DSP based systems, hence allowing us to analyze a signal's spectrum [14].

A.2. Mathematical Background

In mathematical terms, the Fourier Series that describes any periodic wave can be written the following way [45]:

$$f(t) = a_0 + \sum_{n=1}^{N} a_n sin(2\pi nft) + \sum_{n=1}^{N} b_n cos(2\pi nft) \quad \textbf{(A.1)}$$

Where: a_0 is a constant that provides the DC offset from zero; a_0, a_n and b_n are called the Fourier Series Coefficients; N is the number of harmonics used in the summation.

In the equation above, the harmonics do not have to be integer values, and can be real or imaginary. However, the harmonics are integer multiples of the starting frequency. Therefore, the starting frequency defines how finely the signal is decomposed. It is sometimes referred to as the resolution frequency for that reason. The equation below describes the harmonics [45]:

$$f_n(t) = nf(t) = \frac{n}{T} \tag{A.2}$$

Where: T is the period of the first wave; n is the harmonic.

Using Equation (A.2), we can rewrite Equation (A.1) with respect to the period of the fundamental waveform and each harmonic as:

$$f(t) = a_0 + \sum_{n=1}^{\infty} a_n sin\left(\frac{2\pi nt}{T}\right) + \sum_{n=1}^{\infty} b_n cos\left(\frac{2\pi nt}{T}\right) \tag{A.3}$$

In addition, all sine waves can be converted to cosine waves by adding a half-period phase shift. Hence, the equation is rewritten as [45]:

$$f(t) = C_0 + \sum_{n=1}^{\infty} C_n cos\left(\frac{2\pi nt}{T} + \phi_n\right) \tag{A.4}$$

Where: C_0 is the constant that provides the DC offset from zero; C_0 and C_n are the Fourier Series Coefficients; T is the period of the first wave; n is the harmonic.

Using Euler complex representation, the generalized Fourier equation can be represented as follows:

$$f(t) = \sum_{n=1}^{\infty} C_n e\left(\frac{j\pi nt}{T} + \phi_n\right) \tag{A.5}$$

In signal processing, the Fourier Coefficients define the spectral components of a signal. They provide knowledge concerning which frequencies are present in the signal, and on the “amount” of those frequencies.

A.3. Understanding the FFT with *Matlab*

A.3.1. The FFT as a tool for Frequency Spectrum Analysis

Consider a simple sine wave defined as $f(t) = \sin(2\pi f_0 t)$. In this example, the fundamental frequency is $f_0 = 2\ Hz$, corresponding to two cycles per second. To generate harmonics, we must multiply the fundamental frequency by integer values. For instance, the frequency of the second harmonic is $2f_0 = 4\ Hz$, and the third harmonic has frequency $3f_0 = 6\ Hz$.

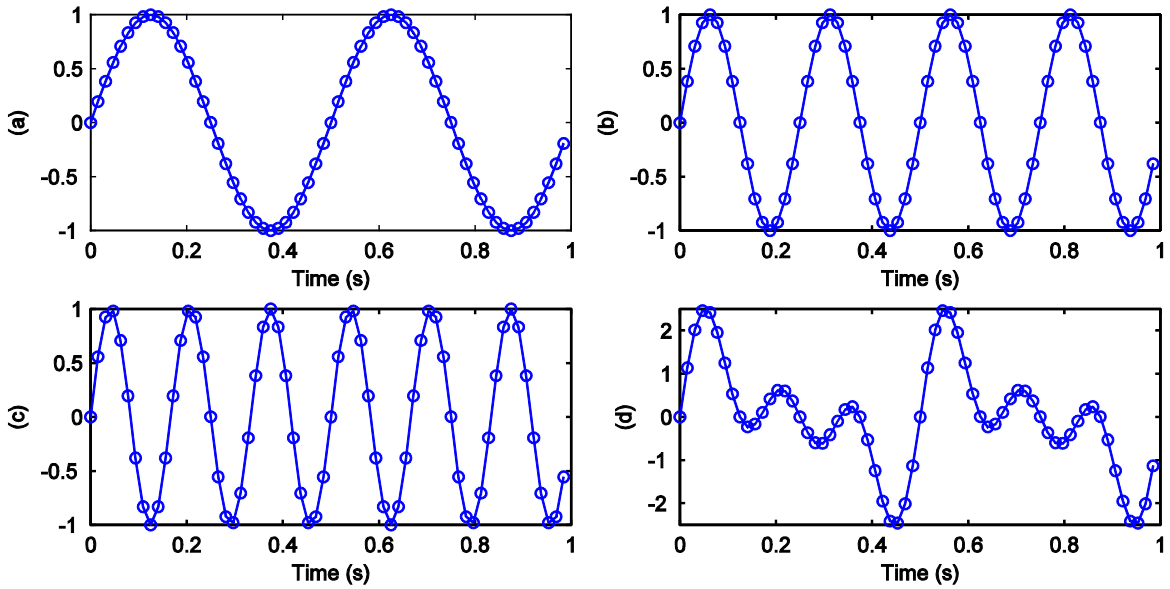

Figure A.1 – (a) Sine wave with f_0 = 2 Hz; (b) Sine wave with f_0 = 4 Hz; (c) Sine wave with f_0 = 6 Hz; (d) The summed sines (a)+(b)+(c)

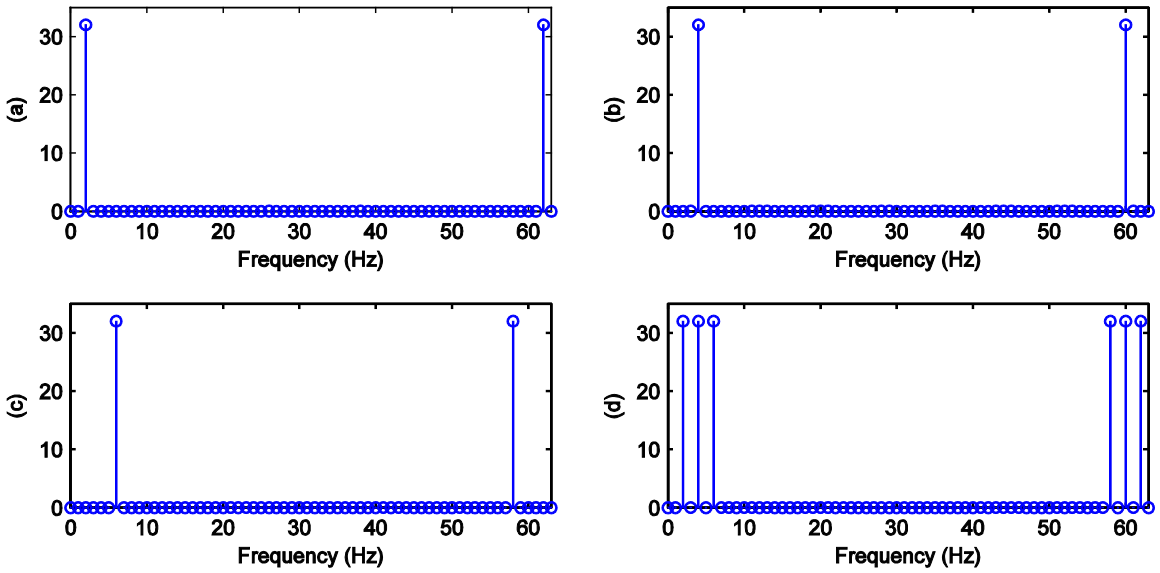

Figure A.2 – Frequency spectrums obtained using the FFT for: (a) a sine wave with f_0 = 2 Hz; (b) a sine wave with f_0 = 4 Hz; (c) a sine wave with f_0 = 6 Hz; (d) the summed sines (a)+(b)+(c).

As mentioned previously, by summing these three periodic sinusoids, a new periodic signal is created, which contains all the frequencies of the summed sinusoids. It can be observed in Figure A.1 that each simple signal is periodic and that the signal composed by the sum of the others appears more complicated and is periodic too.

By performing the FFT operation to the TD signal from Figure A.1 with the *Matlab* built-in *fft()* function, the corresponding frequency spectrums depicted in Figure A.2 were obtained. Notice that in all spectrums the symmetric property can be observed around the Nyquist frequency. As

expected, the frequency related information of the three summed sinusoids is represented in the last frequency spectrum. It has become possible to see how many frequencies exist in that signal. However, by looking at the plots as they are, it is not possible to extract information on the frequency in the sense that there is no indication that the peaks are in the right place. In addition, the amplitudes are very high and the spectrums are not centered around zero.

In order to properly present the frequency spectrum, we can use another *Matlab* built-in function called *fftshift()*. This function swaps the left and right halves of the spectrum. In essence, the negative frequencies that appear on the right side of the spectrum are shifted to the left. By doing this, the frequency spectrum becomes centered and two-sided. Since it is known that the FFT has a periodicity that extends from $f = 0$ to $f = f_s$, the correct frequency axis after the shifting will go from $-0.5f_s$ to $0.5f_s$. In addition, for a proper comparison between frequencies, the amplitude should be normalized. Figure A.3 shows the corrected, meaningful spectrums. At this point, we can see that the information within the spectrum is entirely symmetric. Therefore, by representing only the positive spectrum and discarding the redundant negative section of the spectrum we can still define the frequency spectrum.

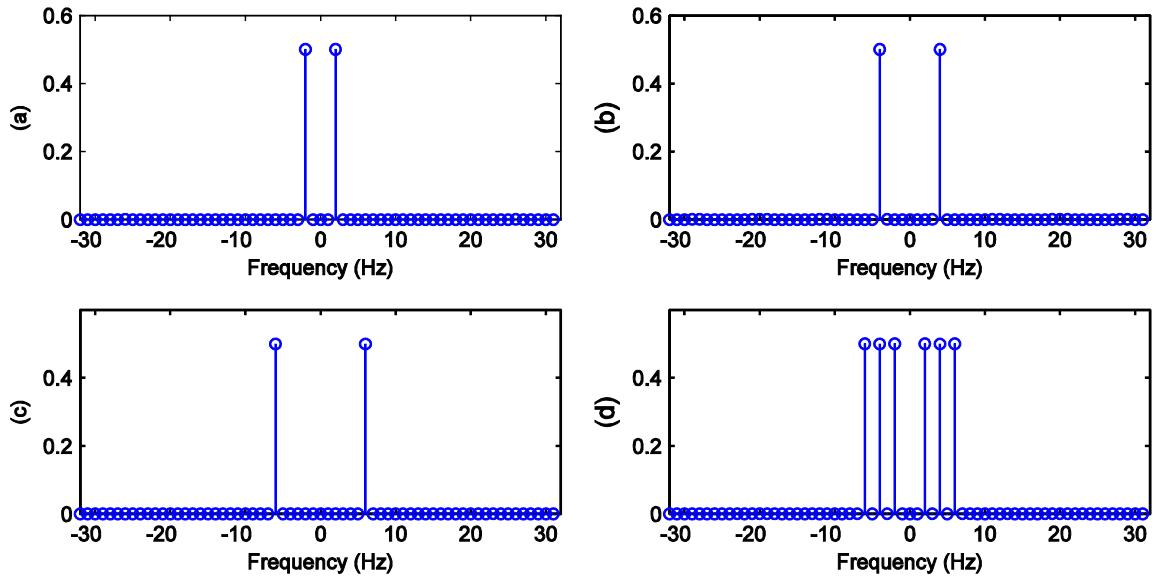

Figure A.3 – Two-sided and centered frequency spectrums with amplitude normalization for: (a) a sine wave with f_0 = 2 Hz; (b) a sine wave with f_0 = 4 Hz; (c) a sine wave with f_0 = 6 Hz; (d) the summed sines (a)+(b)+(c).

A.3.2. The FFT and the effect of Zero Padding

There are two reasons that can justify the use of zero padding. The first reason consists in increasing the efficiency of the FFT computation. Optimal computational efficiency is achieved for FFT lengths that are equal to 2^N samples. The second aspect that motivates the use of zero padding is the need for a greater spectral resolution. In practice, it is generally useful to zero pad a signal up to 4 times its original length, providing a 4-fold increase in the frequency resolution.

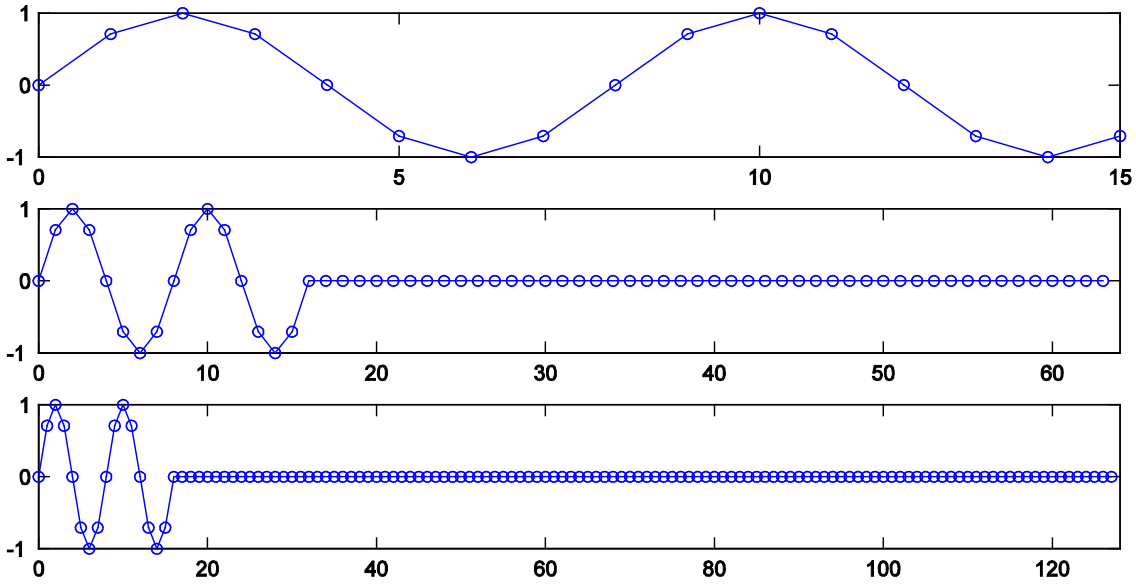

Figure A.4 – Sine wave with f_0 = 4 Hz and 8 samples per period; curve padded with zeros to reach 64 samples; curve padded again with zeros to reach 128 samples.

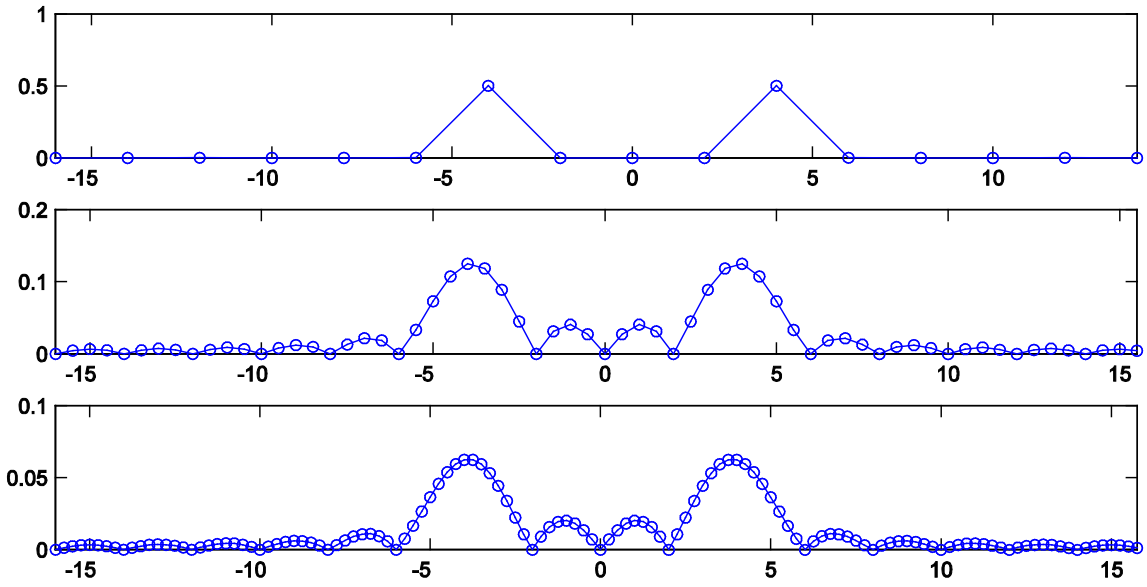

Figure A.5 – Frequency spectrum of: the signal computed with no zero padding; the signal computed with 64 samples; the signal computed with 128 samples.

In this particular example, Figure A.4 shows the original curve, and two curves manually zero padded. In practice, the *fft()* function in *Matlab* will zero pad the input data automatically if the FFT length specified is greater than the number of samples. Figure A.5 illustrates the effect of zero padding for each case. It can be observed that, as the number of samples increases, the shape of the spectrum appears better defined. This is interesting in the sense that it becomes easier to analyze the frequency spectrum.

However, it is very important to understand that in reality only the resolution of the spectrum is increased as more samples define it. Effectively the data is interpolated and more samples are produced, but no additional information is added to the signal.

The next example demonstrates a practical advantage of resolution increase to see more components of a frequency spectrum. Consider a periodic signal composed by a sum of sines such as $f(t) = \sin(2\pi(1.5)t) + \sin(2\pi(2)t) + \sin(2\pi(2.5)t)$. Three similar frequencies exist in this signal. In Figure A.6, we can see the frequency spectrum with and without resolution enhancement. It can be observed that, where only one peak was visible, the "improved" spectrum now shows two more peaks that previously appeared "hidden".

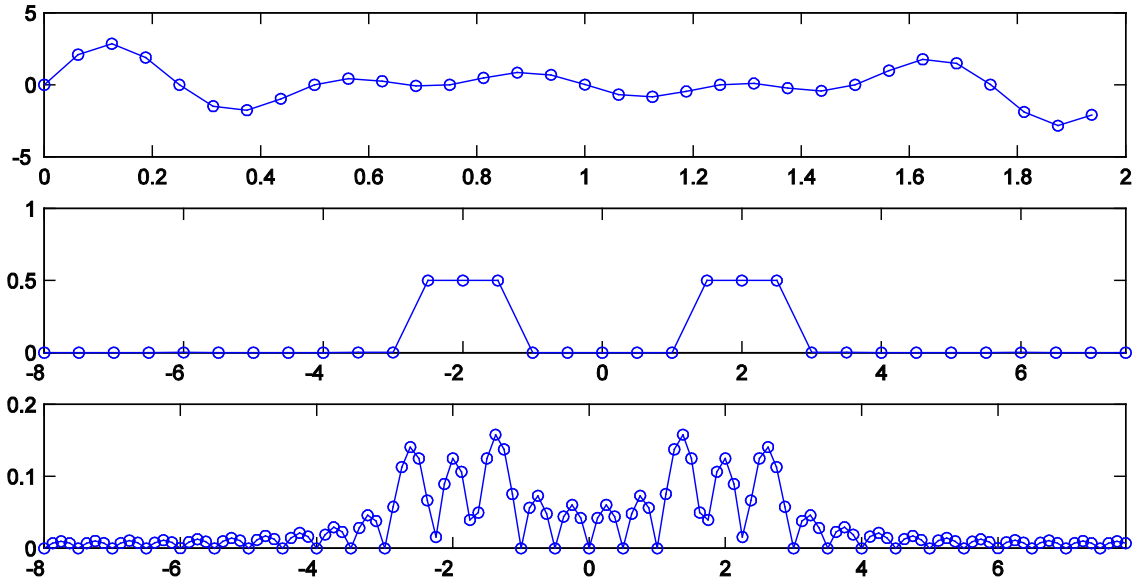

Figure A.6 – The sum of three sine waves at 1.5 Hz, 2 Hz and 2.5 Hz; Frequency spectrum with no zero padding; Frequency spectrum with an 8-fold resolution increase.

Again, it is important to realize that since no new information was added, the information was already there. It is the number of samples that was not high enough to define the existing peaks. In terms of information, as long as the sampling is performed under the Nyquist rate, all the necessary information that defines the continuous-time signal is present. Zero padding in essence consists in interpolating the information with more samples, without really adding any additional information, which has the effect of increasing the spectral resolution.

A.3.3. The FFT as a Modulator and Multiplexer for OFDM Systems

In this section we will see how OFDM technology is implemented using FFT to perform simultaneously both modulation and multiplexing of multiple carriers, while guaranteeing orthogonality between SCs.

Consider the BPSK sequence [-1,-1,-1,-1]. This is the existing information in the FD. To modulate it, we need to translate this information into a TD waveform. In order to do so, we can use the *Matlab* built-in *ifft()* function. In terms of frequencies, if we feed the BPSK sequence to the IFFT function as it is, each sample will represent a distinct frequency. By the DFT definition, each of these frequencies will be a harmonic of the fundamental frequency located at the first sample. Therefore, a single signal containing these four frequencies $1f_0$, $2f_0$, $3f_0$ and $4f_0$ is expected at the IFFT output. This can be verified easily with a few *Matlab* commands:

```
Fo = 1;         % fundamental signal frequency in Hz (periods per second)
Fs = 32;        % sampling rate (samples per second)
N = Fs/Fo;      % samples per period
T = 1;          % period in seconds
Ts = 1/Fs;      % sampling time interval
A = -1/Fs;      % signal peak amplitude
NFFT = 8*Fs;    % FFT length (8-fold resolution increase)
t = 0:Ts:T-Ts; % time vector

NSC = 4;            % number of data subcarriers
a = -ones(1, NSC); % generate BPSK symbols (the information)
b = diag(a);        % each row is a subcarrier with one sample shifted right

x0 = zeros(NSC, Fs);
for k = 1 : NSC
    x0(k,:) = A*exp(1i*2*pi*(k-1)*Fo*t); % periodic signals (DC, harmonics)
end
xx0 = sum(x0, 1);     % sum all the periodic signals (manual)
x1 = ifft(b, Fs, 2); % equivalent periodic signals
xx1 = sum(x1, 1);     % sum all the periodic signals (IFFT)
xx2 = ifft(a, Fs);    % equivalent IFFT operation

[ XX0 F0 ] = fftcenter(xx0, Fs, NFFT); % perform FFT and center spectrum
[ XX1 F1 ] = fftcenter(xx1, Fs, NFFT); % perform FFT and center spectrum
[ XX2 F2 ] = fftcenter(xx2, Fs, NFFT); % perform FFT and center spectrum

figure, subplot(3,1,1), plot(t, real(xx0), 'o-', 'MarkerSize', 3);
title('Manually generated signal'); set(gca, 'XTick', [], 'YTick', []);
subplot(3,1,2), plot(t, real(xx1), 'o-', 'MarkerSize', 3);
title('Multiple IFFT generated signal'); set(gca, 'XTick', [], 'YTick', []);
subplot(3,1,3), plot(t, real(xx2), 'o-', 'MarkerSize', 3);
title('Single IFFT generated signal'); xlabel('Time (s)');
set(gcf, 'Position', [440 436 600 300]); set(gca, 'YTick', []);

figure, subplot(3,1,1), plot(F0, abs(XX0), 'o-', 'MarkerSize', 3);
title('Manually generated signal'); set(gca, 'XTick', [], 'YTick', []);
subplot(3,1,2), plot(F1, abs(XX1), 'o-', 'MarkerSize', 3);
title('Multiple IFFT generated signal'); set(gca, 'XTick', [], 'YTick', []);
subplot(3,1,3), plot(F2, abs(XX2), 'o-', 'MarkerSize', 3);
title('Single IFFT generated signal'); xlabel('Frequency (Hz)');
set(gcf, 'Position', [440 436 600 300]); set(gca, 'YTick', []);
```

The *Matlab* code above allows us to see that, in fact, the IFFT performed to the data samples as a sequence is equivalent to creating a modulated subcarrier for each sample at a harmonic frequency, and summing them together. This small generic simulation confirms in two ways that the IFFT performs both data modulation and subcarrier multiplexing. First, a number of periodic waveforms with harmonically related frequencies are created without using the IFFT, and are

summed together. Second, equivalent periodic waveforms are generated, this time using an IFFT for each, with a shift in the information sample to create the harmonic frequency, and are summed together. Third, a direct IFFT implementation is performed to an equivalent four information samples sequence. It can be observed in Figure A.7 and Figure A.8 that the results are alike in both TD and FD, therefore providing evidence that the IFFT algorithm can perform modulation and multiplexing while ensuring orthogonality.

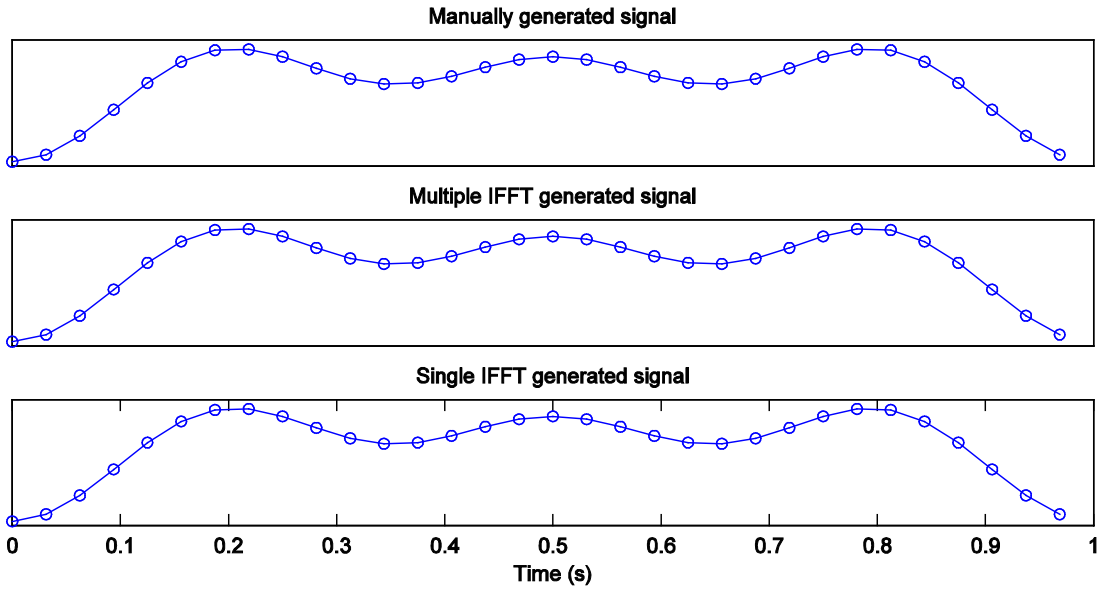

Figure A.7 – A generic OFDM signal generated in three different ways: (a) Periodic waveforms created separately and summed together; (b) Periodic waveforms created separately with IFFT and summed together; (c) A single IFFT operation that provides the same output.

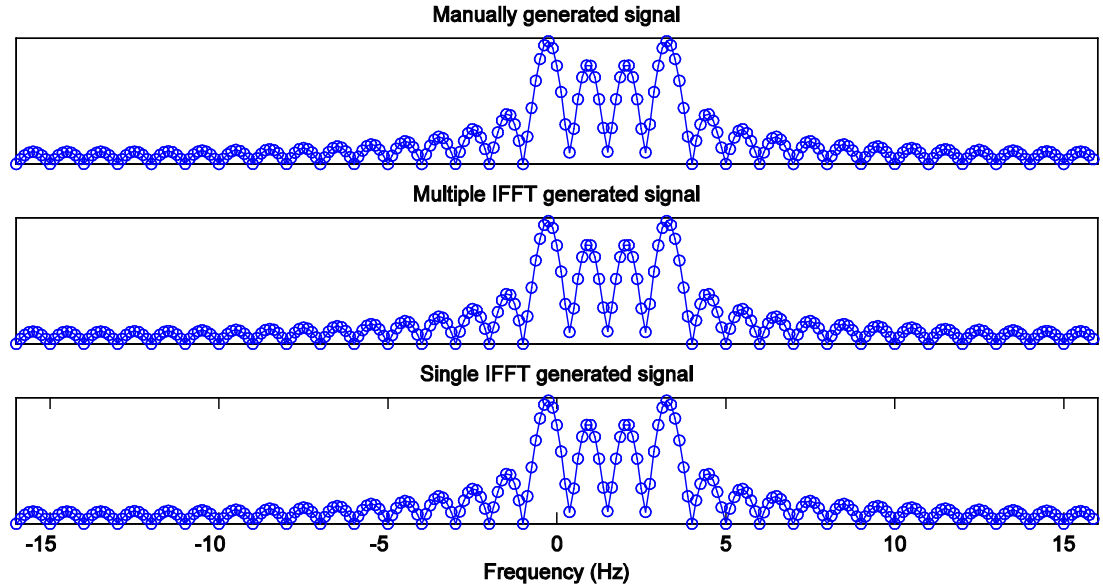

Figure A.8 – Frequency spectrum of: (a) Periodic waveforms created separately and summed together; (b) Periodic waveforms created separately with IFFT and summed together; (c) A single IFFT operation that provides the same output.

Appendix B. Modulating Arbitrary OFDM Signals

B.1. Complex or Real OFDM Modulation

OFDM signals can be created directly and digitally using the IFFT/FFT algorithm. The modulation/multiplexing is performed by taking the IFFT of the chunks of samples in the FD. Before doing so, the samples must be prepared and placed in the correct location, corresponding to the SCs. Two possible outputs samples can be generated by taking the IFFT: complex or real.

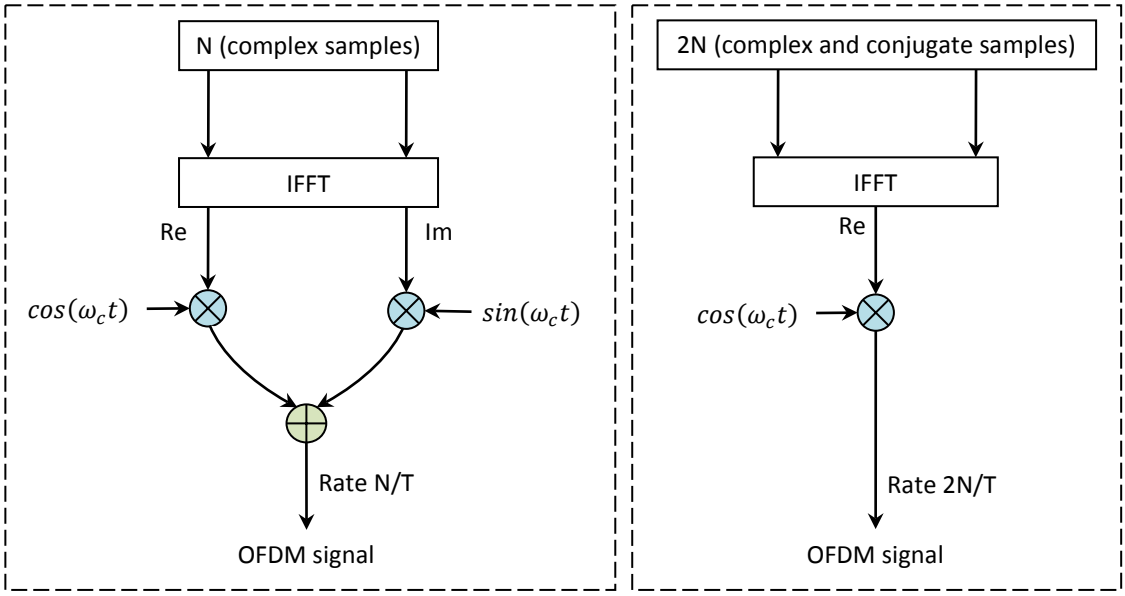

Figure B.1 – Transmission with (left) and without (right) additional IQ modulation [10].

If the transmission is to be made using an IQ modulator, a complex output is expected from the IFFT, which means that the IFFT input must be of N complex modulated data symbols [10]. The complex output is obtained by using both the positive and the negative frequencies to allocate different SCs.

Conversely, the real output is obtained by taking advantage of the Hermitian symmetry property, where the IFFT input must represent an odd function composed by $2N$ samples. That is, N samples are the complex modulated data samples, and the other N samples are the complex conjugate of the original samples [7] [10]. In other words, half of the frequencies contain the information to transmit, and the other half is the complex conjugate of the samples.

B.2. Generating Arbitrary Baseband OFDM Signals

In this section, the process for arbitrary OFDM modulation is illustrated, for the generation of complex and real baseband signals carrying the same information. The following parameters summarize this simulation:

- The channel spacing is 10 MHz;
- The baseband signal is a single packet, with 16 OFDM symbols;
- The base FFT length is 16 samples;
- An oversampling factor of 2 is used;
- The GI is a CP, increasing the symbol length by a quarter of the FFT length;
- The windowed transition is raised-cosine, altering half the GI length;
- Each OFDM symbols has 4 data SCs and 2 pilot SCs;
- The source bits are encoded with convolutional code at rate 3/4;
- The data modulation is 4-QAM constellation.

	N_{FFT}	N_{GI}	N_{WIN}	N_{SYM}	T_{FFT}	T_{GI}	T_{WIN}	T_{SYM}
Complex	16	4	2	20	1.6 µs	0.4 µs	0.2 µs	2 µs
Real	32	8	4	40	3.2 µs	0.8 µs	0.4 µs	4 µs

Table B.1 – Complex and Real OFDM modulation parameters.

The first step of the OFDM system model presented in Chapter 2 suggests source coding to increase the system's robustness against signal degradation. In this example, only FEC coding is performed on the bit stream.

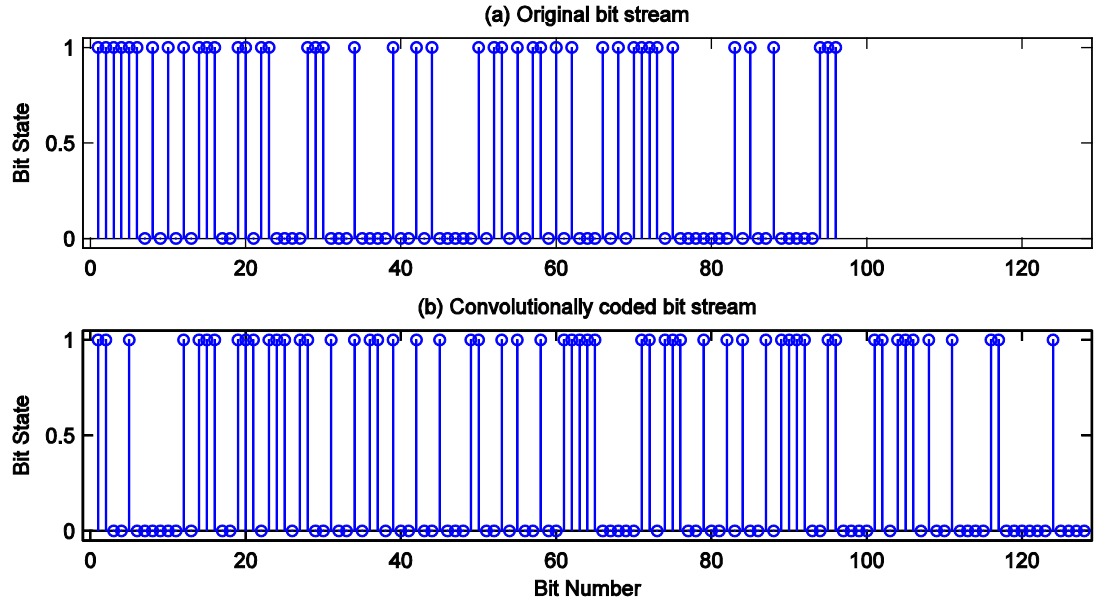

Figure B.2 – a) Original bits stream; b) Convolutionally coded bits stream at rate 3/4.

Consider a serial bit stream composed by 96 pseudo-random bits. By submitting the bit stream to a convolution code with rate 3/4, first a convolutional code with rate 1/2 is applied, meaning that one redundant extra bit is generated for each existing original bit, and then a puncturing pattern is applied to obtain a 3/4 rate. Hence, the number of coded bits to be transmitted is now given by $96/(3/4) = 128$. This implies a loss in transmission efficiency because irrelevant non-information bits are transmitted, thus using additional power and bandwidth, but it is an important characteristic to recover from interferences that can corrupt the data.

At this point, the bit stream can already be split between the several SCs in order to modulate each of them with a different data modulation scheme. However, in this case 4-QAM modulation is applied to all the data SCs, which means that a single modulation can be done on the whole stream.

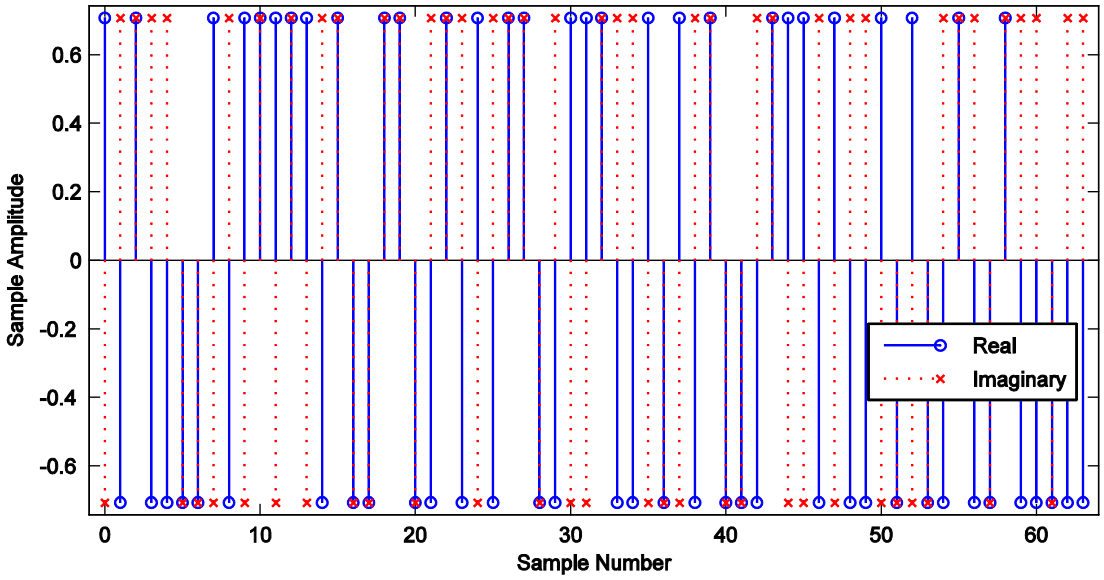

Figure B.3 – Modulated complex data samples using 4-QAM modulation scheme.

With this particular data modulation scheme, the number of bits per data symbol is given by $log_2(4) = 2$. This means that the 128 coded bits are now contained in only $128/2 = 64$ modulated complex data symbols. For this specific example, Figure B.3 shows that the 4-QAM modulated data is given by the following sequence for the first 12 complex data samples, which correspond to the first three OFDM symbols:

DSC0	DSC1	DSC2	DSC3	DSC0	DSC1	DSC2	DSC3	DSC0	DSC1	DSC2	DSC3	…
0,7-0,7j	-0,7+0,7j	0,7+0,7j	-0,7+0,7j	-0,7+0,7j	-0,7-0,7j	-0,7-0,7j	0,7-0,7j	-0,7+0,7j	0,7-0,7j	0,7+0,7j	0,7-0,7j	…

Table B.2 – First 12 samples of 4-QAM modulated data in series.

Now, the modulated data must be prepared for the third part of the OFDM model: the OFDM modulation. Since we are considering 4 data SCs, we know that our 64 modulated samples will be

divided between them, and therefore all the modulated samples will later be distributed through $64/4 = 16$ OFDM symbols. In order to perform OFDM modulation, the modulated data must first undergo serial-to-parallel conversion [15] as shown in Table B.3, where each column represents one of the data SCs, and each segment composed by each row is a data chunk that will be carried into an OFDM symbol.

	DSC0	DSC1	DSC2	DSC3
CHUNK0	0,7-0,7j	-0,7+0,7j	0,7+0,7j	-0,7+0,7j
CHUNK1	-0,7+0,7j	-0,7-0,7j	-0,7-0,7j	0,7-0,7j
CHUNK2	-0,7+0,7j	0,7-0,7j	0,7+0,7j	0,7-0,7j
...	...	...	...	...

Table B.3 – First 3 chunks of 4-QAM modulated samples in parallel.

It was explained that the OFDM modulation can be performed by applying the IFFT algorithm to each data chunk in the FD, thus resulting in TD OFDM symbols. However, the N modulated data samples must first be prepared depending on the output needed from the IFFT. For the OFDM modulation presented in this example, the IFFT output for both complex and real baseband waveforms are implemented. The frequency allocation of the SCs is defined as depicted below for each OFDM symbol.

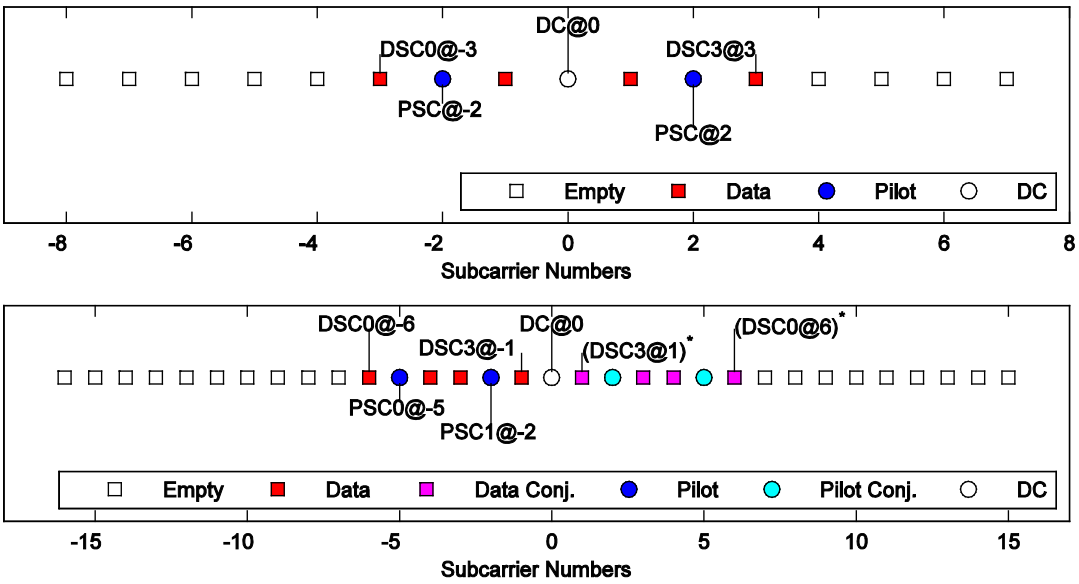

Figure B.4 – SCs frequency allocation before IFFT operation for: a complex output on top; a real output at bottom.

First, a number of empty guard SCs are placed from left to right, leaving enough space for the data SCs and pilot SCs. Then, the complex data SCs can be positioned from left to right at predetermined locations, and the pilot SCs among them. For the complex IFFT output, the N frequencies are placed from -8 to 7, that is, half of the SCs are allocated in the negative frequencies, and the other half on the positive frequencies after DC. For the real IFFT output, N frequencies are

allocated from indexes -15 to -1, as depicted in Figure B.4. At this point, the DC frequency can be reserved at index 0, and the conjugate of the previously allocated SCs going from indexes -6 to -1 can now be placed, flipped from right to left, at indexes going from 1 to 6. The remaining frequencies after the last complex conjugate data SC are empty guard SCs. As a result, all the SCs are allocated amongst $2N$ total frequencies.

N complex samples											
GSC	GSC	GSC	DSC0	PSC0	DSC1	DC	DSC2	PSC1	DSC3	GSC	GSC
...	0	0	0,7-0,7j	1	-0,7+0,7j	0	0,7+0,7j	1	-0,7+0,7j	0	...
...	0	0	-0,7+0,7j	1	-0,7-0,7j	0	-0,7-0,7j	1	0,7-0,7j	0	...
...	0	0	-0,7+0,7j	1	0,7-0,7j	0	0,7+0,7j	1	0,7-0,7j	0	...
...	...	...	...	...	...	...	...	...	...	...	...

Table B.4 – Modulated data prepared for IFFT with a complex output of N samples.

N complex samples									DC+N-1 complex conjugate samples							
GSC	GSC	GSC	DSC0	PSC0	DSC1	DSC2	PSC1	DSC3	DC	DSC3	PSC1	DSC2	DSC1	PSC0	DSC0	GSC	GSC
...	0	0	0,7-0,7j	1	-0,7+0,7j	0,7+0,7j	1	-0,7+0,7j	0	-0,7-0,7j	1	0,7-0,7j	-0,7-0,7j	1	0,7+0,7j	0	...
...	0	0	-0,7+0,7j	1	-0,7-0,7j	-0,7-0,7j	1	0,7-0,7j	0	0,7+0,7j	1	-0,7+0,7j	-0,7+0,7j	1	-0,7-0,7j	0	...
...	0	0	-0,7+0,7j	1	0,7-0,7j	0,7+0,7j	1	0,7-0,7j	0	0,7+0,7j	1	0,7-0,7j	0,7+0,7j	1	-0,7-0,7j	0	...
...	...	...	...	...	...	...	...	...	...	...	...	...	...	...	...	...	...

Table B.5 – Modulated data prepared for IFFT with a real output of 2N samples (Hermitian symmetry).

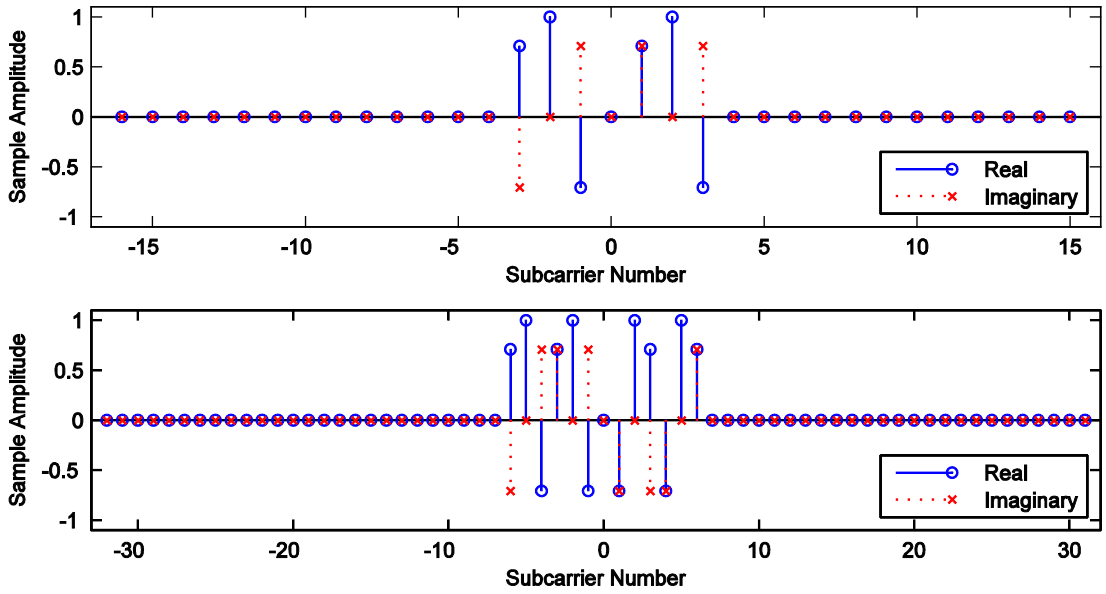

Figure B.5 – The first FD OFDM chunk prepared for the IFFT operation, with 2-fold oversampling by zero padding: complex output on top; real output at bottom.

Again, each column contains one SC and each row is an OFDM symbol in the FD. The pilot SCs are modulated with BPSK scheme and are positioned between sets of data SCs to estimate phase and

frequency shift errors at the receiver. In this case, 2 pilot SCs were used for demonstration purpose. The empty guard SCs also provide a slight resolution improvement, but reduce the bandwidth efficiency.

In this example, $N = 16$ samples were chosen as the base IFFT size. However, for the real IFFT output the number of samples is doubled due to the additional complex conjugate component. In addition, 2-fold oversampling by zero padding is used in this example. Therefore, the IFFT output has $N_{FFT} = 2 \times N = 32$ TD samples for the complex output, and $N_{FFT} = 2 \times 2N = 64$ samples for the real output. In other words, each sample corresponding to each one of the frequencies is multiplexed with the others into one single OFDM symbol. Figure B.4, Table B.4, Table B.5 and Figure B.5 illustrate in detail how the FD construction of OFDM symbols is achieved. Note that in Figure B.5, the SCs require a final shifting before the IFFT operation. After shifting the samples, DC is located at the starting leftmost position. The configuration presented in Figure B.5 includes the zeros padded to achieve 2-fold oversampling.

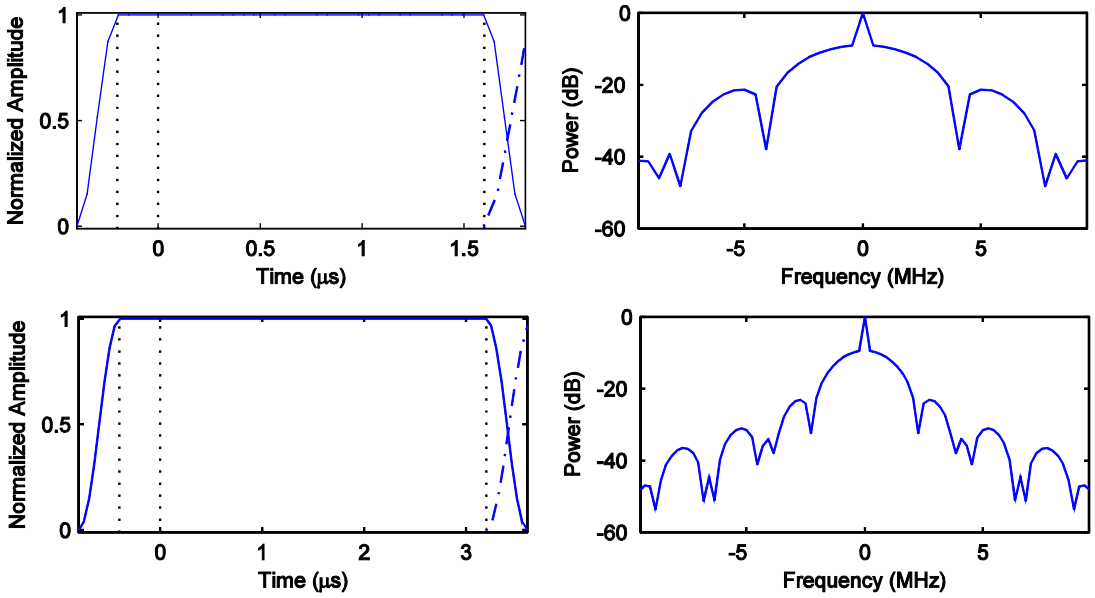

Figure B.6 – Raised-cosine window shape applied to each OFDM Symbol, with 2-fold oversampling: applied to the complex samples on top; applied to the real samples at bottom.

At this point, the IFFT is performed on each chunk to create the TD OFDM symbols. Then, the GI can be generated by extending each symbol with a CP, as introduced in Section 2.3.4. In this example, the CP was defined as a quarter of the length of the FFT. Using the last samples of the effective transmission samples to create this GI has the effect of making the OFDM symbol appear continuous in time. The length of each OFDM symbol in samples with the GI and without oversampling can be found in Table B.1. At present, the GI and the CP are the same extended samples. By applying a window to part of the extended samples, the length of unchanged cyclic extension is reduced, that is, the effective GI duration decreases. On the other hand, the window will

smooth the transition between adjacent OFDM symbols, therefore enhancing the spectral regrowth caused by amplitudes differences. Raised-cosine is a popular window type because it is quite simple, reasonably easy to implement and flexible. For this simulation, a window length with half the length of the cyclic extension is specified, as shown in the raised-cosine window shape from Figure B.6. The window is applied to each OFDM symbol, and the shaped samples from adjacent OFDM symbols are summed as described in Section 2.3.5.

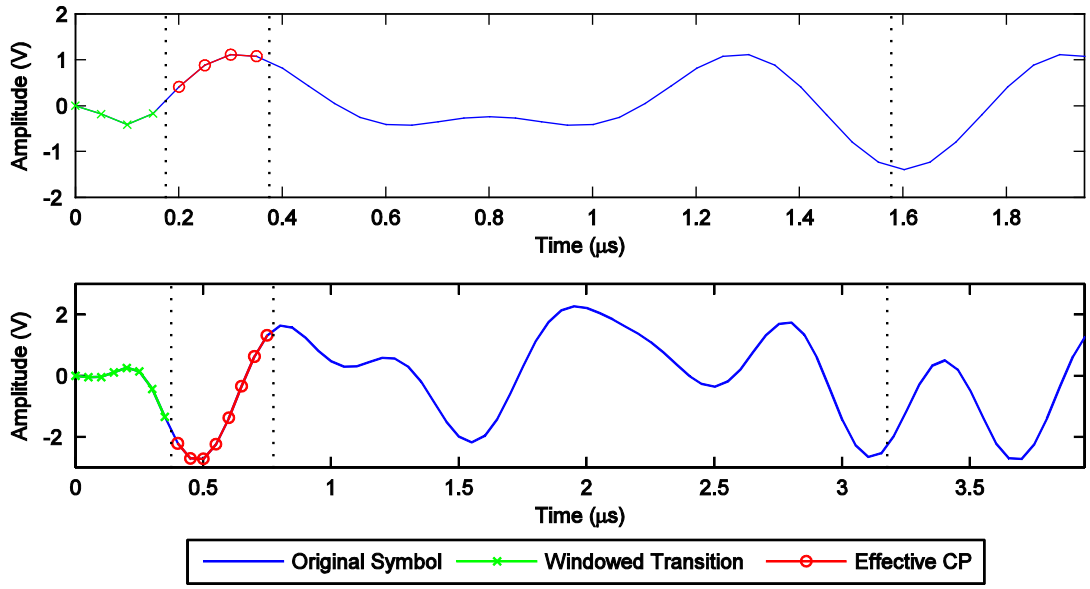

Figure B.7 – The first TD OFDM symbols, with 2-fold oversampling by zero padding: real part of complex output on top; real output at bottom.

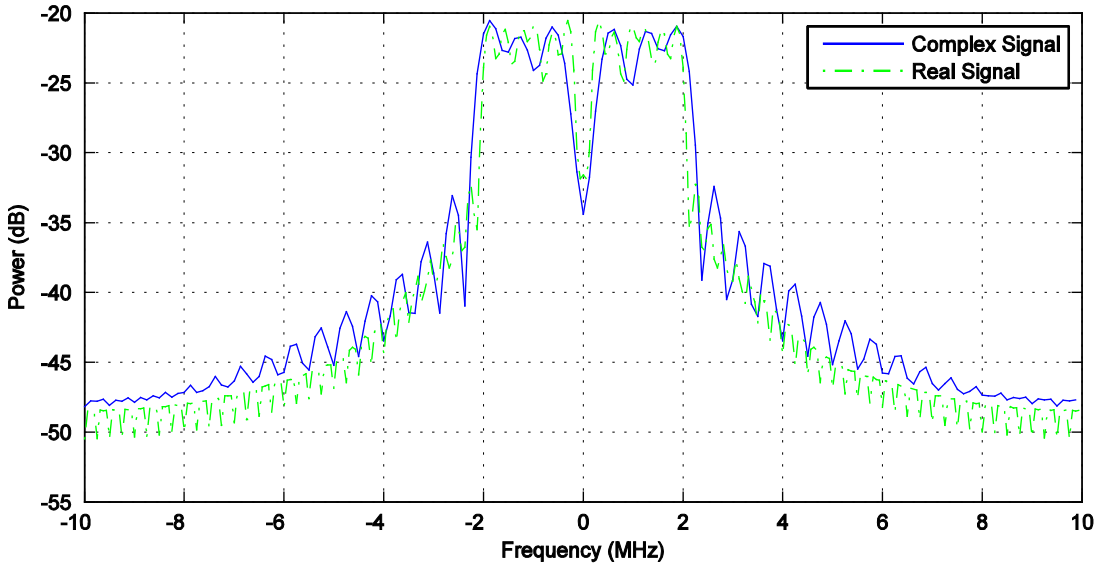

Figure B.8 – Two-sided frequency spectrum of the OFDM signal.

Consider the predefined spectral bandwidth occupancy of $B = 10\,MHz$ per OFDM symbol. Since oversampling is used, to maintain the frequency components at the correct rate, the sampling

rate must be increased to $2B = 20\ MHz$. Therefore, the timing-related parameters from Table B.1 remain the same. The effective component of the OFDM symbol has duration that is resulting from the elementary frequency component, which is the first harmonic. The first harmonic, sometimes referred to as resolution frequency, defines the SC frequency spacing. In this case, it is given by $\Delta F_C = 20\ MHz/32 = 625\ kHz$ for the complex signal, and $\Delta F_R = 20\ MHz/64 = 312.5\ kHz$ for the real signal. However, in reality the GI extends the OFDM symbols, so the OFDM symbol periods become $T_{SYM_C} = 1/(20\ MHz/40) = 2\ \mu s$ and $T_{SYM_R} = 1/(20\ MHz/80) = 4\ \mu s$.

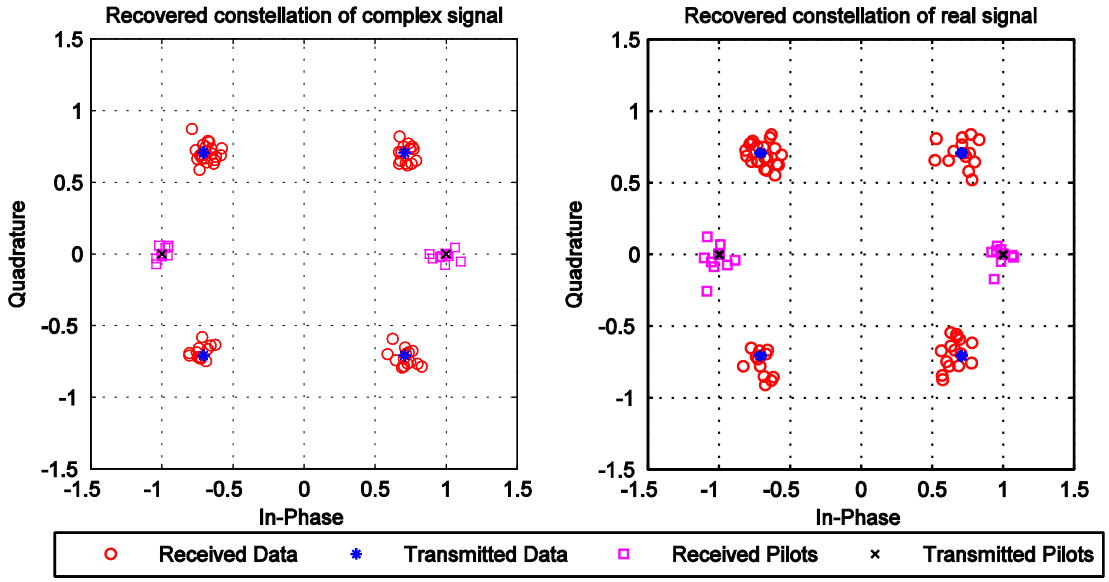

Figure B.9 – Superimposed constellations of the transmitted and recovered SCs.

Knowing the number of SCs per OFDM symbol, the modulation order and the coding rate, the number of information bits per OFDM symbol, that is, the data rate is determined as:

$$N_{BPSC} = N_{SD} \times log_2(M) \times R = 4 \times log_2(4) \times (3/4) = 6$$

$$DR_C = \frac{N_{BPSC}}{T_{SYM_C}} = \frac{6}{2\ \mu s} = 3\ Mbits/s$$

$$DR_R = \frac{N_{BPSC}}{T_{SYM_R}} = \frac{6}{4\ \mu s} = 1.5\ Mbits/s$$

In this case, the simulation is performed with baseband channel effects. The SNR relation is 20 dB in a 2 tap multipath complex random channel, which in this case is still within the GI duration.

From the results it is observed that preparing the IFFT for a real output implies a reduction to half the transmission rate.

Appendix C. Instruments Specifications

C.1. Keithley Model 2910 RF Signal Generator

In ARB waveform mode, the *Keithley Model 2910* expects ARB files with the interleaved IQ samples, the average power factor of the samples and the sampling rate in order to "playback" the transmission. The ARB files can then be loaded into memory and transmitted at the specified sampling rate, with specified center frequency and power. Then, the instrument up-converts the signal by performing IQ modulation with the baseband complex samples from the ARB file to modulate an RF carrier.

Sampling Rate (Hz)			
50000	125000	1250000	10000000
78125	156250	1562500	12500000
	250000	2500000	25000000
	312500	5000000	50000000
	500000	6250000	
	625000		

Table C.1 – Keithley Model 2910 supported sampling rates for ARB waveforms playback [42].

Although the Amplitude is specified in dBm as a parameter external to the ARB file, the Output Power of this instrument takes into account the average power factor of the complex waveform placed in the header of the ARB file to transmit. Therefore, when specifying the Amplitude of the transmission, in order for the Output Power of the instrument to correspond to the power required by the user, the following should be considered:

$$RMS\ Power = \frac{\sqrt{\sum(I^2) + \sum(Q^2)}}{Waveform\ Record\ Size} \tag{C.1}$$

$$Power\ Factor = 10 \times log_{10}(RMS\ Power) \tag{C.2}$$

$$Output\ Power = Amplitude + Power\ Factor \tag{C.3}$$

The equations above are described in [42]. The I and Q values must be normalized to a maximum range of -1.0 to 1.0. Lower distortion should be achieved by limiting the I and Q values to a range of -0.5 to 0.5. By changing the value of the RMS Power, the user can balance the maximum amplitude, distortion and noise performance [42].

C.2. Tektronix RSA 2203A Real-Time Spectrum Analyzer DC-3GHz

The *Tektronix RSA 2203A* receives the RF signal, and converts it into a 20 MHz IF signal. At this stage, the signal is also adjusted for the upcoming ADC conversion with low-noise amplification, fine-tuning attenuation and anti-alias filtering. After being down-converted, the signal enter the ADC with a resolution of 14 bits and a sampling rate of 51.2 MHz. The next signal processing step performed by the receiver is to send the signal to the Digital Down Converter (DDC). At this stage, the 20 MHz real signal is converted into complex components of ±10 MHz. The frequency span is limited to up to 10 MHz, and center frequency fine-tuning is performed. The span is changed by effectively reducing the sampling rate with a decimating filter. A 503-tap FIR filter and a four-stage comb filter allow highly accurate filtering with minimal spurious emissions [41].

When acquiring data with *Tektronix RSA 2203A*, the Acquisition Length and Analysis Length are important parameters to consider, as well as their relation with the instrument capacity. This exposition is particularly relevant when the acquisitions are achieved using a GPIB, because all dimensions are defined in blocks and in samples, instead of time values.

The Acquisition Length is defined by the number of samples per block of frames, and each frame is defined by a fixed number of samples. The Acquisition Length depends on both the frame length and the number of frames. A block of frames is designated as Block Size. Hence, the following relation gives the Acquisition Length in samples [41]:

$$Acquisition\ Length = Block\ Size \times Frame\ Length \tag{C.4}$$

In other words, the Acquisition Length defines the period of time during which the Spectrum Analyzer captures the received information, which is related to its memory capacity. Table C.2 shows that one block can have a maximum of 500 frames, and that each frame contains at most 1024 samples. Based on these specifications, it is determined that the maximum Acquisition Length supported by this receiver is 512000 samples. However, for this number of samples the block duration and definition changes, based on the relations available in Table C.3.

Characteristics	Description
Acquisition mode	Single and Continuous
Acquisition memory size	2 MB
Number of data samples in one frame	1024 (Vector mode)
Block size	1 to 500 frames
A/D converter	14 bits, 51.2 Ms/s
Vector span	10 MHz
Real-time capture bandwidth	RF: 10 MHz; Baseband: 20 MHz (Option 05 only)

Table C.2 – Tektronix RSA 2203A acquisition parameters for IQT data [41].

When the instrument performs several acquisitions of smaller dimension, they are known as the Acquisition History, and they can be accessed by setting the block number. The latest acquisition is number 0, and the remaining are larger negative numbers [41].

The Analysis Length is a range of samples within the specified Acquisition History block. The starting sample is defined by the Analysis Offset, which accounts for the Trigger Position, and is given by a frame number within the acquisition. The Analysis Offset is introduced in sample between 0 and 1024. Therefore, the Analysis Length is limited by the Acquisition Length, the Trigger Position and the Analysis Offset.

If the trigger of the instrument is active, which is normally the case when the receiver is synchronized with a the signal generator, the Spectrum Analyzer requires a Trigger Position to be specified in percentage. Under this condition, the Analysis Length is limited by the Trigger Position within the Acquisition Length:

$$Analysis\ Length = Acquisition\ Length \times (1 - Trigger\ Position/100) - Analysis\ Offset \quad \text{(C.5)}$$

Henceforward, the equation above conditions the length of the analysis, and the Analysis Length is the information that can be fetched or read using the GPIB. Considering for example a Trigger Position of 25% for a maximum Acquisition Length of 512000 samples and an Analysis Offset of 0 samples, the Analysis Length would have 384000 samples.

Span (Hz)	Sampling Rate (Hz)	Frame Time (s)	Resolution Bandwidth (Hz)
100	160	6.4	1
200	320	3.2	1
500	800	1.28	1
1000	1600	0.64	1
2000	3200	0.32	2
5000	8000	0.128	5
10000	16000	0.064	10
20000	32000	0.032	20
50000	80000	0.0128	50
100000	160000	0.0064	100
200000	320000	0.0032	200
500000	800000	0.00128	500
1000000	1600000	0.00064	1000
2000000	3200000	0.00032	1000
5000000	6400000	0.00016	1000
10000000	12800000	0.00008	1000

Table C.3 – Tektronix RSA 2203A span-dependent parameters for IQT acquisition [41].

Another important aspect of the data acquisition resides in the accuracy of the instrument, and the phase/amplitude correction in frequency that should be applied. Tektronix support team provided a document describing the steps to achieve this flatness correction. In the process of correction, the first and last 256 samples are discarded to remove the finite length effect in the signal processing. Therefore, if those samples are discarded, the corrected data is shortened by 512 samples. If these samples are discarded, this must be accounted for.

C.3. Relating the Baseband Transmission to the Acquisition

This section describes a generic transmission example between the instruments involved, which are the *Keithley 2910 RF Signal Generator* and the *Tektronix RSA 2203A Real-Time Spectrum Analyzer*.

Consider an arbitrary transmission composed by N_S complex samples. To transmit the samples at improved conditions, consider also an oversampling factor of N_{OS}. At this point, the transmission length in samples is defined as:

$$TxLen_S = N_{OS} \times N_S$$

These samples in baseband are transmitted as an ARB file into *Keithley Model 2910*. We now need to specify a sampling rate to the Signal Generator. It is known that the ADC at the Spectrum Analyzer samples at 51.2 MHz. Therefore, since the sampling theorem stipulates that the sampling rate should be at least twice the highest frequency of the sampled signal, then ideally the sampling rate for transmission must be underneath:

$$KeiSR = 51.2\ MHz/2 = 25.6\ MHz$$

This is the theoretical limit stipulated by the Nyquist criterion for an ideal situation, requiring extremely accurate instrumentation. In a real system, the limitations of the instruments should be taken into account (for instance, in this dissertation the RoF network has the transmitter, the RSOA, the receiver, etc…), and the sampling rate increased. This is why oversampling should be introduced previously. As it was explained in Section 5.3.2, oversampling provides a greater margin of operation to the anti-aliasing filter, hence improving the reconstruction of the signal. It also improves the SNR. In this description, the closest rate supported by *Keithley Model 2910* that is under the Nyquist rate is 25 MHz. In this case, transmitting the oversampled signal at 25 MHz corresponds, in terms of rate for the original samples, to transmitting the non-oversampled at $25\ MHz/N_{OS}$, that is, the bandwidth has increased with oversampling.

Knowing the sampling rate, we can already determine the duration of the transmission. The sampling time is given by:

$$KeiST = 1/KeiSR = 1/25\ MHz = 0.04\ \mu s$$

Thus, the transmission length in time for this sampling time is given by:

$$TxLen_T = KeiST \times TxLen_S = 0.04\ \mu s \times TxLen_S$$

At this point, the transmission duration is known. To find out the Acquisition Length required in samples, this duration must be related to the timing parameters supported by *Tektronix RSA 2203A*, which depend on the selected frequency span. Consider a frequency span of 10 MHz. From Table C.3 we can get the frame duration associated to this span, which is 0.08 ms. Hence, the number of frames required to acquire the entire transmission, that is, the Block Size is given in frames by the ratio:

$$Block\ Size = ceil(TxLen_T/0.08\ ms)$$

It is known from Table C.2 that each frame contains 1024 samples. Therefore, to acquire completely the transmission the Spectrum Analyzer has to acquire a minimum of $Block\ Size \times 1024$ samples. However, if triggering is used, the Trigger Position in *Tektronix RSA 2203A* will influence the analysis length. For instance, a Trigger Position of 25% will limit the Analysis Length to a fraction of the Acquisition Length. This should be taken into account when data is being fetched from the instrument. Therefore, if a 25% Trigger Position is set, then for this generic example the minimum number of frames to acquire so that a complete acquisition of the transmitted signal is achieved is:

$$Acquisition\ Length = ceil(Block\ Size/(1 - 25/100)) \times 1024$$

Currently, assuming perfect synchronization with triggering, we can transfer the acquired baseband complex samples back into *Matlab* environment. In this example, it is assumed that no Analysis Offset is present. However, these samples are now sampled at a different rate than the original samples, which is again depending on the frequency span used in the acquisition. By consulting Table C.3 we can see that the sampling rate is $TekSR = 12.8\ MHz$, because the acquisition was performed for a frequency span of 10 MHz. Consequently, in order to recover the original samples, we need to find the instrument ration rate while taking into account the oversampling rate introduced before transmitting. This is achieved by doing the following calculation:

$$Ration\ Rate = N_{OS} \times \frac{TekSR}{KeiSR}$$

The ration between these two instruments rate is generally not an integer value. Nonetheless, with rational approximation an estimate can be made on an equivalent fraction of integers. *Matlab* function *rat()* performs this operation for a given tolerance. In this example, we consider that $rat(Ration\ Rate) = NUM/DEN$. The original sampling rate prior to oversampling and

transmission can now be recovered by interpolating the samples by a factor of DEN, and decimating back the samples by a factor of NUM, resulting in the following amount of acquired samples:

$$Acquisition = Block\ Size \times 1024\ \times \mathrm{DEN/NUM}$$

Because the *ceil()* function was applied to define the Acquisition Length, there is probably a small excess in the received samples. In this case, since perfect synchronization is assumed, the received information of interest is found within samples going from 1 to N_S, and the remaining can be discarded. In this dissertation, other mechanisms were implemented to recover the samples in the right position, namely, introducing empty guard intervals between packets, and also using cross-correlation with known sequences to detect the packet starting sample.

Appendix D. Experimental Results for RCE, BER and PER Metrics

The results of the performance analysis achieved for this project are presented here in their numerical form. They are divided in three main groups: the electrical domain acquisitions; the RSOA polarization analysis; the RoF experimental configurations. Although the results discussed in the thesis concern 5-fold oversampling, acquisitions revealing very similar pattern were also made for 2-fold oversampling. In all cases, the oversampling is performed by IFFT/FFT zero padding. Each value is the result of an average computed for 20 packets, with 129 OFDM symbols (SIGNAL+DATA).

D.1. Channel Spacing of 5 MHz, 2-fold Oversampling

Carrier Power (dBm)	Data Rates (Mb/s)	B2B				2C2S				2C2S-IMD			
		RCE (%)	RCE (dB)	BER (%)	PER (%)	RCE (%)	RCE (dB)	BER (%)	PER (%)	RCE (%)	RCE (dB)	BER (%)	PER (%)
-10.5	1.5	0.64	-43.92	0.00	0.00	1.23	-38.21	0.00	0.00	1.35	-37.38	0.00	0.00
	2.25	0.64	-43.86	0.00	0.00	1.23	-38.20	0.00	0.00	1.28	-37.87	0.00	0.00
	3	0.64	-43.87	0.00	0.00	1.24	-38.16	0.00	0.00	1.30	-37.75	0.00	0.00
	4.5	0.63	-44.06	0.00	0.00	1.25	-38.09	0.00	0.00	1.29	-37.76	0.00	0.00
	6	0.64	-43.91	0.00	0.00	1.22	-38.27	0.00	0.00	1.30	-37.72	0.00	0.00
	9	0.66	-43.63	0.00	0.00	1.25	-38.06	0.00	0.00	1.33	-37.51	0.00	0.00
	12	0.64	-43.90	0.00	0.00	1.26	-37.99	0.00	0.00	1.32	-37.57	0.00	0.00
	13.5	0.66	-43.67	0.00	0.00	1.21	-38.32	0.00	0.00	1.31	-37.66	0.00	0.00
0.5	1.5	0.60	-44.44	0.00	0.00	0.48	-46.35	0.00	0.00	0.61	-44.32	0.00	0.00
	2.25	0.60	-44.38	0.00	0.00	0.47	-46.57	0.00	0.00	0.59	-44.64	0.00	0.00
	3	0.62	-44.17	0.00	0.00	0.48	-46.39	0.00	0.00	0.60	-44.40	0.00	0.00
	4.5	0.59	-44.61	0.00	0.00	0.48	-46.29	0.00	0.00	0.60	-44.44	0.00	0.00
	6	0.60	-44.38	0.00	0.00	0.49	-46.24	0.00	0.00	0.60	-44.46	0.00	0.00
	9	0.61	-44.25	0.00	0.00	0.49	-46.21	0.00	0.00	0.60	-44.39	0.00	0.00
	12	0.59	-44.56	0.00	0.00	0.50	-45.96	0.00	0.00	0.61	-44.30	0.00	0.00
	13.5	0.60	-44.37	0.00	0.00	0.48	-46.29	0.00	0.00	0.61	-44.23	0.00	0.00
10.5	1.5	0.60	-44.50	0.00	0.00	0.49	-46.19	0.00	0.00	0.92	-40.77	0.00	0.00
	2.25	0.61	-44.35	0.00	0.00	0.50	-46.02	0.00	0.00	1.23	-38.23	0.00	0.00
	3	0.61	-44.29	0.00	0.00	0.49	-46.26	0.00	0.00	1.23	-38.19	0.00	0.00
	4.5	0.59	-44.60	0.00	0.00	0.48	-46.40	0.00	0.00	1.22	-38.30	0.00	0.00
	6	0.62	-44.10	0.00	0.00	0.50	-45.94	0.00	0.00	1.22	-38.29	0.00	0.00
	9	0.60	-44.49	0.00	0.00	0.48	-46.32	0.00	0.00	1.24	-38.15	0.00	0.00
	12	0.62	-44.21	0.00	0.00	0.48	-46.29	0.00	0.00	1.24	-38.14	0.00	0.00
	13.5	0.62	-44.11	0.00	0.00	0.51	-45.87	0.00	0.00	1.20	-38.38	0.00	0.00

Table D.1 – Results for the electrical configurations, with 2-fold oversampling.

Carrier Power (dBm)	Data Rates (Mb/s)	2C2S-RSOA55				2C2S-RSOA60				2C2S-RSOA65				2C2S-RSOA70				2C2S-RSOA75			
		RCE (%)	RCE (dB)	BER (%)	PER (%)	RCE (%)	RCE (dB)	BER (%)	PER (%)	RCE (%)	RCE (dB)	BER (%)	PER (%)	RCE (%)	RCE (dB)	BER (%)	PER (%)	RCE (%)	RCE (dB)	BER (%)	PER (%)
-10.5	1.5	28.75	-10.83	0.00	0.00	25.81	-11.76	0.00	0.00	29.65	-10.56	0.00	0.00	27.21	-11.31	0.00	0.00	25.88	-11.74	0.00	0.00
	2.25	30.67	-10.26	0.00	0.00	26.04	-11.69	0.00	0.00	29.38	-10.64	0.00	0.00	27.96	-11.07	0.00	0.00	25.55	-11.85	0.00	0.00
	3	29.75	-10.53	0.00	0.00	25.54	-11.85	0.00	0.00	29.06	-10.73	0.00	0.00	27.43	-11.23	0.00	0.00	25.83	-11.76	0.00	0.00
	4.5	30.69	-10.26	0.03	40.00	26.52	-11.53	0.00	5.00	29.26	-10.68	0.02	30.00	27.48	-11.22	0.06	15.00	24.90	-12.08	0.01	10.00
	6	30.78	-10.23	2.19	100.00	26.24	-11.62	0.58	100.00	29.66	-10.56	1.49	100.00	27.33	-11.27	0.76	100.00	25.21	-11.97	0.41	100.00
	9	30.75	-10.24	24.03	100.00	25.80	-11.77	12.09	100.00	28.65	-10.86	20.11	100.00	27.05	-11.36	16.02	100.00	26.39	-11.57	12.75	100.00
	12	30.20	-10.40	45.69	100.00	25.88	-11.74	42.42	100.00	28.77	-10.82	44.88	100.00	28.04	-11.04	43.89	100.00	26.10	-11.67	41.77	100.00
	13.5	31.14	-10.13	48.42	100.00	25.59	-11.84	46.24	100.00	28.75	-10.83	47.71	100.00	28.40	-10.93	47.83	100.00	25.31	-11.94	45.95	100.00
0.5	1.5	8.63	-21.28	0.00	0.00	7.74	-22.22	0.00	0.00	8.44	-21.48	0.00	0.00	7.96	-21.98	0.00	0.00	7.68	-22.30	0.00	0.00
	2.25	8.48	-21.43	0.00	0.00	7.63	-22.35	0.00	0.00	8.49	-21.42	0.00	0.00	7.93	-22.01	0.00	0.00	7.48	-22.52	0.00	0.00
	3	8.76	-21.15	0.00	0.00	7.83	-22.13	0.00	0.00	7.96	-21.98	0.00	0.00	7.70	-22.27	0.00	0.00	7.50	-22.50	0.00	0.00
	4.5	8.72	-21.19	0.00	0.00	7.90	-22.05	0.00	0.00	8.26	-21.66	0.00	0.00	7.92	-22.03	0.00	0.00	7.57	-22.42	0.00	0.00
	6	8.47	-21.44	0.00	0.00	8.12	-21.81	0.00	0.00	8.34	-21.57	0.00	0.00	8.10	-21.83	0.00	0.00	7.62	-22.36	0.00	0.00
	9	8.43	-21.48	0.00	0.00	7.87	-22.08	0.00	0.00	8.20	-21.73	0.00	0.00	7.97	-21.97	0.00	0.00	7.60	-22.38	0.00	0.00
	12	8.66	-21.25	0.25	100.00	7.78	-22.18	0.10	100.00	7.97	-21.97	0.18	100.00	7.86	-22.09	0.12	100.00	7.87	-22.08	0.15	100.00
	13.5	8.67	-21.24	1.22	100.00	7.93	-22.02	0.66	100.00	8.08	-21.86	0.90	100.00	7.90	-22.04	0.68	100.00	7.79	-22.17	0.66	100.00
10.5	1.5	3.07	-30.25	0.00	0.00	2.80	-31.06	0.00	0.00	2.95	-30.59	0.00	0.00	3.02	-30.40	0.00	0.00	2.72	-31.30	0.00	0.00
	2.25	2.94	-30.63	0.00	0.00	2.70	-31.37	0.00	0.00	2.84	-30.92	0.00	0.00	2.89	-30.77	0.00	0.00	2.83	-30.97	0.00	0.00
	3	3.01	-30.44	0.00	0.00	2.70	-31.37	0.00	0.00	2.90	-30.76	0.00	0.00	2.84	-30.95	0.00	0.00	2.75	-31.23	0.00	0.00
	4.5	2.94	-30.64	0.00	0.00	2.73	-31.29	0.00	0.00	3.03	-30.38	0.00	0.00	2.84	-30.93	0.00	0.00	2.83	-30.95	0.00	0.00
	6	2.98	-30.51	0.00	0.00	2.78	-31.11	0.00	0.00	2.96	-30.59	0.00	0.00	2.82	-31.00	0.00	0.00	2.75	-31.23	0.00	0.00
	9	3.03	-30.36	0.00	0.00	2.63	-31.61	0.00	0.00	2.96	-30.57	0.00	0.00	2.91	-30.72	0.00	0.00	2.76	-31.18	0.00	0.00
	12	2.98	-30.53	0.00	0.00	2.72	-31.32	0.00	0.00	2.98	-30.52	0.00	0.00	2.82	-31.01	0.00	0.00	2.82	-30.98	0.00	0.00
	13.5	3.28	-29.67	0.00	5.00	2.72	-31.32	0.00	0.00	3.07	-30.27	0.00	0.00	2.84	-30.93	0.00	0.00	2.79	-31.08	0.00	0.00

Table D.2 – Results for the RSOA polarizations, with 2-fold oversampling.

		2C2S-IMD-RSOA				2C2S-IMD-RSOA-11k				2C2S-RSOA				2C2S-RSOA-11k			
Carrier Power (dBm)	Data Rates (Mb/s)	RCE (%)	RCE (dB)	BER (%)	PER (%)	RCE (%)	RCE (dB)	BER (%)	PER (%)	RCE (%)	RCE (dB)	BER (%)	PER (%)	RCE (%)	RCE (dB)	BER (%)	PER (%)
-10.5	1.5	30.28	-10.38	0.00	0.00	26.91	-11.40	0.00	0.00	25.81	-11.76	0.00	0.00	33.55	-9.49	0.00	0.00
	2.25	30.72	-10.25	0.00	0.00	26.31	-11.60	0.00	0.00	26.04	-11.69	0.00	0.00	33.18	-9.58	0.00	0.00
	3	30.54	-10.30	0.00	0.00	26.80	-11.44	0.00	0.00	25.54	-11.85	0.00	0.00	34.37	-9.28	0.00	0.00
	4.5	30.13	-10.42	0.03	50.00	27.79	-11.12	0.03	25.00	26.52	-11.53	0.00	5.00	33.19	-9.58	0.14	85.00
	6	30.30	-10.37	2.09	100.00	27.98	-11.06	0.96	100.00	26.24	-11.62	0.58	100.00	35.48	-9.00	5.30	100.00
	9	30.18	-10.40	23.25	100.00	27.92	-11.08	18.57	100.00	25.80	-11.77	12.09	100.00	34.80	-9.17	34.33	100.00
	12	30.29	-10.37	46.03	100.00	27.26	-11.29	43.85	100.00	25.88	-11.74	42.42	100.00	35.90	-8.90	48.02	100.00
	13.5	30.11	-10.43	48.62	100.00	27.74	-11.14	47.95	100.00	25.59	-11.84	46.24	100.00	35.67	-8.95	49.25	100.00
0.5	1.5	8.43	-21.49	0.00	0.00	9.52	-20.43	0.00	0.00	7.74	-22.22	0.00	0.00	10.27	-19.77	0.00	0.00
	2.25	7.92	-22.03	0.00	0.00	9.90	-20.09	0.00	0.00	7.63	-22.35	0.00	0.00	10.32	-19.72	0.00	0.00
	3	8.02	-21.92	0.00	0.00	9.79	-20.18	0.00	0.00	7.83	-22.13	0.00	0.00	10.34	-19.71	0.00	0.00
	4.5	8.06	-21.87	0.00	0.00	9.26	-20.67	0.00	0.00	7.90	-22.05	0.00	0.00	10.05	-19.96	0.00	0.00
	6	7.92	-22.03	0.00	0.00	9.68	-20.28	0.00	0.00	8.12	-21.81	0.00	0.00	10.43	-19.63	0.00	0.00
	9	7.95	-22.00	0.00	0.00	9.53	-20.42	0.17	80.00	7.87	-22.08	0.00	0.00	10.27	-19.77	0.00	5.00
	12	8.07	-21.87	0.15	100.00	9.93	-20.06	0.74	100.00	7.78	-22.18	0.10	100.00	10.30	-19.74	0.96	100.00
	13.5	8.25	-21.67	0.93	100.00	9.97	-20.03	4.52	100.00	7.93	-22.02	0.66	100.00	10.17	-19.86	3.75	100.00
10.5	1.5	11.55	-18.75	0.00	0.00	11.17	-19.04	0.00	0.00	2.80	-31.06	0.00	0.00	4.38	-27.18	0.00	0.00
	2.25	11.48	-18.80	0.00	0.00	11.36	-18.89	0.00	0.00	2.70	-31.37	0.00	0.00	4.62	-26.71	0.00	0.00
	3	11.34	-18.91	0.00	0.00	12.22	-18.26	0.00	0.00	2.70	-31.37	0.00	0.00	4.40	-27.13	0.00	0.00
	4.5	11.94	-18.46	0.08	60.00	12.84	-17.83	0.02	25.00	2.73	-31.29	0.00	0.00	4.54	-26.85	0.00	0.00
	6	10.21	-19.82	0.00	0.00	12.88	-17.80	0.00	10.00	2.78	-31.11	0.00	0.00	4.42	-27.10	0.00	0.00
	9	11.75	-18.60	0.51	100.00	12.92	-17.77	0.58	95.00	2.63	-31.61	0.00	0.00	4.45	-27.04	0.00	0.00
	12	10.74	-19.38	0.47	100.00	12.42	-18.12	2.41	100.00	2.72	-31.32	0.00	0.00	4.67	-26.61	0.00	15.00
	13.5	10.45	-19.62	1.43	100.00	12.47	-18.08	5.62	100.00	2.72	-31.32	0.00	0.00	4.52	-26.89	0.00	20.00

Table D.3 – Results for the RoF configurations, with 2-fold oversampling.

D.2. Channel Spacing of 5 MHz, 5-fold Oversampling

		B2B			2C2S			2C2S-IMD		
Carrier Power (dBm)	Data Rates (Mb/s)	RCE (%)	RCE (dB)	BER (%)	PER (%)	RCE (%)	RCE (dB)	BER (%)	PER (%)	RCE (%)	RCE (dB)	BER (%)	PER (%)
-10.5	1.5	0.65	-43.76	0.00	0.00	1.21	-38.37	0.00	0.00	1.33	-37.53	0.00	0.00
	2.25	0.63	-44.01	0.00	0.00	1.17	-38.67	0.00	0.00	1.30	-37.70	0.00	0.00
	3	0.63	-44.00	0.00	0.00	1.18	-38.56	0.00	0.00	1.27	-37.91	0.00	0.00
	4.5	0.64	-43.94	0.00	0.00	1.19	-38.49	0.00	0.00	1.28	-37.86	0.00	0.00
	6	0.65	-43.72	0.00	0.00	1.19	-38.49	0.00	0.00	1.33	-37.55	0.00	0.00
	9	0.66	-43.66	0.00	0.00	1.18	-38.54	0.00	0.00	1.32	-37.56	0.00	0.00
	12	0.64	-43.91	0.00	0.00	1.20	-38.39	0.00	0.00	1.33	-37.54	0.00	0.00
	13.5	0.66	-43.54	0.00	0.00	1.20	-38.44	0.00	0.00	1.28	-37.83	0.00	0.00
0.5	1.5	0.59	-44.62	0.00	0.00	0.49	-46.15	0.00	0.00	0.61	-44.23	0.00	0.00
	2.25	0.60	-44.46	0.00	0.00	0.50	-46.05	0.00	0.00	0.64	-43.88	0.00	0.00
	3	0.59	-44.62	0.00	0.00	0.49	-46.23	0.00	0.00	0.63	-44.03	0.00	0.00
	4.5	0.62	-44.14	0.00	0.00	0.48	-46.46	0.00	0.00	0.62	-44.19	0.00	0.00
	6	0.61	-44.22	0.00	0.00	0.47	-46.61	0.00	0.00	0.63	-43.97	0.00	0.00
	9	0.61	-44.29	0.00	0.00	0.48	-46.37	0.00	0.00	0.64	-43.90	0.00	0.00
	12	0.62	-44.21	0.00	0.00	0.51	-45.79	0.00	0.00	0.62	-44.09	0.00	0.00
	13.5	0.62	-44.20	0.00	0.00	0.50	-45.96	0.00	0.00	0.64	-43.93	0.00	0.00
10.5	1.5	0.60	-44.37	0.00	0.00	0.49	-46.19	0.00	0.00	1.02	-39.81	0.00	0.00
	2.25	0.60	-44.43	0.00	0.00	0.47	-46.48	0.00	0.00	1.07	-39.39	0.00	0.00
	3	0.60	-44.44	0.00	0.00	0.48	-46.44	0.00	0.00	1.31	-37.64	0.00	0.00
	4.5	0.61	-44.22	0.00	0.00	0.49	-46.26	0.00	0.00	1.30	-37.71	0.00	0.00
	6	0.59	-44.64	0.00	0.00	0.48	-46.33	0.00	0.00	1.33	-37.49	0.00	0.00
	9	0.62	-44.12	0.00	0.00	0.49	-46.17	0.00	0.00	1.34	-37.46	0.00	0.00
	12	0.60	-44.46	0.00	0.00	0.48	-46.29	0.00	0.00	1.31	-37.68	0.00	0.00
	13.5	0.59	-44.52	0.00	0.00	0.50	-46.09	0.00	0.00	1.14	-38.85	0.00	0.00

Table D.4 – Results for the electrical configurations, with 5-fold oversampling.

Carrier Power (dBm)	Data Rates (Mb/s)	2C2S-RSOA55				2C2S-RSOA60				2C2S-RSOA65				2C2S-RSOA70				2C2S-RSOA75			
		RCE (%)	RCE (dB)	BER (%)	PER (%)	RCE (%)	RCE (dB)	BER (%)	PER (%)	RCE (%)	RCE (dB)	BER (%)	PER (%)	RCE (%)	RCE (dB)	BER (%)	PER (%)	RCE (%)	RCE (dB)	BER (%)	PER (%)
-10.5	1.5	19.46	-14.22	0.00	0.00	27.00	-11.37	0.00	0.00	34.09	-9.35	0.00	0.00	29.93	-10.48	0.00	0.00	30.40	-10.34	0.00	0.00
	2.25	18.89	-14.47	0.00	0.00	26.13	-11.66	0.00	0.00	33.57	-9.48	0.00	0.00	31.23	-10.11	0.00	0.00	31.19	-10.12	0.00	0.00
	3	19.02	-14.42	0.00	0.00	26.67	-11.48	0.00	0.00	32.88	-9.66	0.00	0.00	31.98	-9.90	0.00	0.00	31.35	-10.08	0.00	0.00
	4.5	19.43	-14.23	0.00	0.00	27.05	-11.36	0.01	20.00	33.03	-9.62	0.18	80.00	31.30	-10.09	0.13	65.00	31.96	-9.91	0.08	75.00
	6	19.43	-14.23	0.02	85.00	26.15	-11.65	0.55	100.00	32.34	-9.80	3.53	100.00	31.77	-9.96	2.04	100.00	31.80	-9.95	2.45	100.00
	9	18.94	-14.45	2.41	100.00	25.97	-11.71	14.18	100.00	33.48	-9.50	30.30	100.00	32.35	-9.80	29.15	100.00	32.46	-9.77	29.40	100.00
	12	18.73	-14.55	24.35	100.00	25.90	-11.73	42.05	100.00	31.92	-9.92	47.00	100.00	33.56	-9.48	47.52	100.00	32.15	-9.86	46.95	100.00
	13.5	18.85	-14.50	37.07	100.00	25.77	-11.78	46.77	100.00	32.44	-9.78	48.84	100.00	30.73	-10.25	48.50	100.00	32.60	-9.74	49.06	100.00
0.5	1.5	6.14	-24.24	0.00	0.00	7.48	-22.52	0.00	0.00	9.22	-20.71	0.00	0.00	8.85	-21.06	0.00	0.00	9.19	-20.74	0.00	0.00
	2.25	5.93	-24.53	0.00	0.00	7.58	-22.41	0.00	0.00	9.17	-20.75	0.00	0.00	8.44	-21.48	0.00	0.00	8.84	-21.07	0.00	0.00
	3	6.16	-24.21	0.00	0.00	7.55	-22.44	0.00	0.00	9.24	-20.69	0.00	0.00	8.52	-21.39	0.00	0.00	9.02	-20.90	0.00	0.00
	4.5	6.29	-24.03	0.00	0.00	7.68	-22.29	0.00	0.00	9.20	-20.72	0.00	0.00	8.37	-21.55	0.00	0.00	9.12	-20.80	0.00	0.00
	6	6.18	-24.18	0.00	0.00	8.02	-21.92	0.00	0.00	9.18	-20.74	0.00	0.00	8.65	-21.26	0.00	0.00	9.29	-20.64	0.00	0.00
	9	6.03	-24.39	0.00	0.00	7.73	-22.24	0.00	0.00	8.85	-21.06	0.00	0.00	8.76	-21.15	0.00	0.00	9.27	-20.66	0.00	10.00
	12	6.03	-24.39	0.01	60.00	7.59	-22.40	0.09	100.00	9.03	-20.89	0.37	100.00	8.74	-21.17	0.27	100.00	9.38	-20.56	0.47	100.00
	13.5	6.00	-24.43	0.05	80.00	7.85	-22.10	0.75	100.00	9.04	-20.87	1.80	100.00	8.87	-21.04	1.38	100.00	9.24	-20.68	1.80	100.00
10.5	1.5	2.18	-33.22	0.00	0.00	2.47	-32.15	0.00	0.00	3.12	-30.11	0.00	0.00	4.49	-26.95	0.00	0.00	4.53	-26.88	0.00	0.00
	2.25	2.24	-33.00	0.00	0.00	2.47	-32.13	0.00	0.00	3.07	-30.26	0.00	0.00	4.50	-26.94	0.00	0.00	4.67	-26.61	0.00	0.00
	3	2.12	-33.49	0.00	0.00	2.55	-31.86	0.00	0.00	2.96	-30.57	0.00	0.00	4.57	-26.80	0.00	0.00	4.63	-26.70	0.00	0.00
	4.5	2.21	-33.10	0.00	0.00	2.48	-32.12	0.00	0.00	3.06	-30.28	0.00	0.00	4.39	-27.15	0.00	0.00	4.62	-26.71	0.00	0.00
	6	2.18	-33.25	0.00	0.00	2.56	-31.85	0.00	0.00	3.09	-30.19	0.00	0.00	4.38	-27.18	0.00	0.00	4.75	-26.46	0.00	0.00
	9	2.19	-33.17	0.00	0.00	2.51	-32.01	0.00	0.00	3.08	-30.22	0.00	0.00	4.56	-26.82	0.00	0.00	4.66	-26.63	0.00	0.00
	12	2.24	-32.99	0.00	0.00	2.62	-31.63	0.00	0.00	3.18	-29.95	0.00	0.00	4.53	-26.87	0.00	5.00	4.67	-26.62	0.00	15.00
	13.5	2.22	-33.08	0.00	0.00	2.59	-31.74	0.00	0.00	3.04	-30.35	0.00	0.00	4.42	-27.09	0.00	10.00	4.69	-26.57	0.00	0.00

Table D.5 – Results for the RSOA polarizations, with 5-fold oversampling.

		2C2S-IMD-RSOA				2C2S-IMD-RSOA-11k				2C2S-RSOA				2C2S-RSOA-11k			
Carrier Power (dBm)	Data Rates (Mb/s)	RCE (%)	RCE (dB)	BER (%)	PER (%)	RCE (%)	RCE (dB)	BER (%)	PER (%)	RCE (%)	RCE (dB)	BER (%)	PER (%)	RCE (%)	RCE (dB)	BER (%)	PER (%)
-10.5	1.5	28.83	-10.80	0.00	0.00	29.70	-10.55	0.00	0.00	27.00	-11.37	0.00	0.00	28.60	-10.87	0.00	0.00
	2.25	27.37	-11.26	0.00	0.00	29.89	-10.49	0.00	0.00	26.13	-11.66	0.00	0.00	30.28	-10.38	0.00	0.00
	3	28.84	-10.80	0.00	0.00	29.66	-10.56	0.00	0.00	26.67	-11.48	0.00	0.00	30.03	-10.45	0.00	0.00
	4.5	28.27	-10.97	0.01	30.00	30.36	-10.35	0.09	65.00	27.05	-11.36	0.01	20.00	29.25	-10.68	0.02	35.00
	6	29.16	-10.70	1.10	100.00	30.37	-10.35	2.77	100.00	26.15	-11.65	0.55	100.00	29.83	-10.51	1.59	100.00
	9	27.99	-11.06	18.11	100.00	30.57	-10.29	24.53	100.00	25.97	-11.71	14.18	100.00	29.73	-10.54	22.25	100.00
	12	27.74	-11.14	44.10	100.00	31.21	-10.11	46.23	100.00	25.90	-11.73	42.05	100.00	29.12	-10.72	45.18	100.00
	13.5	27.95	-11.07	47.74	100.00	30.79	-10.23	48.75	100.00	25.77	-11.78	46.77	100.00	29.77	-10.52	48.38	100.00
0.5	1.5	8.99	-20.92	0.00	0.00	9.43	-20.51	0.00	0.00	7.48	-22.52	0.00	0.00	10.23	-19.80	0.00	0.00
	2.25	8.80	-21.11	0.00	0.00	9.97	-20.03	0.00	0.00	7.58	-22.41	0.00	0.00	10.54	-19.54	0.00	0.00
	3	8.66	-21.25	0.00	0.00	10.21	-19.82	0.00	0.00	7.55	-22.44	0.00	0.00	10.11	-19.91	0.00	0.00
	4.5	8.74	-21.17	0.00	0.00	10.02	-19.98	0.00	0.00	7.68	-22.29	0.00	0.00	10.43	-19.64	0.00	0.00
	6	9.09	-20.83	0.00	0.00	10.05	-19.96	0.00	0.00	8.02	-21.92	0.00	0.00	10.07	-19.94	0.00	0.00
	9	9.03	-20.89	0.00	0.00	10.34	-19.71	0.00	10.00	7.73	-22.24	0.00	0.00	9.94	-20.05	0.00	0.00
	12	8.63	-21.27	0.25	100.00	10.04	-19.96	0.82	100.00	7.59	-22.40	0.09	100.00	10.12	-19.89	0.89	100.00
	13.5	8.77	-21.14	1.44	100.00	10.36	-19.69	4.30	100.00	7.85	-22.10	0.75	100.00	9.72	-20.24	2.70	100.00
10.5	1.5	5.91	-24.57	0.00	0.00	8.68	-21.23	0.00	0.00	2.47	-32.15	0.00	0.00	4.34	-27.25	0.00	0.00
	2.25	5.98	-24.46	0.00	0.00	9.79	-20.18	0.00	0.00	2.47	-32.13	0.00	0.00	4.21	-27.51	0.00	0.00
	3	6.11	-24.28	0.00	0.00	10.56	-19.53	0.00	0.00	2.55	-31.86	0.00	0.00	4.30	-27.33	0.00	0.00
	4.5	6.43	-23.84	0.00	0.00	10.28	-19.76	0.07	50.00	2.48	-32.12	0.00	0.00	4.24	-27.46	0.00	0.00
	6	6.97	-23.13	0.00	0.00	10.36	-19.69	0.00	0.00	2.56	-31.85	0.00	0.00	4.05	-27.86	0.00	0.00
	9	7.44	-22.57	0.07	90.00	10.99	-19.18	0.55	95.00	2.51	-32.01	0.00	0.00	4.22	-27.48	0.00	0.00
	12	8.00	-21.94	0.39	100.00	10.55	-19.53	1.05	100.00	2.62	-31.63	0.00	0.00	4.21	-27.52	0.00	0.00
	13.5	8.09	-21.85	0.81	100.00	10.80	-19.34	2.56	100.00	2.59	-31.74	0.00	0.00	4.05	-27.85	0.00	0.00

Table D.6 – Results for the RoF configurations, with 5-fold oversampling.

References

[1] Gurprakash Singh and Arokiaswami Alphones, "OFDM Modulation Study for a Radio-over-Fiber System for Wireless LAN (IEEE 802.11a)," *ICICS-PCM 2003*, vol. 1-3, pp. 1460-1464, December 2003.

[2] IEEE Computer Society, IEEE Std 802.11TM - Part 11: Wireless LAN Medium Access Control (MAC) and Physical Layer (PHY) Specifications, June 12, 2007, Sponsored by the LAN/MAN Standards Committee.

[3] Ramjee Prasad, *OFDM for Wireless Communications Systems*. Boston - London: Artech House, Inc., 2004.

[4] Pak Kay Tang, Ling Chuen Ong, A. Alphones, Bin Luo, and Masayuki Fujise, "PER and EVM measurements of a radio-over-fiber network for cellular and WLAN system applications," *Journal of Lightwave Technology*, pp. 2370-2376, November 2004.

[5] Jean Armstrong, "OFDM for Optical Communications," *Journal of Lightwave Technology*, vol. 27, no. 3, pp. 189-204, February 2009.

[6] Bao Linh Dang and Ignas Niemegeers, "Analysis of IEEE 802.11 in radio over fiber home networks," *LCN 2005: 30th Conference on Local Computer Networks, Proceedings*, pp. 744-745, 2005.

[7] William Shieh and Ivan Djordjevic, *Orthogonal Frequency Division Multiplexing for Optical Communications*, Academic Press, Ed. United States of America: Elsevier, 2009.

[8] Louis Litwin and Michael Pugel, "The principles of OFDM," *RF signal processing*, vol. 1, pp. 30-48, January 2001.

[9] S. B. Weinstein and Paul M. Ebert, "Data Transmission by Frequency-Division Multiplexing Using the Discrete Fourier Transform," *IEEE Transactions on Communication Technology*, vol. 19, no. 5, pp. 628-634, October 1971.

[10] Ernesto Leite Pinto and Claudio Penedo de Albuquerque, "A técnica de Transmissão OFDM," *Revista Científica Periódica - Telecommunicações*, vol. 5, no. 1, Junho 2002.

[11] Dušan Matiæ, "OFDM as a possible modulation technique for multimedia applications in the range of mm waves," *Introduction to OFDM, II edition*, vol. 1, pp. 10–30, October 1998.

[12] Ahmad R. S. Bahai, Burton S. Saltzberg, and Mustafa Ergen, *Multi-carrier Digital Communications: Theory And Applications Of OFDM*, 2nd ed. Boston, United States of America: Springer Science + Business Media, Inc., 2004.

[13] Guilhermo Acosta, OFDM Simulation Using Matlab, August 2000.

[14] Jesse Hansen and Sambit Bohidar. University of Rhode Island - Department of Electrical, Computer, and Biomedical Engineering. [Online]. http://www.ele.uri.edu/~hansenj/projects/ele436/fft.pdf

[15] Charan Langton. (2004) Intuitive Guide to Principles of Communications. [Online]. http://www.complextoreal.com/chapters/ofdm2.pdf

[16] VOCAL Technologies, Ltd. (2001) 802.11a Wireless LAN. [Online]. http://www.vocal.com/redirect/802_11a.html

[17] Fernando H. Gregorio, 802.11A - OFDM PHY CODING AND INTERLEAVING, 2004.

[18] Werner Henkel, Georg Tauböck, Per Ödling, Per Ola Börjesson, and Niklas Petersson, "The cyclic prefix of OFDM/DMT - An Analysis," in *International Zurich Seminar on Broadband Communications*, Zurich, 2002, pp. 22-22.

[19] Roberto López-Valcarce, "Minimum delay spread TEQ design in multi-carrier systems," *IEEE Signal Processing Letters*, vol. 11, no. 8, pp. 682–685, August 2004.

[20] Marius Oltean and Miranda Naforniţă, "The Cyclic Prefix Length Influence on OFDM-Transmission BER," *Buletinul Ştiinţific al Universităţii "Politehnica" din Timişoara*, vol. 48, no. 62, Fascicola 2003.

[21] Yun Chiu, Dejan Markovic, Haiyun Tang, and Ning Zhang, "OFDM Receiver Design," Electrical Engineering and Computer Sciences, University of California Berkeley, 2000.

[22] Ken Gentile, "The care and feeding of digital, pulse-shaping filters," *RF mixed signal*, vol. 25, pp. 50–58, April 2002.

[23] Eldad Perahia and Robert Stacey, *Next Generation Wireless LANs: Throughput, Robustness, and Reliability in 802.11n*. Cambridge, United Kingdom: Cambridge University Press, 2008.

[24] Agilent Technologies. (2010, May) N7617B Signal Studio for 802.11 WLAN. [Online]. http://wireless.agilent.com/wireless/helpfiles/n7617b/n7617b.htm

[25] Eric Lawrey, "The suitability of OFDM as a modulation technique for wireless telecommunications, with a CDMA comparison," Computer Systems Engineering, James Cook University, Thesis 1997.

[26] K. Fazel and S. Kaiser, *Multi-Carrier and Spread Spectrum Systems: From OFDM and MC-CDMA to LTE and WiMAX*, 2nd ed.: Wiley, 2008.

[27] Juha Heiskala and John Terry, *OFDM Wireless LANs: A Theoretical and Practical Guide*. Indianapolis, Great Britain: Sams, 2002.

[28] Krishna Sankar. (2008, March) DSP log - Signal Processing for Communication. [Online]. http://www.dsplog.com/

[29] Alliance for Telecommunications Industry Solutions. (2007) Telecom Glossary 2000. [Online]. http://www.atis.org/glossary/

[30] Christian Olgaard, "Using advanced signal analysis to identify sources of WLAN transmitter degradations," *RF design*, October 2004, www.rfdesign.com.

[31] National Instruments. Modulation Error Ratio (MER) and Error Vector Magnitude (EVM). [Online]. http://zone.ni.com/devzone/cda/tut/p/id/3652

[32] Rishad Ahmed Shafik, Md. Shahriar Rahman, AHM Razibul Islam, and Nabil Shovon Ashraf, "On the error vector magnitude as a performance metric and comparative analysis," in *2nd International Conference on Emerging Technologies*, Peshawar, 2006, pp. 27–31.

[33] The MathWorks, Inc. (2010, September) MathWorks. [Online]. http://www.mathworks.com/help/toolbox/comm/ref/commmeasure.evm.html

[34] Sanjeev Kumar and Swati Sharma, "Error Probability of Different Modulation Schemes for OFDM based WLAN standard IEEE 802.11a," *International Journal of Engineering (IJE)*, vol. 4, no. 4, pp. 262-267, October 2010.

[35] Hisham A. Mahmoud and Hüseyin Arslan, "Error Vector Magnitude to SNR Conversion for Nondata-Aided Receivers," *IEEE TRANSACTIONS ON WIRELESS COMMUNICATIONS*, vol. 8, no. 5, pp. 2694-2704, May 2009.

[36] Khaled M. Gharaibeh, Kevin G. Gard, and Michael B. Steer, "Accurate Estimation of Digital Communication System Metrics — SNR, EVM and ρ in a Nonlinear Amplifier Environment," in *ARFTG Microwave Measurements Conference*, Raleigh, 2004, pp. 41-44.

[37] Department of Communications and Networking (Comnet). Advanced Error Control Schemes. [Online]. http://www.comlab.hut.fi/opetus/311/ofdm_mod.pdf

[38] The MathWorks, Inc. (2010, December) MathWorks. [Online]. http://www.mathworks.com/products/matlab/

[39] Johan Kirkhorn, Introduction to IQ-demodulation of RF-data, September 15, 1999, IFBT, NTNU.

[40] Keithley Instruments, Inc, Advanced Measurement Techniques for OFDM- and MIMO-based Radio Systems: Demystifying WLAN and WiMAX Testing, 2009, 1st Revised Edition.

[41] Tektronix, Inc., RSA2203A & RSA2208A 3 GHz & 8 GHz Real-Time Spectrum Analyzers User Manual, This document applies to firmware version 3.20 and above.

[42] Agilent Technologies, Inc., Agilent Series V2900 Help, 2010, Help system build 2010.04.13.1815

for firmware version 5.0.

[43] John Watkinson, *The Art of Digital Audio*, 3rd ed. England: Focal Press, 2001.

[44] Wallace C. Babcock, "Intermodulation Interferences in Radio Systems," *The Bell System Technical Journal*, pp. 63-74, January 1953.

[45] Charan Langton. (1998) Intuitive Guide to Principles of Communications. [Online]. http://www.complextoreal.com/chapters/fft1.pdf

[46] J. McNames. (2006, June) The Computer Action Team - Electrical and Computer Engineering. [Online]. http://web.cecs.pdx.edu/~ece2xx/ECE223/Slides/CTFourierTransformx4.pdf

[47] Quan Quach. (2008, March) Blinkdagger - an Engineering and MATLAB blog. [Online]. http://blinkdagger.com/fourier/linear-time-invariant-systems-the-backbone-of-fourier-theory/